Proceedings of The International Conference

SN 1987A, Quark Phase Transition in Compact Objects and Multimessenger Astronomy

Institute for Nuclear Research
of the Russian Academy of Sciences

Федеральное государственное
бюджетное учреждение науки
Институт ядерных исследований
Российской академии наук

Посвящается 50-летию
Баксанской нейтринной обсерватории ИЯИ РАН

Сверхновая SN 1987A, кварковый фазовый переход в компактных объектах и многоволновая астрономия

Труды
Международной конференции

Российская Федерация
Кабардино-Балкария, Терскол (БНО)
КЧР, Нижний Архыз (САО)
2-8 июля 2017

Ответственные редакторы:
В.В. Соколов, Т.Н. Соколова, В.Б. Петков,
В.В. Синев, Е.А. Горбачева

Институт ядерных исследований
Российской академии наук (ИЯИ РАН)
Москва
2018

Dedicated to 50-th Anniversary
of Baksan Neutrino Observatory INR RAS

Proceedings
of The International Conference

SN 1987A, Quark Phase Transition in Compact Objects and Multimessenger Astronomy

Russia
KBR, Terskol (BNO)
KChR, Nizhnij Arkhyz (SAO)
July 2-8 2017

Edition board:
V.V. Sokolov, T.N. Sokolova, V.B. Petkov,
V.V. Sinev, E.A. Gorbacheva

Moscow, Institute for Nuclear research
of Russian academy of Sciences
Moscow
2018

УДК 524-7 (063)
Q24

Научное издание

Ответственные редакторы:
В.В. Соколов, Т.Н. Соколова, В.Б. Петков, В.В. Синев, Е.А. Горбачева

Q24 **Сверхновая SN 1987A, кварковый фазовый переход в компактных объектах и многоволновая астрономия.**
Труды Международной конференции
(Российская Федерация, Кабардино-Балкария, Терскол (БНО)
На английском языке. М.: ИЯИ РАН, 2018 — 266 с.

ISBN 978-5-94274-327-7

В сборнике представлены доклады международной конференции «Сверхновая SN 1987A, кварковый фазовый переход в компактных объектах и многоволновая астрономия», состоявшейся 2–8 июля 2017 г. в Терсколе-Нижнем Архызе. Конференция посвящена взаимодействию астрономии с нейтринной и гамма астрономией. Представлены доклады по важным задачам: отождествление наблюдаемых объектов с источниками нейтринных и гамма всплесков, разработка новых приборов для наблюдения, анализ данных гравитационных антенн и ряд других.

УДК 524-7 (063)

ISBN 978-5-94274-327-7

Conference participants from left on right:

First row: T. Sokolova, I. Savanov, O. Zhelenkova, V. Petkov, V Vlasyuk, V. Sokolov;

Second row: A. Valeev, G. Beskin, V. Goransky, I. Dzaparova, N. Oborina, V. Kasalov, A.Gangapshev;

Third row: A. Johannes Stasik, A. Marukhno, T. Fatkhullin, S. Semenov, S. Yakimenko, S. Trushkin, A. Yudin, L. Fesik, V. Sinev, O. Sholukhova, A. Kurenya, A.Vinokurov

Content

Preface

The international conference on this urgent topic was held in Russia for the second time. The success of the first workshop held in October 2015 persuaded the organizers that such meetings arranged in locations of unique Russian Observatories – Special Astrophysical Observatory of RAS (SAO RAS) and Baksan Neutrino Observatory of Institute for Nuclear Research of RAS (BNO INR RAS) – are well needed.

The feature of this conference was that it was related to two significant dates: the 50-th anniversary of Baksan Neutrino Observatory and the 30-th anniversary of the supernova SN 1987A. Observation of its neutrino signal was the direct experimental confirmation of the extremely important role of neutrino in the process of explosion of massive stars. The Baksan Underground Scintillation Telescope (BUST) was one of the four neutrino detectors which registered neutrino events from SN 1987A.

The holding of the conference by efforts of BNO INR RAS and SAO RAS was determined by the character of fundamental problems of the modern astrophysics included in its program. Solution of such problems demands development of methods combining optical ground-based and space observations and experiments with neutrino telescopes, cosmic-ray recording sets and detectors of gravitational waves.

The scientific program of our conference covers a wide range of problems of the modern theoretical astrophysics including the problem of existence of quantum-chromodynamic (QCD) phase transitions and matter states at high temperatures and densities. Such conditions are likely to be achievable only in astrophysical objects – collapsars of stellar mass, for example, the objects whose formation is related with collapse and explosion of hot and dense cores of massive stars observable as gamma-ray bursts and supernovae.

Nowadays the quark-gluon plasma is a new direction both in the high-energy physics and in the study of stellar compact objects. The phase transition to the state of quark-gluon plasma is surely related to the mechanism itself of explosion of massive supernovae (such as SN 1987A), and the energy of such a transition can be a source of cosmic gamma-ray bursts. Neutrinos which are observed with modern detectors (including domestic ones, such as BUST) can be signals of transition of matter to quark matter. Equipment of modern gravitational detectors is also developed for such signals registration.

Participation of astronomers in the programs aimed at the study of neutrino and gravitational events localization boxes was discussed many times already (e.g., see the report of a special commission: The summary of the EMMI Rapid Reaction Task Force on "Quark Matter in Compact Stars", October 7-10, 2013, FIAS, Goethe University, Frankfurt, Germany, arXiv:1402.6911).

At the conference a considerable part of time was dedicated to up-to-date opportunities of experimental observation (electromagnetic identification) of sources of cosmic neutrino and gravitational waves, and to discussion about prospects of development of studies in this field. The conference included review lectures of leading experts in the conference topic and original oral presentation. A special session was dedicated to the supernova SN 1987A. Presentations by young Russian researchers were especially welcomed. Participation of leading Russian and foreign scientists promoted the further achievements in the study of this field of astrophysics in Russia and the training of skilled researchers.

The adopted Conference's resolution reads the following: the results of the second conference on this urgent topic are appreciated as successful; the idea of holding such a conference by joint efforts of two unique Russian Observatories was fruitful; it is recommended to continue a series of such conferences in SAO RAS and BNO INR RAS. Special notification was made on concentration of efforts of all Russian observers on all aspects of Multi-Messenger Astronomy studies.

Organizing committee of the conference

Gravitation theory in multi-messenger astronomy I: comparison of geometrical and field approaches to the physics of gravitational interaction

Yu.V. Baryshev[1], S.A. Oschepkov[2]

[1]Astronomical Department, Saint Petersburg State University, Saint-Petersburg, Russia;
yubaryshevl@mail.ru

[2]Taurida Academy, V.I. Vernadsky Crimean Federal University, Simferopol, Russia

Abstract In modern theoretical physics there are two alternative possibilities of the description of gravitation: geometrical theory of the General Relativity Theory (GRT) of Einstein and non-metric theory of the material tensor Field Gravitation Theory (FGT) of Feynman. In this first report general provisions of these theories are stated: basic principles, Lagrangians, equations of the field and equations of the motion. These equations will be used for interpretations of observations in multimessenger astronomy, which discussed in our second report.

Keywords: relativistic astrophysics, gravitation, lagrangian formalism, quantum field theory.

1. Gravity physics as the bases of relativistic astrophysics.

The multi-messenger astronomy deals with the most energetic processes in the Universe such as compact relativistic objects (neutron and quark stars), candidates of black holes having stellar and galactic masses, gravitational radiation, massive supernova explosions, gamma ray bursts, jets from active galactic nuclei. Relativistic gravitational collapse is the source of the highest energy extraction from astrophysical objects and this is why the gravitation theory is the fundamental basis for interpretation of violent events in multi-messenger astronomy.

Since the beginning of the 20th century there are two really alternative approaches for the description of gravitational interaction in theoretical physics: material field in Mincowski space-time and curvature of Riemannian space-time itself.

Because of great success of the **General Relativity Theory** (GRT) in explanation of the existing experimental and observational facts in gravitation physics, the theory of gravitation as the theory of the field has still been deprived of the general attention and only GRT is considered in textbooks - Landau & Lifshitz 1971 [1]; Misner, Thorne & Wheeler 1973 [2]; Straumann 2013 [3] and others

However already Einstein in 1926 in work "Non-Euclidean Geometry and Physics" (“Nichtenklidische Geometrie in der Physik”) has allocated two alternative approaches to interrelation of geometry and physics. He called it Helmholtz’s and Poincare's approaches. In particular he wrote "We will accept the first (geometrical) point of view as the most answering to the current state of our knowledge". But he noted also that development in particular of the quantum theory will perhaps force to reconsider our point of view.

Field approach to gravitation has been partially developed by number of the famous physicists (e.g. Thirring 1961 [4]; Kalman 1961 [5]). A general base for relativistic quantum **Field Gravitation Theory** (FGT) was presented by Feynman in his Caltech 1962/63 lectures (see Lecture 1 – "A Field Approach to Gravitation" in Feynman, Morinigo & Wagner 1995 [6]). The gravitation phenomena in FGT are described by the relativistic quantum field which theoretically presented by the second rank symmetric tensor ψ_{ik} in Minkowski space with metric tensor η_{ik} .

A decisive step in the frame of FGT was done by Sokolov & Baryshev 1980 [7] where they founded the crucial role of the scalar (spin-0) component of the symmetric tensor field, i.e. its trace $\psi(r, t) = \eta^{ik} \psi_{ik}$, which is the irreducible part of the symmetric tensor representation (together with the spin-2 traceless irreducible representation). The most important new aspect of the field gravitation theory is that the gravity force (Newtonian and relativistic) actually consists of the two types of fields – attraction spin-2 field and repulsion spin-0 field. Note that this fact was missed by many physicists who tried to prove the identity of the Einstein's geometrical and Feynman's relativistic quantum field descriptions of the gravitation. As it was demonstrated by Sokolov & Baryshev 1980 [7] the scalar part (trace) of the symmetric tensor potential is the true dynamical repulsive field with positive energy density, and it is not a "ghost" with negative energy density.

Recent review of the FGT results was done by Baryshev 2017 [8]. It was demonstrated that the FGT is principally different from GRT, though main really observed relativistic gravity effects have the same values in both approaches.

The reason that the intrinsic scalar field disappears in GRT but is the essential part of FGT follows from strict mathematical properties of tensors in Minkowski space. Indeed, the strict properties of the metric tensor of the Riemannian space and the general tensor rules for physical quantities in Minkowski space demand that for the sum of two quantities $\eta_{ik} + h_{ik}$ and $\eta_{ik} + \psi_{ik}$ one gets the following expressions (where g^{ik} - metric tensor of the Riemannian space, η_{ik} - metric tensor of the Minkowski space, h_{ik} and ψ_{ik} are small quantities of the first order):

Geometrical approach:		Field approach:
$g_{ik}(r, t) = \eta_{ik} + h_{ik}(r, t)$	and	$f_{ik}(r, t) = \eta_{ik} + \psi_{ik}(r, t)$
$g^{ik}(r, t) = \eta^{ik} - h^{ik}(r, t)$	while	$f^{ik}(r, t) = \eta^{ik} + \psi^{ik}(r, t)$
$g^{i}_{\ k} = \delta^{i}_{\ k}$	while	$f^{i}_{\ k}(r, t) = \delta^{i}_{\ k} + \psi^{i}_{\ k}(r, t)$
$g_{ik}\, g^{ik} = 4$	while	$f_{ik}\, f^{ik} = 4 + 2\psi(r, t)$

From these relations we see that there is principle difference between geometrical and field-theoretical approaches. Indeed, in the frame of the FGT the consistent description of the sum of two tensors does not allow to change the sign for the parts. Hence tensor f^{ik} cannot be the metric tensor of a Riemannian space and in the geometrical approach the scalar part of the symmetric tensor field is lost. So a "repairing" of the field approach, suggested in [2], in fact means replacing the field-theoretical approach in Minkowski space by the geometrization principle of the geometrical approach in the Riemannian space.

It leads to the new FGT predictions: that there is EMT (positive energy density of the gravitational field for both spin-2 and spin-0 parts), that besides tensor gravitational waves there are also scalar waves, and there are relativistic compact objects without horizons instead of black holes with unphysical one way surfaces.

2. General Relativity Theory: basic principles, main equations and predictions.

To understand the physical difference between GRT and FGT description of gravitation we start from consideration of the:

GRT basic principles:

1) ***The principle of geometrization***. General relativity is based on the principle of geometrization which indicates that all gravitational phenomena have to be described by a metrics of Riemannian space. The role of the gravitational "potential" is played by the metric tensor g_{ik} which determines the 4-interval of the corresponding Riemannian space:

$$ds^2 = g_{ik}\, dx^i dx^k \qquad (1)$$

Thus, gravitation is not a material physical field in flat space-time, but is only manifestation of curved space-time.

A test particle moves along a geodesic line of the Riemannian space. Note that geodesic motion is a form of the equivalence principle, which actually has many "non-equivalent" formulations like universality of free fall or philosophical equivalence of the inertial reference frames to the reference frames accelerated by homogeneous gravity field. Equivalence principle played an important role when general relativity was born, while now the basic principle is the principle of geometrization, having clear mathematical formulation.

2) ***The principle of least action***. The field equations in Einstein's GRT are derived from the principle of the least action at a variation of a metric tensor g_{ik} in action S (matter + gravitational field). It is important to note that instead of three parts (field-interaction-matter of full action in the standard field theory) here full action contains only two parts:

$$S = S_{(m)} + S_{(g)} = \frac{1}{c}\int\left(\Lambda_{(m)} + \Lambda_{(g)}\right)\sqrt{-g}\, d\Omega \qquad (2)$$

There is no Lagrangian function for interaction because in GRT gravitational interaction isn't considered while interaction Lagrangian exists for other physical fields, which is contained in the interaction part $S_{(int)}$.

Basic equations of general relativity:

1) ***Einstein's field equations***. Variation δg_{ik}, with restriction $g_{ik}g^{ik} \equiv 4$ gives from $\delta(S_{(m)} + S_{(g)}) = 0$ the following field equations:

$$\mathfrak{R}^{ik} - \frac{1}{2}\, g^{ik}\, \mathfrak{R} = \frac{8\pi G}{c^4}\, T^{ik}_{(m)} \qquad (3)$$

where $\mathfrak{R}_{ik}$ is the Ricci tensor, $T^{ik}_{(m)}$ is the energy-momentum tensor (EMT) of the matter.

Note that $T^{ik}_{(m)}$ does not contain the energy-momentum tensor of the gravity field itself, because gravitation is not a material field in General Relativity (as also discussed below).

2) ***The equation of motion of test particles***. A mathematical consequence of the field equations (3) is that due to Bianchi identity the covariant derivative of the left side equals

zero, so for the right side we also have

$$T^{ik}_{(m)\,;i} = 0 \tag{4}$$

This continuity equation also gives the equations of motion for a considered matter. It implies the geodesic equation of motion for a test particle:

$$\frac{du^i}{ds} = \Gamma^i_{kl}\, u^k u^l \tag{5}$$

$u^i = dx^i/ds$ is the 4-velocity of the particle and Γ^i_{kl} is the Christoffel symbol.

Major predictions for experiments/observations are:

All predictions of the General Relativity (both for weak and for strong fields) are derived from Einstein's field equations and the equations of motion.

The classical weak gravity effects have been tested with accuracy of about 0.1-1%. Among these experimentally verified effects are:

- Universality of free fall for non-rotating bodies,
- Deflection of light by massive bodies,
- Gravitational frequency-shift,
- Time delay of light signals,
- Perihelion shift of a planet,
- Lense-Thirring effect,
- Geodetic precession of a gyroscope,
- The emission and detection of the quadrupole gravitational waves,

The fundamental prediction of GRT for the strong gravity is:

- Existence of the event horizon and singularity of Black Holes.

However in GRT there are also conceptual problems. The so called “energy problem” can be demonstrated with the simplest case of a spherically symmetric weak static gravity field. For instance, in harmonic coordinates the Landau-Lifshiz [1] symmetric pseudo-tensor gives negative energy density of the static spherically symmetric gravity field

$$\varepsilon_{(g)}(\boldsymbol{r}) = t^{00}_{LL}(\boldsymbol{r}) = -\frac{7}{8\pi G}(\nabla\varphi_N)^2 \tag{6}$$

The “final” energy-momentum tensor of the gravity field, which was derived by Grishchuk, Petrov & Popova [9], also has a negative energy density of the weak static field:

$$t^{00}_{GPP}(\boldsymbol{r}) = -\frac{11}{8\pi G}(\nabla\varphi_N)^2 \tag{7}$$

while Einstein’s pseudo-tensor gives:

$$t^{00}_{E}(\boldsymbol{r}) = +\frac{1}{8\pi G}(\nabla\varphi_N)^2 \tag{8}$$

Hence, according to the LL-pseudo-tensor and the GPP-tensor the energy density of the static gravitational field is negative, which conflicts with the quantum field theories of other fundamental interactions. We note also that the traces of all these EMPTs do not vanish for static fields, while it should be for massless fields.

3. Relativistic Quantum Field Gravitation Theory: basic principles, main equations and predictions.

In Sec.1 we have emphasized that the field gravitation theory has its roots in papers by Birkhoff, Thirring, Kalman, and was formulated as a relativistic quantum field by Feynman [6].

Feynman [6] has shown that gravitational interaction can be described as the interaction of matter with the field of a symmetric tensor of the second rank in Minkowski's space based on a Lagrangian formalism of the field theory. He discussed a quantum field approach to the gravity just as the next fundamental physical interaction and claimed that "the geometrical interpretation is not really necessary or essential to physics" ([6] p. 113).

In the frame of the field gravitation theory the crucial role of the intrinsic scalar part (the trace $\psi(r, t) = \eta_{ik}\psi^{ik}$) of the reducible symmetric tensor potentials $\psi_{ik}(r, t)$ was discovered and studied by Sokolov & Baryshev 1980 [7] (recent review in Baryshev 2017 [8].

Basic principles of Relativistic Quantum Field Gravitation Theory include:

- the inertial reference frames and Minkowski space with metric η_{ik};
- the reducible symmetric second rank tensor potential $\psi^{ik}{}_{(r,t)}$ and especially its trace $\psi_{(r,t)} = \eta_{ik}\,\psi^{ik}$ describe gravitational interaction;
- the Lagrangian formalism and Stationary Action principle:

$$S = S_{(m)} + S_{(int)} + S_{(g)} = \frac{1}{c}\int\left(\Lambda_{(m)} + \Lambda_{(int)} + \Lambda_{(g)}\right)\sqrt{-g}\,d\Omega \tag{9}$$

where

$$\Lambda_{(int)} = -\frac{1}{c^2}\,\psi_{ik}T^{ik} \tag{10}$$

- the principle of consistent iterations;
- the universality of gravitational interaction $\Lambda_{(int)}$;
- the conservation law of the energy-momentum;
- the gauge invariance of the linear field equations;
- the positive localizable energy density and zero trace of the gravity field EMT;
- the quanta of the field energy as the mediators of the gravity force;
- the uncertainty principle and other quantum postulates of the QFT.

Basic equations of the Field Gravity Theory:

1) ***FGT field equations***.

Using the variation principle to obtain the field equations from the action (9) one must assume that the sources T_{ik} of the field are fixed (or the motion of the matter given) and vary only the potentials ψ_{ik} (serving as the coordinates of the system). On the other hand, to find the equations of motion of the matter in the field, one should assume the field to be given and vary the trajectory of the particle (matter). So keeping the total EMT of matter in (10) fixed and varying $\delta\psi_{ik}$ in (9) we get the following field equations (see [8]):

$$-\psi_l^{ik,l} + \psi_l^{il,k} + \psi_l^{kl.i} - \psi^{,ik} - \eta^{ik}\psi^{lm}_{,lm} + \eta^{ik}\psi_l^{,l} = \frac{8\pi G}{c^2}T^{ik} \tag{11}$$

The trace of the field equations (11) gives the scalar equation for generating the scalar part of the symmetric second rank tensor – its trace $\psi(r, t)$, in the form

$$-2\psi_{l}^{,l} + 2\psi_{,lm}^{lm} = \frac{8\pi G}{c^2} T \tag{12}$$

An important conceptual difference between the coordinate's transformation in GRT and the gauge transformation of the gravitational potentials in FGT is that these gauge transformations are performed in a fixed inertial reference frame. The gauge freedom allows one to put four additional conditions on the potentials, in particular a Lorentz invariant gauge – the Hilbert-Lorentz gauge:

$$\psi_{,k}^{ik} = \frac{1}{2}\,\psi^{,i} \tag{13}$$

With the gauge (13) the field equations get the form of wave equation:

$$\left(\nabla - \frac{1}{c^2}\,\frac{\partial^2}{\partial t^2}\right)\psi^{ik} = \frac{8\pi G}{c^2}\left[T^{ik} - \frac{1}{2}\,\eta^{ik}\,T\right] \tag{14}$$

which describes two types of waves: first, the spin-2 traceless irreducible representation $\psi_{\{2\}}^{ik} = \psi^{ik} - (1/4)\,\psi(r, t)\,\eta^{ik}$ and second, the scalar (spin-0) component of the symmetric tensor field, i.e. its trace $\psi(r, t) = \eta^{ik}\,\psi_{ik}$, which is the second irreducible part of the symmetric tensor representation.

2) Equation of motion:

Equation of motion for test particles in the field gravity theory ([8]):

$$A_k^i\,\frac{d(m_0 u^k)}{ds} = -m_0 B_{kl}^i u^k u^l \tag{15}$$

where $m_o u_k = p_k$ is the 4-momentum of the particle, and

$$A_k^i = \left(1 - \frac{1}{c^2}\,\psi_{ln}u^l u^n\right)\eta_k^i - \frac{2}{c^2}\,\psi_{kn}u^n u^i + \frac{2}{c^2}\,\psi_k^i \tag{16}$$

$$B_{kl}^i = \frac{2}{c^2}\,\psi_{k,l}^i - \frac{1}{c^2}\,\psi_{kl}^{,i} - \frac{1}{c^2}\,\psi_{kl,n}u^n u^i \tag{17}$$

Relativistic gravity experiments/observations in FGT:

- Universality of free fall for non-rotating bodies,
- The deflection of light by massive bodies,
- TheGravitational frequency-shift,
- The time delay of light signals,
- The perihelion shift of a planet,
- The Lense-Thirring effect,
- The geodetic precession of a gyroscope,
- The quadrupole spin-2 and monopole spin-0 gravitational radiation

For the strong gravitational field the fundamental prediction is:

- Relativistic Compact Objects without horizon, instead of Black Holes.

In this theory there is no problem with energy of gravitational field. In calculations Oschepkov 1995 [10] it is shown that energy density of static spherically symmetric gravitational field not only is positive for canonical EMT, but also for Gilbert's EMT:

$$T^{00}_{(canon)} = T^{00}_{(Gilbert)} = + \frac{1}{8\pi G}(\nabla\varphi_N)^2 \qquad (18)$$

In the following report "Gravitation theory in multimessenger astronomy II: crucial observational tests based on GW and optical observations" we consider applications of metric and field gravitation theories for interpretations of astrophysical observations.

References

[1] Landau, L.D., Lifshitz, E.M., 1971, The Classical Theory of Fields. (Pergamon, Oxford) (1971)

[2] Misner, C., Thorne, K., Wheeler, J. Gravitation. Freeman, San Francisco (1973)

[3] Straumann N., General Relativity. Springer (2013)

[4] Thirring W. E., An alternative approach to the theory of gravitation. Ann. of Phys. 16, 96 (1961)

[5] Kalman G., Lagrangian formalism in relativistic dynamics. Phys.Rev. 123, 384 (1961)

[6] Feynman R., Morinigo F., Wagner W., Feynman Lectures on Gravitation, Addison-Wesley Publ. Comp. (1995)

[7] Sokolov V.V., Baryshev Yu.V., Field-theoretical approach to gravitation: energy-momentum tensor of the field, Gravitation and Relativity Theory, Kazan State University, vyp.17, 34 (1980)

[8] Baryshev Yu.V., Foundation of relativistic astrophysics: Curvature of Riemannian Space versus Relativistic Quantum Field in Minkowski Space. Arxiv 1702.02020 (2017).

[9] Grischuk, L.P., Petrov, A.N., Popova, A.D., Exact theory of the (Einstein) gravitational field in an arbitrary background space-time, Commun. Math. Phys., 94, 379 (1984)

[10] Oschepkov S.A, Energy of static spherical-symmetrical field in Gravidynamics, Gravitation, Vol. 1, Issue 1, 1995, pp. 36-40. (http://astro.okis.ru/files/1/7/2/172962/04_oshepkov_en.pdf)

Gravitation theory in multimessenger astronomy II: crucial observational tests based on GW and optical observations

Yu.V. Baryshev[1], S.A. Oschepkov[2]

[1]Astronomical Department, Saint Petersburg State University, Saint-Petersburg, Russia;
yubaryshevl@mail.ru

[2]Taurida Academy, V.I. Vernadsky Crimean Federal University, Simferopol, Russia

Abstract Multimessenger astronomy provides crucial observational tests of gravity physics for two alternative theories of gravitation – Einstein's geometrical General Relativity Theory (GRT) and Feynman's non-metric field gravitation theory (FGT), which we considered in the first report. Such tests are able to clarify the key question on the nature of gravitational interaction: is gravity the curvature of space? or is gravity a material field in Minkowski flat space as other physical forces? Up to now all actually performed experiments/observations do not allow to distinguish between these two alternatives in gravity physics, however forthcoming multimessenger astronomy will bring the answer to this fundamental question.

Keywords: relativistic astrophysics, gravitation, observational tests, relativistic compact objects.

1. Introduction

Multimessenger astronomy deals with all four fundamental physical forces – strong, weak, electromagnetic and gravitational interactions. The corresponding messenger particles - cosmic rays, neutrinos, photons and gravitons (gravitational waves), provide crucial information on the most violent phenomena in the Universe. Simultaneous study of these particles may help us answer fundamental questions in high-energy astrophysics, including the nature of massive supernova explosions, gamma-ray busts, active galactic nuclei and relativistic jets. Especially important fact is that the nature of all these phenomena is based on the gravitation theory.

Hence multimessenger astronomy provides crucial observational tests of gravity physics for two alternative theories of gravitation – Einstein's geometrical General Relativity Theory (GRT) and Feynman's non-metric field gravitation theory (FGT). Basic initial principles, field equations and the equations of motions for these alternative theories of gravitation (GRT and FGT) have been given in our first report "Gravitation theory in multimessenger astronomy I: comparison of geometrical and field approaches to the physics of gravitational interaction". In this part we discuss differences in interpretation of some astrophysical observations when one uses GRT or FGT.

2. Crucial observational tests

2.1 Localization of Gravitational Waves which carry positive energy

Recently gravitational-wave signals were detected by using Advanced LIGO and Virgo interferometric antennas (Abbott B. et al. [1], [2]). This means that the positive gravitational field energy carried by gravitational waves, was localized by a GW detector, i.e. free gravitational field energy can be transformed to the kinetic energy of the moving LIGO mirrors. An interpretation of the GW detector length variations as a contracting and stretching the "space-time" without energy taking from gravitational wave is a nonphysical approach.

Though it is possible in the frame of GRT to introduce non-covariant description of GW energy-momentum (Maggiore 2008 [3]), however it leads to some conceptual problems because of giving up the general covariance principle in geometrical description of the gravitational field energy. Indeed, according to Landau & Lifshitz 1971 [4] (§101, p.307): "...it has no meaning to speak of a definite localization of the energy of the gravitational field in space..." and "so that it is meaningless to talk of wether or not there is gravitational energy at a given place". Also according to Misner, Thorne & Wheeler 1973 [5] (§20.4, p.467): "...gravitational energy... is not localizable. The equivalence principle forbids", and (§35.7, p.955): "...the stress-energy carried by gravitational waves cannot be localized inside a wavelength" and "...one can say that a certain amount of stress-energy is contained in a given 'macroscopic' region of several wavelengths' size".

In part I we have described the equations of scalar and tensor gravitational radiation in FGT. The equations corresponds to the radiation of two types – pure tensor gravitons (traceless, spin-2) and scalar gravitons (trace of the tensor potential, spin-0). In the frame of FGT the generation of scalar wave can be calculated by using retarded potentials, which give in the case of the wave zone approximation the following expression:

$$\psi(\boldsymbol{r},t) \approx \frac{2GM_0}{r} - \frac{2GE_k}{rc^2} + \frac{2GM_0}{r\,c}\left(\boldsymbol{n}\cdot\dot{\boldsymbol{R}}\right) + \frac{G}{r\,c^2}\,n_\alpha n_\beta \ddot{I}_{\alpha\beta} + \cdots \,, \tag{1}$$

where $M_0 = \Sigma\, m_a$, $E_k = ½\, \Sigma\, m_a\, v_a^{\,2}$, $\boldsymbol{R} = \Sigma\, m_a\, r_a / \Sigma\, m_a$, $I_{\alpha\beta} = \Sigma\, m_a\, x_a^{\,\alpha}\, x_a^{\,\beta}$.

Taking derivative of (1) over time (at fixed point r) and excluding non-contributing terms, we get following equation for the time derivative of the scalar potential:

$$\dot{\psi}(\boldsymbol{r},t) = -\frac{2\,G\,\dot{E}_k}{r\,c^2} \tag{2}$$

It means that the scalar gravitational radiation is the second order monopole radiation, and there is no first order monopole, dipole and quadrupole scalar radiation. Using the expression (2) for the energy density in the scalar wave, we get

$$T^{00}_{(g)\{0\}} = \frac{G\,\dot{E}_k^2}{8\pi c^6 r^2} \tag{3}$$

The energy flux is $cT^{00}{}_{\{0\}}$, so the additional loss of energy (in 4π steradian) due to the scalar monopole radiation is

$$L_{\{0\}} = \frac{G}{2c^5}\,\dot{E}_k^2 \tag{4}$$

so the scalar gravitational (actually "anti-gravitational") radiation has the same order $1/c^5$ as

the tensor of quadrupole radiation.

The test for correctness of gravitational radiation formulas is a double systems of a pulsars. For a binary system the loss of energy due to the pure tensor gravitational radiation is given by the quadrupole luminosity (which is the same in FGT and GRT)

$$L_{\{2\}FG} = \frac{G}{45c^5} \dddot{D}^2_{ab} \tag{5}$$

where $D_{\alpha\beta}$ is the quadrupole moment of the system. We note that tensor gravitational wave in the frame of FGT is transversal and has localizable positive energy.

For a binary system the quadrupole luminosity is

$$< \dot{E} >_{\{2\}} = \frac{32G^4\, m_1^2 m_2^2\, (m_1+m_2)(1+\frac{73}{24}e^2+\frac{37}{96}e^4)}{5c^5 a^5 (1-e^2)^{7/2}} \tag{6}$$

here m_1, m_2 are masses of the two stars, a is the semimajor axis and e is the eccentricity of the relative orbit.

For a binary star system the orbital additional energy loss via scalar waves (according to Eq.(4)) is

$$< \dot{E} >_{\{0\}} = \frac{G^4\, m_1^2 m_2^2\, (m_1+m_2)(\, e^2+\frac{1}{4}e^4)}{4c^5 a^5 (1-e^2)^{7/2}} \tag{7}$$

Hence the ratio of the scalar to tensor luminosity is

$$\frac{<\dot{E}>_{\{0\}}}{<\dot{E}>_{\{2\}}} = \frac{5}{128} \cdot \frac{(\, e^2+\frac{1}{4}e^4)}{(1+\frac{73}{24}e^2+\frac{37}{96}e^4)} \tag{8}$$

The value of this ratio lies in interval 0 - 1.1% depending on the value of the eccentricity e, and for a circular orbit equals zero. Note that for PSR1913+16 binary pulsar the observer excess of the energy loss is (+0.848 +/-0.041)%, while the FGT prediction for additional scalar radiation is +0.735% (see discussion in [11]).

However, for a spherically-symmetric pulsating body the radiation of the scalar gravitational field becomes dominating because quadrupole radiation is absent.

2.2 Existence of Black Holes event horizon and singularity.

There are several paradoxes related to the concept of black hole horizon, which were emphasized by Einstein 1939 [6]. Einstein wrote in [6] - "Schwarzschild singularity cannot exist in physical reality". The information paradox was recently discussed by Hawking 2014 [7] and the incompatibility of classical and quantum concepts of the BH horizon was considered by Chowdhury & Krauss 2014 [8]. The infinite time formation of the classical BH event horizon (in the distant observer's coordinates) and finite time of BH quantum evaporation means that a BH should evaporate before its formation ([8]). Stephen Hawking claimed in [7] that "There would be no event horizons and no firewalls. The absence of event horizons mean that there are no black holes - in the sense of regimes from which light can't escape to infinity". Though there is no escape from a black hole in classical theory, but in quantum theory, energy and information can escape from a black hole. It means that an explanation of the gravity physics requires a theory that successfully merges gravity with the quantum fields of other fundamental forces of nature.

In FGT there is no black holes, horizons and singularities, and no such limit as the

Oppenheimer-Volkoff mass (review in [11]). This means that compact massive objects in binary star systems and active galactic nuclei are good candidates for testing GRT and FGT theories. According to FGT for a static weak field conditions the positive energy density of the gravitational field around an object with mass *M* and radius *R* is

$$\varepsilon_g = \frac{(\nabla\varphi_N)^2}{8\pi G} = \frac{GM^2}{8\pi r^4} \tag{9}$$

It is positive, localizable, and does not depend on a choice of the coordinate system.

A very general mass-energy argument shows that in FGT there is the limiting radius of any self-gravitating body and there is no singularities. This argument is a precise analogue to that of the classical radius of electron. Indeed, the total mass-energy of the gravitational field existing around a body is given by

$$E_{field} = \int_{R_0}^{\infty} \frac{(\nabla\varphi_N)^2}{8\pi G}\, 4\pi r^2\, dr = \frac{GM^2}{2R_0} \tag{10}$$

This energy should be less than the rest mass-energy of the body, which includes the energy of the gravity field. From this condition it follows that:

$$E_{field} < Mc^2 \quad => \quad R_0 > \frac{G\,M}{2\,c^2} \tag{11}$$

If one takes into account the non-linearity of the gravity field and the internal energy-part inside the object, then the value of the limiting radius further increases, because ”the energy of the field energy” should be added. As the gravitational radius Rg for any massive body in the field gravity we define the radius, where mass-energy of the gravitational field equals to half of its mass-energy measured at infinity, so:

$$R_g = \frac{G\,M}{c^2} = \frac{1}{2}\, R_{Sch} \tag{12}$$

Recent surprising observational fact [13] is that the estimated radius of the inner edge (Rin) of the accretion disk (around black hole candidates has sizes about $(1.2{-}1.4)R_g = (0.6{-}0.7)R_{Sch}$ points to a suggestion, that instead of a Kerr BH rotating with velocity about 0.998*c*, we observe ordinary RCO having radius close to its limiting FGT value R_g (Eq.12).

Also VLBI observations, using submm wavelength Event Horizon Telescope (EHT), have unique angular resolution which will achieve event-horizon-scale structure in the supermassive black hole candidate at the Galactic Centre (SgrA*) and M87. The first results of EHT observations at 1.3mm surprisingly has demonstrated that for the RCO in SgrA* there are no expected for BH the light ring at radius $5.2R_{Sch}$ ([9], [10], [14]). Again this may points to a possibility the existence of limiting FGT RCO having finite gravity force at its surface which does not produce light rings. So in the frame of FGT there is prediction, that forthcoming EHT observations at 0.6 mm will discover a combination of radiation from a central RCO, accretion disc and the origin of relativistic jet from the surface of the RCO (without black hole horizon in the center energy source).

2.3 Relativistic Compact Objects.

Observations of the stellar mass BH candidates surprisingly discovered a preferred value of RCO mass about 7 M_Θ ([15], [16]). Intriguingly in the frame of Quantum Gravidynamics (which is extension of FGT into the strong field regime) a quantum consideration of the

macroscopic limiting high density quark-gluon bag gives self-gravitating configurations with preferred mass 6.7 $M_\odot$ and radius 10 km [16]. So, quantum gravidynamics predicts two peaks in mass distribution of the stellar-mass relativistic compact objects: 1.4$M_\odot$ for neutron stars and 6.7$M_\odot$ for quark stars.

In the weak field regime the post-Newtonian equation of hydrostatic equilibrium of a spherically symmetric body in FGT is:

$$\frac{dp}{dr} = -\frac{G(\rho_0+\delta\rho)M_r^*}{r^2} \tag{13}$$

where

$$\delta\rho = \frac{e+p}{c^2} + 2\rho_0\frac{\Phi}{c^2}\ , \tag{14}$$

and

$$M_r^* = \int_0^r 4\pi r'^2\left(\rho_0 + \frac{e+3p}{c^2} + 2\frac{\rho_0\,\Phi}{c^2} + \frac{(d\Phi/dr)^2}{8\pi G c^2}\right)dr' \tag{15}$$

The most important difference of the Eq.(13) of hydrostatic equilibrium in FGT is that the Tolman-Oppenheimer-Volkoff equation in GRT has the form:

$$\frac{dp}{dr} = -\frac{G\left(\rho+\frac{p}{c^2}\right)(M+4\pi p r^3/c^2)}{r^2\,(1-r_{Sch}/r)} \tag{16}$$

According to the Tolman-Oppenheimer-Volkoff equation the factor $1/(1 - r_{Sch}/r)$ leads to an infinite pressure gradient for $r \to r_{Sch}$. This has a deep consequence: there is an upper limit for the mass of static compact relativistic stars, around 2 - 3 $M_\odot$. According to the standard GR compact objects with larger masses may exist only as black holes.

According to FGT the relativistic gravity corrections lead to a decrease of the gravitating mass (and so gravitational force) relative to its Newtonian value (due to the negative value of the gravitational potential ($\Phi = \psi^{00} < 0$)). According to Eq.(13) a hydrostatic configuration is possible for any large mass. Another important prediction of the FGT is that the supermassive stars (suggested as a possible source of energy in quasars) are stable to small adiabatic pulsations [17]. Whereas the first calculations in FTG on the equation (13) give extreme masses of 5 - 6 $M_\odot$ for EOS FPS and SLy4.

3. Conclusion

Decisive role of optical observations in multimessenger astronomy relates to the very large potential informativity of classical spectral analysis. Especially localization and identification of the GW sources can solve the riddle of the nature of the gravitational interaction.

The crucial astrophysical phenomena for testing Einstein's geometrical General Relativity Theory (GRT) and Feynman's non-metric field gravitation theory (FGT) are ([11],[12],[15],[16]):

- The additional acceleration in translational motion of rotating bodies (according to FGT is~ $\mathbf{V^2_{rot} / c^2}$)should be tested in orbital motion of binary neutron stars;
- The scalar-tensor nature of symmetric tensor potentials $\boldsymbol{\psi^{ik}(r,t)}$, $\boldsymbol{\psi(r,t) = \eta_{ik}\ \psi^{ik}}$

(repulsion by the trace part of the symmetric tensor) will change the structure, masses and sizes of Relativistic Compact Objects (Neutron Stars, Quark Stars and Super Massive RCO having radiuses $\mathbf{r \sim R_g = GM/c^2 = R_{Sch}/2}$) and origin their relativistic jets;

- The emission of gravitational waves of spin 2 and spin 0 during massive supernovae explosion and GRB events, and detection these GWs by means of interferometric antennas (in FGT energy density of gravitational waves: $\mathbf{T_{\{2\}}^{00}}$ and $\mathbf{T_{\{0\}}^{00}}$ is positive and localizable).

References

[1] Abbott B. et al. (LIGO Scientific Collaboration and Virgo Collaboration), Observation of Gravitational Waves from a Binary Black Hole Merger, Phys. Rev. Letters 116 , 061102 (2016)

[2] Abbott B. et al. (LIGO Scientific Collaboration and Virgo Collaboration), GW170817: Observation of Gravitational Waves from a Binary Neutron Star Inspiral, Phys. Rev. Letters 119 , 161101 (2017)

[3] Maggiore M., Gravitational Waves, Oxford Univ. Press (2008)

[4] Landau, L.D., Lifshitz, E.M., 1971, The Classical Theory of Fields (Pergamon, Oxford) (1971)

[5] Misner, C., Thorne, K., Wheeler, J. Gravitation. Freeman, San Francisco (1973)

[6] Einstein, A. On a stationary system with spherical symmetry consisting of many gravitating masses, Ann. of Phys., 40, 922 (1939)

[7] Hawking S., Information Preservation and Weather Forecasting for Black Holes. ArXiv: 1401.5761 (2014)

[8] Chowdhury B. and Krauss L., Hawking Evaporation is Inconsistent with aClassical Event Horizon at r = 2M, ArXiv: 1409.0187 (2014).

[9] Doeleman S. et al., Imaging an Event Horizon: submm-VLBI of a Super Massive Black Hole, Science White Paper submitted to the ASTRO2010 Decadal ReviewPanels, arXiv:0906.3899 (2009)

[10] Falcke H., Markoff S., Toward the event horizon - the supermassive black hole in the Galactic Center, Class. Quant. Grav.,30, iss. 24, id. 244003 (2013) arXiv:1311.1841

[11] Baryshev Yu.V., Foundation of relativistic astrophysics: Curvature of Riemannian Space versus Relativistic Quantum Field in Minkowski Space. ArXiv 1702.02020.

[12] Baryshev Yu.V., Paturel G., Sokolov V.V. Sidereal time analysis as a tool for detection of gravitational and neutrino signals from the core-collapse SN explosions in the inhomogeneous Local Universe, Proceedings of the International Workshop on Quark Phase Transition in Compact Objects and Multimessenger Astronomy: Neutrino Signals, Supernovae and Gamma-Ray Bursts, KChR, Nizhnij Arkhyz (SAO), KBR, Terskol (BNO), pp 23 - 34 (2016).

[13] Wilkins D. and Gallo L. Driving extreme variability: The evolving corona and evidence for jet launching in Markarian 335, MNRAS, 454, 4440 (2015).

[14] Doeleman S. et al., Event-horizon-scale structure in the supermassive black hole candidate at the Galactic Centre, Nature, 455, 78 (2008) arXiv:0809.2442

[15] Sokolov V.V., The gamma-ray bursts and core-collapse supernovae – global star forming rate peaks at large redshifts, in Proceedings of the XXIX International Workshop on High Energy Physics: New Results and Actual Problems in Particle & Astroparticle Physics and Cosmology (HEPFT2013), 26-28 June 2013, Protvino, Moscow region, Russia, (2014)

[16] Sokolov V.V., On the Observed Mass Distribution of Compact Stellar Remnants in Close Binary Systems and Localizability of Gravitational Energy, International Journal of Astronomy, Astrophysics and Space Science 2(6): 51-58 (2015).

[17] Oschepkov S.A. & Raikov A.A. Post-Newtonian politrops in alternative gravitation theories, Gravitation, v.1, N.1, (1995) (http://astro.okis.ru/files/1/7/2/172962/05_oshepkov_raikov_en.pdf)

High time resolution multi-band photo-polarimetric observations of the binary millisecond redback pulsar J1023+0038 with the BTA

G.M. Beskin[1,2], S.V. Karpov[1,2], V.L. Plokhotnichenko[2], Yu.A. Shibanov[3,4], D.A. Zyuzin[3], A.F. Kholtygin[5], V.V. Sokolov[2], Yu.V. Baryshev[5]

[1]Special Astrophysical Observatory, Nizhnij Arkhyz, Karachaevo-Cherkessia, 369167, Russia

[2]Kazan Federal University, 16a Kremlyovskaya St., Kazan 420008, Russia

[3]Ioffe Institute, Politekhnicheskaya 26, St.-Petersburg, 194021, Russia

[4]Peter the Great Saint Petersburg Polytechnic University, Politekhnicheskaya 29, St.-Petersburg, 195251, Russia

[5]Saint-Petersburg State University, Universitetskij pr. 2 8, St.-Petersburg, 198504, Russia

Abstract We briefly report first results of high time resolution optical multiband panoramic photo-polarimetric observations of the eclipsing binary millisecond redback pulsar J1023+0038 obtained in February 2017 with the 6 m BTA telescope. Our data show that the pulsar still remained in the low-mass X-ray binary stage, which is characterised by rapid flaring at time scales of 10-100 s with amplitudes of 0.2-0.5 mag. We resolved a fine structure of the flares at time scales of 0.1–10 s. The polarimetry at the time scale of 12 s shows no variable polarization with an upper limit of 2-4% for the linear polarization degree in the flaring and quiet stages. We shortly outline implications of the results.

Keywords: Pulsars: Individual: Psr J1023+0038 — Techniques: Photometric — Techniques: Polarimetric — Accretion

1. Introduction

Rotation powered millisecond pulsars (RMSPs) were discovered in the radio about 35 yr ago, the first one was PSR B1937+21 [1]. Two independent groups immediately suggested that RMSPs were spun-up (”recycled”) by accretion in close binary systems [2, 3]. The mechanism was proposed early [4]. A long time this idea was only supported by the fact that most RMSPs are in binary systems with ordinary stellar companion. The discovery of 401 Hz X-ray coherent pulsations from the accretion powered neutron star (NS) in low mass X-ray binary (LMXB) SAX J1808.4-3658 [5] was the first direct evidence of the accretion spin-up.

Compact RMSPs binaries with binary period Pb $\leq$ 1 day show two distinct sub-classes: “black widows” (BWs; [6]) with sub-stellar companion masses M $\leq 0.1 M_\odot$ and “redbacks” with M $\geq 0.1 M_\odot$ bloated companions close to filling their Roche lobes [7]. The LMXB - RMSP connection was finally firmly established by three recently discovered redbacks: PSR

J1023+0038 [8], XSS J12270-4859 [9, 10], and PSR J1824-2452I [11]. They directly demonstrated transformation from the accretion to the rotation powered MSP stages.

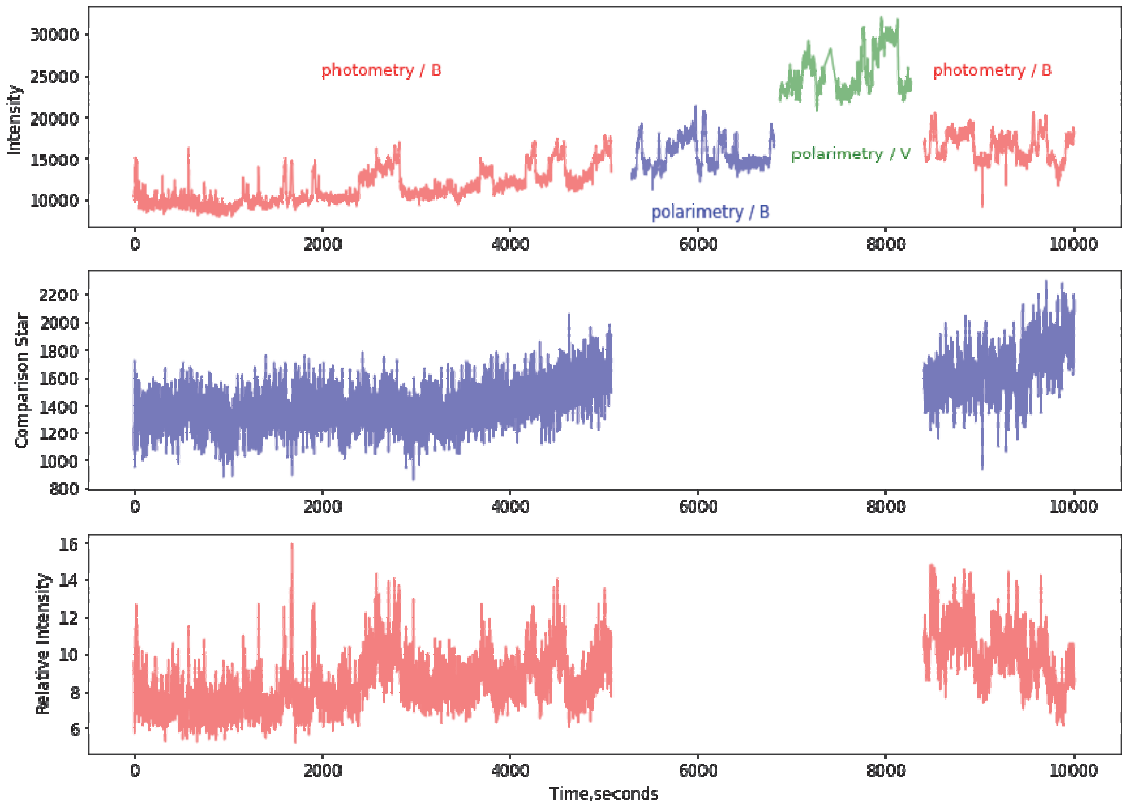

Fig1. *Total light curves in counts vs time in seconds from the start of observations of J1023+0038 (top) and the comparison star (middle) in the B band and their ratio (bottom). The data are binned to the bin size of 1.2 s.*

Among these three, PSR J1023+0038 is a most studied and intriguing object. It has shown the LMXB to radio RMSP transition in 2003 [8] and then suddenly returned back to a low luminosity accretion stage in 2013 [12]. This demonstrates that the transition itself is a complicated multistage process challenging additional studies. J1023+0038 is an eclipsing binary 1.64 ms pulsar with the 4.754 h orbital period and the ~0.2$M_{\odot}$ non-degenerate G-class secondary star. The parallax based distance is 1.37 kpc [13]. Owing to its puzzling behaviour, this object is monitored in different spectral domains from the radio to γ-rays. Its redback nature follows from the modulation of the optical flux and colour with Pb: the pulsar heats the companion's face [14]. The X-ray flux is also modulated with Pb, which is interpreted as the presence of an intro-binary shock. The latter supported by gamma-ray observations [15]. After the transition to the LMBX stage, sporadic switchings between high and low luminosity modes are observed in X-rays on time scales form minutes to hours accompanied by occasional bright flares. Coherent X-ray pulsations with the pulsar period are detected in the high mode, likely due to channeled accretion onto magnetic poles of the NS [16]. It is unusual as compared to typical AMXPs as the implied accretion rate appears to be too low that the accreted matter could overcome the centrifugal barrier of the pulsar. It is also intriguing, that measured spin-down rates in LMBX and RMSP stages is almost the same [17] suggesting that the pulsar wind continues to operate. This is supported by radio brightening detections within the low X-ray mode intervals [18].

In the optical, J1023+0038 is a relatively bright, V ≈ 16.7, and low reddened, E(B − V) ≈ 0.07, object. First optical high-time resolution observations with the ULTRACAM in the accretion stage also showed occasional flares and deeps at a 0.1-1 magnitude level and time scales from 20 s to 10 min [14]. Implied spatial scales of the regions responsible for bright flares can be as small as $0.3R_{\odot}$, which is comparable with accretion disk size. However, many flares and deep fronts are not resolved due to a limited time resolution of about 0.3 s. Higher time resolution observations would be useful to study the variability nature.

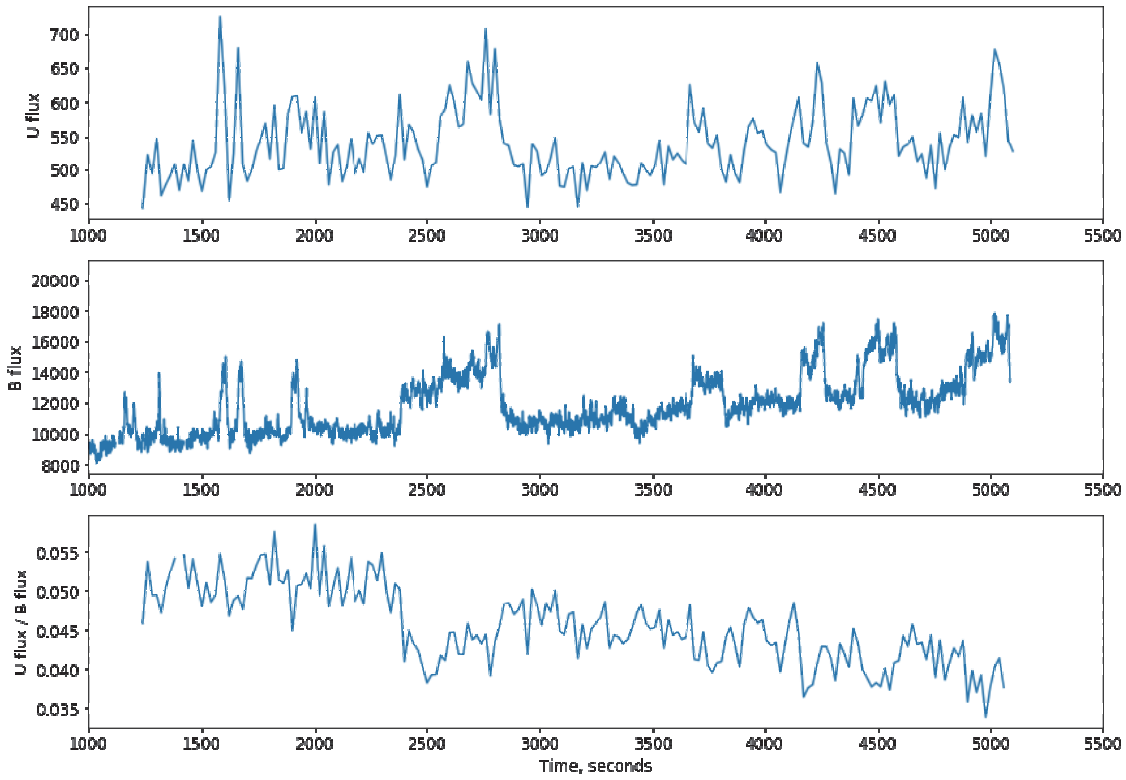

Fig2. *Comparison of the U (top) and B (middle) band light curves fragments at bin sizes of 20 and 1.2 s, respectively. Their ratio is shown in the bottom panel.*

2. Observations

PSR J1023+0038 was observed in February 17, 2017 during 3.5 h with the Russian 6-m BTA telescope using the Multicolor Panoramic Photo-Polarimeter (MPPP) [19], which is a part of the MANIA experiment [23]. Conditions were clean and seeing was about 1.7″. The MPPP allows to register photons from the target in four photometric bands and/or to obtain three Stocks parameters simultaneously. Photons can be registered by two detectors: the microchannel plate based position sensitive photon counter (PSD) [24] with multi-alcali photocathode, equipped with the Quantochron 4-48 data acquisition system [25] providing the time resolution up to 100 ns; the low readout noise PhotonMax 512B EMCCD from Princeton Instruments with the resolution up to 1 ms. In our photometric observations we employed both simultaneously in a

"wide-field" regime where the area of 40″ with the target and a comparison star was observed using the EMCCD in the B band with 0.12 s exposures, and using PSD in U band with 1 μs resolution. Also, a part of time, the polarimetric regime was used when only the target in a square 10″ x 10″ diaphragm was observed in four polarization orientations simultaneously with EMCCD. The latter regime of MPPP is analogous to the one used in [20, 21]. The summary of the observations is listed in ***Table1.***

Table1. *Summary of observations of PSR J1023+0038 on t**he** Russian 6-m BTA telescope*

Start time, UT	**End time, UT**	**Duration, seconds**	**Detector**	**Filter**	**Regime**
2017-02-17 18:49:25	2017-02-17 20:14:10	5085	EMCCD	B	photometry
2017-02-17 19:10:06	2017-02-17 20:14:56	3890	PSD	U	photometry
2017-02-17 20:17:33	2017-02-17 20:43:02	1529	EMCCD	B	polarimetry
2017-02-17 20:44:00	2017-02-17 21:07:06	1386	EMCCD	V	polarimetry
2017-02-17 21:09:31	2017-02-17 21:36:07	1596	EMCCD	B	photometry

3. Results

In ***Fig1***. the total background subtracted light curve of J1023+0038 in the B band binned to 1.2 s resolution is shown. The data for the stable comparison star and the ratio of the target to this star intensities are presented as well to demonstrate the stability of the instrument performance. The gap in the data correspond to the interval of the polarimetric observations where no comparison star data are available. Several bright flares of different duration are seen in the light curve when the emission intensity sharply increases by a factor of 1.5. Some of them are unresolved at the selected time binning. Unfortunately, in the U band, where we had much higher time resolution, J1023+0038 is much fainter while detector quantum efficiency is lower, and the light curve at the same resolution is much noisier. Nevertheless, main features seen in B are resolved in U, particularly when we use large binning (see ***Fig*2.). The ratio of U/B shows that during bright episodes J1023+0038 becomes redder, which is consistent with results by Shahbaz et al. [14].

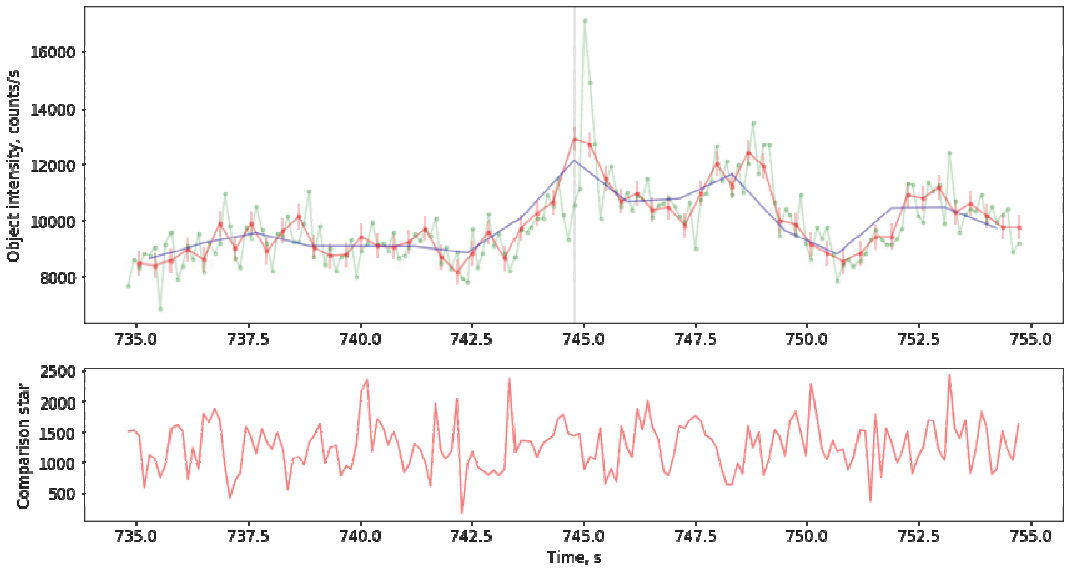

Fig3. *Fragment of the B band light curve with a sharp flare. Green, red and blue lines correspond to the native resolution of 0.12 s and binning with 0.4 and 10 s, respectively. The flare disappears with time resolution decrease.*

We resolved, for the first time, very sharp bright flares with durations and rising **times** down to about 0.4 and 0.2 s, respectively. An example is shown in ***Fig3.*** where we demonstrate also that such flares can hardly be detected at a factor of two-three lower resolution. In some episodes of the observations we see signatures of a periodic flux modulation. Using the Lomb-Scargle periodogram method we found a significant periodicity with the period of 7.6 s and the duration of about 100 seconds in the initial part of the B-band light curve (***Fig4.***). No events of similar significance are seen later.

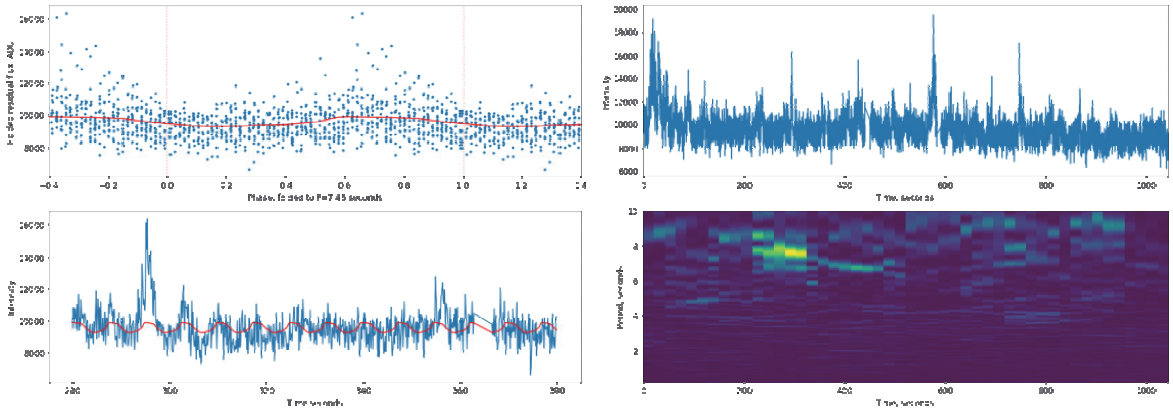

Fig4. *Left: initial part of the B band light curve (top) and running Lomb-Scargle periodogram of this curve (bottom) computed using the 100 s window. The peak near t ~300 s at the periodogram has a significance better than 10^{-6} and probably displays a frequency drift. The best fit period P=7.6 s is derived using phase-dispersion minimization (PDM) method. Right: the folded (top) and un-folded (bottom) light curve around the peak. The red line corresponds to the curve derived by smoothing the folded light curve.*

The overall light curve (***Fig1.***) seems to demonstrate a transition from a nearly constant and relative low initial (until about 2000 s) intensity level with very short bright spikes towards a stage where sharp sporadic switchings between the low and a bright intensity intervals of

several minutes durations are observed. The latter is reminiscent of the low/high luminosity mode transitions observed in X-rays [18]. This effect definitely needs additional observations in order to properly describe and characterize it.

The Stokes parameters derived at a 12 seconds resolution scale during polarimetric observations are presented in ***Fig5***. We find no obvious correlation of the polarization with the intensity variations on the level greater than 2-4% on time scales larger than 12 seconds. Shorter flashes also do not display any polarization greater than 10%.

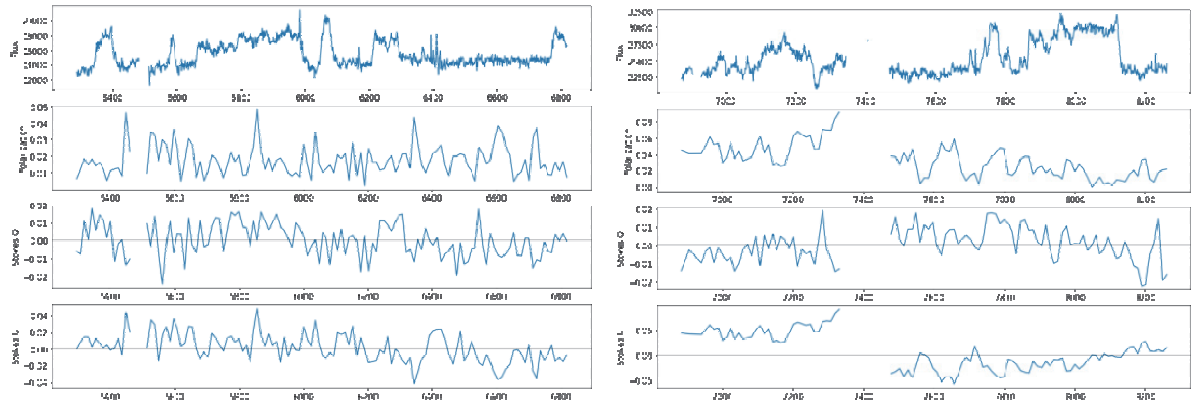

Fig5. *From top to bottom: the time variation of the B (left panel) or V (right panel) band flux intensity, the polarization degree, and Stokes parameters Q and U. The time bin is 12 s. Long-term trends in Stokes parameters are due to not fully corrected instrumental polarization depending on the object position on detector. There is no evident correlation of the polarization with large flares in the intensity.*

4. Discussion and Conclusions

The temporal resolution of our observations is by a factor of three better as compared with previous observations [14]. This allowed us to resolve, for the first time, the bright flares in the optical emission of J1023+0038 with the durations down to hundred milliseconds. This is in remarkable agreement with predictions of accretion models by Romanova et al. [22] constructed for different propeller regimes. The models suggest a characteristic variability scale in a range of 50–100 ms for the parameters of the J1023+0038 system. Thus, J1023+0038 is likely to be in an unstable propeller regime. We plan to continue observations increasing the time resolution to find the lowest variability scale and to perform detailed comparison with models. Coordinated optical-X-ray-radio high time resolution observations would be very useful to better understand the nature of processes in this remarkable object.

Acknowledgements

The work is performed according to the Russian Government Program of Competitive Growth of Kazan Federal University. Development of hardware for high temporal resolution observations on BTA and data analysis are supported by the Russian Science Foundation grant No. 14-50- 00043 and by RFBR project No. 17-52-45048.

References

[1] Backer D C, Kulkarni S R, Heiles C, Davis M M and Goss W M 1982 Nature 300 615–618

[2] Alpar M A, Cheng A F, Ruderman M A and Shaham J 1982 Nature 300 728–730

[3] Radhakrishnan V and Srinivasan G 1982 Current Science 51 1096–1099

[4] Bisnovatyi-Kogan G S and Komberg B V 1974 SvA 18 217

[5] Wijnands R and van der Klis M 1998 Nature 394 344–346

[6] Fruchter A S, Gunn J E, Lauer T R and Dressler A 1988 Nature 334 686–689

[7] Roberts M S E 2013 Neutron Stars and Pulsars: Challenges and Opportunities after 80 years (IAU Symposiumvol 291) ed van Leeuwen J pp 127–132 (Preprint 1210.6903)

[8] Archibald A M, Stairs I H, Ransom S M, Kaspi V M, Kondratiev V I, Lorimer D R, McLaughlin M A, Boyles J, Hessels J W T, Lynch R, van Leeuwen J, Roberts M S E, Jenet F, Champion D J, Rosen R, Barlow B N, Dunlap B H and Remillard R A 2009 Science 324 1411 (Preprint 0905.3397)

[9] Bassa C G, Patruno A, Hessels J W T, Keane E F, Monard B, Mahony E K, Bogdanov S, Corbel S, Edwards P G, Archibald A M, Janssen G H, Stappers B W and Tendulkar S 2014 MNRAS 441 1825–1830 (Preprint1402.0765)

[10] Roy J, Ray P S, Bhattacharyya B, Stappers B, Chengalur J N, Deneva J, Camilo F, Johnson T J, Wolff M, Hessels J W T, Bassa C G, Keane E F, Ferrara E C, Harding A K and Wood K S 2015 ApJ 800 L12(Preprint 1412.4735)

[11] Papitto A, Ferrigno C, Bozzo E, Rea N, Pavan L, Burderi L, Burgay M, Campana S, di Salvo T, Falanga M, Filipovi´c M D, Freire P C C, Hessels J W T, Possenti A, Ransom S M, Riggio A, Romano P, Sarkissian J M, Stairs I H, Stella L, Torres D F, Wieringa M H and Wong G F 2013 Nature 501 517–520 (Preprint 1305.3884)

[12] Halpern J P, Gaidos E, Sheffield A, Price-Whelan A M and Bogdanov S 2013 The Astronomer's Telegram 5514

[13] Deller A T, Archibald A M, Brisken W F, Chatterjee S, Janssen G H, Kaspi V M, Lorimer D, Lyne A G, McLaughlin M A, Ransom S, Stairs I H and Stappers B 2012 ApJ 756 L25 (Preprint 1207.5670)

[14] Shahbaz T, Linares M, Nevado S P, Rodr´ıguez-Gil P, Casares J, Dhillon V S, Marsh T R, Littlefair S, Leckngam A and Poshyachinda S 2015 MNRAS 453 3461–3473 (Preprint 1507.07473)

[15] Takata J., Li K. L. ,Leung G.C.K., Kong A. K. H., Tam P. H. T., Hui C. Y., Wu E.M.H., Xing Y., Cao Y., Tang S., Wang Z. and Cheng K. S. 2014 ApJ 785 131 (Preprint 1312.0605)

[16] Archibald A M, Bogdanov S, Patruno A, Hessels J W T, Deller A T, Bassa C, Janssen G H, Kaspi V M, Lyne A G, Stappers B W, Tendulkar S P, D'Angelo C R and Wijnands R 2015 ApJ 807 62 (Preprint 1412.1306)

[17] Jaodand A, Archibald A M, Hessels J W T, Bogdanov S, D'Angelo C R, Patruno A, Bassa C and Deller A T2016 ApJ 830 122 (Preprint 1610.01625)

[18] Bogdanov S, Deller A T, Miller-Jones J C A, Archibald A M, Hessels J W T, Jaodand A, Patruno A, BassaC and D'Angelo C 2017 ArXiv e-prints (Preprint 1709.08574)

[19] Plokhotnichenko V L, Beskin G M, de Bur V G, Karpov S V, Bad'in D A, Lyubetskaya Z V, Lyubetskij A Pand Pavlova V V 2009 Astrophysical Bulletin 64 308–316

[20] Beskin G, Karpov S, Plokhotnichenko V, Stepanov A and Tsap Y 2017 Stars: From Collapse to Collapse (Astronomical Society of the Pacific Conference Series vol 510) ed Balega Y Y, Kudryavtsev D O,Romanyuk I I and Yakunin I A p 303

[21] Beskin G, Karpov S, Plokhotnichenko V, Stepanov A and Tsap Y 2017 PASA 34 e010 (Preprint 1702.06660)

[22] Romanova M M, Blinova A A, Ustyugova G V, Koldoba A V and Lovelace R V E 2017 ArXiv e-prints(Preprint 1704.08336)

[23] Shvartsman, V. F. 1977, Soobshch. Spets. Astrofiz. Obs., Vyp. 19, p. 5 – 38

[24] Debur, V. et al., 2003, Nuclear Instruments and Methods in Physics Research Section A, Volume 513, Issue 1-2, p. 127-131

[25] Plokhotnichenko, V., Solin, V. and Tikhonov, A. 2009, Astrophysical Bulletin, v.64 issue 2, pp 198–206

New vision of problem of Geoneutrinos and Earth heat fluxes

L. B. Bezrukov[1], A.S. Kurlovich[1], B. K. Lubsandorzhiev[1], A. K. Mezhokh[1], V.P. Morgalyuk[2], V. V. Sinev[1],*, and V. P. Zavarzina[1]

[1] Institute for Nuclear Researches of Russian Academy of Sciences, Prospekt 60-letia Oktyabrya 7a, 115409 Moscow, Russia, vsinev@inr.ac.ru

[2] A. N. Nesmeyanov Institute of Organoelement Compounds of Russian Academy of Sciences, Vavilova 10, 115409 Moscow, Russia

Abstract The Hydride Earth model predictions of geoneutrino flux and intrinsic Earth heat flux are discussed. The geoneutrino flux predicted by the model can be adjusted to the experimental one. The predicted intrinsic Earth heat flux is significantly larger than model dependent experimental value obtained under assumption that the main heat transfer mechanism is a thermal conductivity. We introduce an additional mechanism of heat transfer in the Earth's crust, namely the energy transfer by hot gases produced in the Earth crust at great depths. The experimental data supporting this idea, in particular the temperature profiles measured in the Kola super deep borehole, are discussed.

Keywords: Earth heat flux, geoneutrinos

1. Introduction

So far there are only two detectors, Borexino [1] and KamLAND [2], which reported registration of geoneutrino signals. Geoneutrinos are electron antineutrinos produced in beta-decays of radioactive elements in natural families of ^{238}U, ^{232}Th and ^{40}K, accumulated inside the Earth. Geoneutrino flux on the Earth surface depends on the amounts of ^{238}U, ^{232}Th and ^{40}K in the Earth and their distribution with the depth.

Amounts of ^{238}U, ^{232}Th and ^{40}K in the Earth and their distribution are different in existing models of the Earth. The theory most popular at the moment is called the Bulk Silicate Earth (BSE) [3, 4]. Its main idea is that element abundances are the same as in meteorites. Based on this idea the amounts of ^{238}U, ^{232}Th and ^{40}K were obtained for the Earth:

$$M_{BSE}(U) = 0{,}81\cdot10^{17} \text{ kg}, M_{BSE}(Th) = 3{,}16\cdot10^{17} \text{ kg and } M_{BSE}(^{40}K) = 5{,}73\cdot10^{16} \text{ kg}. \quad (1)$$

These masses are distributed mainly in the Earth crust and partially in its mantle, but they are absent in its core. Experimentally observed antineutrino flux is in agreement with ^{238}U and ^{232}Th amounts from (1) under the assumption that they are distributed in the crust and in the upper mantle [1] only.

Each radioactive decay accompanied by a definite thermal energy emission. If we know the total amounts of ^{238}U, ^{232}Th and ^{40}K in the Earth, the value of radiogenic heat flux can be predicted and it can be compared with experimentally measured one.

The Earth thermal flux on continents in boreholes is explored by the measurement of the temperature gradient at depths of ~500 meters. The thermal flux in oceans is measured by dedicated apparatus which penetrates to the bottom floor by several meters and measures the temperature gradient. To calculate the value of thermal flux one uses the idea that the main thermo-transfer mechanism is a thermal conductivity. Presently the value obtained from

experimental measurements assuming the foregoing point of view is 47±2 TW.

The calculated inner Earth thermal flux appears to be equal to 17.5 TW. In this calculation the total masses of ^{238}U, ^{232}Th and ^{40}K in the Earth were taken from (1). Comparison of this value with experimental one did not confirm correctness of the BSE basic assumptions. Researches started to look for additional heat sources.

In this paper we will use an alternative Earth model, so called the Hydride Earth model (HE) [5], and discuss how predictions of geoneutrino and thermal fluxes are correspond to the observed data.

2. Hydride Earth model and geoneutrinos

The main idea of the HE model is the following: a planet element composition depends on the distance from the Sun. That is why the Earth's element composition should differ from composition of asteroids in the asteroid belt which is the source of meteorites. Vladimir Larin [5] proposed and used for element composition calculations the following equation:

$$(X_M/X_{Si})_{Earth} = (X_M/X_{Si})_{Sun} \cdot F(E_{IP}(M)), \quad (2)$$

where X_M – the share of element M in the Earth mass, X_{Si} – the share of Silicon in the Earth mass, $F(E_{IP}(M))$ – the mass share of chemical element M from the mass of this element in the Sun that existed at the Earth's orbit at its formation, $E_{IP}(M)$ – the ionization potential of element M.

In [6] the function F was proposed as an exponential one [6]:

$$F(E_{IP}(M)) = A \cdot \exp\{- B \cdot E_{IP}(M)\}, \quad (3)$$

where coefficients A and B were chosen from the known element composition of the Sun and Earth's crust.

We can estimate the total masses of ^{238}U, ^{232}Th and ^{40}K in the Earth using a method of calculation proposed in [7] and quoting the value of $E_{IP}(M)$ and function $F(E_{IP}(M))$ from [8] and [6] respectively:

$$M_{HE1}(U) = 3{,}18 \cdot 10^{17}\ \text{kg},\ M_{HE1}(Th) = 1{,}0 \cdot 10^{18}\ \text{kg and}\ M_{HE1}(^{40}K) = 2{,}6 \cdot 10^{19}\ \text{kg} \quad (4)$$

It is noteworthy that the use of function $F(E_{IP}(M))$ as in [6] results in the values of ^{238}U and ^{232}Th masses roughly three times less than in (4) - $M_{HE}(U) = 1{,}1 \cdot 10^{17}$ kg, $M_{HE}(Th) = 3{,}6 \cdot 10^{17}$ kg.

As it is shown above, predictions of the HE model depends strongly on the $F(E_{IP}(M))$ function, which is known in its turn rather crudely. It is of fundamental importance that the HE model leaves room for larger values of the total masses of ^{238}U, ^{232}Th and ^{40}K in the Earth as well as allows considering ^{238}U, ^{232}Th and ^{40}K present in the Earth core in the primordial amount, i.e. at the moment of the Earth formation. In particular the total mass of potassium is much more than predicted by the BSE model because of its small ionization potential.

In our previous paper [9] an attempt was done to estimate the maximal values of ^{238}U, ^{232}Th and ^{40}K masses in the Earth which are allowed by the modern experimental data on geoneutrino fluxes and the Earth thermal flux. Our analysis provided the following results:

$$M_{HE2}(U) = 1{,}7 \cdot 10^{17}\ \text{kg},\ M_{HE2}(Th) = 6{,}7 \cdot 10^{17}\ \text{kg and}\ M_{HE2}(^{40}K) = 1{,}2 \cdot 10^{19}\ \text{kg}. \quad (5)$$

In the estimates we expanded potassium abundance known for the Earth's crust to the Earth whole volume.

Comparing estimates made by the HE and BSE models, (5) and (1) respectively, one can

conclude that they are rather close, although the HE values are slightly larger.

Taking into account that the HE model predicts the total masses of ^{238}U, ^{232}Th and ^{40}K in the Earth's core in primordial abundances experimental arrays for ^{238}U and ^{232}Th geoneutrino flux detection should have substantially larger events statistics in comparison with the present arrays in order to have capabilities to distinguish those two models.

The total mass of ^{40}K predicted by the HE model is more than two orders of magnitude larger than the mass predicted by BSE model. In [10] the capability to detect the large geoneutrino flux due to ^{40}K flux by modern detectors was analyzed. The conclusion is done that sensitivity of presently operating detectors is not sufficient for such a purpose. But for next generation detectors with significantly lower background and larger target possibility to measure geoneutrino flux due to ^{40}K should be conspicuously high. It is also important to have independent measurements of CNO cycle neutrinos spectrum, which is rather close to the spectrum shape of ^{40}K neutrinos.

3. Hydride Earth model and thermal flux of the Earth

One can calculate steady thermal flux of the inner Earth heat knowing the value of the heat energy released per radioactive decay. Thermal flux corresponding to the foregoing mass values of ^{238}U, ^{232}Th and ^{40}K in case of the HE model (5) turns out to be 304 TW. This huge amount of heat is the consequence of the larger amount of potassium in the Earth predicted by the HE model.

At first glance, comparison of the HE value with the experimentally measured one of 47 TW leads to the idea that the HE model is wrong. Indeed, the large amount of potassium follows from the basic HE postulates claiming that ionization potential determines a share of chemical element mass which existed in a planet's orbit at the moment of its formation. If to assume that the HE model is correct than it is necessary to bring forward arguments allowing understanding of so large difference between values of thermal fluxes predicted by the HE model and measured experimentally in boreholes by the temperature gradient method.

Furthermore let's consider here the experimental data of the Earth thermal flux different from the value in 47 TW.

The results of the temperature profile measured in super deep boreholes are rather easy to understand in the framework of the HE model. But, on contrary, the results were not predicted by the BSE model at all.

Scientific results of the Cola super deep borehole were published in [11]. The depth of 12 262 meters was achieved there. In fact all ideas of the Earth's core structure obtained from the measurements in the borehole were inconsistent with expectations. With the deepening the rocks do not get denser and their porosity does not decrease as it was expected earlier. On the contrary, the rocks at the multi-kilometer depth are penetrated by multiple pores and broken by cracks.

It was a sensation that there existed hydrogen and hydrogen-containing gases, in particular water, at high depth where the pressure reaches hundreds of atmospheres.

Finally, it appeared that the Earth is significantly hotter than it was assumed earlier. At the depth of 5 km the temperature exceeds 70°C and passes 120°C and 220°C at 7 km and 12 km depths respectively. The latter is 100°C more than the temperature extrapolated from the value measured at 1 km depth.

The HE model predicts element composition of the primordial Earth. Hydrogen should constitute about 18% of mass and it could be accumulated in the hydride form. Radiogenic heating of the Earth's core results in the production of free hydrogen at the border between the core and mantle. The HE model predicts existence of degasification processes from the Earth's surface, basically by hydrogen containing gases, e.g. water vapor. Gases should be produced at

high depth where appropriate temperatures could exist. The gases provide production of multiple cracks and pores in rocks at high depth.

These gases could be the main carrier of thermal energy. Cracks and pores allow gases to move up to the surface. The heat could bypass the thermometers measuring the temperature gradient at the depths of about 500 meters or at the ocean bottom by two ways. The first one is absorption of thermal energy during gas production process. Thermal energy is transferred to the internal energy of gas molecules which is released later by exothermic decomposition reactions at small depths. The second one is transfer of thermal energy to the Earth surface by narrow jets of hot gases. These jets should have substantial distances between them. Existence of such vertical jets leads at large depths to the emergence of horizontal component of gas velocity. Therefore, only a fraction of heat at the depths of about 500 meters takes part in the process of vertical heat transfer by thermo-conductivity mode. The most part of heat energy is carried out by hot gases. We note that boreholes do not drilled at outlets of gas jets because on continental platforms gas outlets look like lakes or swamps. Volcanoes are gas outlets too.

The existence of the forgoing heat transfer mechanism, additional to thermo-conductivity, allows an understanding of unexpected high temperatures at large depths. It also helps to resolve contradiction between the large heat flux predicted by the HE model and results of temperature gradient measurements.

The ARGO experiment published recently interesting results showing temperature increasing of the world ocean in 2005–2010 [12]. Despite that period has been the period of the minimum of solar activity, the world ocean has been warming up. To provide such heating there is a need to have additional energy flux of 0.58 ± 0.15 W·m^{-2} for 6 years. If to multiply this value by the Earth surface area we will get the Earth thermal flux of 300 ± 80 TW.

In the context of the HE model, this experimental fact could be explained by an increase of gases outcome into the ocean and existence of exothermic reactions with gases in the ocean volume. The model includes an idea that the gas flux is not stable but cyclic. We can consider the present ocean heating is observed due to an increase of the Earth's internal heat flux during of the Earth's exit from the small ice age. The value of the heat flux necessary for the observed ocean heating does not cause surprise in frame of the HE model.

It is noteworthy to mention studies done at the Lebedev Physical Institute of the Russian Academy of Sciences (LPI) [13]. In that study the Moon thermal flux was measured by detection of radio wave emission from the Moon. The authors of the paper consider that the heat flux comes from deep interior of the Moon and has the same radiogenic nature as on the Earth. Basing on the idea that the Moon and Earth have the same element composition we can calculate the Earth heat flux using some scaling factor:

$$H_{\text{earth}} = H_{\text{moon}} \cdot M_{\text{earth}} / M_{\text{moon}} = 170 \text{ TW}. \quad (6)$$

Where: H_{moon} – the measured heat flux at the Moon, M_{earth} and M_{moon} – the Earth and Moon masses respectively. It is necessary to note that on the Moon, according to the HE model, degasification process finished because of its small size and practically all radiogenic energy comes out of the Moon by thermo-conductivity way. The heat flux value calculated using (6) supports the correctness of the HE model. It is important to note that the Moon thermal flux measurements by the radio wave emission method average the Moon thermal flux on the visible Moon surface and gives us the mean value.

In two different points on the Moon surface measurements of thermal flux were done by drilling boreholes during Apollo 15 and Apollo 17 missions. Basing on the Apollos data and using equation (6) it is possible to recalculate the Earth thermal flux. The resulting values are 43 and 65 TW. It is believed that these data do not contradict to LPI measurements because in that Apollo missions landing places the thermal fluxes should be significantly less than the mean

value. It is supported by the Moon pictures made by the infrared telescope installed on board of the NASA satellite Lunar Reconnaissance Orbiter in 1996 during the full lunar eclipse.

Finally, let's estimate the upper limit of the Earth thermal flux. There are certain places on the Moon surface which are never illuminated by the Sun. The places have always constant temperature. We can assume that only radiogenic internal heat determines their temperature. So, the energy flux emitted by the Moon surface unit can be estimated according to the Stephan-Boltzmann law. Then it is possible to calculate the total thermal flux of the Moon. The Earth thermal flux recalculated using (6) is 420 TW. The value is obtained taking into account the temperature of 40°K in places never illuminated by the Sun at the Moon's South Pole region. The value of 420 TW for the Earth thermal flux can be regarded as an upper limit. This upper limit shows that the ^{238}U, ^{232}Th and ^{40}K masses in the Earth presented in (4) are too large. Whereas the masses shown in (5) result in the Earth thermal flux of 304 TW. The last value is smaller than the upper limit.

4. Conclusion

1. The HE model is a convenient tool for analysis of events taking place on the Earth. We demonstrated in the framework of the HE model that many complicated phenomena could find explanations in a natural way basing on just one model. Those are the geoneutrino fluxes, temperature profiles of super deep boreholes and experimentally observed increase of the ocean temperature.

2. It was shown that the HE model introduces the large concentrations of ^{238}U, ^{232}Th and ^{40}K in the Earth and allows their existence in the Earth core in primordial amount with correction for the elements decay. The most prominent amount appeared to be for potassium in comparison with the Bulk Silicate Earth model prediction due to its small ionization potential.

3. An assumption was done that the modern value of the Earth thermal flux resulting from the temperature gradient measurements does not take into account significant amount of heat transferred by hot gases. The Hydride Earth model predicts production of gases at high depths. The existence of this kind of heat transfer mechanism, additional to thermal conductivity, allows understanding of high temperature existing at big depths in deep boreholes on continents and in oceans.

Acknowledgments

Authors are grateful to the organization committee of The International Conference SN 1987A, Quark Phase Transition in Compact Objects and Multimessenger Astronomy (held at 2-8 July of 2017, KBR, Terskol (BNO INR); KChR, Nizhnij Arkhyz (SAO)) for their kind invitation to present the talk. Also authors thank Igor Tkachev (INR RAS) for fruitful discussion, Allen Caldwell (MPI) for the opportunity to talk at MPI seminar and valuable discussion, Leo Stodolsky (MPI) for inspiring discussion, and in particular for his question on temperature profiles in continental platforms at existence of thermal energy transfer by hot gases.

5. References

[1] *Agostini M. et al. (Borexino Collab.)* Spectroscopy of geoneutrinos from 2056 days of Borexino data // Phys. Rev.D., 92, 031101, 2015.

[2] *Gando A. et al. (KamLAND Collab.)* Reactor on-off antineutrino measurement with KamLAND // Phys. Rev.D. 2013. V. 88. P. 033001; arXiv:1303.4667v2 [hep-ex].

[3] *Bellini G., Ludhova L., Ianni A., Mantovani F., McDonough W.F.* Geo-neutrinos // Progress in Particle and Nuclear Physics, 73, 1, 2013.

[4] *Yu Huang, Viacheslav Chubakov, Fabio Mantovani, Roberta L. Rudnick, William F. McDonough* A reference Earth model for the heat producing elements and associated geoneutrino flux. arXiv:1301.0365v2 [physics.geo-ph]

[5] *Larin,V. N.* Hydridic Earth: the New Geology of Our Primordially Hydrogen-Rich Planet ed. C. Warren Hunt. Calgary, Alberta, Canada: Polar Publishing, 1993.

[6] *Herve Toulhoat, Valerie Beaumont, Viacheslav Zgonnik, Nikolay Larin, Vladimir N. Larin.* Chemical Differentiation of Planets: A Core Issue. arXiv:1208.2909 [astro-ph.EP].

[7] *Bezrukov L.* Geoneutrino and Hydridic Earth Model. Version 2. Preprint INR 1378/2014. M., 2014. 12 p; arXiv:1308.4163[astro-ph.EP].

[8] *David R. Lide (ed)*. CRC Handbook of Chemistry and Physics, 84th Edition, Section 10, Atomic, Molecular and Optical Physics; Ionization Potentials of Atoms and Atomic Ions Boca Raton, Florida: CRC Press, 2003.

[9] *L. B. Bezrukov, A. S. Kurlovich, B. K. Lubsandorzhiev, V. P. Morgalyuk, V. V. Sinev and V. P. Zavarzina* On geoneutrino // EPJ Web of Conference, QUARKS-2016. 2016. V. 125. 02004.

[10] *V. V. Sinev, L. B. Bezrukov, E. A. Litvinovich, I. N.Machulin, M.D. Skorokhvatov, S. V. Sukhotin* Looking for antineutrino flux from ^{40}K with large liquid scintillator detector // EPAN Letters, 46, 339, 2015; arXiv:1405.3140 [hep-ex].

[11] Cola super deep hole. Scientific results and research experience // Ed. board: P. A. Brodsky, D. M. Guberman, V. I. Kazansky, O. L. Kuznetsov, V. B. Mazur, N. V. Militenko, F. P. Mitrofanov, A. F. Morozov, L. A. Pevzner, B. N. Chachaev, Yu. N. Yakovlev, Moscow: MF "Technoneftegaz", 1998.

[12] *J. Hansen, M. Sato, P. Kharecha, and K. von Schuckmann*. Earth's energy imbalance // Atmos. Chem. Phys. 2011. V. 11, P. 13421-13449.

[13] *Krotikov V.D., Troitskyi V.S.* Radio emission and nature of the Moon // Soviet Phys. Uspekhi. 1964. V. 6. P. 841-871.

Search for astrophysical neutrino sources at the Baksan Underground Scintillation Telescope

M.M. Boliev[1], A.V. Butkevich[1], I.M. Dzaparova[1,2], M.M. Kochkarov[1], R.V. Novoseltseva[1], V.B. Petkov[1,2] P.S. Striganov[1],V.I. Volchenko[1] and A.F. Yanin[1]

[1]Institute for Nuclear Research of RAS, Moscow, Russia; boliev2005@yandex.ru

[2]Institute of Astronomy of RAS, Moscow, Russia

Abstract Baksan Underground Scintillation Telescope is an underground detector located at the Northern Caucasus (Russia). The BUST can detect an astrophysical flux of neutrinos from Galactic sources as an excess of cosmic ray muon neutrinos arriving from the source direction. The search performed using 38 years (live time = 31.05) of the BUST dataset to look for a statistically significant excess of events arriving within a solid angle. No significant excess of events produced by astrophysical sources is found. Since the number of detected events is compatible with the number of expected background events upper limit on the muon neutrino flux is determined.

Keywords: Cosmic Rays, Neutrino, Astrophysics, Galaxies, Local Sources

1. Experimental Data

The Baksan Underground Scintillation Telescope (BUST) [l] is located in the underground laboratory at the effective depth of 850m.w.e. The detector itself is a parallelepiped 16.7 x 16.7 x ll m^3, all sides of which are entirely covered by liquid scintillator counters of the standard type (0.7m x 0.7m x 0.3m). There are also two additional horizontal layers inside, at distances of 3.6 and 7.2 meters from the bottom. Thus the detector consists of four horizontal and four vertical planes, each separated from the other by m160g/cm2 of absorber. The total number of the detectors is 3180. Every counter is viewed with one PMT (the 15 cm diameter photocathode). The construction of BUST allows one to identify tracks of muons crossing the telescope. Separation of arrival directions between up and down hemispheres is made by time-of-flight (TOF) method with time resolution 5 ns [2]. The angular resolution of the BUST for reconstructed events is about 1.6°.The detection of upward-going muons is performed by means of the time-of-flight method. In first period (1978 – 2000) two hardware triggers are used in order to reject downward-going atmospheric muons. Trigger I covers the zenith angle range 95° — 180°, while trigger II selects horizontal muons in the range 80° — 100°, for more details see ref [3,4]. Since 2000 year no use hardware triggers for select neutrino events.

The data used for this analysis have been collected from December of 1978 until June of 2017, for a total of 31.05 live-years. It was found that 1635 events survived these cuts.

2. **Search for astrophysical sources**

In this work we calculate real live-time for selected astrophysical objects. ***Fig1*** shows dependence of BUST detector live-time for declination (δ). The search for a neutrino induced signal has been performed within angular windows of 5° around a exact coordinates of selected astrophysical objects. The size of the window was derived by Monte Carlo simulations of point-like neutrino sources with power law spectra (γ =2.5), and is the cone opening angle including 90% of the effect. The scattering angle between incident neutrino and daughter muon, multiple Coulomb scattering of the muon in the rock, and the angular resolution of the detector have been taken into account.

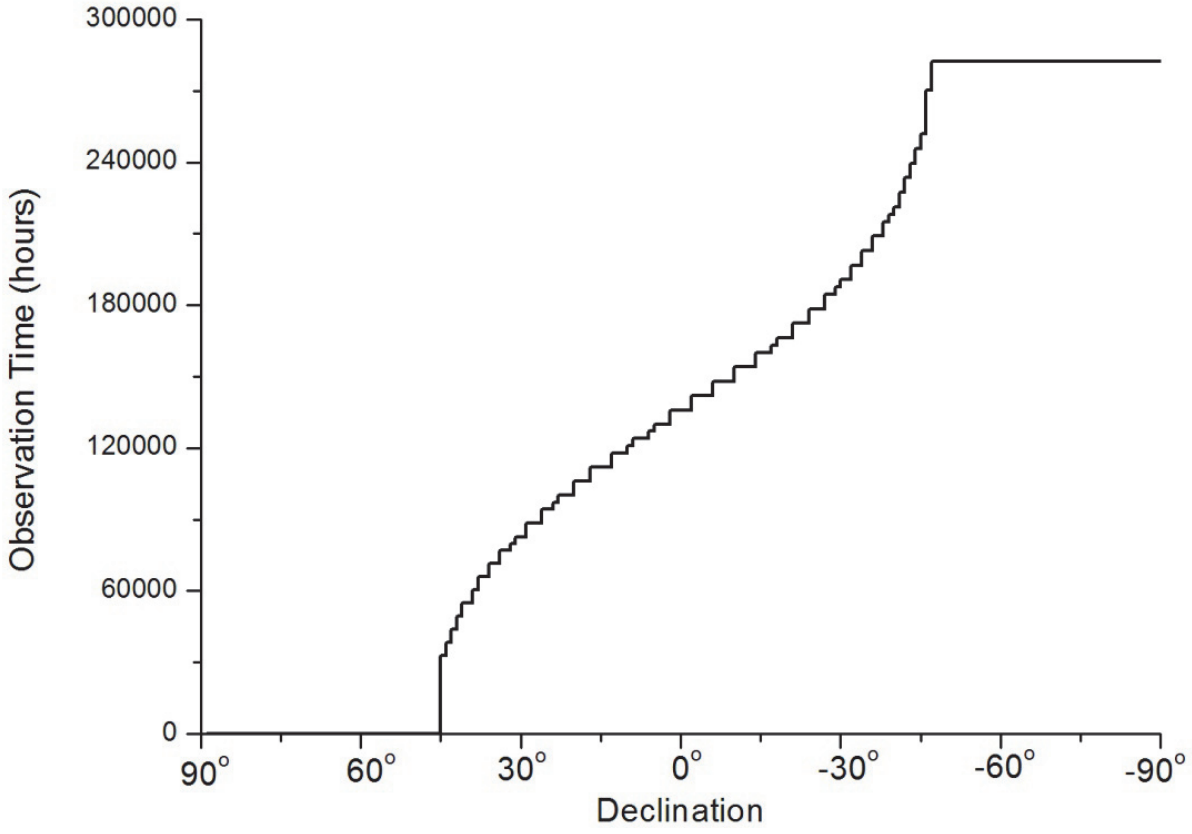

Fig1. *Dependence live-time according by declination - δ*

Table1 shows the number of upward-going muons observed within the window and the expected background, which was evaluated from simulations of the angular distribution of atmospheric neutrino induced muons and randomization of the event arrival times. The neutrino flux of [5] has been used. No evidence is found for any excess, and 90% C.L. limits for muon fluxes are given in fifth column of ***Table1***. For this search we have used the entire sample of 1635 events.

Table1. *Baksan flux limits on astrophysical muon neutrino sources*

Object	α(°)	δ(°)	Background	Events	μ Flux (cm-2 s-1) 90% C.L.
G.C.	265.6°	- 28.9	6.5	5	$0.32 \cdot 10^{-14}$
NGC 1952	83.6	+22.0	1.9	0	$0.87 \cdot 10^{-14}$
Vela X-1	135.5	-40.3	6.5	4	$0.15 \cdot 10^{-14}$
SS433	288.0	+5.0	2.8	1	$0.63 \cdot 10^{-14}$
3c273	187.3	+2.0	2.9	4	$0.52 \cdot 10^{-14}$
NGC 5128	201.4	-43.0	6.8	5	$0.15 \cdot 10^{-14}$
Cen. X-3	170.3	-60.6	6.3	3	$0.11 \cdot 10^{-14}$
Cyg. X-3	307.7	+40.8	0.1	0	$0.99 \cdot 10^{-14}$
Gem. SN437	98.5	+17.8	2.1	2	$1.35 \cdot 10^{-14}$
Scorp. X-1	245.0	-15.6	4.2	3	$0.37 \cdot 10^{-14}$

Acknowledgments

This study is performed with a part of the instrument certified as a Unique Scientific Facility (Baksan Underground Scintillation Telescope) and at an office that is an item of the Shared Research Facilities state program (Baksan Neutrino Observatory of the Institute for Nuclear Research).

References

[1] Alexeyev E.N. et al., Proc. of the l6th ICRC, v. 10, p. 276 (1979)

[2] Yu.M. Andreyev et al. Proc. of 16 ICRC. 1979. V.10. P.184. http://adsabs.harvard.edu/abs/1979ICRC 10.184A

[3] Boliev M.M. et al., Proc. of the 3rd Int. Workshop on Neutrino Telescopes, p.235 (1991).

[4] Boliev M.M. et al., Proc. of the 24th ICRC, Roma, v.1 p.686 (1995).

[5] Volkova L.V., Sov. J. Nucl. Phys., 31 (1980) 784

Gamma-ray bursts: Historical afterglows and early-time observations

Alberto J. Castro-Tirado[1,2] , Vladimir V. Sokolov[3] and Sergey S. Guziy[4]

[1] Instituto de Astrofísica de Andalucía (IAA-CSIC), P.O. Box 03004, E-18080 Granada, Spain; ajct@iaa.es

[2] Departmento de Ingeniería de Sistemas y Automática (Unidad Asociada al CSIC), Escuela de Ingeniería Industrial, Universidad de Málaga, Spain

[3] Special Astrophysical Observatory (SAO-RAS), Zelenchuk, Karachai-Cherkessia, Russia

[4] Astronomical Observatory, Mykolaiv National University, Mykolaiv, Ukraine

Abstract We discuss two historical afterglows (GRB 920723 and 920925C) prior to the Afterglow Era that started in 1997. We show how the use of both the 6-meter BTA in Zelenchuk (Russia) and 10.4-m GTC in La Palma (Spain) have benefited the study of GRB afterglows and their host galaxies. Moreover, when completed with our BOOTES Global Network of 0.6-meter robotic telescopes, this result had completed studying the early phases starting seconds after the trigger.

Keywords: Gamma-Ray Bursts, Afterglows, Early-Time Observations

1. Introduction

Since the discovery of the afterglows to Gamma-Ray Bursts (GRBs) in 1997, much has been advanced in the field, with several hundreds of counterparts in the last 20 yr in all the electromagnetic range from radio to gamma-rays, ending up with the detection of gravitational waves associated to a short-duration GRB in 2017.

2. Historical GRB afterglows

In 1997 the first counterpart at longer wavelengths was detected thanks to *BSAX* satellite. We always refer to 'the Afterglow era' to the period starting in 1997, following the important *BSAX* discovery of X-ray afterglows [1] followed by counterparts at other wavelengths. But we wonder whether there were other afterglows prior to 1997 serendipitously reported.

2.1. GRB 920723: the first X-ray afterglow?

An X-ray afterglow was pinpointed 5 yr before the *BSAX* detection of GRB 970228, which started the so-called Afterglow Era. This was the cased for GRB 920723, detected by the WATCH all-sky monitor on *Granat* ([2], [3]). See Fig. 1. Indeed Terekhov et al. refer to it as "afterglow" in their above-mentioned work published in 1993 [2].

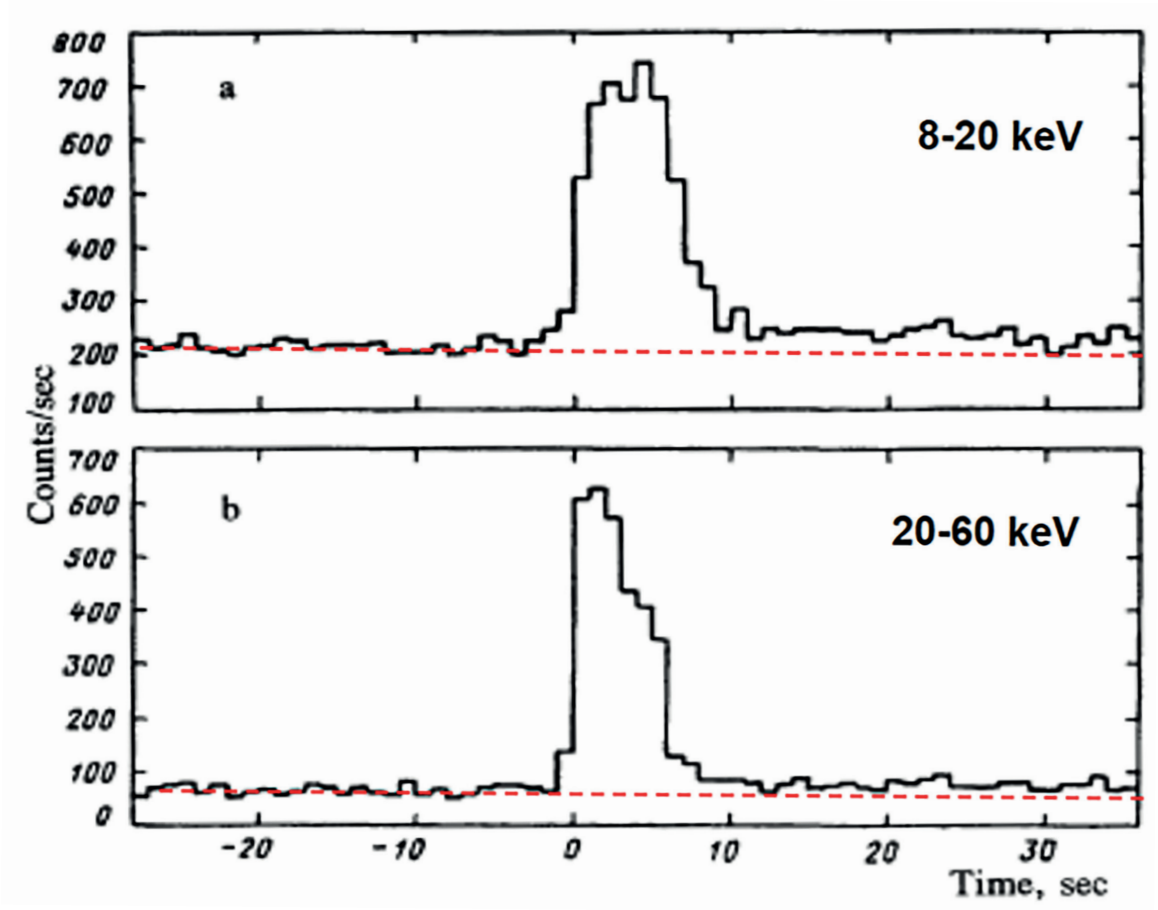

Fig 1. GRB 920723 as detected by WATCH on board Granat in the low energy range (8-15 keV, panel a) and in the high energy range (20-60 keV, panel b). See in a) how the low-energy emission above the background (red dotted line) extends significantly while the high energy emission (in b) has ceased. Adapted from [3].

2.2. GRB 920925C: the first optical afterglow?

GRB 920925C was a 400s long-duration GRB detected by WATCH/ *Granat* [3] and reported 4.5 yr prior to the famous GRB 970228, yet its optical afterglow (OA) needed 10 yr to be discovered once the corresponding POSS-II plates were checked! (and reported in [4]). A 2.6m Shajn initial search at Crimean Astrophysical Observatory was carried [5], reporting an upper limit of 25th mag. Deeper imaging conducted at the OA position revealed in

2013 a GRB 920925C candidate host galaxy and the very deep 10.4m GTC multicolour imaging performed in 2014 and 2017 showed a blue galaxy, as found in many other events. See Fig. 2.

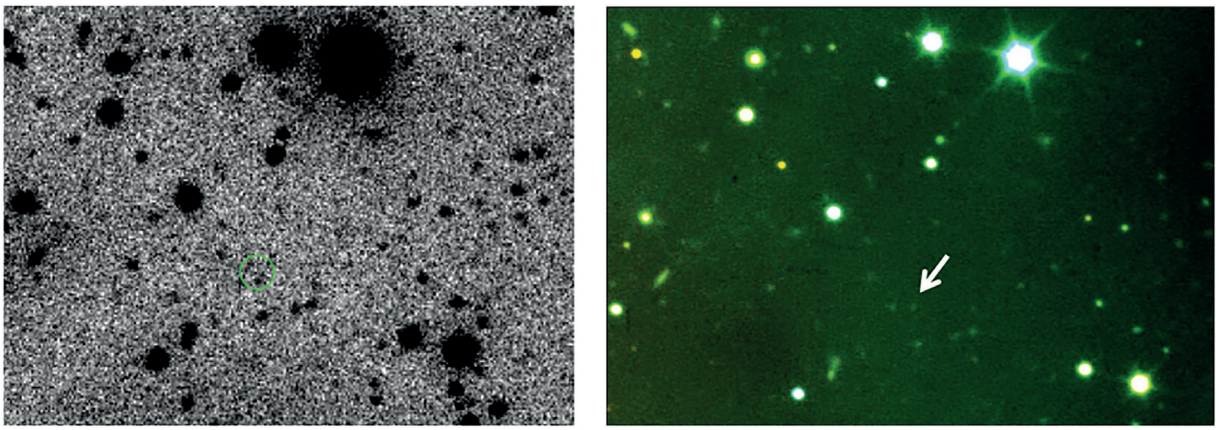

Fig 2. The green circle in the SAO image (left) represents the optical afterglow position found in [4] in the POSS-II plates, superimposed to the BTA deep V-band image, taking under Sokolov's GRB program in 2013. The GTC image (right) shows a color image as a result of combining g'r'i' images taken by the 10.4m GTC under the Castro-Tirado GRB program in 2013 and 2017. The arrow points to the candidate host galaxy. The field of view is 1.8' x 1.3'. North is up and east to the left.

3. Early observations of optical GRB afterglows

3.1. Reverse shocks

The strength of the reverse shock (RS) depends on magnetization content of the ejecta. See [6]. One such example is GRB 060117 [7]. See Fig.3.

3.2. Forward shocks

From the peak time of the rising OA lightcurves the initial Lorenz factor Γ_0 can be determined [8]. The rising lightcurves are also important to understand the onset of the afterglow [9] : $\alpha \sim 2$ ($\nu_c < \upsilon_{optical}$) or $\alpha \sim 3$ ($\nu_c > \nu_{optical}$) in the case of ISM or $\alpha \sim 0.5$ for a WIND density profile. And they also help to constrain off-axis and structured jet models [10].

3.3. Automated and Robotic telescopes: advantages for GRB afterglow follow-ups

The automatization and robotizacion of existing telescopes, or the installation of newly developed robotic telescopes is greatly helping the early detection of the GRB afterglows, thus completing the rapid response for the space (e.g. by the *Swift* satellite). A further step is the deployment of networks of robotic telescopes, such as MASTER [11] and BOOTES [12], amongst others.

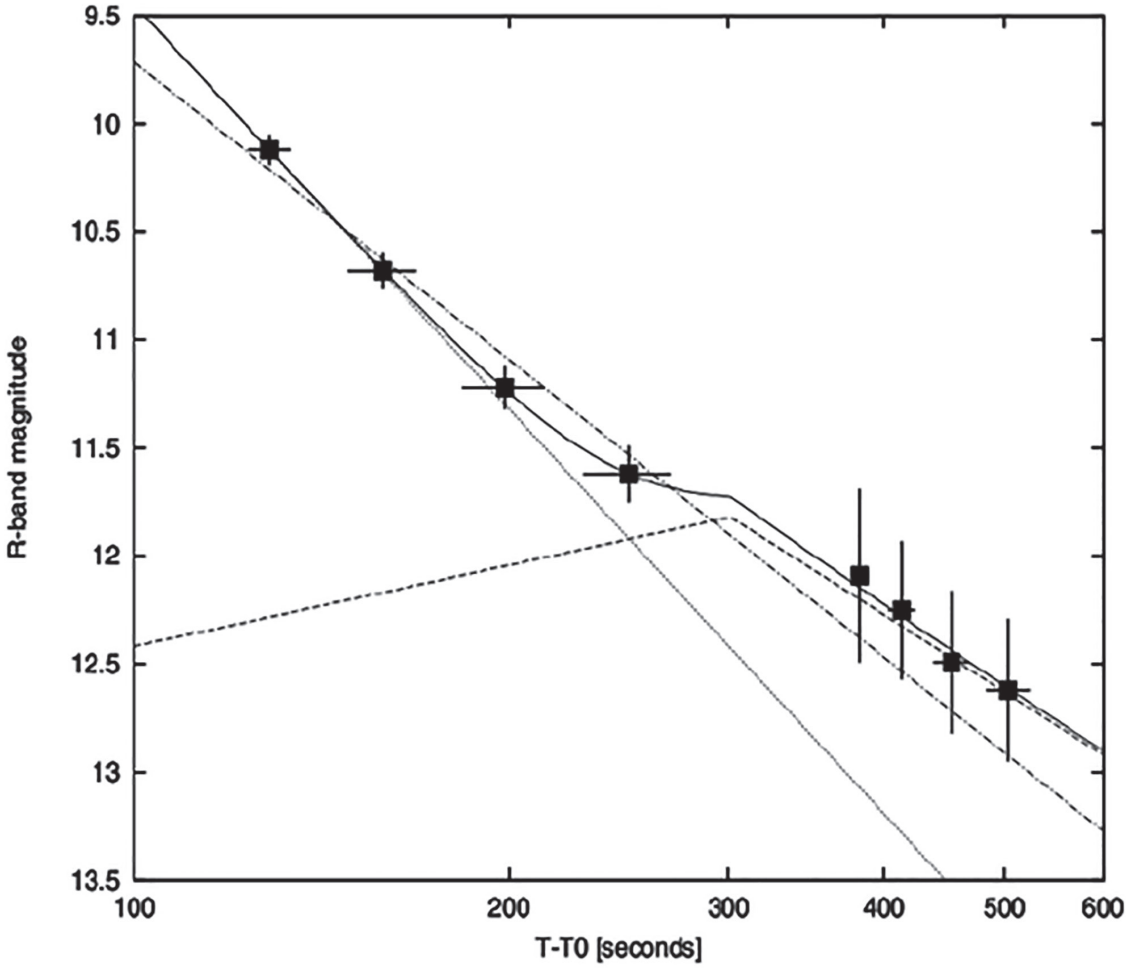

Fig 3. The early optical light curve of GRB 060117 (filled squares), fitted by a rapidly declining reverse shock and a forward shock peaking at about 300s (dotted lines resulting in the continuous line. Adapted from [7].

Fig 4. Some of the BOOTES stations worldwide. Robotic telescopes with a diameter of 60cm attached to EMCCD cameras. See [13] for further details.

BOOTES (Burst Observer and Optical Transient Exploring System), is becoming a worldwide network (with 4 units so far) of 0.6-meter ∅ identical robotic telescopes, attached to electro multiplying charged couple device cameras (EMCCD) cameras and filters (clear and g'r'i'ZY) which should help rapidly pointing to GRBs as soon as they go off. The next station (BOO-6) is opened in 2018 at the Boyden Observatory (South Africa). See Fig. 4.

A compilation of several early-time optical light curves provided by BOOTES-1 and -2 is shown in Fig. 5. 71 follow-ups in the period 2004-2013 resulted in 21 detections.

In some cases, the prompt discovery by one of the BOOTES telescope has led to trigger the 10.4-m GTC telescope, confirming the suspected high-redshift for the GRB itself. See Fig. 6.

4. 6.0-meter BTA & 10.4-meter GTC complementary observations

Following the 6.0-meter BTA, the largest telescope in the world in 1976, the 10.4-meter GTC is now the largest diameter optical telescope so far. See Fig. 7.

Some highlights follow:

a) Redshifts determination for about 20 GRBs (the first one: GRB 100316A, the last one: GRB 170626A). Redshift confirmation for another dozen of them. For instance, for GRB 100316A: the redshift was determined by GTC (z = 3.20). For GRB 140629A, the redshift was determined by BTA (z = 2.27, Hu et al. 2018). See Fig.8.

b)The extraordinarily bright and nearby (z = 0.340) GRB 130427A at the BTA & GTC, which was associated to a highly energetic supernova (SM2013cq). Spectroscopy was obtained at 6 different epochs. Work in progress. See Fig. 9. See also [17].

c) Searches for medium size GRB (few arcmin diameter) error boxes: discovery of a quasar in the short-duration GRB 140606A error box [18]. See Fig. 10.

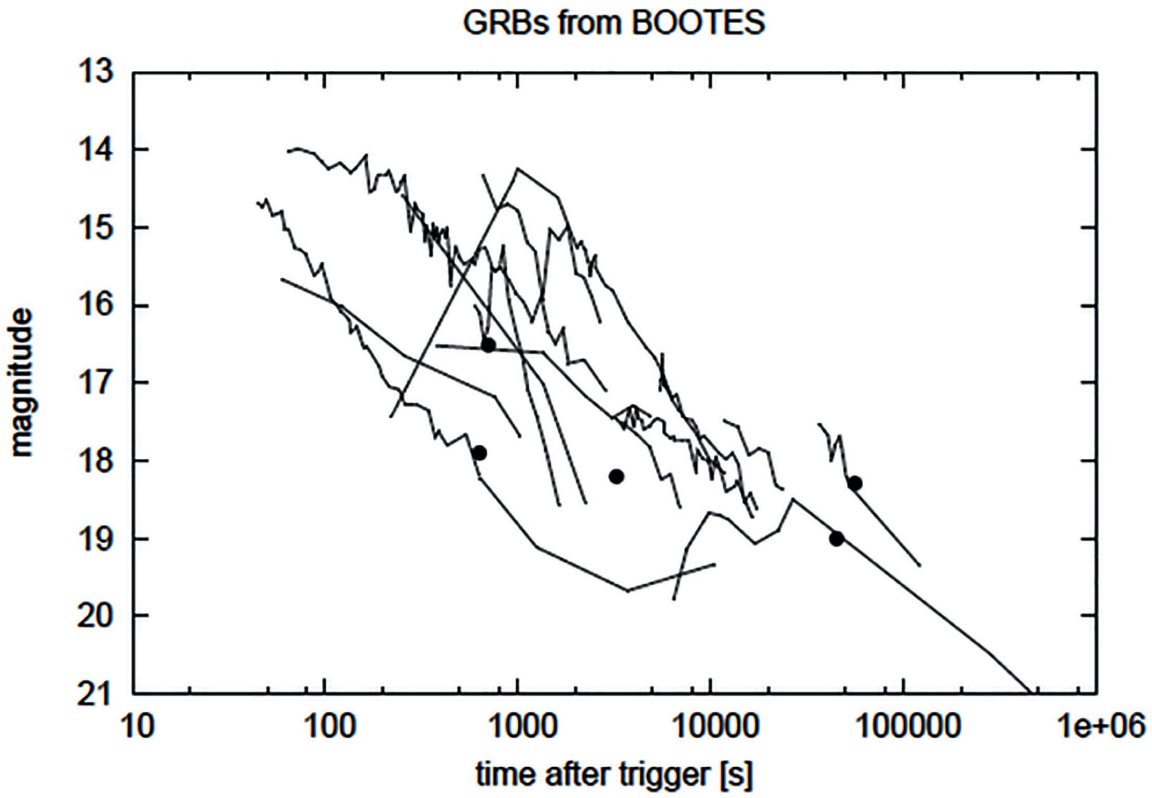

Fig 5. Some early light curves obtained by BOOTES-1 and -2 stations in South Spain. Adapted from [14].

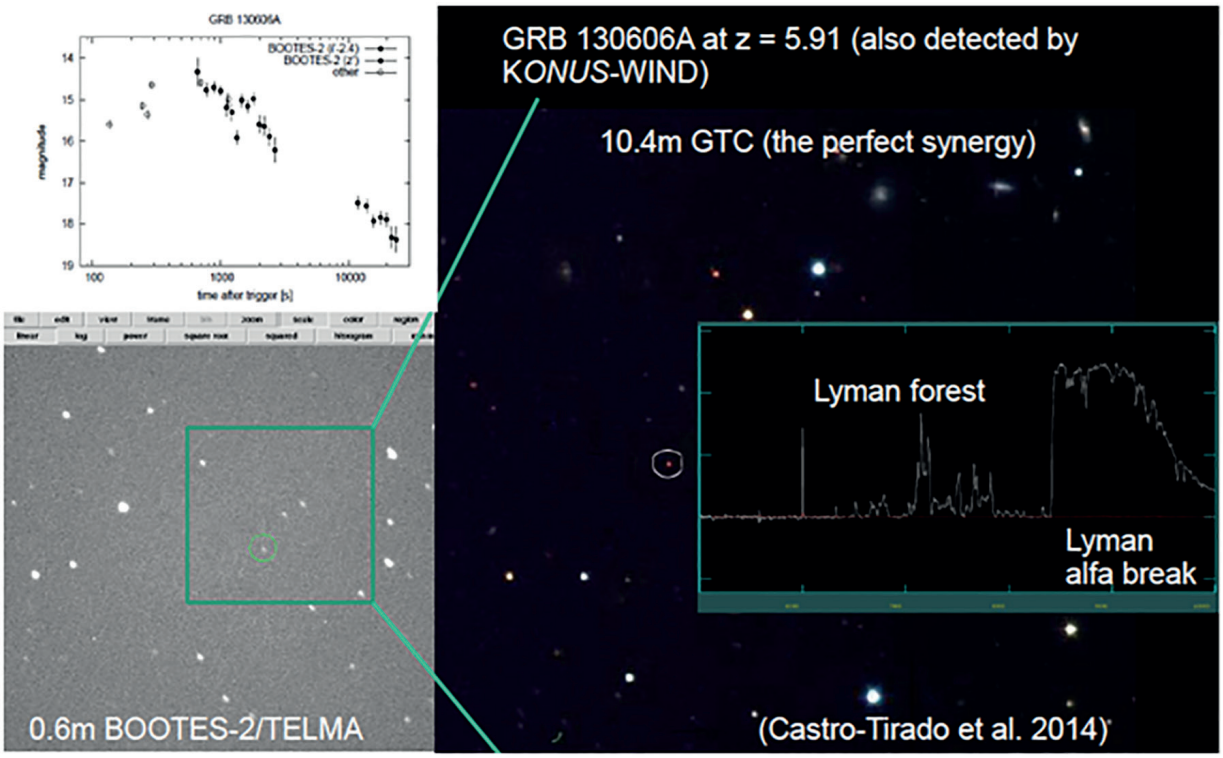

Fig 6. GRB 130606A at z = 5.91, first discovered by BOOTES-2 (lower left image), sampling the optical afterglow lightcurve (upper left) with the GTC showing the very highly reddened afterglow (right) at the z = 5.91 redshift determined by the GTC (insert). Adapted from [15].

Fig 7. Left: The dome of the 6-meter BTA telescope of SAO RAS. Right: The dome of the 10.4-meter Gran Canarias Telescope (GTC) (top) and the telescope itself (bottom).

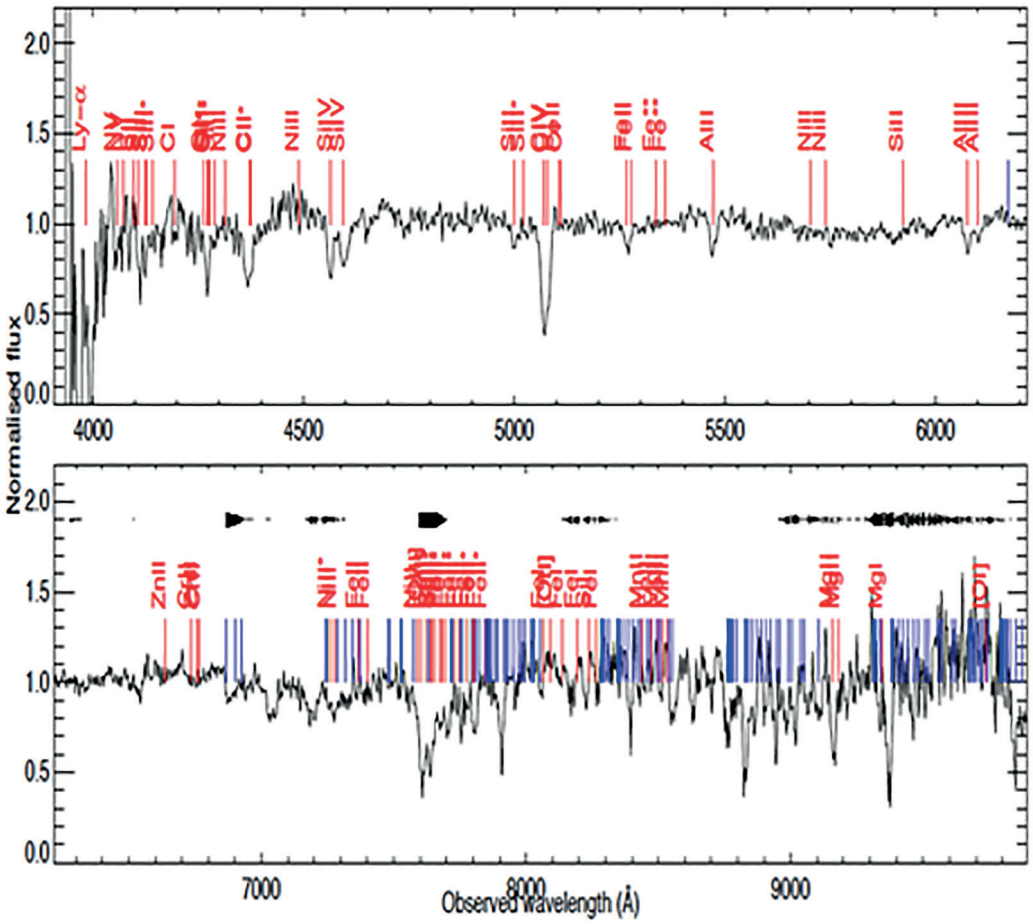

Fig 8. BTA optical spectrum of GRB 140629A obtained only 4.1-h after the detection of the GRB. It shows the Lyman-alpha emission line arising from the host galaxy plus some of the most prominent absorption line systems at the host galaxy redshift (in red). For completeness, the foreground system at z = 2.275 is also shown (in blue). Adapted from [16].

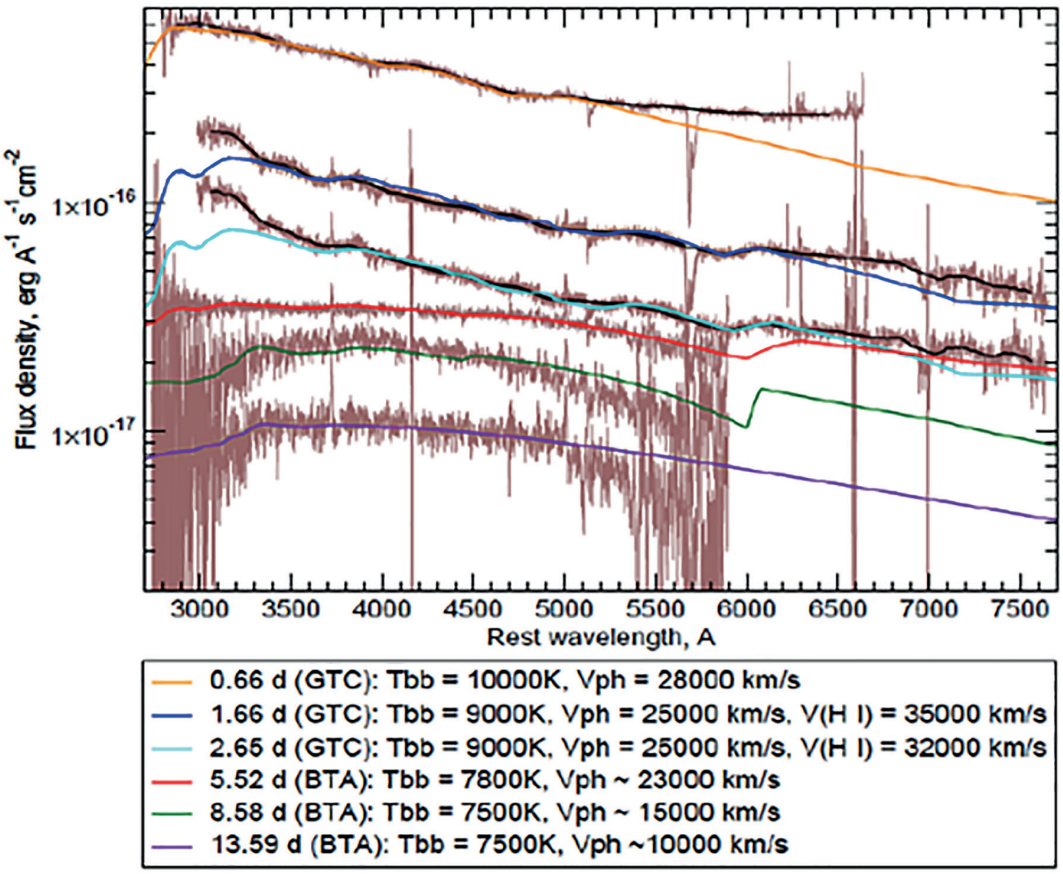

Fig 9. Multiepoch optical spectroscopy for GRB 130427A (z = 0.340) obtained at both the BTA and GTC, showing the velocity of the ejecta as a function of time.

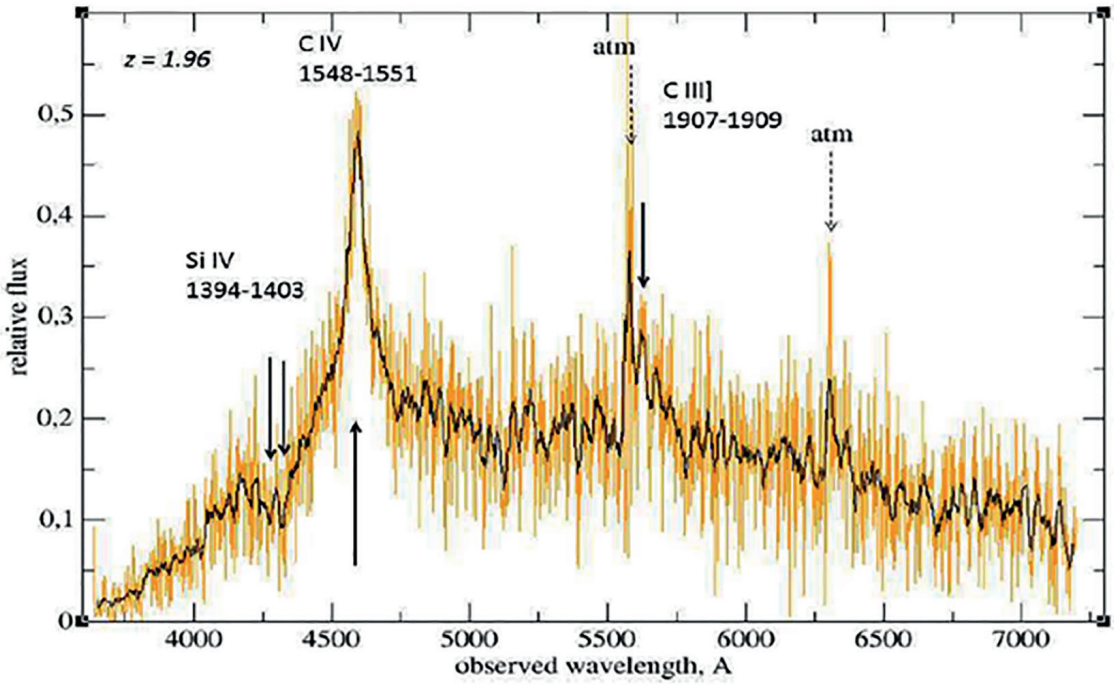

Fig 10. The BTA spectrum of the new quasar discovered in the GRB 140606A error box showing the typical emission lines at a redshift z = 1.96. Adapted from [18].

5. Conclusion

We discuss two historical afterglows (GRB 920723 and 920925C) prior to the Afterglow Era that started in 1997.

Afterglow emission can be detected in all the electromagnetic range (especially for long-duration events), in all timescales from seconds to months (the later in some cases). A variety of features can be studied by different techniques (photometry, spectroscopy, polarimetry) to gain insight into the progenitors, environments, abundances, metallicities, host galaxies... Multi-messenger information is also highly valuable, in the light of the recent detections of gravitational waves associated with the short-duration GRB 170817 (see [19] and references therein).

Automated and Robotic telescopes (such as the BOOTES Global Network) are very useful to study the early phases starting seconds after the trigger. This can be later completed by large diameter telescopes in the optical (e.g. 6.0-meter BTA, 10.4-meter GTC).

Acknowledgements

We acknowledge fruitful discussions with the rest of the ARAE and BTA teams. On the IAA-CSIC side, the project is funded by the Spanish Ministry's projects AYA 2012-39727-C03-01 and AYA2015-71718R, and the Junta de Andaluc a's project TIC-2839.

References

[1] Costa, E. et al. 1997. Discovery of an X-ray afterglow associated with the gamma-ray burst of 28 February 1997; Nature, 387: 783

[2] Terekhov. O. V., et al. 1993. Observations of a cosmic gamma-ray burst on 23 July 1992 with the WATCH instrument onboard the Granat Observatory, Pis`ma Astron. Zh. 19: 686

[3] Castro-Tirado, A. J. 1994. The WATCH experiment: 1000 days observing the X-ray Universe, University of Copenhagen

[4] Denisenko, D. V. & Terekhov, O. V. 2007. Discovery of an optical afterglow from the cosmic GRB 920925C, Astr. Let. 34:298

[5] Pozanenko, A. S. et al. 2008. Searching for the host galaxy of GRB 920925C, Astr. Let. 34:141

[6] Zhang, B., Kobayashi, S. and Meszaros P. 2003. Gamma-ray burst early optical afterglow: implications for the initial Lorentz factor and the central engine, ApJ 595:950

[7] Jel nek, M. et al. 2006. The bright optical flash from GRB 060117, A&A 454: L119

[8] Molinari, E. et al. 2007. REM observations of GRB 060418 and GRB 060607A: the onset of the afterglow and the initial fireball Lorentz factor determination, A&A 469:L13

[9] Sari, R. and Piran, T. 1999. Predictions for the very early afterglow and the optical flash, ApJ 520: 641

[10] Painatescu, A., M sz ros, P. and Rees, M.J. 1998. Multiwavelength afterglows in gamma-ray bursts: refreshed shocks and jets effects, ApJ 503:314

[11] Lipunov, V. V. et al. 2016. MASTER Global Robotic Net: new sites and new result, Rev. Mex. A&A Conf. Ser. 48:42

[12] Castro-Tirado, A. J. et al. 2012. Building the BOOTES Network of Robotic Telescopes, ASI Conf. Ser., 7:313

[13] (2018) The BOOTES website. [Online]. Available: http://bootes.iaa.es

[14] Jel nek, M. 2014. Study of gamma-ray bursts with Robotic telescopes, Ph.D. Thesis, Universidad de Granada

[15] Castro-Tirado, A.J. et al. 2014. GRB 130606A within a sub-DLA at redshift 5.91, A&A, submitted (astro-ph/1312.5631)

[16] Hu, Y. et al. 2018. A burst with a jet break in the optical and X-ray afterglow, A&A, submitted

[17] Sokolov, V.V., Castro-Tirado A.J., and Sokolova, T.N. 2018, The core collapse supernovae, gamma-ray bursts and SN1987A, These Proceedings

[18] Pandey, S. B. et al. 2018. Multiwavelength analysis of short-duration GRBs observed between 2012 and 2015, A&A, submitted

[19] Zhang, B.-B. et al. 2018. A peculiar low-luminosity short gamma-ray burst from a double neutron star merger progenitor, Nature Communications, in press (arXiv171005851Z)

The Carpet-3 EAS array to search for cosmic diffuse ultra-high energy gamma-rays

D.D. Dzhappuev[1], V.B. Petkov[1], A.S. Lidvansky[1], V.I. Volchenko[1], G.V. Volchenko[1], E.A.Gorbacheva[1], I.M. Dzaparova[1], A.U. Kudzhaev[1], N.F. Klimenko[1], A.N. Kurenya[1], O.I. Mikhailova[1], K.V. Ptitsyna[1], M.M. Khadzhiev[1], A.F. Yanin[1]

[1]Institute for Nuclear Research, Russian Academy of Sciences; Moscow, Russia;
dzhappuev@mail.ru

Abstract At the moment an experiment for measuring the flux of cosmic diffuse gamma rays with energy higher than 100 TeV (experiment Carpet-3) is being prepared at the Baksan Neutrino Observatory. The preparation of the experiment implies considerable enlargement of the area of both muon detector and surface part of the shower array. Sensitivity of the experiment to showers generated by primary gamma rays is estimated for different configurations of the future array. Also presented are the results of measurements made with a smaller area of the muon detector (the Carpet-2 experiment) for a net exposure of 9.2 years. Preliminary estimates of the upper limit on the flux of diffuse cosmic gamma rays with energies above 930 TeV are derived.

Keywords: Cosmic Rays, Extensive Air Showers, Primary Diffuse Gamma Rays, Muon-poor Showers

1. Introduction

To measure the flux and spectrum of diffuse primary cosmic gamma rays with energies higher than 100 TeV is of great interest for solving the problem of origin of cosmic rays, one of the most important in high energy astrophysics. As opposed to ordinary cosmic rays (protons and nuclei of heavier elements) that are charged particles and deflect in interstellar magnetic fields, the primary gamma rays can give information about the spatial distribution and characteristics of places of acceleration of cosmic rays, as well as about the density of cosmic rays in the interstellar space. Investigation of diffuse gamma rays at such energies is carried out by the EAS method in experiments in which one can separate the showers produced by primary photons and nuclei. Such a separation is possible due to the fact that showers from primary photons are essentially less abundant with hadrons (and, as a result, they are muon-poor) in comparison with showers from primary protons and (the more so) nuclei. Thus, if one selects hadron-poor or muon-poor EAS, there is a hope to effectively distinguish between the showers produced by primary gamma rays and by nuclei. For the first time this method was suggested in paper [1]. Since then, many experiments were carried out to search for gamma ray showers in a wide energy range. One can find reviews on these experiments in papers [2-5]. The experiments with air shower arrays at Mt. Chakaltaya, Tien Shan, Yakutsk and Lodz reported about some positive results for gamma rays in the energy

range 10^{14}-5x10^{17} eV. However, these results had low statistical significance and were not confirmed afterwards.

Later, high-energy primary gamma rays were searched for in the energy range 3×10^{14} – 5×10^{16} eV by the air shower arrays EAS-TOP, CASA-MIA, and KASCADE and at energies above 10^{18} eV by the arrays Haverah Park, AGASA, Yakutsk, Pierre Auger, and Telescope Array. All these experiments obtained only the upper limits on flux values, which appeared to be much lower than previously measured fluxes in early experiments.

Many years ago the experiment aimed at searching for local sources of gamma rays with energy higher then 100 TeV was made with the Carpet air shower array of the Baksan Neutrino Observatory of INR of RAS. A burst of gamma radiation with energy $E_\gamma \geq 100$ TeV was detected from the Crab Nebula [6], while for other possible sources of gamma rays the flux upper limits were obtained [7].

The interest to searching for primary gamma rays with energies higher than 100 TeV has recently greatly increased in connection with the results of the IceCube experiment, where high energy neutrinos of astrophysical origin were found. In [8] it was suggested that such neutrinos are a result of decays of charge pions in the Galaxy. If so, the neutral pions of the same energy should exist, whose decays produce a considerable flux of gamma rays in the energy range 10^{14} - $5\cdot10^{17}$ eV. The flux of diffuse galactic gamma rays predicted in this paper is close to available experimental limits in the energy range lower than approximately 5 PeV, and it can be detected in the Carpet-3 experiment. This project is a further development of the Carpet-2.

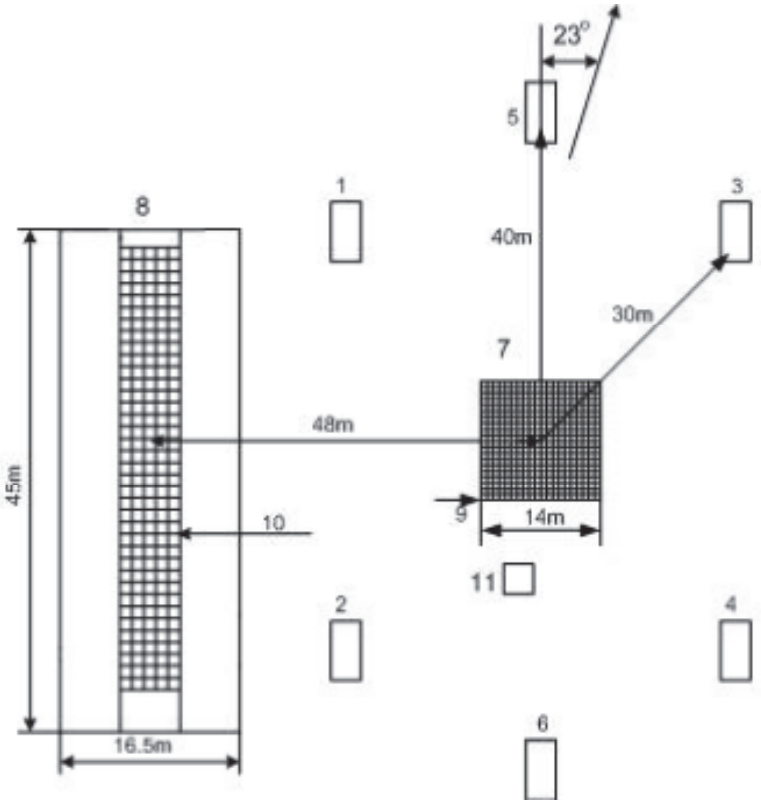

Fig1. *Layout of the Carpet-2 array detectors: 1-6 are huts with liquid scintillation detectors, 7 is the Carpet of liquid scintillators, 8 is the muon detector (MD), 10 are its plastic scintillators, and 11 is the neutron monitor. The arrow in the upper part of the figure shows the direction to the north.*

2. The Carpet-2 experiment

The Carpet-2 air shower array [9, 10] of the Baksan Neutrino Observatory is located at North Caucasus near Mt. Elbrus at an altitude of 1700 m above sea level (the atmospheric thickness is 840 g/cm^2 and geomagnetic cutoff rigidity is 5.6 GV). It consists (***Fig1***) of a surface part, the Carpet with six external huts (EH) and underground muon detector (MD). The distance between centers of the Carpet and MD is 48 m. The Carpet that detects the EAS electron-photon component includes 400 scintillation counters forming a square (20x20) with a total area of 196 m^2. Each EH contains 18 counters (9 m^2) of the same type as those in the Carpet. The muon detector records the muon component with energy threshold of 1 GeV. It has 175 plastic scintillation counters, each of area of 1 m^2. Anode pulses of PM tubes of these detectors are joined in groups of 35 to feed 5 analog summators. The summed signals come to inputs of charge-to-digital converters (CDC) whose threshold of actuation is 0.5 r.p. (1 r.p. or relativistic particle corresponds to the most probable energy release of a single particle in a detector, it equals 10 MeV for MD counters and 50 MeV counters of the Carpet and EH). Pulses from CDC are sent to input of the scheme of event selection (SES), which generates an output trigger signal when 2 or more pulses appear at its input. This signal permits data recording for a particular event in the MD data acquisition system. Signals of six EH are used to determine the shower arrival directions. For EAS having axes within the Carpet the accuracy of determining their coordinates is no worse than 0.7 m, while the angular accuracy of shower direction determination is about 3°. The Carpet and MD operate independently of each other, and their recording systems have different dead times. However, since time tags of events in the MD and Carpet are produced by one and the same clock, coincident events are reliably identified within the time interval $\Delta t = 1$ ms.

The total number of relativistic particles within the Carpet ($N_{r.p.}$) and the number n_μ of muons recorded by the MD are the experimentally measured quantities used to determine the energy of EAS and the total number of muons in it, respectively. The events satisfying the following conditions are included into processing:

1. shower axes are well within the Carpet;
2. zenith angles of showers $\theta < 40°$;
3. the total energy release in the Carpet $N_{r.p.} \geq 10^4$.
4. the number of counters in the Carpet with signals exceeding 10 r.p. is ≥ 300.

After such a selection, the number of showers recorded in the period since 1999 to 2011 is equal to 1.3x10^5. The net exposure time for this period is 3390 days ($\approx$ 9.2 years). The CORSIKA code v. 6720 (the QGSJET01C model for high energies FLUKA 2006 for low energies) [11] was used for modeling the showers. 5400 showers from primary protons were simulated within the energy interval (0.316–31.6) PeV, as well as 815 showers from primary gamma rays in the range (0.3–9) PeV. As a result of modeling, the averaged energy dependence was obtained for N_e, and n_μ was determined as a function of E_0 and N_e.

3. Upper limit on diffuse flux of cosmic gamma rays

In order to distinguish the showers from primary gamma rays on the background of ordinary EAS, we have analyzed correlation dependences in the plane $n_\mu - N_e$ for detected and simulated events (***Fig2***). In this paper we consider the energy region $N_e \geq 6\times10^5$ where, with the used method of processing experimental data, one can separate simulated gamma-ray showers from ordinary EAS events.

To evaluate the efficiency of selection of gamma-ray showers at $N_e \geq 6\times10^5$, $N_e \geq 10^6$, and $Ne \geq 5\times10^6$ we isolated on the plane $n_\mu - N_e$ the area where only simulated gamma-ray showers are present, and there are no really detected showers. The boundary of this region is shown by a broken line in ***Fig2***.

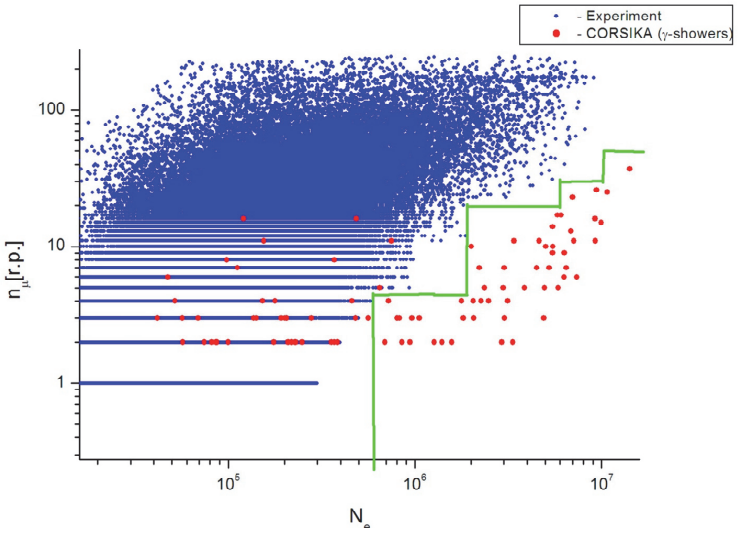

Fig2. *The n_μ versus N_e dependence: experiment and CORSIKA gammas.*

The ratio ε_γ of the number of simulated gamma-ray showers in a particular area to the total number is the efficiency of detection for this area. For three intervals $N_e \geq 6\times10^5$, $N_e \geq 10^6$, and $N_e \geq 5\times10^6$ the calculated values of ε_γ are equal to 0.95, 0.9, and 1.0, respectively. Based on the fact that there are no detected events in a specified region (no background, N_B=0), one can use the following formula for estimation of the flux of primary gamma rays at 90% confidence level:

$$I_\gamma = \frac{2.3}{S \cdot T \cdot \Omega \cdot \varepsilon_\gamma}$$

where S = 200 m^2 is the detection area for EAS axes, T is the net exposure (data taking) time, and ε_γ is the detection efficiency for showers from primary gamma-rays. Using the above derived values for efficiency, the upper limits were obtained for $E_\gamma \geq 9.3\times10^{14}$ eV, ($N_e \geq 6\times10^5$), $E_\gamma \geq 1.3\times10^{15}$ eV ($N_e \geq 10^6$), and $E_\gamma \geq 3.2\times10^{15}$ eV ($N_e \geq 5\times10^6$) (see ***Table1*** below).

Table1.

N_e	E_γ[eV]	N_B	ε_γ	log10(E_γ I_γ(>E)) [eV cm^{-1}sec^{-1} sr^{-1}]
$\geq 6\times10^5$	$\geq$ 9.3×10^{14}	0	0.95	0.61
$\geq 10^6$	$\geq$ 1.3×10^{15}	0	0.99	0.85
$\geq 5\times10^6$	$\geq$ 3.2×10^{15}	0	1.0	0.92

Fig3 presents the limits on the integral flux of cosmic diffuse gamma rays as a function of energy of primary photons together with the results of other experiments. It should be noted that our results present in this paper are preliminary, and the upper limits presented in ***Fig3*** and Table can be refined after more careful analysis of experimental data.

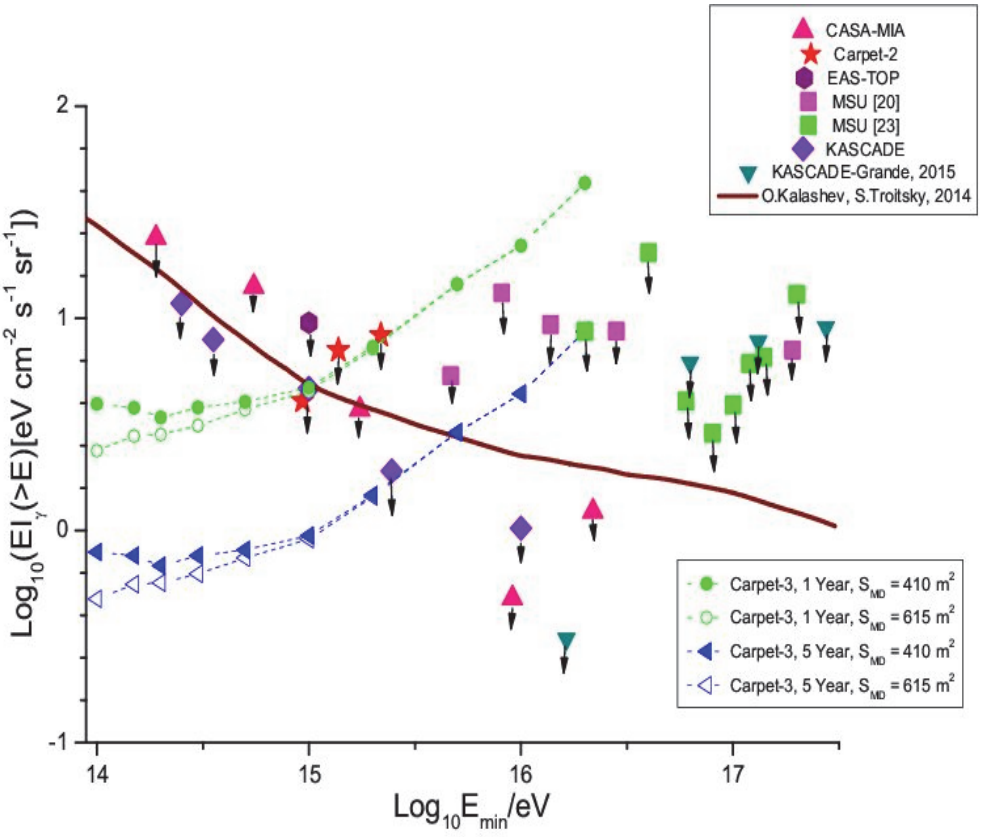

Fig*3.* *The Carpet-3 sensitivity to the flux of diffuse cosmic gamma rays.*

4. The Carpet-3 experiment

Preparation of the experiment suggests a step-by-step increase of the MD's continuous area: at first up to 410 m^2 and then up to 615 m^2. The area of EAS axes detection also will be increased. For this purpose 20 additional modules will be installed with 9 scintillation counters of area 1 m^2 each (see ***Fig4***).

At the moment 410 plastic scintillation counters with the total area of 410 m^2 are installed in the MD underground tunnels. They are fully equipped with necessary electronic circuits. Also the work on adjustment of these counters and on creation of the special data acquisition system for a new configuration of the MD is in progress.

At the same time, calculations have been carried out to estimate the efficiency of selection of gamma rays and the sensitivity of different configurations of the new array to air showers initiated by primary gamma rays. ***Fig3*** demonstrates the expected limits on the flux of diffuse cosmic gamma rays for two configurations of the Carpet-3 array and for two periods of data accumulation. One can see that even at the MD area equal to 410 m^2 the new array will have the world-best sensitivity to the flux of cosmic gamma rays with energies in the range 100 TeV – 1 PeV.

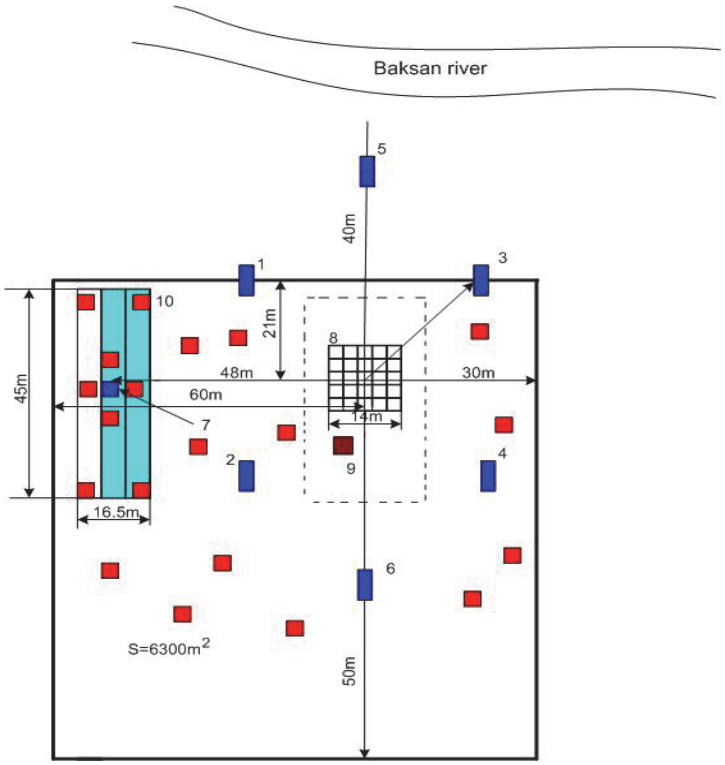

Fig4. *The layout of the Carpet-3 air shower array. The big blue rectangle shows the MD area filled with plastic scintillation counters. The dark blue and red patches present outdoor huts (modules) with scintillation detectors.*

5. Conclusions

1. From the results of the Carpet-2 air shower array the upper limits on the flux of diffuse cosmic gamma rays with energy above 900 TeV are derived.
2. In order to provide for efficient detection of air showers initiated by gamma rays with energies higher than 100 TeV, it is necessary to perform the array modernization with a considerable increase of the Muon Detector area (The Carpet-3 experiment).
3. In this case, several years of data accumulation will make it possible to improve significantly the results currently available on measuring the 100 TeV flux of cosmic diffuse gamma rays.
4. This work is now in progress.

Acknowledgments

This study is performed with a part of the instrument certified as a Unique Scientific Facility (Baksan Underground Scintillation Telescope) and at an office that is an item of the Shared Research Facilities state program (Baksan Neutrino Observatory of the Institute for Nuclear Research). The work is supported by the Russian Foundation for Basic Research, project numbers 16-02-00687 and 16-29-13049-OFI-M).

References

[1] Maze R, Zawadzki A, On an attempt of detection of primary cosmic photons of very high energy. Nuovo Cim. 1960; 17: 625.

[2] Fomin YuA, Kalmykov NN, Kulikov GV, Sulakov VP, Troitsky SV. J. Exp. Theor. Phys. 2013; 117: 1011. [arXiv: 1307.4988 [astro-ph.HE]].

[3] Fomin YuA, Kalmykov NN, Karpikov IS, Kulikov GV, Kuznetsov MYu, Rubtsov GI, Sulakov VP, Troitsky SV. JETP Letters. 2015; 100: 699. [arXiv: 1410.2599 [astro-ph.HE]].

[4] Fomin YuA, Kalmykov NN, Karpikov IS, Kulikov GV, Kuznetsov MYu, Rubtsov GI, Sulakov VP, Troitsky SV. No muon excess in extensive air showers at 100-50 PeV primary energy: EAS-MSU results. Astropart. Phys. 2017; 92: 1. [arXiv: 1609.05764 [astro-ph.HE]].

[5] Fomin YuA, Kalmykov NN, Karpikov IS, Kulikov GV, Kuznetsov MYu, Rubtsov GI, Sulakov VP, Troitsky SV. Constraints on the flux of (10^{16} – $10^{17.5}$) eV cosmic photons from the EAS-MSU muon data. Report INR RAS INR-TH-2017-005.[arXiv: 1702.08024].

[6] Alexeenko VV, Andreyev YuM, Chudakov AE, Elensky YaS, Lidvansky AS, Ozrokov SKh, Stenkin YuV, Tizengauzen VA, Graham LJ, Osborne JL and Wolfendale AW. The ultra-high energy gamma-ray burst from the Crab Nebula observed by the Baksan EAS array. 1992 J. Phys. G: Nucl. Part. Phys.; 18: L83-L88.

[7] Alekseenko VV, Lidvanskii AS, Metlinskii NA, Ozrokov SKh, Sklyarov VV, Tizengauzen VA, Khaerdinov NS, Chudakov AE, Possible flare of the source Cyg X-3 at E > 10^{14} eV. JETP Letters; 44: 258

[8] Kalashev OE, Troitsky SV, IceCube astrophysical neutrinos without a spectral cutoff and (10^{15}–10^{17}) eV cosmic gamma radiation. JETP Lett. 2015; 100: 761. [arXiv: 1410.2600].

[9] Dzhappuev DD, Alekseenko VV, Volchenko VI, et al., Modernization of the Carpet-2 array of the Baksan Neutrino observatory. Bull. Russ. Acad. Sci. Phys. 2007; 71: 525-28.

[10] Dzhappuev, DD, Alekseenko VV, Lidvansky AS, Stenkin YuV, Petkov VB, Mikhailova OI, Kudzhaev AU, Chernyaev AB, and Tsyabuk AL, Study of EAS hadronic component with hadron energy > 50 GeV. Proc. 30th ICRC, Merida, 2007, vol. 4, p. 19.

[11] Heck D et al., The Air Shower Simulation Program CORSIKA. Report FZKA 6019 (1998), Forschungszentrum, Kalrsruhe.

Localization of gravitational waves as a test of gravitation theory

Liudmila Fesik[1]

[1]Saint-Petersburg State University, Saint-Petersburg, Russia; lucia555@yandex.ru

Abstract Detection of the gravitational wave events by Advanced LIGO antennas has opened the new possibility for the study high energy astrophysical processes and also fundamental physics of the gravitational interaction. A new method is presented for measuring the polarization state of an incoming GW by using localization of GW sources along the apparent circle of a detected event. The method takes into account the antenna-pattern functions for different polarization modes and the the detected strain ratio. In is shown that the apparent circles on the sky for allowed positions of the GW sources for the GW150914, GW151226 and LVT151012 events are parallel to the plane of the disc-like large scale structure known as the Local Super-Cluster (LSC) of galaxies which extends up to radius ~100 Mpc and having thickness ~30 Mpc.

Keywords: Gravitational Waves, Detection of gravitational waves, Source localization

1. Introduction

In the 1980's, the Laser Interferometer gravitational wave Observatory (LIGO) was proposed for detecting gravitational waves with the principal goal to study astrophysical GWs and stimulate research in fundamental physics concerning the nature of gravity. Recent detection of gravitational wave signals by Advanced LIGO antennas has opened such possibility for study physics of the gravitational interaction.

In the situation when there is no reliable optical (and other electromagnetic bands) identification of the GW events, the interpretation of the physics of the GW source is still uncertain. Even though the model of tens solar masses binary black holes coalescence at the distance 400 - 1000 Mpc is consistent with existing GW data (Abbott et al. [2016a], Abbott et al. [2016b]), one should also test alternative possibilities which are allowed by modern theories of the gravitational interaction (Eardley et al. [1973], Maggiore and Nicolis [2000], Will [2014], Baryshev [2017]).

Here we develop a method based on very general physical arguments, which allows us to distinguish between tensor and scalar polarization states predicted by the scalar-tensor gravitation theories. In particular, for the case of two antennas actual position of the GW source at the apparent circle on the sky can be used for determination of the polarization state of the detected GW. Hence, our method allows testing astrophysical models proposed for explanation of the physical processes generating the gravitational waves.

2. Polarization states of a gravitational wave in the modern theories of gravity

There are two main approaches to study the physics of gravitational interaction: the geometrical one, known as General Relativity Theory (hereafter GR) proposed by A. Einstein, and the field theory approach introduced by R. Feynman. In the frame of both approaches, there is predicted the existence of gravitational waves (hereafter, GW) as a result of massive bodies interaction.

The first approach is the geometrical Einstein's general relativity theory (GRT, also called "geometrodynamics"), which is based on the concept of metric tensor g^{ik} of curved Riemannian space-time (Einstein [1916], the standard textbooks on GRT: Landau and Lifshitz [1988], Misner et al. [1973]). The second approach, the Feynman's field gravitation theory (FGT, also called "gravidynamics") is a non-metric relativistic quantum theory, where the gravitational interaction is described by a symmetric second rank tensor potential ψ^{ik} in the Minkowski space-time (Feynman [1971], Feynman et al. [1995]).

A gravitational wave is characterized by its polarization state, which reflects the response of test bodies on the propagation of the wave. Modern theories of gravitation predict the existence of several GWs modes generally divided on tensor and scalar, longitudinal and transverse. A certain polarization state of a received GW significantly depends on the nature of a GWs source. In particular, a merging binary system of stars is expected to give a GW with a tensor transverse polarization state but not a scalar one, whereas a symmetric core-collapse supernovae might be capable to produce a scalar GW mode without a tensor component.

On the other hand, a polarization state is limited by circumstances of a chosen theory. Thus, GR takes under consideration only tensor transverse modes, whereas some modified GR theories as well as field gravitation theory apart from tensor consider also the existence of scalar modes. Therefore, the detection of a certain polarization state of an incoming GW provides a test on a theory of gravitation.

3. Interferometric antennas and polarization states of GWs

Let us consider a GW antenna based on a Michelson-type interferometer with two orthogonal arms having four test masses at their ends. The receiver is at the rest in the local proper reference frame, with the origin of spatial coordinates in the corner of the system and the X and Y axes along the antenna's two arms, ***Fig1***. The GW passing through the antenna displaces the test masses, thereby changing the length of each arm from its initial length L_0 (for LIGO detectors L_0 = 4 km). The monitored by laser difference between lengths of these arms $\Delta L(t) = L_X - L_Y$ normalized by the initial length of the arm L_0 gives the observed at the antenna strain $\bar{h}(t) = \Delta L(t)/L_0$.

For laser interferometers, the general form of the signal $\bar{h}$ is a composition of antenna-pattern functions F with waveform $h(t)$ for the corresponding polarization mode (Will [2014]):

$$\bar{h}(t; \zeta, \Phi, \Psi) = F_{SL}(\zeta, \Phi)h_S(t) + F_{ST}(\zeta, \Phi)h_S(t) + F_+(\zeta, \Phi, \Psi)h_+(t) + F_\times(\zeta, \Phi, \Psi)h_\times(t) \quad (1)$$

Waveforms $h(t)$ are critically dependent on the nature of a source and the processes producing this GW, whereas antenna-response functions $F(\zeta,\Phi,\Psi)$ depend only on the

position of the source on the sky relative to the antenna characterized by zenith angle ζ and azimuth Φ in the horizontal coordinate system of the antenna. Therefore, for the same source, a received by several antennas GW with a certain waveform has different antenna response functions.

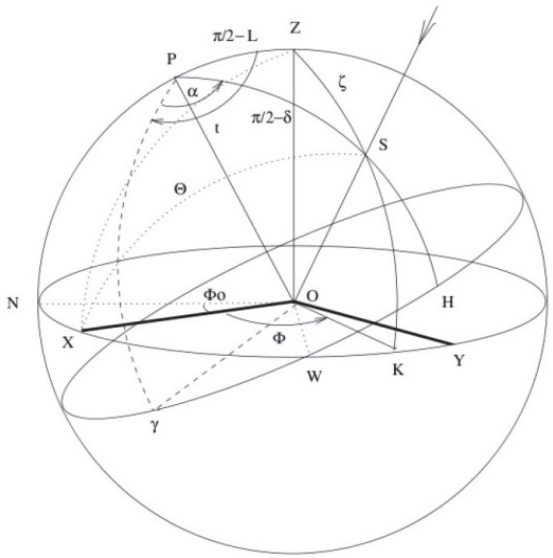

Fig1. *Equatorial and horizontal coordinate systems of an interferometric antenna for the GW source S. Z is the zenith, P – the northern pole, γ defines the sidereal time, α – the right ascension (RA), δ – the declination (DEC), ζ – the zenith angle. The reference direction of the detector is the direction OX with the azimuth Φ0.*

3.1. Antenna-response functions of two-arms interferometric antennas

Antenna-pattern functions $F(\zeta,\Phi,\Psi)$ are determined for each polarization state (see, e.g., Will [2014]) by the angles (ζ,Φ) of a source position in the horizontal coordinate system (hereafter CS) of an antenna, ***Fig1***.), and polarization angle Ψ in the case of tensor GW (for definition see p. 366 Hawking and Israel [1989]):

$$F_{+}(\zeta,\Phi,\Psi) = ½\,(1+\cos^2\zeta)\cos2\Phi\cos2\Psi - \cos\zeta\sin2\Phi\sin2\Psi \quad (2a)$$

$$F_{\times}(\zeta,\Phi,\Psi) = ½\,(1+\cos^2\zeta)\cos2\Phi\sin2\Psi - \cos\zeta\sin2\Phi\,\mathrm{cow}2\Psi \quad (2a)$$

It is convenient to represent these functions in three dimensions as beam patterns of a detector, Figs 2a, 2b. From these pictures, it can be seen clearly that beam patterns for tensor cross × and plus + polarization states are different, therefore, an interferometric (two-arms) antenna-detector allows us to distinguish between these polarizations.

Regarding antenna response on a scalar polarization state, which might be longitudinal (SL) or transverse (ST), it can be shown that the functions are different only by a sign Will [2014]:

$$F_{SL}(\zeta,\Phi) = ½\sin^2\zeta\cos2\Phi \quad (3a)$$

$$F_{ST}(\zeta,\Phi) = -½\sin^2\zeta\cos2\Phi \quad (3b)$$

Therefore, beam patterns of an interferometric antenna are the same for scalar longitudinal and transverse polarizations, Fig.2c It means that it is not possible to recognize scalar modes by means of a typical two-arms interferometer.

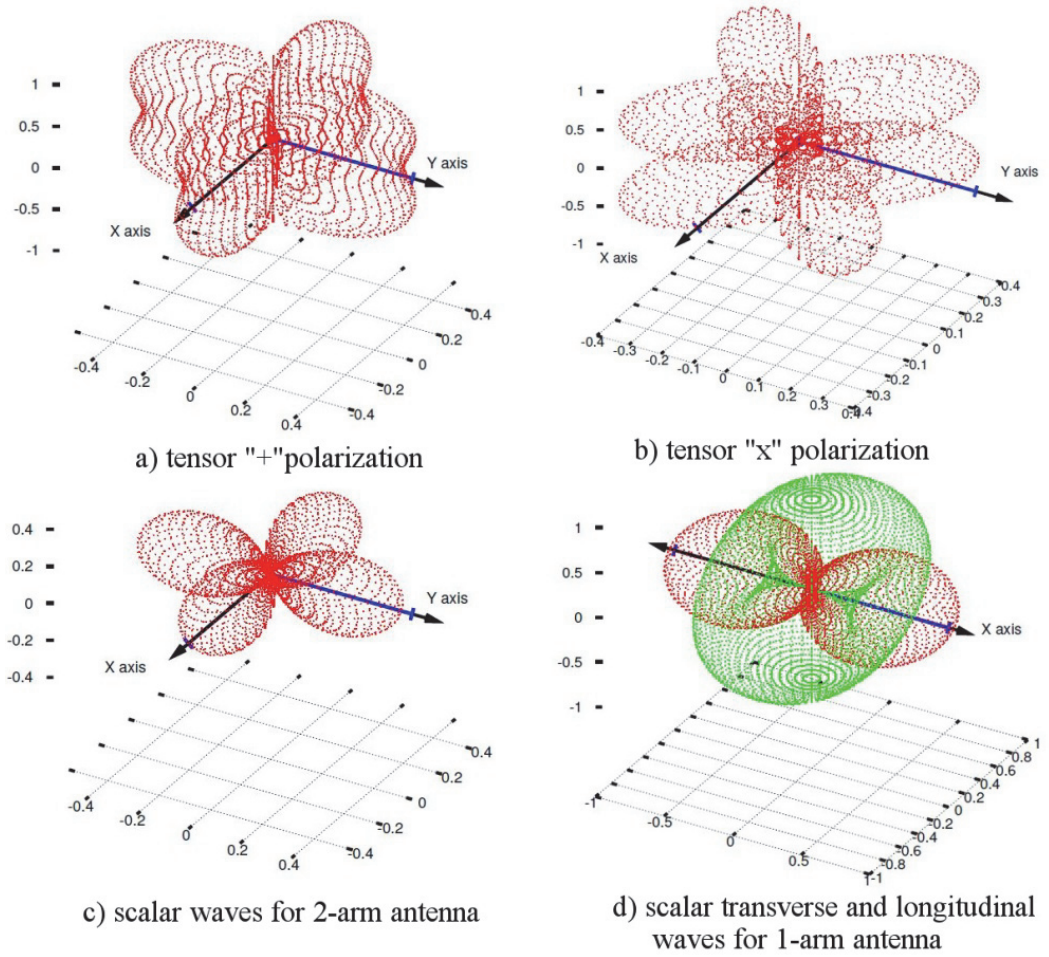

Fig2. *Antenna beam patterns for different polarizations of an incoming GW. Blue lines indicate the arms of the detectors along the X and Y axis. Red points are the beam pattern depending on the location of a GW source on the sky. Green points in (2d) are the antenna response for scalar transverse wave in the case of one-arm mode.*

3.2. Antenna-response functions of one-arm interferometric antennas

To tackle the problem of indiscernibility between scalar longitudinal and transverse modes by a two-arms interferometer, there has been proposed a modification of an interferometric detector as one-arm antenna (one-arm mode) having one working arm with two test masses Baryshev and Paturel [2001]. Then, the observed strain is given by the length change of the working arm (X-axis) relative to the length L_0 of the fixed (former Y-axis) arm: $\Delta L(t) = L_X - L_0$. The amplitude of the arm-length variation $h^0 = \Delta L_{max}/L_0$ can be used as a normalization constant.

The antenna-response functions for scalar longitudinal and transverse modes are the following (Baryshev and Paturel [2001]):

$$F_{SL}(\zeta,\Phi) = \cos\Theta = \sin\zeta\cos\Phi \tag{4a}$$

$$F_{ST}(\zeta,\Phi) = \sin\Theta \tag{4b}$$

where Θ is the angle between the direction of a GW propagation and X-axis of the antenna, Fig1.

The beam-patterns are depicted in Fig. (2d), where the red points indicate the response of the antenna on the scalar longitudinal and the green – on the scalar transverse. Thereby, applying one-arm modification of the interferometric antenna, it is possible to recognize scalar longitudinal and transverse polarization modes.

4. Method description

The proposed method for source localization is based on the considered properties of antenna-response functions and the possibility to recognize a polarization state of an incoming GW. The method uses the value of the maximal amplitude of the detected strain *h(t)* at each antenna in the network during so-called "pre-coalescence" phase, sidereal time (ST) of the signal arrival, time delay Δ between signal registration at the antennas as well as the position of antennas in the equatorial CS.

The detected time delay Δ between registrations determines a radius of an apparent circle (hereafter AC) on the unit sky sphere, along which the source of GW might be located. The centre of the AC is defined by the direction of the vector joining the two antennas at the sidereal time (ST) of the event. In the equatorial CS, each point at the AC is defined by right ascension (RA) α and declination (DEC) δ. Regarding the detector, the considered point as possible source S has horizontal coordinates: zenith angle ζ and azimuth Φ, Fig1. The antenna-pattern functions $F(\zeta,\Phi,\Psi)$ are different for distinct antennas in the network.

Table 1. *Detection parameters of LIGO events. ST is the sidereal time of the event, h0 – the strain as the maximal amplitude normalized by 10-21, ΔLH – the time delay between registrations at Livingston and Hanford antennas. ST is the sidereal time of the event given in hours.*

GW event	(UTC)	ST	Δ_{LH} [ms]	h^0
GW150914	(09:50:45)	3.33	$6.9^{+0.5}_{-0.4}$	0.6
LVT151012	(09:54:43)	5.24	– 0.6±0.6	0.3
GW151226	(03:38:53)	3.89	1.1±0.3	0.3
GW170104	(10:11:59)	11.1	$-3.0^{+0.4}_{-0.5}$	0.3

A typical detected strain *h(t)* can be theoretically decomposed into the purely time-dependent part, which is a waveform *s(t)*, and time-independent part or geometrical factor $G(\zeta,\Phi,\Psi)$, which depends only on the position of the source in the horizontal CS of an antenna.

$$h(t) = \frac{\Delta L(t)}{L_0} = h^0 s(t) G(\zeta, \Phi, \Psi) \tag{5}$$

where h^0 is the amplitude of the signal.

The geometric factor $G(\zeta,\Phi,\Psi)$ is determined by the relative orientation of an antenna with respect to the position of the source on the sky at the sidereal time (ST) of the detection, angles (ζ,Φ), as well as by the polarization angle Ψ for tensor GW. In the particular case of an incoming GW in a single polarization mode, the G-factor is equivalent to the antenna-pattern function ($G \equiv F$) for this mode. In a general case, the G-factor represents a composition of antenna-pattern functions F weighted by coefficients identifying the entering polarization states (1).

Regarding the time-dependent part of a strain, it is worth to mention that the normalized waveform *s(t)* depends only on the nature of the source and, consequently, is the same at each antenna in the network for a particular GW event.

Then the following relation holds at the fixed sidereal time:

$$\frac{h_1}{h_2} = \frac{G_1}{G_2} = \frac{G(\zeta_1,\Phi_1,\Psi_1)}{G(\zeta_2,\Phi_2,\Psi_2)} \tag{6}$$

where "1" and "2" indicate the values related to the considered antennas.

Thus, the calculated ratio of G-factors G_1/G_2 for a certain point on an AC predicts the ratio of the strains h_1/h_2, which should be observed in the case of an incoming GW of a certain polarization state. In other words, it means that a point at the AC being the real source of a GW of a certain polarization should produce the ratio of geometrical factors, which is equal to the ratio of the strains h_1/h_2. Therefore, it is possible to highlight such points on the AC, where the calculated G_1/G_2 is approximately equal to the observed h h_1/h_2. This is the main principle of the method.

It is important to emphasize that the detected strain ratio does not depend on the nature of the source but only on the antenna position relative to the source and polarization state of the incoming GW.

5. Application of the method for the source localization of events

In order to show the method application, let us consider three GW events 2015: GW150914, GW151226 and LVT151012 (Abbott et al. [2016a]), as well as the event GW170104. The used data are given in Table1. For the reported GW events, there were only two antennas in operation: LIGO Hanford and Livingston. The time delay ΔLH between the signal registration at these antennas together with the sidereal time ST of the event determine the AC on the sky, along which the GW sources will be searched.

To select the points of possible GW localization for each event, there should be calculated the G-factors and their ratio for the assumed polarization states of the GWs and compared with the observed ratio of the strains at the antennas couple. The points, for which the ratio G_L/G_H for the considered polarization states is approximately equal to the observed h_L/h_H with the error of observations ≈ 1.0 ± 10%, are highlited by red in Fig. 3 for a tensor transverse plus polarization and for scalar polarization.

5.1. Representation of the results in the supergalactic CS

Besides the most common representation of the GW source localization in the equatorial CS, there can be taken into account other coordinate systems, which are capable to show the possible coincidence of the source localization with the galaxies distribution.

In particular, there has been introduced the supergalactic (hereafter SG) coordinate system (see eg., Courtois et al. [2013]) for the convenience of considering the Local Super-Cluster of galaxies (hereafter LSC). The LSC has the _lamentary disc-like structure with the radius ~ 100 Mpc, the thickness ~ 30 Mpc and the centre roughly in the Virgo cluster (*SGL* = 104º; *SGB* = 22º), and the North Pole *SGB* = 90º with galactic coordinates *l* = 47.37º, *b* = 6.32º (Courtois et al. [2013], de Vaucouleurs [1953], de Vaucouleurs [1958], di Nella and Paturel [1995]).

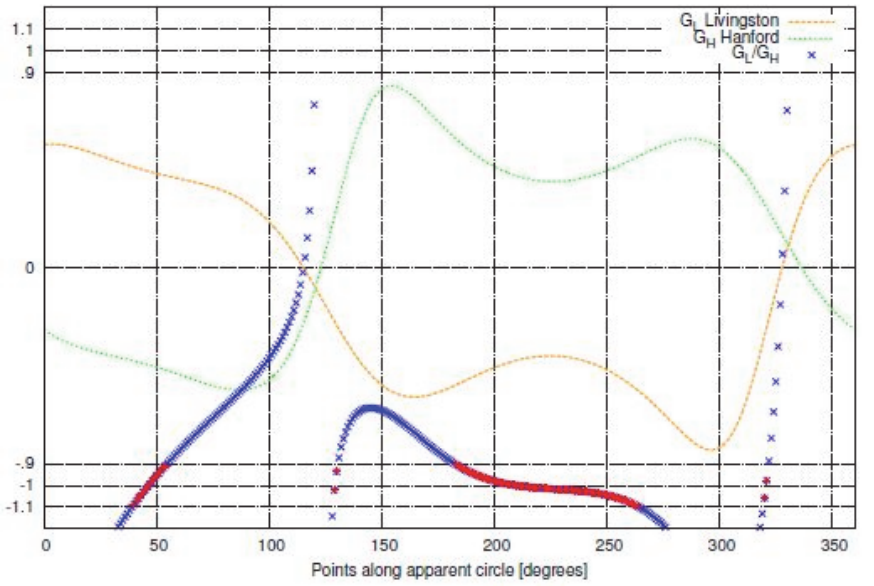

for tensor "+" GW

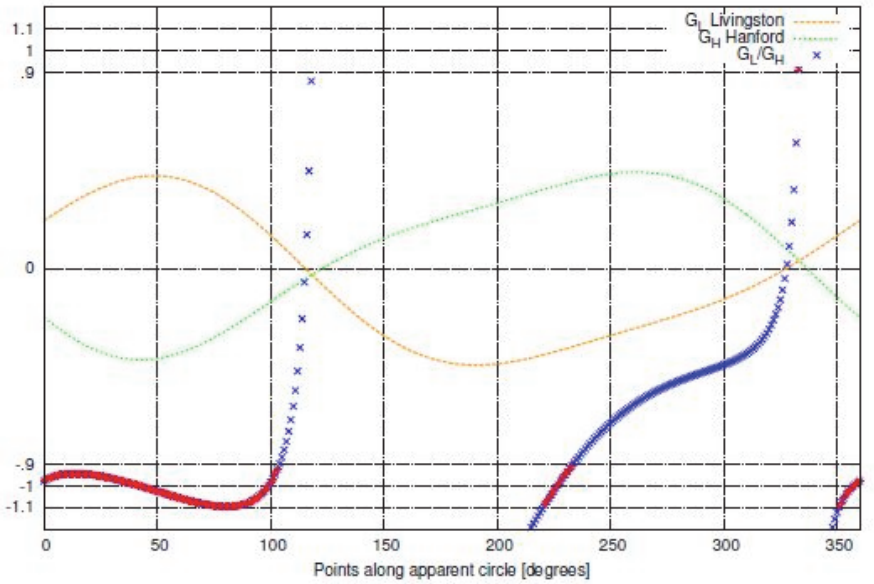

for scalar (transverse or longitudinal) GW

Fig3. *G-factors for possible polarization states of GW150914. The orange and green thin curves represent the G-factors along the AC calculated with LIGO Livingston and Hanford coordinates respectively. Blue dots curve shows the ratio GL/GH. The allowable places of the GW source are highlighted by red corresponding to the condition GL/GH ≈ 1 ± 10%.*

In Figs. (4, 5) the LSC is represented in SG CS with the background projection of the 2MRS catalogue of galaxies, which is the result of the 2MASS all-sky IR survey (Huchra et al. [2012]) and includes the redshifts of 43 533 galaxies. There have been taken the subsample containing 32 656 galaxies with $z \leq 0.025$, which corresponds to the spatial distribution of the galaxies within ~ 100 Mpc known as the Local Super-Cluster or Laniakea Super-Cluster or Home Super-Cluster (hereafter LSC, de Vaucouleurs [1958], di Nella and Paturel [1995], Tully et al.).

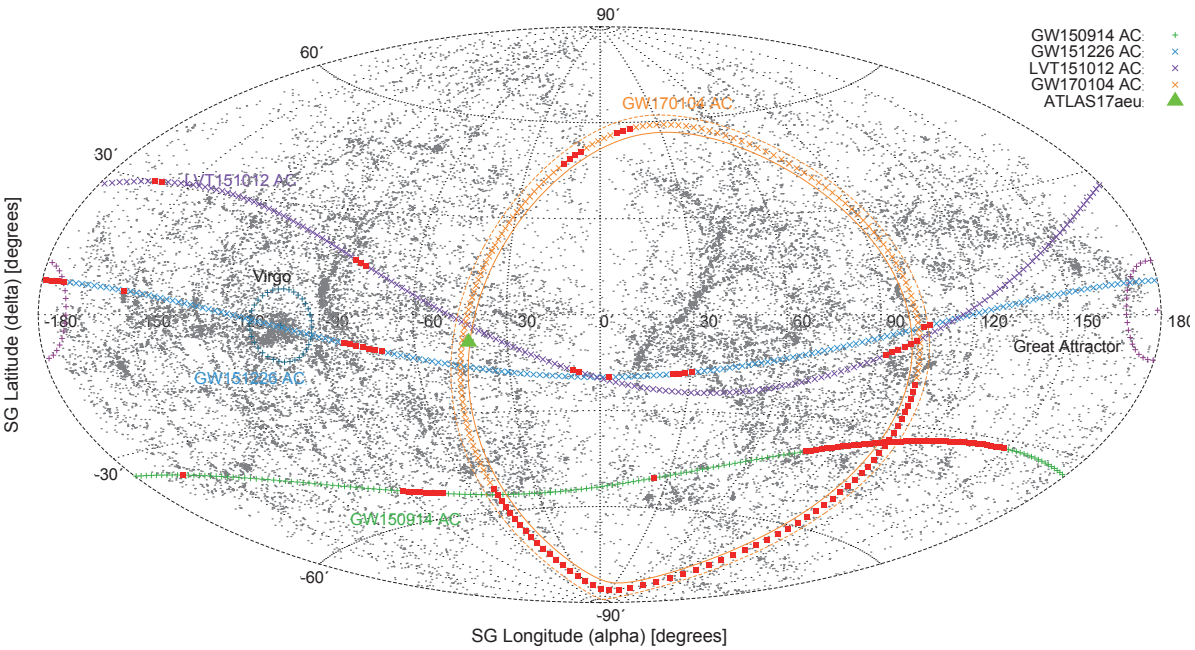

Figure 4: *ACs for LIGO events in supergalactic coordinates. The red points corresponding to the condition $G_L/G_H \approx 1 \pm 10\%$ represent the allowed source positions in the case of tensor "+" ($\Psi = 0$) incoming GW. The green triangle denotes the possible optical counterpart ATLAS17aeu for the GW170104.*

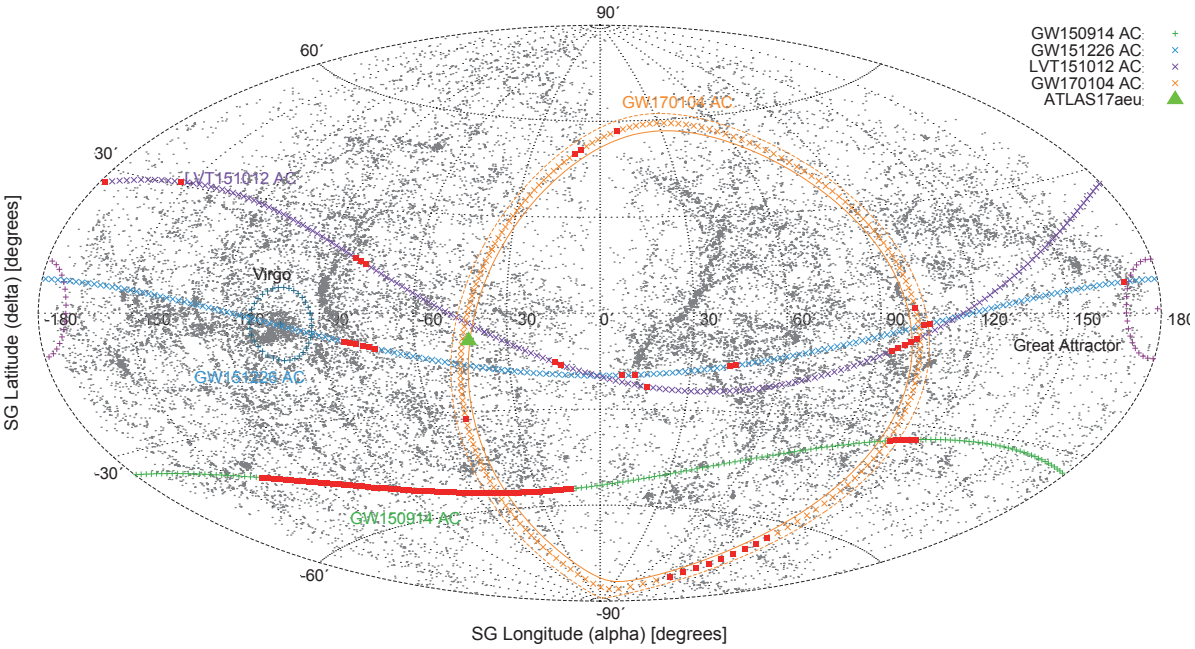

Figure 5*: ACs for LIGO events in supergalactic coordinates. The red points corresponding to the condition $G_L/G_H \approx 1 \pm 10\%$ represent the allowed source positions in the case of scalar (transverse or longitudinal) incoming GW. The green triangle denotes the possible optical counterpart ATLAS17aeu for the GW170104.*

The results of the construction of ACs in SG CS together with the predicted by the method GW source localization (red points) are shown in Fig. (4) for the scalar (longitudinal or transverse) and on the Fig. (5) – for the tensor plus ($\Psi = 0$) polarization of an incoming GW. Interestingly, the ACs for all GW events detected in 2015 lie along the supergalactic plane of

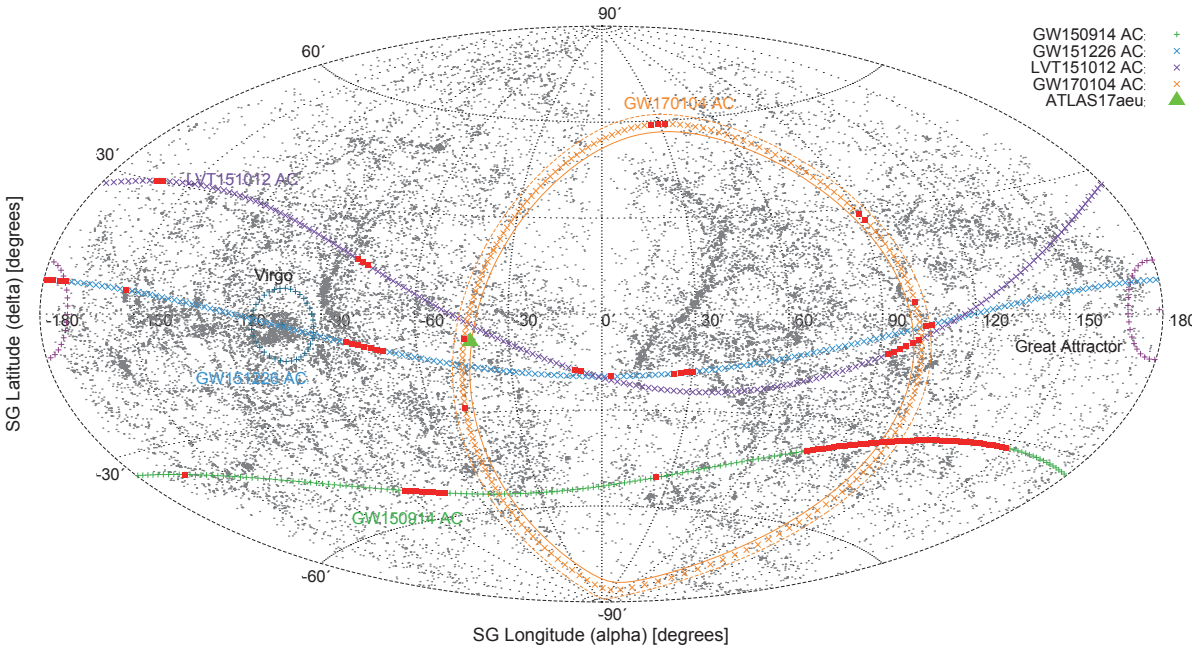

***Figure 6**: ACs of the predicted source positions for LIGO events in the case of tensor transverse GW ($G = 1.5F_+ + \sqrt{2}\,F_\times$) in SG coordinates. Red points correspond to the condition $G_L/G_H \approx 1 \pm 10\%$. The green triangle denotes the possible optical counterpart ATLAS17aeu for the GW170104.*

the LSC with a range of possible positions within ±30º SGB. This fact may witness that the possible GW sources are capable to belong to the LSC, i.e. on the distances less than 100 Mpc, which contradicts the currently accepted assumption about these sources as binary coalescences at the distances 400 – 1000 Mpc (Abbott et al. [2016a]). Nevertheless, if such a correlation between the positions of ACs and the SG plane is confirmed by the forthcoming GW observations, it should be also necessary to consider alternative mechanisms of the original GW radiation. For instance, in the context of scalar-tensor metric theories as well as the field gravitation approach, some authors (Novak and Ibanez [2000], Maggiore and Nicolis [2000], Coccia et al. [2004], Maggiore [2006], Baryshev, Yu. V. [1990]) predict existence of a scalar GW radiation from a symmetric core-collapse Supernova (CCSN).

The detected GRB-like afterglow ATLAS17aeu as a possible counterpart event of the GW170104 is indicated by the green triangle. The AC of the GW170104 is depicted taking into account the error in the determination of the time delay ±0.5 ms, Table1, which allows us to represent the realistic possible area for the forthcoming search of electromagnetic transients for this event. Besides this, Fig. (6) presents the case of a mixture of tensor transverse modes with $G = 1.5F_+ + \sqrt{2}F_\times$, where the covering area is coincide with the position of the ATLAS17aeu. Thereby focusing on the fact that there may exist such polarization states of an incoming GW providing various localization areas including those within the SG plane.

6. Conclusions

We have presented the new method for a GW source localization on the sky in the case of a GW detection by two interferometric antennas. The method is based on the antennas beam patterns for a supposed polarization state of the incoming GW together with the measurements of the arrival time delays between antennas and the ratio of the detected strains at each antenna.

It has been shown that a network of LIGO-type two-arm antennas can distinguish between tensor and scalar, but not between scalar longitudinal and transverse polarizations, which is possible by means of one-arm interferometric (as well as bar) detectors.

We have demonstrated that there is an interesting possibility for the polarization state recognition by means of actual localization on the sky a GW source. For this purpose, there has been considered a network of three antennas LIGO-Virgo. The theoretical conclusions concerning beam patterns for different polarization states were applied to the calculations of the strain ratio for each antenna couple in order to offer a test on the polarization state of the GW coming from a definitely located source.

For three aLIGO events: GW150914, GW 151226 and LVT151012, the apparent circles of the allowed GW source positions are parallel to the supergalactic (SG) plane of the Local Super-Cluster of galaxies. Such fact indicates that GW sources of these events might belong to this structure. It is worth noting that if the detected three events did not belong the LSC, then we would have a rare chance of accidentally correlated direction of GW sources positions on the sky, especially for the sources at very high distances such the currently proposed 400 – 1000 Mpc for the LIGO events 2015 (Abbott et al. [2016a], Abbott et al. [2016b]). Moreover, if these GW sources are related to the LSC, then we have to consider distances to them within ~ 100 Mpc.

Interestingly, for the new aLIGO event GW 170104, the apparent circle is perpendicular to the supergalactic equator with only some parts within SG plane (±30º SGB), nevertheless the possible optical counterpart ATLAS17aeu to this event (Stalder et al. [2017]) belongs to the Local Super-Cluster plane, which is also consistent with our supposition about the special role of the LSC.

The next aLIGO observing runs are proposed to test the reality of clustering the GW events along the SG plane. Future identification of GW sources with electromagnetic counterparts is crucial for the physics of the gravitational interaction. Especially, follow-up observations are of great importance for the fundamental physics and they should take into account the experience in GRB optical identification.

Acknowledgements

This work was supported by the Saint Petersburg State University.

References

B. P. Abbott et al. Observation of Gravitational Waves from a Binary Black Hole Merger (LIGO and Virgo Scienti_c Collaboration). *Phys. Rev. Letters*, 116(061102), 2016a. doi: 10.1103/PhysRevLett.116.061102.

Benjamin P. Abbott et al. The basic physics of the binary black hole merger GW150914 (LIGO and Virgo Scientific Collaboration). *Annalen Phys*., 2016b. doi: 10.1002/andp.201600209.

Yu. V. Baryshev and G. Paturel. Statistics of the detection rates for tensor and scalar gravitational waves from the local galaxy universe. *Astron. Astrophys*., 371:378, 2001. doi: 10.1051/0004-6361:20010349.

Yurij V. Baryshev. Foundation of relativistic astrophysics: Curvature of Riemannian Space versus Relativistic Quantum Field in Minkowski Space. 2017.

Baryshev, Yu. V. *Introduction to the tensor _eld theory of gravitation*. Saint Petersburg State University (unpubl.), 1990.

Eugenio Coccia, Florian Dubath, and Michele Maggiore. On the possible sources of gravitational wave bursts detectable today. *Phys. Rev.*, D70:084010, 2004. doi: 10.1103/PhysRevD.70.084010.

Helene M. Courtois, Daniel Pomarede, R. Brent Tully, and Denis Courtois. Cosmography of the Local Universe. *Astron. J.*, 146:69, 2013. doi: 10.1088/0004-6256/146/3/69.

G. de Vaucouleurs. On the distribution of mass and luminosity in elliptical galaxies. *MNRAS*, 113:134, 1953. doi: 10.1093/mnras/113.2.134.

G. de Vaucouleurs. Further evidence for a local super-cluster of galaxies: rotation and expansion. *Astronomical Journal*, 63:253, July 1958. doi: 10.1086/107742.

H. di Nella and G. Paturel. Possible Connection Between Largescale Structures. *Proceedings of the Astronomical Society of Australia*, 12:26, April 1995.

D. M. Eardley, D. L. Lee, A. P. Lightman, R. V. Wagoner, and C. M. Will. Gravitational-wave observations as a tool for testing relativistic gravity. *Phys. Rev. Lett*., 30:884{886, 1973. doi: 10.1103/PhysRevLett.30.884.

A. Einstein. Approximative Integration of the Field Equations of Gravitation. *Preuss. Akad. Wiss. Berlin, Sitzber*., 688, 1916.

R. Feynman. *Lectures on Gravitation*. California Institute of Technology, 1971.

R. Feynman, F. Morinigo, and W. Wagner. *Feynman Lectures on Gravitation*. Addison-Wesley Publ. Comp., 1995.

S. W. Hawking and W. Israel. *Three Hundred Years of Gravitation*. Cambridge University Press, 1989.

J. P. Huchra et al. The 2MASS Redshift SurveyDescription and Data Release. *The Astrophysical Journal Supplement*, 199: 26, April 2012. doi: 10.1088/0067-0049/199/2/26.

L. D. Landau and E. M. Lifshitz. *The Classical Theory of Fields*. Nauka, fourth edition, 1988.

Michele Maggiore. Gravitational waves and fundamental physics. In *Sense of Beauty in Physics: Miniconference in Honor of Adriano Di Giacomo on his 70th Birthday,* Pisa, Italy, January 26-27, 2006, 2006.

Michele Maggiore and Alberto Nicolis. Detection strategies for scalar gravitational waves with interferometers and resonant spheres. *Phys. Rev*., D62:024004, 2000. doi: 10.1103/PhysRevD.62.024004.

C. Misner, K. Thorne, and J. Wheeler. *Gravitation*. Freeman and Company, Physics Series, 1973.

Jerome Novak and Jose M. Ibanez. Gravitational waves from the collapse and bounce of a stellar core in tensor scalar gravity. *Astrophys. J.*, 533: 392-405, 2000. doi: 10.1086/308627.

B. Stalder et al. Observations of the GRB afterglow ATLAS17aeu and its possible association with GW170104. *Astrophys. J*., 850(2):149, 2017. doi: 10.3847/1538-4357/aa95c1.

R. B. Tully et al. The Laniakea supercluster of galaxies. *Nature*.

M. Will. The Confrontation between General Relativity and Experiment. *Living Rev. Relativity*, 17(4), 2014.

GW170104 optical counterpart and possible scenarios of gravitational waves generation

Liudmila Fesik[1]

[1]Saint-Petersburg State University, Saint-Petersburg, Russia; lucia555@yandex.ru

Abstract The gravitational wave event GW170104 detected by aLIGO is of an especial interest for a range of reasons. Firstly, it provides a test on different mechanisms of GW radiation. Besides the most common view on the GW source as a coalescing binary, in this work has been considered the scenario for a core-collapse supernova including a spherically-symmetric one and a massive supernova proposed by Imshennik and Nadezhin. The theoretical predictions have been applied to estimate physical parameters of such objects in order to provide the criteria for the electromagnetic transients search. Secondly, there has been used the proposed by authors method for source localization based on the construction of an apparent circle (AC) on the sky together with the beam pattern to the polarization state of an incoming GW. Interestingly, the AC for GW170104 is perpendicular to the Local Super-Cluster plane with some parts within it. Thus, the predicted positions of the source may belong to the LSC plane, which is consistent with detection of possible optical counterpart ATLAS17aeu.

Keywords: Gravitational Waves, Localization of GW, GW Sources, Optical Counterparts

1. Introduction

Despite the fact that GW radiation was theoretically predicted by A. Einstein as far back as 1916, the question about a practical detection of GWs remained open for decades (Rudenko, V. N. [2017]). The GW radiation should be powerful enough to give amplitude necessary for the detection by the currently working gravitational-waves antennas. Given the current sensitivity of the modern interferometric antennas, the most promising for being detectable are GWs from compact binary coalescence (CBC) and core-collapse supernovae (CCSN). The possibility of detecting waves from each kind of sources depends on the energy radiated in GWs, the distance to the object, the pulse duration and the frequency.

Examining the possible nature of the sources of the LIGO events, there is analyzed the prediction of the existence of scalar wave from a CCSN. Firstly, it is motivated by the possibility of the sinusoidal signal similar to the detected ones, due to spherically symmetric core pulsations. While the tensor waveform by asymmetric collapse is expected to be more complex (see eg., Hawking and Israel [1989], Thorne [1989]). Secondly, as will be shown, the radiated energy as a result of the CCSN is estimated to be orders of magnitude more than ones due to the asymmetric collapse. Consequently, it is possible to detect the GWs from CCSN by the antennas of the current sensitivity ($h \sim 10^{-23}$, LIGO and Virgo) at the distances up to 100 Mpc.

2. Possible sources of GW radiation

Compact binary coalescence (CBC) is a class of GW sources with two relativistic compact objects (hereafter RCOs) on a common orbit. Gravitational radiation during the orbital motion of such objects "takes away" from the system both the energy and the angular momentum, which causes a decrease in orbital radius up to the merger into one RCO. This class of GW sources is of particular interest because the stage of the orbital motion just prior to the merger – the so-called "inspiral" phase can be accurately modeled, which makes the predictions about the waveform and the frequency of a GW signal depending on the masses of the incoming objects. Therefore, observations of CBC can provide us with an excellent test of gravitation theories. In the case of identification of a GW event with its counterpart in the EM branch, it is possible to determine the position of the GW source as well as the distance to it precisely.

Another type of GW events is connected with the explosions of massive supernovae. GW radiation arises as a result of the gravitational collapse of the degenerate core of the star in the late stages of its evolution, resulting in the formation of a compact object such as a neutron star or RCO. In this case, a huge amount of energy is released, of the order of $M_{\odot}c^2$, most of which is carried away by neutrinos and some (still undetermined) portion – by GWs.

An important scenario of the core-collapse of a massive supernova was proposed in the works of Imshennik and Nadezhin (Imshennik [2010]): due to a strong rotation of the core, there firstly occurs the formation of an RCO binary radiating tensor GWs, and then merging into a single RCO with the possible scalar GW radiation.

Although supernovae may be a powerful source of gravitational radiation, up to now there are many uncertainties in the modeling of the collapse mechanism itself. Therefore, it is difficult to make sufficiently reliable assumptions about the amplitude and the waveform of a GW from a supernovae (Thorne [1989], Maggiore [2006], Coccia et al. [2004], Burrows [2013]). Massive supernovae can differ greatly in the nature of the processes occurring in them but for the purposes of GW study, the SN bursts are divided into two types: those resulting from an asymmetric collapse of the core (in the GR) and others as a result of a spherically symmetric core-collapse (in the scalar-tensor theories of gravitation). In addition, the speed of rotation and the presence of a magnetic field should be taken into account. The modern theories of CCSN make it possible to explain the stages of the evolution of a massive star before and after an explosion but there is still no theory that would explain accurately the relativistic collapse stage itself in order to calculate the energy of GW radiation and the observed waveform (see eg. discussion Imshennik [2010], Burrows [2013]). This uncertainty motivates the further studying of the detected GW events from the point of view of the possible origin of such a signal from a collapsing supernova such as CCSN.

The importance of a separate consideration of these types lies in the fact that according to the GR, tensor waves can arise only from an asymmetric collapse (Misner et al. [1973]), whereas both the scalar-tensor metric theories and the FGT predict the existence of a scalar GW mode, which may occur as a result of a spherically-symmetric core-collapse (CCSN) (Novak and Ibanez [2000], Maggiore and Nicolis [2000], Coccia et al. [2004], Maggiore [2006], Baryshev, Yu. V. [1990], Baryshev [2017]).

3. Search for the follow-ups

The detection of transients accompanying a GW signal in the electromagnetic (hereafter EM) branch of the spectrum is of fundamental importance in the analysis of GWs physics.

Firstly, the identification of the detected GW signal with an EM counterpart will increase the confidence that there has occurred a real astrophysical event. Secondly, the joint GW and EM observations complement each other significantly in the understanding of the causing physical processes. The form of a GW signal as well as its frequency, amplitude and polarization state may provide the specific information about the mass motions necessary for the source simulation. While the identification of the GW signal with an EM transient gives it possible to estimate the physical parameters of the environment surrounding the RCO, as well as to localize the source on the sky with the calculation of the distance to it.

According to the GRT, the black holes coalescence in the vacuum does not produce any EM radiation. The same is true for the case of such a merger in the interstellar medium, where the gas density and the magnitude of the magnetic fields are too small to give a noticeable EM "follow-up". However, the RCOs coalescence in clusters, dense molecular clouds and in galactic centers may have some peculiarities in the EM spectrum due to the interaction with gas and magnetic fields.

In the case when a CBC includes at least one neutron star (or an RCO without the events horizon Sokolov and Zharykov [1993], Sokolov [2015], Baryshev [2017]), it can produce the EM radiation in a wide range of wavelengths and on different time scales. Thus, a number of studies has shown (Piran [2004], Nakar [2007]) that there may be expected the short-hard gamma-ray bursts (hereafter SGRBs) with the duration of 2 seconds or less from NS-NS and NS-BH CBCs. In the review (Lipunov and Panchenko [1996]) has been discussed that there may present short radio or optical non-thermal radiation from CBCs including at least one magnetic NS.

Another class of objects expected to give the GW radiation is the CCSN, which may produce the long-soft gamma-ray bursts (LGRBs) (Woosley [1993], MacFadyen and Woosley [1999], Piran [2004]).

4.1. Energy and amplitude estimations for CCSN

According to the theoretical predictions, the tensor GW can be radiated only due to an asymmetric or axisymmetric core-collapse supernova (see eg., Hawking and Israel [1989], Thorne [1989]). However, despite the long-term theoretical study of the gravitational core-collapse of the stars, there is still no reliable estimates of the rate of asymmetry in such processes, which in turn causes uncertainty in the estimates of the radiated energy in the form of GWs.

Thus, studying the dynamics of the asymmetric collapse of the rotating SN core, the authors, Zwerger and Mueller [1997], came to the conclusion that the energy released into the GW is around $E_{GW} = 10^{-11} - 10^{-8}\ M_{\odot}c^2$, which corresponds to the amplitude of the tensor wave $4 \cdot 10^{-25} \leq h \leq 4 \cdot 10^{-23}$ from the source at the distance 10 Mpc. To a similar result came Bonazzola et al. [1993] for the case of an axisymmetric rotating core with the asymmetry rate $s < 0.1$. On the other hand, examining a fast-rotating core-collapse, Stark and Piran [1985] have given an estimate of the energy radiated in the "+" or "×" polarization mode as $E_{GW} \leq 10^{-3} M_{\odot}c^2$.

Scalar-tensor metric theories predict apart from tensor waves, the presence of the scalar radiation, which may arise as a result of the spherically-symmetric Core Collapse Supernova (CCSN) (Novak and Ibanez [2000]). In this case, the GW energy is expected to be up to $E_{GW} \leq 10^{-3}\ M_{\odot}c^2$.

In this way, despite the uncertainty in the explosion mechanism itself, the estimations of the energy emitted in scalar GWs as a result of a spherically-symmetric CCSN are on

average by an order of the magnitude higher than such estimations for tensor GWs by an asymmetric or an axisymmetric rotating collapse. In both cases, the duration of a pulsation is estimated to be of the order of 0.5 – 5 ms, the duration of the whole pulse – 1 ms, and the GW frequency is around f ≈ 10^2 – 10^3 Hz (Zwerger and Mueller [1997]).

A typical GW signal from a CCSN pulsation can be represented as a unit pulse with the amplitude h_0, the frequency f_0 and the total duration τ. There can be estimated the characteristic amplitude of the scalar GW from a typical CCSN burst at the distances at around ~ 1 Mpc, with the duration τ = 0.1 s and emitted during this time the energy ΔE_{GW} = 10^{-3} $M_\odot c^2$ at the frequency f = 100 Hz:

$$h_0^{sc} \approx 1.36 \cdot 10^{-20} \left(\frac{\Delta E}{10^{-3}}\right)^{\frac{1}{2}} \left(\frac{0.1s}{\tau}\right)^{\frac{1}{2}} \left(\frac{100Hz}{f}\right) \left(\frac{1Mpc}{r}\right) \quad (1)$$

While the tensor GW strain (from an asymmetric CCSN) is expected to be approximately 2 times less (see eg., Schutz and Ricci [2010]):

$$h_0^{tens} \approx 6 \cdot 10^{-21} \left(\frac{\Delta E}{10^{-3}}\right)^{\frac{1}{2}} \left(\frac{0.1s}{\tau}\right)^{\frac{1}{2}} \left(\frac{100Hz}{f}\right) \left(\frac{1Mpc}{r}\right) \quad (2)$$

Thus, with the considered parameters, the emitted GW of both kinds of polarization give the strain large enough to be detected by the modern interferometric antennas LIGO, Virgo with the current sensitivity threshold ($h \approx 10^{-23}$, Abbott et al. [2016]).

In contrast to the most common view regarding the mechanism of the CCSN in the frames of GRT and the scalar-tensor metric theories, in the FGT approach (Baryshev [2017]), the upper limit on the radiated in GW energy is established only by the mass of the object itself, which may amount to the several solar masses.

It can be shown that the characteristic amplitude of the scalar wave from a source at the distance of ~ 100 Mpc with the GW energy of the order of several solar masses is:

$$h_0^{sc} \approx 4.34 \cdot 10^{-21} \left(\frac{\Delta E}{M_\odot c^2}\right)^{\frac{1}{2}} \left(\frac{0.1s}{\tau}\right)^{\frac{1}{2}} \left(\frac{100Hz}{f}\right) \left(\frac{1Mpc}{r}\right) \quad (3)$$

Thus, the GW from a CCSN at the distance r = 100 Mpc radiating GW with the energy $\Delta E_{GW} \sim 10^{-2}$ $M_\odot c^2$ is expected to give the detected strain $h \approx 0.5 \cdot 10^{-21}$.

Comparing the results for the scalar-tensor radiation from CCSN in the frames of both the metric gravitation theories and the FGT, the following conclusion can be made. In contradistinction to the tensor-scalar metric theories, there is no absolute restriction on the radiated into GW energy in the FGT. This allows one to consider the objects as GW sources at farther distances and, consequently, with larger total masses, which might provide corresponding energy on the GW radiation. That in turn establishes the lower limit on the rest mass of the SN collapsing core. Identifying the GW signal as the CCSN, for instance, by the analysis of the follow-up events in the electromagnetic spectrum, the relationship (3) suggests a test for the existence of such objects as supermassive SN. Thus, with the known distance to the object from the EM observations of the transient, and with the detected GW amplitude, it is possible to estimate the energy radiated into GW in the units of solar masses.

Further in this work, there will be given the analysis of the LIGO events in 2015 – 2017 to get estimates on the possible physical parameters of such a CCSN.

4.2. Scalar wave from CCSN in the FGT

As has been discussed, as a result of a spherically-symmetric core-collapse SN, there is predicted the scalar GW radiation (see review Baryshev [2017]). In this case, the expected signal might be in the form of a sinusoidal pulse with the increasing frequency of the pulsations. Further discussion is motivated by the LIGO observations in 2015, which is a fairly correct sinusoidal pulse with the known average frequency and amplitude. In this part will be considered the general relations between the detected values of a GW signal: its "strain" h, (average) period P_0, average frequency f_0, and the physical parameters of the pulsating object: its density P_0, radius R_0, as well as the distance r to the object.

For a CCSN with the characteristic period of the pulsations $P_0 \sim 1/f_0 \sim 1/\sqrt{G\rho_{eff}}$ (Baryshev, Yu. V. [1990]), there can be determined the effective density ρ_{eff} taking into account the inhomogeneity of the mass distribution along the radius of the object:

$$\rho_{eff} \sim \frac{1}{P_0^2 G} \tag{4}$$

Let us introduce the parameter characterizing the relationship between the effective density ρ_{eff} and the average density $\rho_0 = M_0 \left(\frac{4}{3}\pi R_0^3\right)$, where R_0 is the radius of the object, and M_0 – its (average) mass.

$$\gamma = \frac{\rho_{eff}}{\rho_0} \tag{5}$$

The next parameters can be introduced: α characterizing the pulsations velocity $v_0 \sim R_0/P_0$ relative to the speed of light c, and β – for the ratio of the average radius R_0 of the object to its gravitational radius R_G:

$$\alpha = \frac{v_0}{c} \tag{6a}$$

$$\beta = \frac{R_0}{R_G} \tag{6b}$$

The compatibility condition for the entered parameters can be written as:

$$\frac{\gamma}{\beta} = \frac{4}{3}\pi\alpha^2 \tag{7}$$

which means that the relationship γ/β can be determined by the known or estimated parameter α. The parameter limiting conditions: $0 \le \alpha \le 1$; $0 \le \gamma \le 1$; $\beta \ge 1$ are presented in ***Fig1***.

The amplitude of a GW at the distance r from the source can be obtained as:

$$h_0 \sim \frac{R_G}{r}\alpha^2 \tag{8}$$

where $R_G = GM_0/c^2$ is the gravitational radius of the collapsing core.

Using the derived above relationships, there can be represented the relation "the distance to the object r – the registered strain h" in the form depending only on the observed period of the pulsations P_0 and the parameter of the changing rate α:

$$h_0 \sim \frac{4}{3}\pi c \cdot \frac{P_0}{r} \cdot \alpha^5 \sim c \cdot \frac{P_0}{r} \cdot \frac{\gamma}{\beta} \cdot \alpha^3 \qquad (9)$$

Thereby, with the observed data h, P_0 and an supposed GW energy ΔE_{GW}, there can be estimated (9) the introduced source parameters α, β, γ connected by the compatibility condition (7). Which give the estimates of the radius R0, mass M_0 and density ρ_0 of the CCSN.

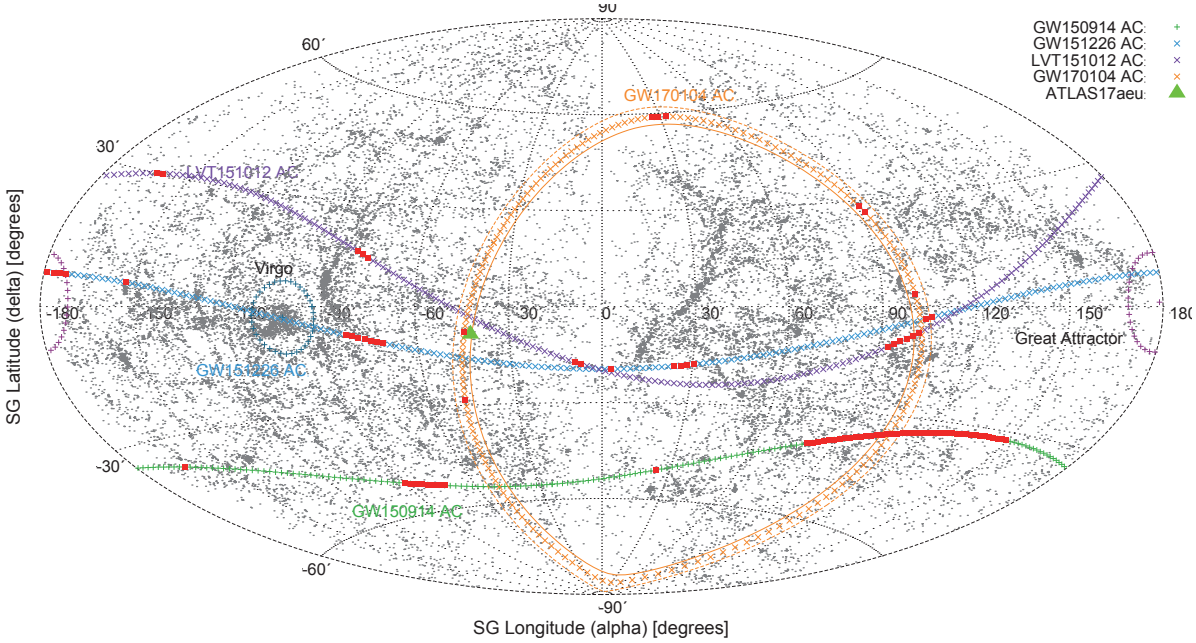

***Fig1**. Possible localization of a GW source along the ACs for the LIGO event GW170104, in the supergalactic CS. The red points corresponding to the condition $G_L/G_H \approx 1 \pm$ 20% represent the allowed source positions in the case of the mixed tensor polarization state ($G = 1.5F_+ + \sqrt{2}\,F_\times$) of the incoming GW calculated by the method (Fesik et al. [2017]). The green triangle marks the position of the possible transient ATLAS17aeu.*

5. Analysis of GW events detected by LIGO in 2015 – 2017

5.1. GW event from Core-Collapse Supernova

According to the considered above approaches to the study of a CCSN, metric and field, there is established a different limit on the radiated into GWs energy. Thus, according to the scalar- tensor metric theories, this limit is estimated to be $\Delta E_{GW} \leq 10^{-3} M_\odot c^2$, while in the FGT, the amount of the radiated energy is limited only by the rest mass of a collapsing, which can amount several solar masses. In this connection, it can be shown what difference is expected in the parameters of a CCSN radiating GWs of different energy, with a frequency and amplitude similar to those detected by LIGO in 2015.

The calculations have been made using formulae (1) for scalar and (2) for tensor GW mode, which illustrate the dependence of the GW amplitude h0 on the distance to the object r for a typical CCSN with radiated GW energy of the order $\Delta E_{GW} = 10^{-3} M_\odot c^2$, according to the discussed above the estimates of the maximal energy possible to be radiated in GWs in the frames of the scalar-tensor metric theories. Besides this, there has been done the calculation for a scalar wave from spherically-symmetric CCSN with the radiation energy $\Delta E_{GW} = 1 M_\odot c^2$, which is possible in the frame of the FGT.

Table 1. *Calculated parameters for a CCSN under the condition that the detected GW signal has average frequency f = 100 Hz. r_1 is the distance to the object corresponding to the detected strain $h = 0.6 \cdot 10^{-21}$ (GW150914), r_2 – to the case of $h = 0.25 \cdot 10^{-21}$ (GW170104). Mass of the Sun $M_\odot \approx 2 \cdot 10^{33}$ g, the gravitational radius $R_G = GM_0/c^2$, and the assumed parameter $\gamma = \rho_{eff}/\rho_0 \equiv 1$ gives the effective density $\rho_{eff} = 0.15 \cdot 10^{12}$ g/cm^3.*

ΔE [$M_\odot c^2$]	r_1 [Mpc]	r_2 [Mpc]	v_0/c	R_0/R_G	$M_0/M_\odot$
10^{-6}	0.72	1.74	0.06	58.44	2.22
10^{-3}	22.88	54.92	0.13	14.68	17.64
1	723.57	1736.57	0.35	3.69	140.08

The average data of the GW signals detected by LIGO in 2015{2017: frequency $f_0 = 100$ Hz, pulse duration $\tau = 0.1$ s. As has been mentioned, with the same detected strain, the GW with higher energy will come from a more distant object. There can be estimated the parameters of a CCSN at such distances, radiating a scalar GW with an average period $P_0 = 1/f_0 = 0.01$ s. The relationship for a CCSN (9) give the parameter $\alpha = v_0/c$ as well as the parameter ratio γ/β (7). The results for typical values of radiated energy: $\Delta E_{GW} = 10^{-6}$; 10^{-3}; $1\ M_\odot c^2$ are given in the Table1. The calculations have been made for the average detected strain values: $h = 0.6 \cdot 10^{-21}$ (GW150914) $h = 0.25 \cdot 10^{-21}$ (GW170104), with the assumed $\gamma \equiv 1$, i.e. $\rho_0 = \rho_{eff} = 0.15 \cdot 10^{12}$ g/cm^3. For these amplitude values, there are no strong differences in the CCSN parameters but the estimated distances to the objects are clearly different: denoted by r_1 and r_2 respectively.

There should be noted that these calculations are model and use average values of the detection parameters without taking into account the variation with the time. To sum up, a CCSN radiating GW with the energy of the order of the solar mass should have a high pulsation rate, a radius close to the gravitational one, and a mass close to the extreme estimates for a massive pre-star of the CCSN, to give a signal with the detected amplitude.

6. Localization for GW170104. Possible transient ATLAS17aeu

In this section, we will discuss an optical event discovered by the ATLAS team to be a follow-up for the GW event GW170104 detected by LIGO on 1 January 2017 at 10:11:59 UTC (Abbott et al. 2017). The alert for the counterparts search was reported 6.6 hours later.

The ATLAS is the Asteroid Terrestrial-impact Last Alert System (Stalder et al., 2017) specializing in the near- Earth survey of asteroids. The ATLAS uses the follow-ups search program Pan-STARRS Smartt et al. [2016]. The ATLAS system comprises two half-meter wide-field telescopes, of which at that time only the Haleakala telescope in the Hawaiian archipelago was in operation.

The observations by the ATLAS team were conducted targeting the fields of the GW170104 localization provided by LIGO. This is the banana shaped skymap with coordinates from RA=108:79, DEC=7:662 to RA=170:55, DEC=72:314 (Fig. 1 in Stalder et al., 2017).

23 hours after the registration of the GW170104, a bright optical transient was detected – ATLAS17aeu – with a rapid decrease in luminosity during the next 2 hours, at the coordinates RA=138.30789, DEC=+61.09267 (09:13:13.89, +61:05:33.6). Besides optics, the ATLAS17aeu was observed in the x-ray by the team Swift (Evans et al. 2017b), as well

as in radio – by the AMI (Arcminute MicroKelvin Imager; Mooley et al. 2017) and the VLA (Very Large Array; Corsi et al. 2017).

In addition, independently of these observations, a gamma burst GRB170105 was discovered by the POLAR group (Marcinkowski et al., 2017), also observed by several satellite missions: AstroSat CZTI (Sharma et al. 2017), Konus-Wind, INTEGRAL SPI-ACS (Svinkin et al. 2017). This gamma burst is considered to be a "long-soft" with the redshift $1 \leq z \leq 2.9$. However, both the localization of this burst and its detection time differ from the localization and time of the optical ATLAS17aeu, which indicates the different origin of their sources.

To sum up, at the present time there is considered the possibility that two astrophysical events: the GW170104 and the optical ATLAS17aeu, both occurred during the day and being spatially close, originate from the same source.

Concerning the nature of the source of this GW event, there is adopted a version about a coalescing binary (CBC) being the most probable source, which may give a quasi-sinusoidal signal similar to the detected by LIGO. Thus, within the framework of the GR, it is assumed that the source of the GW170104 is the CBC BH-BH (comprising two black holes) with masses $20 - 50M_{\odot}$, which are obtained by the analysis of the waveform and frequency of the signal. However, taking into account the field approach to the theory of gravity (the FGT), such masses may belong to RCOs without events horizons, which may provide a sufficient amount of matter to generate the observed optical transient ATLAS17aeu.

It can be noted that in the case of tensor radiation from a source such as a CBC, a combination of tensor modes "+" and "×" is expected to observe. In particular, for tensor waves with some variation of weight coefficients, there is predicted a region of a source localization calculated by the method Fesik et al. [2017], which matches with the position of the possible transient ATLAS17aeu, Fig1.

Besides this, within the framework of the FGT, a possible interpretation of the detected pulsating GW signal is also the existence of a scalar GW with a quasi-sinusoidal waveform from the spherically-symmetric CCSN (Ch. 4). Therefore, considering the localization regions that depend on the assumed polarization state of the GW (Fesik et al. [2017]), it is necessary to take into account the results for both tensor and scalar modes.

Using the method Fesik et al. [2017], there were constructed apparent circles together with the possible localization for the cases of the scalar and the tensor "plus" modes in the supergalactic (SG) CS, taking into account the error in the measurement of the time delay between the signal receiving 3 ± 0.5 ms (see Table1). It should be noted that the coordinates of the optical event ATLAS17aeu are within the SG plane, which is consistent with such an interpretation of the nature of this event as a CCSN in the local super-cluster of galaxies (LSC) at the distances 100 Mpc. The corresponding projections of the positions of galaxies from the 2MRS catalogue are plotted on the map. However, the calculated localization region with the observed strains ratio $h_L/h_H \approx 1 \pm 20\%$ for the assumed scalar polarization mode is located away from the position of the ATLAS17ae, ***Fig. 1***. For the concrete coordinates of the ATLAS17aeu, the method predicts the strains ratio to be $h_L/h_H \approx G_L/G_H = 19.0$.

7. Conclusions

Within the framework of the General Relativity, there exists only tensor GW radiation, which can occur as a result of a compact binary coalescence (CBC) or an asymmetric core-collapse supernova (CCSN). Analyzing the waveform of the LIGO signals in 2015 – 2017, there has been made the conclusion about the nature of all these sources being CBCs.

For such a system, with the registered signal parameters, there can be drawn sufficiently reliable conclusions about the size of the system, the masses of the incoming bodies, the distances to it, and the GW energies. Thus, in the case of the GW150914, the distance to the generating CBC is estimated to be ~ 440 Mpc. An important test of the model of a CBC is the identification of a detected GW event with the optical and X-ray transients, which are possible only in the case of the coalescence of RCOs without the events horizon, which is possible within the frame of the field theory of gravity ("gravidynamics").

In the frame of GTR modifications (the scalar-tensor metric theories), as well as in the field approach to describing gravity (the FGT), there is predicted the existence of scalar GW radiation from a spherically-symmetric pulsating core (CCSN), with the waveform expected to be close to a sinusoidal with a varying frequency similar to the waveform from a CBC. The principal difference between the predictions of the metric theories based on the GR and the FGT is the limit for the radiated in GWs energy. According to the scalar-tensor metric theories, there is presupposed the GW energy radiated from a CCSN to have a limit of $\sim 10^{-3} M_{\odot} c^2$, while the FGT makes the limitation on the radiated energy only by the rest mass of the collapsing SN core itself.

The carried out in this paper evaluations for the scenarios of scalar wave radiation as a result of a CCSN from the point of view of the metric theories and in the FGT approach showed that at the same recorded wave amplitude but at different limiting energies, the sources should be at different distances and have different internal characteristics such as mass, radius and kinetic energy of pulsations. The observational test of the existence of spherically-symmetric pulsations in the core of supermassive SNs will be the identification of the GW event with the associated SN counterpart in the electromagnetic spectrum. This also will allow us to estimate the distance to the object and, as a consequence, the limits of the mass and density of the object.

Acknowledgements

This work was supported by Saint-Petersburg State University.

References

B. P. Abbott et al. Binary Black Hole Mergers in the first Advanced LIGO Observing Run (LIGO and Virgo Scientific Collaboration). *Phys. Rev.*, X6(4):041015, 2016. doi: 10.1103/PhysRevX.6.041015.

B. P. Abbott et al., "Gw170104: Observation of a 50-solar-mass binary black hole coalescence at redshift 0.2", *Phys. Rev. Lett.* 118 Jun (2017) 221101.

Yurij V. Baryshev. Foundation of relativistic astrophysics: Curvature of Riemannian Space versus Relativistic Quantum Field in Minkowski Space. 2017.

Baryshev, Yu. V. *Introduction to the tensor field theory of gravitation*. Saint Petersburg State University (unpubl.), 1990.

S. Bonazzola, E. Gourgoulhon, M. Salgado, and J. A. Marck. Axisymmetric rotating relativistic bodies: A new numerical approach for "exact" solutions. *Astronomy and Astrophysics*, 278: 421-443, November 1993.

Adam Burrows. Colloquium: Perspectives on core-collapse supernova theory. *Rev. Mod. Phys*., 85:245, 2013. doi: 10.1103/RevModPhys.85.245.

Eugenio Coccia, Florian Dubath, and Michele Maggiore. On the possible sources of gravitational wave bursts detectable today. *Phys. Rev.*, D70:084010, 2004. doi: 10.1103/PhysRevD.70.084010.

L. E. Fesik, Yu. V. Baryshev, V. V. Sokolov, and G. Paturel. LIGO-Virgo events localization as a test of gravitational wave polarization state. 2017, arXiv:1702.03440

S. W. Hawking and W. Israel. *Three Hundred Years of Gravitation*. Cambridge University Press, 1989.

V. S. Imshennik. Rotational explosion mechanism for collapsing supernovae and the two-stage neutrino signal from supernova 1987a in the large magellanic cloud. *Usp. Fiz. Nauk*, 180(11):1121-1134, 2010. doi: 10.3367/UFNr.0180.201011a.1121. URL http://ufn.ru/ru/articles/2010/11/b/.

V. M. Lipunov and I.E. Panchenko. *Astronomy and Astrophysics*, 312:937, 1996.

A. I. MacFadyen and S. E. Woosley. Collapsars: Gamma-Ray Bursts and Explosions in “Failed Supernovae". *Astrophysical Journal*, 524:262-289, October 1999. doi: 10.1086/307790.

Michele Maggiore. Gravitational waves and fundamental physics. In *Sense of Beauty in Physics: Miniconference in Honor of Adriano Di Giacomo on his 70th Birthday Pisa, Italy, January 26-27, 2006,* 2006.

Michele Maggiore and Alberto Nicolis. Detection strategies for scalar gravitational waves with interferometers and resonant spheres. *Phys. Rev.*, D62:024004, 2000. doi: 10.1103/PhysRevD.62.024004.

C. Misner, K. Thorne, and J. Wheeler. *Gravitation*. Freeman and Company, Physics Series, 1973.

E. Nakar. Short-hard gamma-ray bursts. *Physics Reports*, 442:166{236, April 2007. doi: 10.1016/j.physrep.2007.02.005.

Jerome Novak and Jose M. Ibanez. Gravitational waves from the collapse and bounce of a stellar core in tensor scalar gravity. *Astrophys. J.*, 533:392-405, 2000. doi: 10.1086/308627.

Tsvi Piran. The physics of gamma-ray bursts. *Rev. Mod. Phys.*, 76:1143-1210, 2004. doi: 10.1103/RevModPhys.76.1143.

Rudenko, V. N. Gravitational-wave experiment in Russia. *UFN*, 2017. doi: 10.3367/UFNe.2016.11.038088.

Bernard F Schutz and Franco Ricci. Gravitational Waves, Sources, and Detectors. 2010.

B. Stalder et al., “Observations of the GRB afterglow ATLAS17aeu and its possible association with GW170104”, arXiv:1706.00175

Stephen J. Smartt et al. Pan-STARRS and PESSTO search for an optical counterpart to the LIGO gravitational wave source GW150914. *Mon. Not. Roy. Astron. Soc.*, 462(4):4094{4116, 2016. doi: 10.1093/mnras/stw1893.

V. V. Sokolov. On the Observed Mass Distribution of Compact Stellar Remnants in Close Binary Systems and Localizability of Gravitational Energy. *International Journal of Astronomy, Astrophysics and Space Science*, 2(6):51-58, 2015.

V. V. Sokolov and S. V. Zharykov. Masses of macroscopic quark configurations in metric and dynamic theories of gravitation. *Astrophysics and Space Science*, 201(2):303{319, 1993. ISSN 1572-946X. doi: 10.1007/BF00627203. URL http://dx.doi.org/10.1007/BF00627203.

Richard F. Stark and Tsvi Piran. Gravitational-wave emission from rotating gravitational collapse. *Phys. Rev. Lett.*, 55: 891-894, Aug 1985. doi: 10.1103/PhysRevLett.55.891. URL

https://link.aps.org/doi/10.1103/PhysRevLett.55.891.

K. S. Thorne. *Gravitational Waves: A New Window onto the Universe*. unpublished, 1989.

S. E. Woosley. Gamma-ray bursts from stellar mass accretion disks around black holes. *Astrophysical Journal*, 405:273-277, March 1993. doi: 10.1086/172359.

T. Zwerger and E. Mueller. Dynamics and gravitational wave signature of axisymmetric rotational core collapse. *Astronomy and Astrophysics*, 320:209-227, April 1997.

Search for the resonance absorption of solar axions emitted in the M1 transition of ^{83}Kr and ^{57}Fe nuclei in the Sun

A.M. Gangapshev[1],*, Z.A. Akhmatov[5], S.S. Berezin[4], Yu.M. Gavrilyuk[1], A.V. Derbin[3], I.S. Drachnev[3], V.V. Kazalov[1], A.Kh.-A. Khokonov[5], V.V. Kuzminov[1], V.N. Muratova, S.I. Panasenko[2], S.S. Ratkevich[2], D.A. Tekueva[1], S.P. Yakimenko[1], E.V. Unzhakov[3], A.Yu. Zavrazhnov[4]

[1] Institute for Nuclear Research RAS, Moscow, Russia; gangapsh@list.ru

[2] Kharkov National University, Ukraine

[3] St. Petersburg Nuclear Physics Inst., NRCKI, Gatchina, Russia

[4] Voronezh state university, Voronezh, Russia

[5] Kabardino-Balkarian State University, Nalchik, Russia

Abstract A search for resonant absorption of the solar axions by ^{83}Kr nuclei was performed using the proportional counter installed inside the low-background setup at the Baksan Neutrino Observatory. The obtained model independent upper limits on axion-nucleon, - photon,- electron couplings are $|g^3_{AN}-g^0_{AN}|\leq 8.4\times10^{-7}$, $|g_{A\gamma}\times m_A|\leq 6.3\times10^{-17}$, $|g_{Ae}\times m_A|\leq 1.4\times10^{-9}$ eV. The upper limit on axion mass is $m_A\leq$ 65 eV at 95% C.L. New experiment using resonant absorption of the solar axions by Fe-57 nuclei is proposed. Different materials containing of Fe-57 which can be used as detectors working media are described

Keywords: Axion, Solar model, Proportional counter, Krypton, Iron.

1. Introduction

A solution of the strong CP problem based on the global chiral symmetry U(1) was proposed by Peccei and Quinn (PQ) [1]. The existence of the axions was predicted by Weinberg [2] and Wilczek [3] as result of spontaneous breaking of the PQ-symmetry at the energy f_a. The axion mass (ma) and the strengths of an axion's coupling to an electron (g_{ae}), a photon ($g_{a\gamma}$) and nucleons (g_{aN}) are proportional to the inverse of f_a. At the moment there are two classes of models for the axion: KSVZ-model (hadronic axion) [4, 5] and DFSZ-model [6, 7].

"Axions are among the most fascinating particles on the long list of those proposed but not yet observed or ruled out. Their existence would provide an elegant resolution of the strong CP problem. Even more exciting is the possibility that the missing mass needed to close the universe is composed of axions, and that axions are «cold dark matter» which seems to be necessary for galaxy formation" [8].

"The composite axion is a particular example of a "hadronic" axion, resulting from a theory where only exotic fermions carry U(1)PQ charges. Hadronic axions don't couple to leptons, which are neutral under SU(3)xU(1)PQ. Nor do they couple to heavy quarks, which are integrated out of the theory above 1GeV, where QCD gets strong. Hadronic axions will still

couple to nucleons as well as to photons" [9].

The axion mass in both models is defined as:

$$m_a = \frac{f_\pi m_\pi}{f_A}\left(\frac{z}{(1+z+w)(1+z)}\right), \quad (1)$$

where $f_\pi \approx 93$ MeV - pion decay constant, $z = m_u/m_d \approx 0.56$ and $w = m_u/m_s \approx 0.029$ - quark-mass ratios. It gives m_A [eV] $\approx 6.0 \times 10^6/f_A$ [GeV].

The main difference between models is that in contrast to the DFSZ-model in KSVZ-model axions have no coupling to leptons and ordinary quarks at the tree level. As result the interaction of the KSVZ axion with electrons through radiatively induced coupling is strongly suppressed [8].

If axions do exist, then the Sun and other stars should be an intense source of these particles. In 1991 Haxton and Lee calculated the energy loss of stars along the red-giant and horizontal branches due to the axion emission in nuclear magnetic transitions in ^{57}Fe, ^{55}Mn, and ^{23}Na nuclei [10]. In 1995 Moriyama proposed experimental scheme to search for 14.4 keV monochromatic solar axions that would be produced when thermally excited ^{57}Fe nuclei in the Sun relax to its ground state and could be detected via resonant excitation of the same nuclide in a laboratory [11]. Searches for resonant absorption of solar axions emitted in the nuclear magnetic transitions were performed with ^{57}Fe [12, 13, 14, 15, 16, 17], ^{7}Li [18, 19, 20] and ^{83}Kr [21] nuclei.

The expected rate of resonance axion absorption by the ^{83}Kr nucleus as a function of the probability for axion emission ω_A/ω_γ; the parameter (g_3-g_0), which describes axion-nucleon interaction; and the axion mass in the KSVZ model can be represented in the form (S=0.5, z= 0.56)[22]:

$$R_A = [g^{-1}day^{-1}] = 4.23 \cdot 10^{23}\left(\omega_A/\omega_\gamma\right)^2 \quad (2)$$

$$= 8.53 \cdot 10^{21}(g_3 - g_0)^2\left(p_A/p_\gamma\right)^6 \quad (3)$$

$$= 2.41 \cdot 10^{-10}(m_A)^4\left(p_A/p_\gamma\right)^6. \quad (4)$$

2. Experimental setup

The experimental technic is based on registration of the γ-quantum and conversion electrons appearing after deexcitation of the ^{83}Kr nuclei. To register this process a large proportional counter (LPC) with a casing of copper is used. The krypton enriched with ^{83}Kr (99.9%) is used as working media of the LPC. The LPC is a cylinder with inner and outer diameters of 137 and 150 mm, respectively. A gold-plated tungsten wire of 10 μm in diameter is stretched along the LPC axis and is used as an anode. To reduce the influence of the counter edges on the operating characteristics of the counter, the end segments of the wire are passed through the copper tubes (3 mm in diameter and 38.5 mm in length) electrically connected to the anode. These segments operate as an ionization chamber with no gas amplification. Taking into account teflon insulators dimensions, the distance from operation region to the flange is 70 mm. The fiducial length of the LPC is 595 mm, and the corresponding volume is 8.77 L. Gas pressure is 1.8 bar, and corresponding mass of the ^{83}Kr-isotope in fiducial volume of the LPC is 58 g. The LPC is surrounded by passive shield made of copper (~20 cm), lead (~20 cm) and polyethylene (8 cm).

The setup is located in the Deep Underground Low-Background Laboratory at BNO INR

RAS [23], at the depth of 4700 m w.e., where the cosmic ray flux is reduced by ~ 10^7 times in comparison to that above ground, and valuated as $(3.0 \pm 0.1) \times 10^{-9}$ cm−2 s^{-1} [24].

3. Results with ^{83}Kr

The background spectra collected during 613.25 days and fit result curve are presented in ***Fig1.*** Two peaks are clear visible in the energy range (4-26) keV. The peak with energy 8.05 keV associates with the detection of $K_{\alpha 1,2}$ X-rays of copper. The structure of the second peak is more complicated, it is mixture of Kr and Br $K_{\alpha 1,2}$ X-rays and 13.5 keV from K-capture of cosmogenic ^{81}Kr. It is seen that the 9.4 keV peak is not manifested. The maximum likelihood method was used to determine the intensity of the peak. The fit of spectrum corresponding to the minimum χ^2 is shown by red solid line in Fig. 1. The minimum of χ^2 corresponds to the nonphysical value of the area of the 9.4 keV peak S_A=−(102±92) events. The standard χ^2-profile method was used to determine the upper bound on the number of events in the peak.

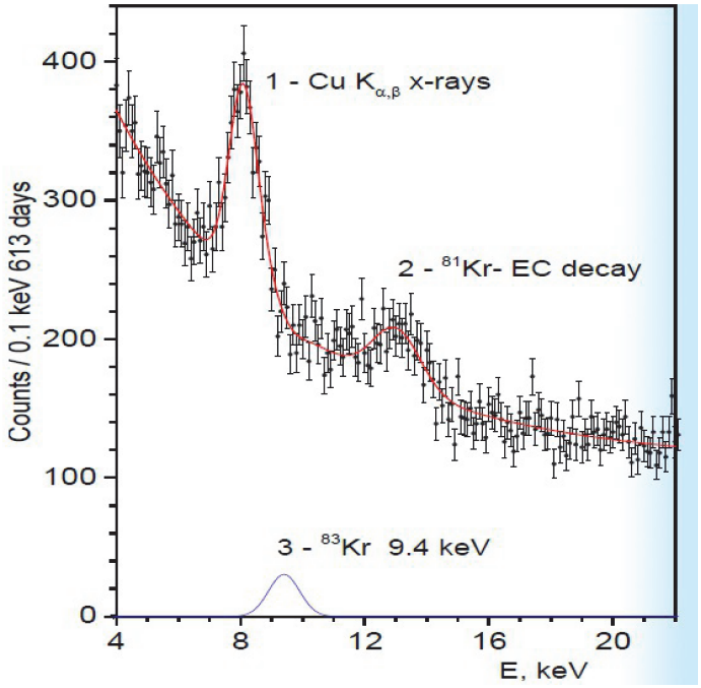

Fig1. *Energy spectra of the Kr LPC measured for 613 days, fitting results (red line) and expected axion peak for* $3S_{lim}$ *(blue line).*

The upper bound thus determined for the number of events in the peak is S_{lim}= 127 for 95 % C.L.

The expected number of registered axions is

$$S_A = RMT\epsilon \leq S_{lim} \ , \qquad (5)$$

where M = 58 g is mass of ^{83}Kr isotope, T = 613.25 days is time of data taking, and ε = 0.825 is the detection efficiency. The upper limit on the excitation rate of ^{83}Kr by solar hadronic axions is defined as $R_{exp}=4.29\times10^{-3}g^{-1}day^{-1}$. The relation $R_A \leq R_{exp}$ limits the region of possible values of the coupling constants g_0,g_3 and axion mass m_A. In accordance with Eqs. (2-4), and on

condition that $(p_A/p_\gamma) \cong 1$ provided for $m_A < 3$ keV one can obtain:

$$\left(\omega_A/\omega_\gamma\right) \leq 1.0 \cdot 10^{-12} \ , \tag{6}$$

$$|g_3 - g_0| \leq 8.4 \cdot 10^{-7} \ , \tag{7}$$

$$m_A \leq 65\ eV \ \ at\ 95\%\ C.L. \tag{8}$$

The limit (8) is stronger than the constrain obtained with 14.4 keV ^{57}Fe solar axions [17]) and is stronger than our previous result obtained in ^{83}Kr experiment [25]. As in the case of 57Fe nucleus the obtained limit on axion mass strongly depends on the exact values of the parameters S and z.

4. Proposal with ^{57}Fe

Another possible way to search for the hadronic soar axions is to use detector with a working media containing ^{57}Fe. One of the possible candidates for a such media is Pyrite. The mineral pyrite, or iron pyrite, also known as fool's gold, is an iron sulfide with the chemical formula FeS_2. Pyrite has been proposed as an abundant, inexpensive material in low-cost photovoltaic solar panels. Synthetic iron sulfide was used with copper sulfide to create the photovoltaic material.

Pyrite is a semiconductor, the band gap in pyrite is about 0.95 eV and the dominant charge carriers can be either electrons or holes. Sometimes, both n-type and p-type semiconducting regions can be found within single naturally occurring crystals. Resistivity (natural crystals): $10^{-5} \div 10^{0} Om * m$. On the other hand, the high purity pyrite should have much higher resistivity (comparable with high purity germanium) and so could be used as semiconductor detector.

Now we are working on development a new semiconductor detector based on high purity pyrite or solid solution GaS:Fe or Ga_2S_3:Fe. The main profit of use these materials is much higher expected rate of resonance axion absorption by the ^{57}Fe in comparison with ^{83}Kr. The ratio of rates is:

$$\frac{R_{Fe-57}}{R_{Kr-83}} = 3.51 \cdot 10^3 \tag{9}$$

Using the semiconductor detector with the iron contaminating working media will allow one to search for hadronic axions with masses below 10 eV – most interesting mass region.

Acknowledgements

This work was supported by the Russian Foundation of Basic Research (grants 17-02-00305A, 16-29-13014ofi-m, 16-29-13011ofi-m, 15-02-02117A, 14-02-00258A).

References

[1] Peccei R. D. and Helen R. Quinn, "Constraints imposed by CP conservation in the presence of pseudoparticles", Phys. Rev. D. 1977. V.16. P.1791;

[2] Weinberg S., "A New Light Boson?", Phys. Rev. Lett. 1978. V.40. P.223;

[3] Wilczek F. , "Problem of Strong P and T Invariance in the Presence of Instantons", Phys. Rev. Lett. 1978. V.40. P.279;

[4] Kim J.E., "Weak-Interaction Singlet and Strong CP Invariance", Phys. Rev. Lett. 1979. V.43. P.103;

[5] Shifman M.A., Vainstein A.I., Zakharov V.I., "Can confinement ensure natural CP invariance of strong interactions?", Nucl. Phys. B. 1980. V.166. P.493;

[6] Zhitnitskii A.R., "О возможности подавления аксион-адронных взаимодействий", Yad. Fiz. 1980. V.31. P.497;

[7] Dine M., Fischler F., Srednicki M., "A simple solution to the strong CP problem with a harmless axion", Phys. Lett. B. 1981. V.104. P.199;

[8] Srednicki M., "Axion couplings to matter: (I). CP-conserving parts", Nucl. Phys. B. 1985. V.250. P.689;

[9] Kaplan David B., "Opening the axion window", Nucl. Phys. B. 1985. V.260. P.215;

[10] Haxton W.C. and Lee K.Y., "Red-giant evolution, metallicity, and new bounds on hadronic axions", Phys. Rev. Lett. 1991. V.66. P.2557;

[11] Moriyama S., "Proposal to Search for a Monochromatic Component of Solar Axions Using ^{57}Fe", Phys. Rev. Lett. 1995. V.75 P.3222;

[12] M.Krčmar, Z.Krečak, M.Stipčević, A.Ljubičić, D.A.Bradley, Phys. Lett. B 442, (1998) p.38;

[13] A.V. Derbin, A.I. Egorov, I.A. Mitropol'sky, V.N. Muratova, N.V. Bazlov, S.V. Bakhlanov, D.A. Semenov, E.V. Unzhakov, "Search for resonant absorption of solar axions emitted in an M1 transition in ^{57}Fe nuclei", JETP Lett. 2007. V.85 p.12;

[14] Namba T., "Results of a search for monochromatic solar axions using ^{57}Fe", Phys. Lett. B 2007. V.645 p.398;

[15] A. V. Derbin, A. I. Egorov, I. A. Mitropol'sky, V. N. Muratova, D. A. Semenov, E. V. Unzhakov, "Search for resonant absorption of solar axions emitted in M1 transition in ^{57}Fe nuclei", Eur. Phys. J. C 2009. V.62. P.755;

[16] F. A. Danevich, O. V. Ivanov, V. V. Kobychev, and V. I. Tretyak. "Heat Flow of the Earth and Resonant Capture of Solar 57Fe Axions", Kinematics and Physics of Celestial Bodies. 2009. V25. P.102;

[17] A. V. Derbin, V. N. Muratova, D. A. Semenov, E.V. Unzhakov, "New limit on the mass of 14.4-keV solar axions emitted in an M1 transition in ^{57}Fe nuclei", Phys. At. Nucl. 2011. V.74. p.596;

[18] M. Krčmar, Z. Krečak, A. Ljubičić, M. Stipčević, and D. A. Bradley, "Search for solar axions using", Phys. Rev. D 2001. V.64 p.115016;

[19] A. V. Derbin, A. I. Egorov, I. A. Mitropolsky, V. N. Muratova, "Search for solar axions emitted in an M1 transition in ^{7}Li* nuclei", JETP Lett. 2005. V.81. p.365;

[20] P. Belli, R. Bernabei, F. Cappella, R. Cerulli, F. A. Danevich, A. d'Angelo, A. Incicchitti, V. V. Kobychev, M. Laubenstein, O. G. Polischuk, V. I. Tretyak, "Search for ^{7}Li solar axions using resonant absorption in LiF crystal: Final results", Phys. Lett. B 2012. V.711. P.41;

[21] K. Jakovcic, Z. Krecak, M. Krcmar, A. Ljubicic, "A Search For Solar Hadronic Axions Using Kr-83", Radiat.Phys.Chem. 2004. V71. P.93; arXiv:nucl-ex/0402016v1;

[22] Yu.M. Gavrilyuk, A.M. Gangapshev, A.V. Derbin et al., "First result of the experimental search for

the 9.4 keV solar axion reactions with ^{83}Kr in the copper proportional counter", Physics of Particles and Nuclei 46, pp 152–156 (2015);

[23] Ju.M. Gavriljuk, A.M.Gangapshev, A.M. Gezhaev, V.V. Kazalov, V.V. Kuzminov, S.I. Panasenko, S. S. Ratkevich, A.A.Smolnikov, S.P.Yakimenko, "Working characteristics of the New Low-Background Laboratory (DULB-4900)", Nucl. Ins. Meth. A. 2013. V.729. P.576;

[24] V.N. Gavrin, V.I. Gurencov, V.N. Kornoukhov, A.M. Pshukov and A.A. Shikhin, "Intensity of muon space beams in laboratory deep location GGNT" Preprint INR RAS,1991. P-698;

[25] Yu.M. Gavrilyuk, A.M. Gangapshev, A.V. Derbin et al., "New experiment on search for the resonance absorption of solar axion emitted in the M1 transition of ^{83}Kr nuclei", JETP Letters, 101, 664 (2015)

Searching for fast optical transients with Mini-MegaTORTORA wide-field monitoring system

S. Karpov[1,3],*, G. Beskin[1,3], A. Biryukov[3,4], S. Bondar[2], E. Ivanov[2], E. Katkova[2], N. Orekhova[2], A. Perkov[2], V. Plokhotnichenko[1], V. Sasyuk[3], J. Pandey[5]

[1]Special Astrophysical Observatory of Russian Academy of Sciences, Russia; karpov.sv@gmail.com

[2]Research and Production Corporation "Precision Systems and Instruments", Russia

[3]Kazan Federal University, Russia

[4]Moscow State University, Russia

[5]Aryabhatta Research Institute of Observational Sciences (ARIES), Nainital-263002, India

Abstract Here we present the summary of first years of operation and the first results of a novel 9-channel wide-field optical monitoring system with sub-second temporal resolution, Mini-MegaTORTORA (MMT-9), which is in operation now at Special Astrophysical Observatory on Russian Caucasus. The system is able to observe the sky simultaneously in either wide (~900 square degrees) or narrow (~100 square degrees) fields of view, either in clear light or with any combination of color (Johnson-Cousins B, V or R) and polarimetric filters installed, with exposure times ranging from 0.1 s to hundreds of seconds. The real-time system data analysis pipeline performs automatic detection of rapid transient events, both near-Earth and extragalactic. The objects routinely detected by MMT include faint meteors and artificial satellites.

Keywords: telescopes — instrumentation: miscellaneous — gamma-ray burst: general — meteorites, meteors, meteoroids

1. Introduction

Mini-MegaTORTORA is a novel robotic instrument just commissioned for the Kazan Federal University and developed according to the principles of MegaTORTORA multi-channel and transforming design formulated by us earlier [1]-[4],[24],[25]. It is a successor to the FAVOR [5]-[7] and TORTORA [8] single-objective monitoring instruments we built earlier to detect and characterize fast optical transients of various origins, both cosmological, galactic and near-Earth. The importance of such instruments became evident after the discovery and detailed study of the brightest ever optical afterglow of a gamma-ray burst, GRB080319B [9],[10].

The Mini-MegaTORTORA (MMT-9) system includes a set of nine individual channels (see ***Fig1***) installed in pairs on equatorial mounts (see ***Fig2***). Every channel has a celostate mirror installed before the Canon EF85/1.2 objective for a rapid (faster than 1 second) adjusting of the objective direction in a limited range (approximately 10 degrees to any direction). This allows for either mosaicking the larger field of view, or for pointing all the channels in one direction. In the latter regime, a set of color (Johnson's B, V or R) and polarimetric (three different

directions) filters may be inserted before the objective to maximize the information acquired for the observed region of the sky (performing both three-color photometry and polarimetry).

The channels are equipped with an Andor Neo sCMOS detectors having 2560x2160 pixels 6.4μm each. Field of view of a channel is roughly 9x11 degrees with angular resolution of 16″ per pixel. The detector is able to operate with exposure times as small as 0.03 s, in our work we use 0.1 s exposures providing us with 10 frames per second as on higher frame rates we are unable to process the data in real time.

Every channel is operated by a dedicated PC which controls its hardware, acquires the images from the detector and performs the data processing. The amount of data acquired by a single channel is about 3Tb in 8 hours of observations. The complex as a whole is being controlled by a separate PC.

Initial tests show that the FWHM of the stars as seen by MMT channels is around 2 pixels wide. The detection limit in white light for 0.1 s exposure is close to 11 mag, when calibrating to V band magnitudes.

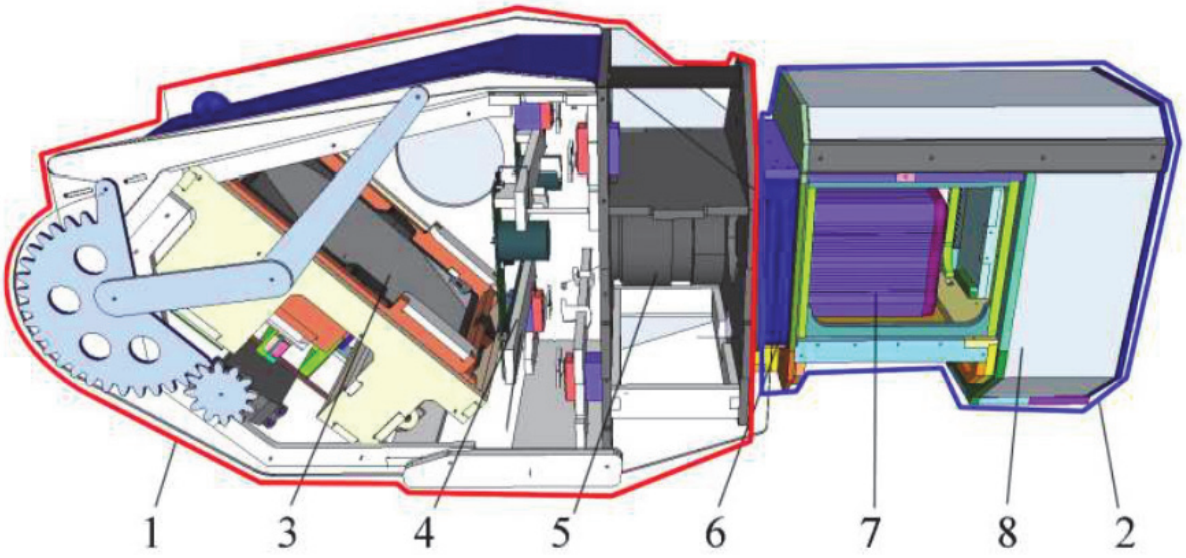

Fig1. *Schematic view of a MMT channel. 1 – celostate unit, 2 – camera unit, 3 – celostate mirror which can rotate for ~ 10 degrees around two axes, 4 – installable color and polarimetric filters, 5 – Canon EF85/1.2 objective, 6 – optical corrector, 7 – Andor Neo sCMOS detector, 8 – conditioner to keep stable environmental conditions inside the channel.*

2. Mini-MegaTORTORA operation

Mini-MegaTORTORA started its operation in June 2014, and routinely monitor the sky since then. The observations are governed by the dedicated dynamic scheduler optimized for performing the sky survey. The scheduler works by selecting the next pointing for Mini-MegaTORTORA by simultaneously optimizing the following parameters: distances from the Sun, Moon and the horizon should be maximized, distances from the current pointings of Swift and Fermi satellites should be minimized, and the number of frames already acquired on a given sky position that night should be minimized. In this way more or less uniform survey of the whole sky hemisphere is being performed while maximizing the probability of observations of gamma-ray bursts. As an unoptimized extension, the scheduler also supports the observations of pre-selected targets given by their coordinates, which may be performed in various regimes

Fig2. *Photo of the all 9 channels of MMT installed on 5 mounts in the single cylindrical dome, which is open at that moment. Russian 6-m telescope may be seen in the background.*

supported by Mini-MegaTORTORA (wide-field monitoring of a given region of the sky with or without filters, narrow-field multicolor imaging or polarimetry with lower temporal resolution, etc).

2.1. Real-time transient detection

The main regime of Mini-MegaTORTORA operation is the wide-field monitoring with high temporal resolution and with no photometric filters installed. In this regime, every channel acquires 10 frames per second, which corresponds to 110 megabytes of data per second. To analyze it, we implemented the real-time fast differential imaging pipeline intended for the detection of rapidly varying or moving transient objects – flashes, meteor trails, satellite passes etc. It is analogous to the pipeline of FAVOR and TORTORA cameras [11],[7], and is based on building an iteratively-updated comparison image of current field of view using numerically efficient running median algorithm, as well as threshold image using running similarly constructed *median absolute deviation* estimate, and then comparison of every new frame with them, extracting candidate transient objects and analyzing lists of these objects from the consecutive frames. It then filters out noise events, extracts the meteor trails by their generally elongated shape on a single frame, collects the events corresponding to moving objects into focal plane trajectories, etc. Data on detected transients are stored to the database and are partially published online [1].

Every 100 frames acquired by a channel are being summed together, yielding "average" frames with 10 s effective exposure and better detection limit. Using these frames, the astrometric calibration is being performed using locally installed ASTROMETRY.NET code [12]. Also the rough photometric calibration is being done. These calibrations, updated every 10

1 Public databases of meteors [15] and artificial satellites [16] observed by Mini-MegaTORTORA are available at project website at http://mmt.favor2.info

seconds, are used for measuring the positions and magnitudes of transients detected by the real-time differential imaging pipeline. The "average" frames are stored permanently (in contrast to "raw" full-resolution data which is typically erased in a day or two after acquisition) and may be used later for studying the variability on time scales longer than 10 s.

The Mini-MegaTORTORA typically observes every sky field continuously for 1000 seconds before moving to the next pointing. Before and after observing the field with high temporal resolution, the system acquires deeper "survey" images with 60 seconds exposure in white light in order to study the variability of objects down to 14-15 magnitude on even longer time scales; typically, every point of the northern sky is covered by one or more such images every observational night.

Mini-MegaTORTORA real-time transient detection system routinely extracts various kinds of transient from the data stream – rapid flashes, meteors, satellites etc.

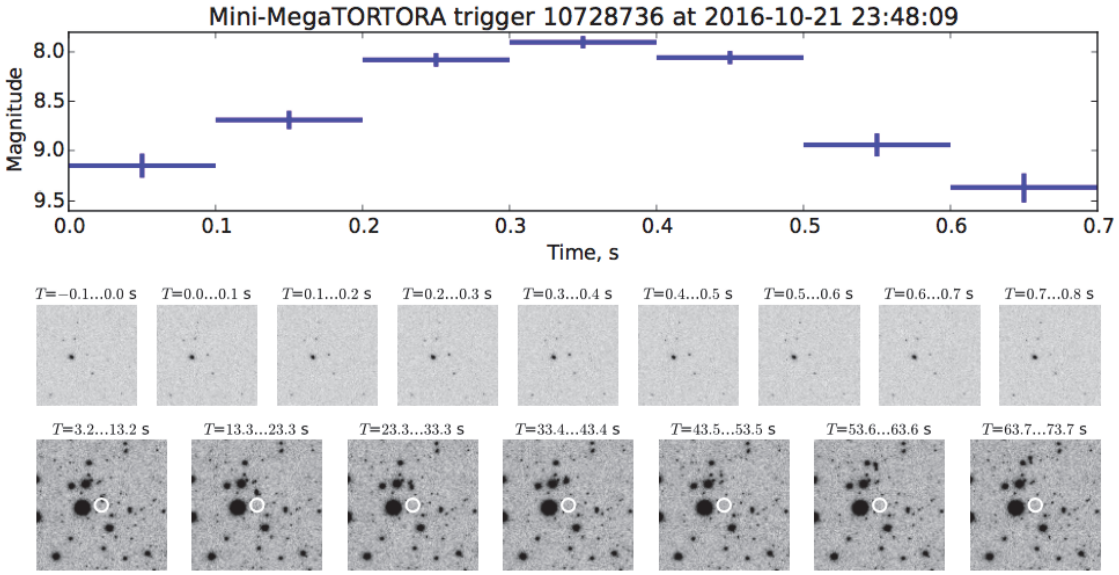

***Fig3**. Example of a rapid optical flash independently detected and followed-up by Mini-MegaTORTORA and not identified with satellites from NORAD database. Upper panel – light curve with 0.1 s temporal resolution, middle panel – corresponding detection images (50' x 50' around the event), lower panel – follow-up images with 10 s exposures that clearly reveal a satellite slowly moving away from the flash position.*

The rapid flashes – i.e. the optical transients rapidly changing their brightness and not displaying signs of motion – are then matched against stellar catalogues to exclude events due to stellar scintillations, and against public NORAD database of satellite orbits [13] to filter out satellite flashes. All the remaining flashes have the same characteristic properties – durations, shapes, peak magnitudes (see ***Fig4***) – as the ones caused by identified satellites, and we may suggest that they are also due to satellites, but either missing from public database of orbits, or having quite large errors in their orbital parameters. Moreover, immediate follow-up observations using Mini-MegaTORTORA rapid reaction mode (see ***Fig3*** for a typical example) often reveal faint satellite trails leading from the event location. Therefore we may conclude that no bright rapid flashes of astrophysical origin are detected in 2.5 years of Mini-MegaTORTORA operation.

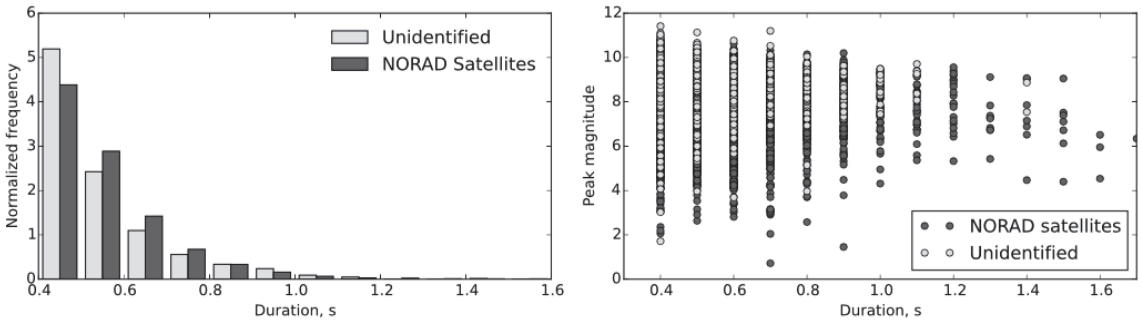

***Fig4**. Comparison of durations (left panel) and brightness (right panel) of rapid flashes detected by Mini-MegaTORTORA and identified/non-indentified with NORAD satellites.*

2.2. Follow-up observations of external triggers

Mini-MegaTORTORA also performs follow-up of Swift, Fermi and LIGO-Virgo triggers. Its large field of view, allowing for simultaneous observations of ~900 sq.deg. sky regions, makes it the perfect instrument for following up events with poor localization accuracy. On the other hand, the triggers with better localizations may be observed in multicolor and/or polarimetric regimes simultaneously.

Since mid-2015, 4 of 89 Swift GRBs have been followed up in narrow-field polarimetric mode in 30 to 60 seconds since trigger distribution through GCN network, with no optical emission detections. 9 of 250 Fermi GBM triggers have been also followed up in wide-field mode in 20 to 90 seconds from the trigger. All other events were either below the horizon or occurred in bad weather conditions.

2.3. Simultaneous observations of Fermi GRB151107B

The localization of Fermi GBM trigger GRB151107B [17],[18] has been observed before, during and just after the trigger time, covering nearly all its error box (see ***Fig5***) simultaneously since T-329.3 s till T+25.7 (including brightest part of first gamma-ray peak) with temporal resolution of 0.1 s in white light. Dedicated real-time transient detection pipeline did not detect any events longer than 0.3 s and brighter than approximately V=10.5 mag. Inspection of co-added images with 10 s effective exposure has not revealed any variable source down to V=12.0 mag during that interval.

After receiving GCN trigger the system initiated a wide-field follow-up and since T+62.7 s (during the continuing gamma-ray activity) till T+666.7 s acquired 20x9 deep images with 30 s exposures in a 30x30 degree field of view covering the whole final 1-sigma localization box. Analysis of the acquired data has not revealed any variable object down to roughly V=13.5 mag over the time interval [18].

3. Detection of the optical counterpart of Fermi GRB 160625B

One more Fermi event, GRB 160625B, has been followed up in the widefield regime, with bright optical flash of GRB 160625B clearly detected during the gamma activity [19].

The on-sky position of the Fermi gamma-ray burst GRB 160625B has been observed before, during and just after the LAT trigger time (T = 2016-06-25 22:43:24). Mini-MegaTORTORA reacted to the Fermi GBM trigger no. 488587220 generated as a result of the detection of the precursor and started observing its error box 52 seconds after it and 136 seconds before LAT trigger. Due to large size of GBM error box, the observations have been performed in “wide-

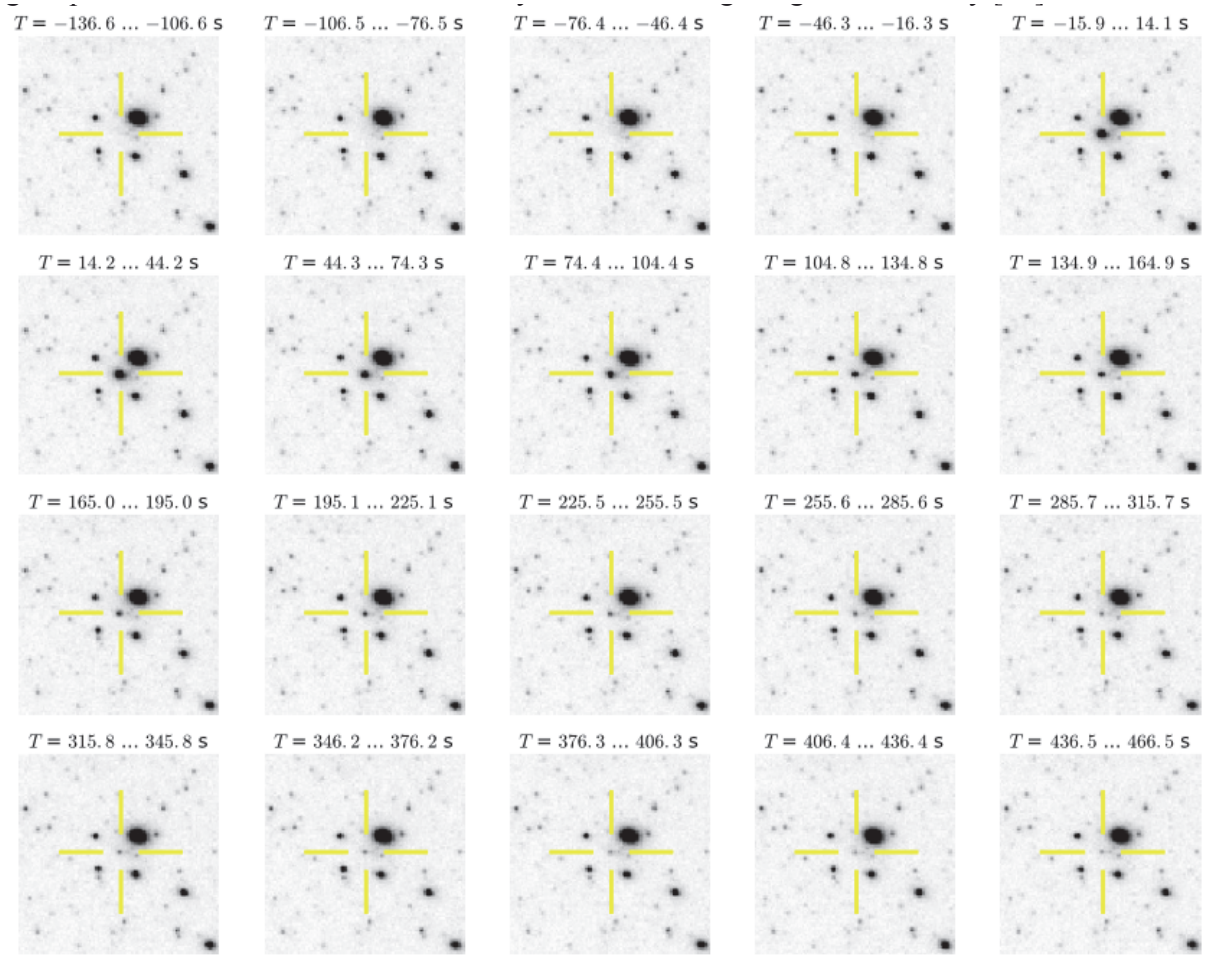

Fig 5*. The final localization region of GRB 160625B as seen by Mini-MegaTORTORA (20 unfiltered images with 30-s exposures). The peak brightness of transient object is V=8.8 mag.*

field+deep" regime, with channels simultaneously covering 30x30 deg field of view (see ***Fig3***) with 30 s exposures in white light to achieve deepest detection limit. The system acquired 20 frames in such regime, covering time interval from T − 136 to T + 466 s, and detected a bright optical transient with a mag- nitude of about V = 8.8 mag on a frame coincident with LAT trigger time (T − 15.9 – T + 14.1 s) at the coordinates consistent with the afterglow [20]. On the consecutive frames, the transient brightened for about 0.1 mag, and then faded following nearly smooth power-law decay with slope of about −1.6, down to V = 12.2 at last acquired frame. The images acquired prior to LAT trigger do not display any object at that position down to about V = 13.5 mag. This sequence of frames (20′ subimages centered on the transient) is shown in ***Fig5.***

The system also responded to the second GBM trigger no. 488587880 with a somewhat different coordinates. This response resulted in the acquisition of 20 more frames covering burst position in the time interval from T + 1691 to T +2264 s. In this sample no transient objects brighter than V = 13.5 mag were detected.

The optical light curve shown in ***Fig6*** displays an initial peak with duration similar to the one of the gamma-ray peak and seemingly corresponding to the prompt phase of emission, gradually transforming into the afterglow about 50 s after the onset of the gamma-ray event. Such a behavior – the absence of the intensity dip between the prompt optical emission

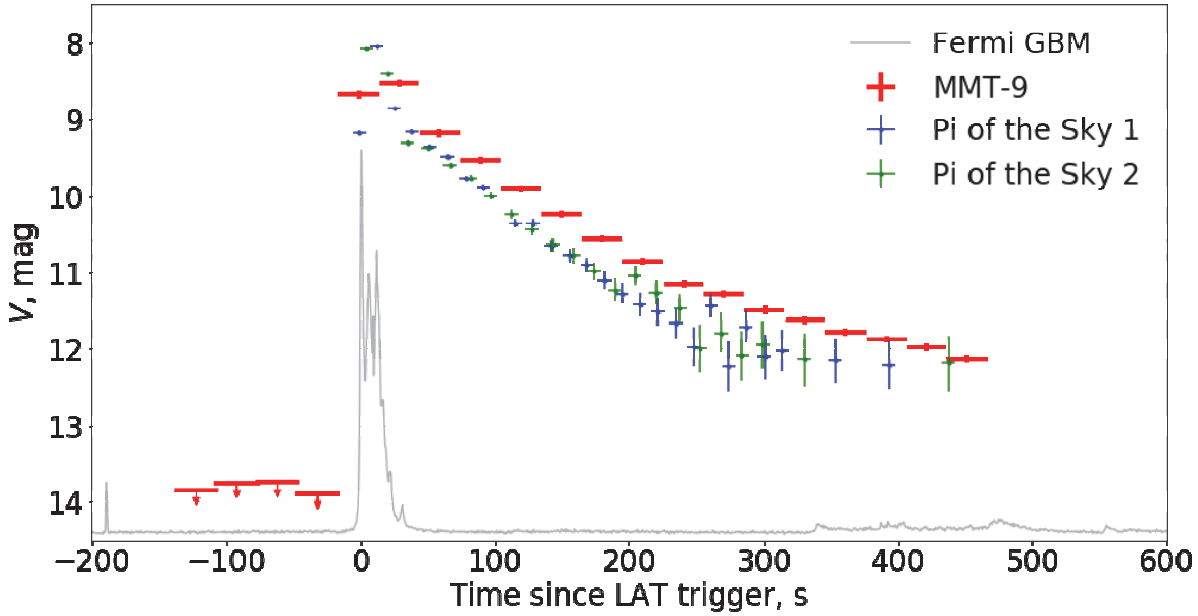

Fig.6. *The light curve of optical transient that accompanied the second gamma activity episode of GRB 160625B, as seen by Mini-MegaTORTORA. Also, the data acquired by Pi~of~the~Sky cameras [22] are shown.*

accompanying the gamma-ray burst and the afterglow – is typical for several most powerful bursts including GRB 080319B (Naked-Eye Burst) [9]. This is not the only similarity between these two events. Indeed, in both cases the intensity of the optical emission accompanying the gamma-ray burst exceeds the extrapolation of the gamma-ray spectrum to the optical range, which indicates different generation mechanisms of these two emission components. Moreover, gamma-ray peaks precede the corresponding optical flashes in time. Indeed, a comparison of the light curves of GRB 160625B in different spectral intervals (see ***Fig6*** where we used both the Mini-MegaTORTORA data and the results obtained by Pi of the Sky wide-field monitoring system [22]) shows that optical and gamma-ray emission in the second activity episode are correlated, and the latter precedes the optical flash by 2–4 s. Given the measured redshift of the object, which was found to be close to 1.4 [21], we find that in the comoving frame optical emission lags behind gamma-ray emission for 1–2 s, like in the Naked-Eye Burst where the same lag was found. We may conclude that in both cases optical photons are born 10–100 times farther away from the "central engine" than high-energy photons, i.e., in jet regions that are spaced apart [9], and that in the GRB 160625B electrons are heated by internal shocks originating from the residual collisions of filaments ejected in the jet, and the observed emission is generated by their synchrotron energy release [23].

4. Photometric analysis of Mini-MegaTORTORA data

Most of the Mini-MegaTORTORA observational time since its commissioning in mid-2014 is dedicated to the high temporal resolution (with exposure of 0.1 s and limit of about V=11 mag) wide-field monitoring of the sky in order to detect and classify rapid optical transients in real time, and to perform their follow-up. In addition to this "monitoring" operation, the system performs deeper "survey" imaging of the sky (one to few frames per night per field with 20 to 60 s exposure and limit down to V=14.5 mag; more than 300000 frames to date). Moreover, during the monitoring, intermediate depth "running sums" images with 10 s effective exposures (limit of about V=12.5 mag), amounting typically for 100 consecutive images, spanning 1000 seconds in total, per field, are generated and stored.

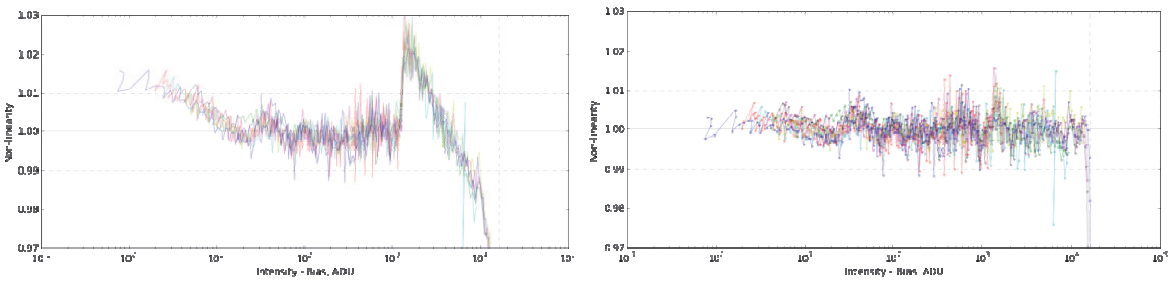

Fig7. *Left – non-linearity of Andor Neo sCMOS detector in global shutter mode as a function of intensity due to its dual-amplifier design. Right – the same after applying linearization correction defined as a piecewise fourth-order polynomial with parameters calibrated on a per-pixel basis.*

Mini-MegaTORTORA has not been originally designed to be a precise photometric instrument, as it uses fast but less reliable Andor Neo sCMOS detectors in place of more typical and accurate CCDs. Due to it, precise calibration of imaging data from Mini-MegaTORTORA requires thorough study of peculiarities, non-linearity (see ***Fig7***) and stability of its detectors, which is now ongoing.

In general, the archive of Mini-MegaTORTORA images represents a time-domain picture of the sky on time scales ranging from tens of seconds to years, with hundreds to tens of thousands points for every object, and in principle allows to extract and characterize the majority of variable objects down to V=14.5 mag. Examples of data extracted from the archive for different classes of variable objects are shown in ***Figs 8,9,10.***

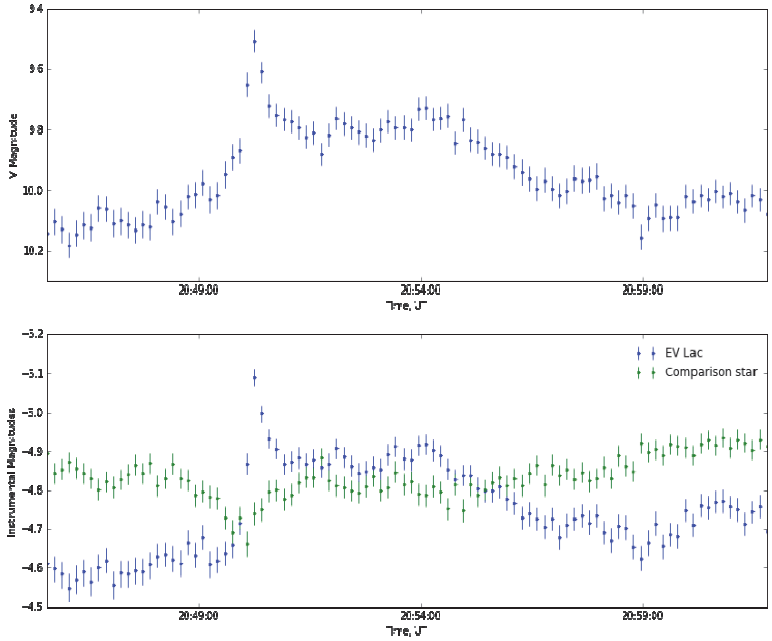

Fig8. *Light curve of EV Lac flaring star extracted from "running sum" frames (10 s effective exposure, derived by averaging 100 consecutive frames acquired in monitoring) in Mini-MegaTORTORA archive. The unfiltered instrumental magnitudes (lower panel) are calibrated to V band (upper panel) by using the comparison star of similar color to the object. The noise in the frames is estimated as a spatial variance and is mostly due to sCMOS non-uniform bias map. Instrumental magnitudes demonstrate temporally correlated trents due to drifting of pixel bias values and slow motion of the stars over different pixels due to imperfect tracking.*

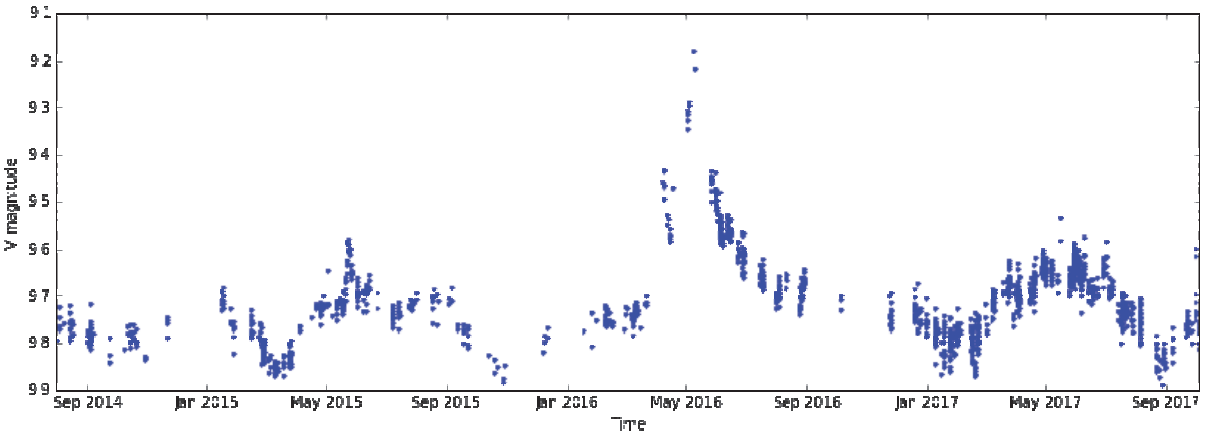

Fig9. *Light curve of AG Dra symbiotic binary star extracted from "survey" images stored in Mini-MegaTORTORA data archive. The large outburst around May 2016 is clearly visible, along with some smaller ones before and after.*

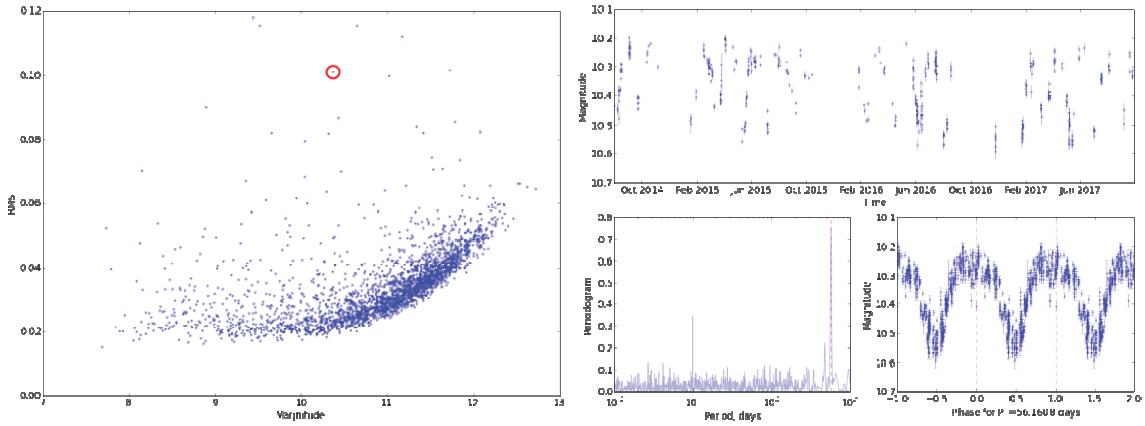

Fig10. *New variable star detected in the Mini-MegaTORTORA data. Left – scatter vs mean magnitude plot with the star marked by a red circle. Right – light curve, periodogram and a folded light curve corresponding to the best period detected in periodigram for the star.*

Acknowledgements

This work was supported by the grant of RFBR No.17-52-45048. Mini-MegaTORTORA belongs to Kazan Federal University and the work is performed according to the Russian Government Program of Competitive Growth of Kazan Federal University. Observations on Mini-MegaTORTORA are supported by the Russian Science Foundation grant No. 14-50-00043.

References

[1] Beskin, G., Bondar, S., Karpov, S., Plokhotnichenko, V., Guarnieri, A., Bartolini, C., Greco, G., Piccioni, A., & Shearer, A. 2010a, Advances in Astronomy, 2010

[2] Beskin, G. M., Karpov, S. V., Plokhotnichenko, V. L., Bondar, S. F., Perkov, A. V., Ivanov, E. A., Katkova, E. V., Sasyuk, V. V., & Shearer, A. 2013, Physics Uspekhi, 56, 836

[3] Beskin, G., Karpov, S., Bondar, S., Perkov, A., Ivanov, E., Katkova, E., Sasyuk, V., Biryukov, A., & Shearer, A. 2014, in Revista Mexicana de Astronomia y Astrofisica Conference Series, Vol. 45, Revista Mexicana de Astronomia y Astrofisica Conference Series, 20

[4] Biryukov, A., Beskin, G., Karpov, S., Bondar, S., Ivanov, E., Katkova, E., Perkov, A., & Sasyuk, V. 2015, Baltic Astronomy, 24, 100

[5] Zolotukhin, I., Beskin, G., Biryukov, A., Bondar, S., Hurley, K., Ivanov, E., Karpov, S., Katkova, E., & Pozanenko, A. 2004, Astronomische Nachrichten, 325, 675

[6] Karpov, S., Beskin, G., Biryukov, A., Bondar, S., Hurley, K., Ivanov, E., Katkova, E., Pozanenko, A., & Zolotukhin, I. 2005, Nuovo Cimento C, 28, 747

[7] Karpov, S., Beskin, G., Bondar, S., Guarnieri, A., Bartolini, C., Greco, G., & Piccioni, A. 2010, Advances in Astronomy, 2010

[8] Molinari, E., Bondar, S., Karpov, S., Beskin, G., Biryukov, A., Ivanov, E., Bartolini, C., Greco, G., Guarnieri, A., Piccioni, A., Terra, F., Nanni, D., Chincarini, G., Zerbi, F., Covino, S., Testa, V., Tosti, G., Vitali, F., Antonelli, L., Conconi, P., Malaspina, G., Nicastro, L., & Palazzi, E. 2006, Nuovo Cimento B, 121, 1525

[9] Beskin, G., Karpov, S., Bondar, S., Greco, G., Guarnieri, A., Bartolini, C., & Piccioni, A. 2010b, ApJ, 719, L10

[10] Beskin, G. M., Karpov, S. V., Bondar, S. F., Plokhotnichenko, V. L., Guarnieri, A., Bartolini, C., Greco,G., & Piccioni, A. 2010c, Physics Uspekhi, 53, 406

[11] Beskin, G., Biryukov, A., Bondar, S., Hurley, K., Ivanov, E., Karpov, S., Katkova, E., Pozanenko, A., & Zolotukhin, I. 2004, Astronomische Nachrichten, 325, 676

[12] Lang, D., Hogg, D. W., Mierle, K., Blanton, M., & Roweis, S. 2010, AJ, 139, 1782

[13] US Department of Defence. 2015, Database of satellite orbital parameters, available at http://www.space-track.org/

[14] McCants, M. 2015, Satellite Tracking TLE page, available at https://www.prismnet.com/~mccants/tles/index.html

[15] Karpov, S., Katkova, E., Beskin, G., et al. 2016b, Revista Mexicana de Astronomia y Astrofisica Conference Series, Vol. 48, 112–113

[16] Karpov, S., Orekhova, N., Beskin, G., et al. 2016c, Revista Mexicana de Astronomia y Astrofisica Conference Series, Vol. 48, 97–98

[17] Stanbro, M. & Meegan, C. 2015, GRB Coordinates Network, 18570

[18] Karpov, S., Beskin, G., Bondar, S., et al. 2015, GRB Coordinates Network, 18574

[19] Karpov, S., Beskin, G., Bondar, S., et al. 2016a, GRB Coordinates Network, 19603

[20] Troja, E., Butler, N., Watson, A. M., et al. 2016, GRB Coordinates Network, 19588

[21] Xu, D., Malesani, D., Fynbo, J. P. U., et al. 2016, GRB Coordinates Network, 19600

[22] Batsch, T., Castro-Tirado, A. J., Czyrkowski, H., et al. 2016, GRB Coordinates Network, 19615

[23] Li, Z. & Waxman, E. 2008, ApJ, 674, 65

[24] Beskin, G., Karpov, S., Biryukov, A. et al. 2017, Astrophysical Bulletin, Volume 72, Issue 1, pp.81-92

[25] Karpov, S., Beskin, G., Biryukov, A. et al. 2016, Revista Mexicana de Astronomía y Astrofísica (Serie de Conferencias) Vol. 48, pp. 91-96

Fast neutron background in BUST for core-collapse supernova searches

M.M. Kochkarov[1]*, M.M. Boliev[1], Yu.F. Novoseltsev[1],
R.V. Novoseltseva[1], V.B. Petkov[1,2], P.S. Striganov[1]

[1] Institute for Nuclear Research of the Russian Academy of Sciences, Moscow, Russia;
kchkrv@rambler.ru

[2] Institute of Astronomy of the Russian Academy of Sciences, Moscow, Russia

Abstract The natural neutron background influences the maximum achievable sensitivity in most deep underground physics experiments. Baksan Underground Scintillation Telescope (BUST) is a multipurpose neutrino detector. The detector BUST able to detect core collapse neutrino burst via the inverse beta decay. The irreducible background is the neutron flux present at the experimental site, since neutrons produce the same signals as neutrinos do. In this paper we discuss our technique to measure low-intensity neutron fluxes and the application of this technique to the study of the neutron background from rock at the BUST experiment.

Keywords: Neutron background, Core Collapse Supernovae, Underground physics, Neutrino

1. Introduction

Deep underground sites provide a unique opportunity to explore the rare events (dark matter, neutrinoless double beta decay, core collapse neutrinos etc.). Most of underground experiments are located at deep underground to reduce the background of cosmic rays. As high-energy muons can penetrate deep underground and generate background to physics experiments, these experiments require precise knowledge of the muon-induced background from surrounding rock.

Cosmic ray muons can be easily vetoed and they do not directly constitute a serious problem. But, the high-energy muons can induce spallation neutrons at the rock surrounding experimental setup. These spallation neutrons have a very broad spectrum that extends up to several GeV in neutron energy. They can travel a long distance into the detector and are difficult to tag. Neutron scattering and capture within the target can restrict experimental sensitivities or bring false positive signals in the studies of rare events. Background from muon-induced neutrons is one of the most important limitations to detector sensitivity for rare event searches. 1The fast neutrons, from (α, n) reactions and fission in the surrounding rocks, are lower in energy than muon-induced neutrons and thus easier to be shielded. It is difficult to suppress background constituted by the fast neutrons with energy above 10 MeV so that they contribute to the total background of an experiment. Measurements of muon-induced neutron flux are important for estimating the sensitivity of an experiment and constructing future detectors. There are the estimation of muon-induced neutrons in an organic liquid scintillator at the depth 850 m water equivalent. In general, such estimation require detailed and experiment-specific Monte Carlo simulations to correct for the neutron contribution from rock, but this is difficult, in particular for the older experiments. In this paper, we present the results of a study of muon-induced fast neutrons from rock for the BUST experiment.

2. Detector and measurements

The BUST [1] is a liquid scintillation detector whose major purpose is the investigation of cosmic ray muons and neutrinos. To shield cosmic ray background, the BUST experiment is located in an excavation under the slope of Mt. Andyrchy (North Caucasus, 43.28^0 N and 42.69^0 E) at the depth of about 300 m or 850 m.w.e. The walls of the excavation are covered with low radioactivity concrete and lined with steel sheets.

The experimental setup consists of an array of 3186 scintillation counters (see ***Fig1***) distributed over eight planes (4 vertical and 4 horizontal). Six of the eight planes form a parallelepiped structure, the other two are located in it at equidistant from each other. The distance between the neighboring horizontal planes is 3.6 m. The frame of the facility is a metallic carcass of steel beams and channels. The inner part of the parallelepiped is framed in the form of a vertical wall of low radioactivity concrete blocks and two storeys. Each storey consisting of an iron sheet and a layer of low radioactivity gravel is covered by concrete. The counters of the horizontal planes are placed on the concrete layers.

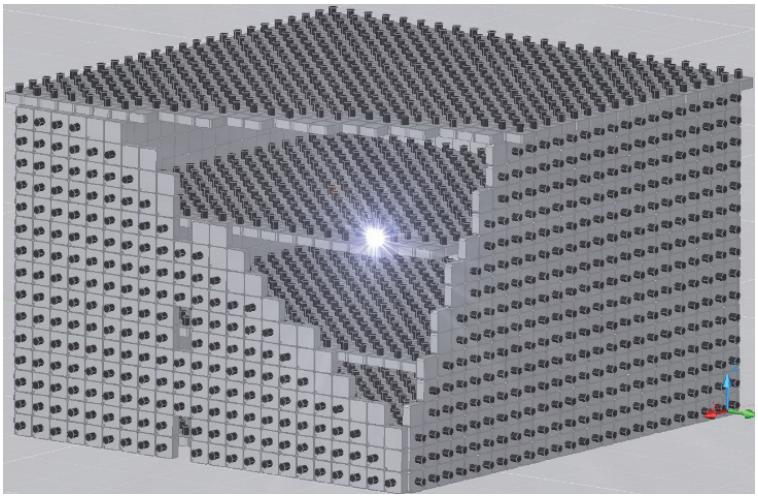

Fig1. *Schematic view of the Baksan Underground Scintillation Telescope of BNO INR RAS.*

The upper horizontal plane consists of 24 × 24 scintillation counters, the rest three horizontal planes accommodate 20 × 20 counters each. Three vertical planes have 15 × 24 counters and one vertical plane is built of 15 × 22 counters. The upper horizontal plane and all vertical planes are serving as an active shield for the internal planes. The total mass of the liquid scintillator contained in 3186 counters is 330 tons. The internal planes have the effective target mass 130 tons and are used for monitoring the Galaxy to study neutrino bursts from gravitational stellar collapses [2]. A standard scintillation counter of the BUST is an aluminium parallelepiped container (see ***Fig2***) with sizes 0.7 × 0.7 × 0.3 m^3 viewed from the top by a 15 cm diameter photomultiplier (PMT) through an organic glass illuminator. A PMT is placed in an iron protective casing.

The pulse discriminator-shaper and LC-converter are attached to the surface of the protective casing. The LC-converter is designed to provide information on the energy deposition in the counter if it exceeds 500 MeV by converting the pulse amplitude from 5th dynode of the PMT to the output pulse duration. The BUST liquid scintillator is a mixture of hydrocarbons (C_9H_{20})

also known as white spirite. The design of the BUST allows to monitor the operation and to process data from each counter. This is useful for a wide range of problems like the study of muon groups or the neutrino signal registration. For registration of rare events such as neutrino from gravitational stellar collapses, the internal planes of the telescope are used. The coordinate information of a triggered counter is constituted by an output signal from the pulse discriminator, which is based on a signal from the 12th dynode of the PMT. The threshold of the pulse discriminators for the horizontal planes is 8 MeV and 10 MeV for the vertical ones. On each plane the anode signals are integrated through a chain of summators. This scheme allows to get information about the energy deposition in the plane and to measure the time of flight of muons as well as to reconstruct their trajectories. Since 2001, the facility is operating in the continuous data acquisition mode using a passive and active shielding to reduce backgrounds. The scintillator serving as a passive hydrogen-rich shielding and the counters as the active charged-particle detectors used to moderate neutrons and veto muon-induced events, respectively.

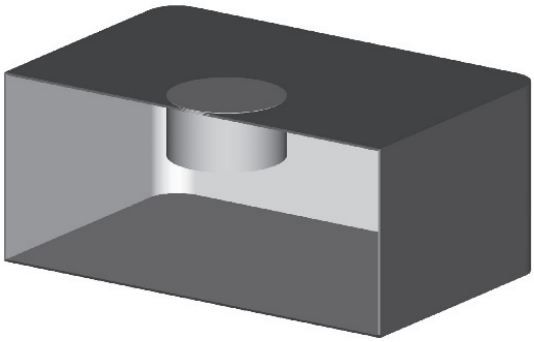

Fig2. *Schematic view of the standard scintillation counter tank.*

In experiments searching for rare events, signals from neutrons have the same signature as the useful signal. In particular, the registration of electron anti-neutrinos [2] at the BUST made mainly through the inverse beta-decay reaction of electron antineutrinos on protons $\tilde{\nu_e}$ + p → e^+ + n. The signal from the positron appears as a single operation of one of the internal counters, at the absence of signals from the other counters. Since the cross sections of reactions with neutrinos are relatively small, all possible reactions with neutrons effectively mimic signals from neutrinos. Neutrons produce background via elastic scattering on protons. At the same time, inelastic neutron-induced reactions with the carbon of the scintillator allow to measure the neutron flux with sufficient accuracy. During the passage of the neutrons through the scintillator unstable radioactive isotopes are generated.

Neutron induced reactions in organic scintillator are interest due to possibility to get information about neutron background. Significant in this respect are the reactions leading to the emission of charged particles. Among them the $^{12}C(n, p)^{12}B$ reaction leads to the emission of protons and energetic electrons above the threshold of BUST counters. The prompt signal from the proton and the delayed signal from the electron from the unstable isotope beta decay constitute the double signature. The BUST can detect unstable radioactive isotope formation and its subsequent beta decay. The $^{12}C(n, p)^{12}B$ reaction has been exploited in the present analysis. Theoretically ^{12}N isotope is known to be not directly produced by the primary neutron, but rather the recoil proton (n + p → n + p) interacting with the ^{12}C: $^{12}C(p, n)^{12}N$. The ^{12}N decay has the same signature as the ^{12}B decay reaction, so this background events can only be statistically subtracted from the data.

A large number of pairs of signals allow to construct the distribution of the time intervals between the signals in the pair. The approximation of distribution of the time intervals between

the signals in the pair by a decay curve makes it possible to estimate the number of radioactive isotopes produced during the observation time. The produced number of ^{12}B nuclei neutrons N_B related to the neutron flux j(E) through the following expression:

$$N_B = n \cdot f \cdot t \cdot \int_{E_{thr}}^{E_{max}} \sigma(E) \cdot j(E) dE \quad (1)$$

where *n* the numbers of target nuclei, *f* is the detection efficiency, *σ(E)* is the differential cross section of the reaction, *t* is the observation time. The energy range covered by the integral spans from the counter threshold for neutrons up to highest neutron energy E_n .

The values of the cross section largely vary depending on the selected model. We use as a benchmark for the predictions of the model calculations the integral measurement of the $^{12}C(n, p)^{12}B$ reaction performed at the neutron time-of-flight facility [3] at CERN. The best evidence for the $^{12}C(n, p)^{12}B$ cross-section comes from n_TOF experiment. The n_TOF result has been compared with evaluated cross-sections used in GEANT4. Among models in GEANT4 good agreement is noticed only with a combined Bertini/Binary cascade model. In this work the neutron flux was estimated on the basis of the cross-section from the Binari/Bertiny model evaluation up to 100 MeV. The neutron flux from the rock above 10 MeV is roughly inversely proportional to the neutron energy [4]. In this case, equation (1) reduces to

$$N_B = n \cdot f \cdot t \cdot k \cdot \int_{E_{thr}}^{E_{max}} \sigma(E)/E \, dE \quad (2)$$

This allows one to determine the proportionality factor *k*. Thus, the differential neutron flux can be written as:

$$j(E) = \frac{N_B}{n \cdot f \cdot t \cdot \int_{E_{thr}}^{E_{max}} \sigma(E)/E dE} \cdot \frac{1}{E} \quad (3)$$

Because of the quenching of the proton light yield in scintillator [5], and taking into account the detector energy threshold (E = 8 MeV), the neutrons with the double signature have energies greater than 28.6 MeV (i.e. E_{thr} = 28.6 MeV).

3. Data analysis and results

To estimate the neutron flux, the BUST data collected from 2001 to 2017 were used. Only those events that appear as two consecutive signals from the same counter in the absence of any signal from the other counters were selected. From each counter, we get information which includes the coordinate of the triggered counter, energy deposition in the volume of the counter and the time information. To have the decay of a ^{12}B nucleus with high probability, the time interval between a pair of events was chosen to be equal to 6 half-lives of ^{12}B. We fitted the distribution of the signal pairs per counter by the Poisson distribution throughout the observation time. The counters which gave the number of signals pairs exceeding that predicted by Poisson distribution were excluded from the data processing. The presence of the radioactive boron is indicated by fitting the distribution of the time intervals (see ***Fig3***) between each pair of signals by the decay curve $F(t) = a \exp(-\Delta t/\tau_B) + a_N \exp(-\Delta t/\tau_N) + b$ (τ_B and τ_N is the mean lifetime of ^{12}B and ^{12}N respectively).

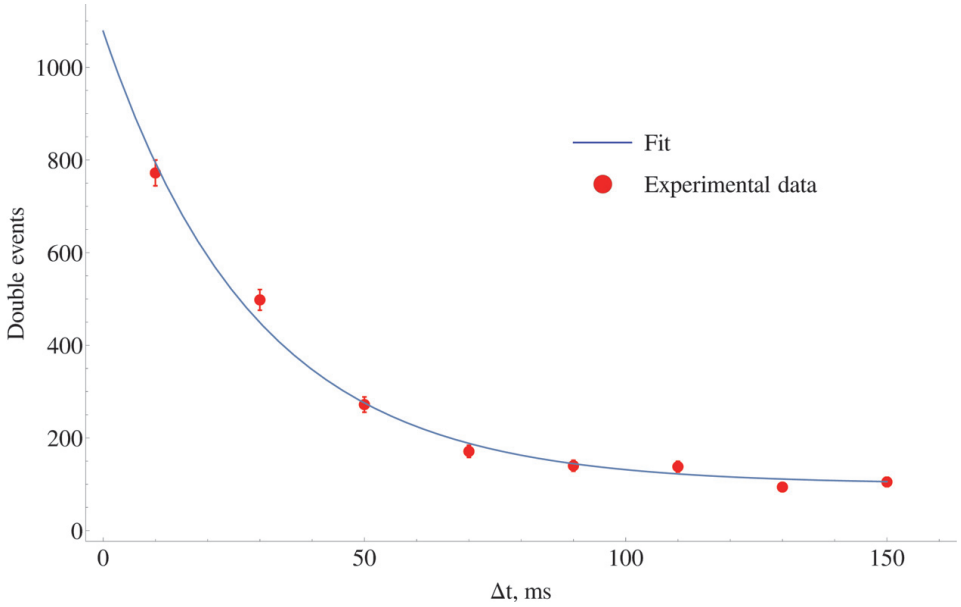

Fig3. *Fitting the distribution of the time intervals between each pair of signals by the decay curve (for upper plane of BUST).*

From the parameter a we obtain the number of ^{12}B isotopes, while b and a_N gives the level of background events. The chi-square distribution minimization method was applied to fitting. Subsequently, the number of the produced ^{12}B nuclei was converted into the neutron flux according to equation (3). The response function f of individual counter to double event reactions has been evaluated using Monte Carlo code. All the involved processes, including energy loss, multiple scattering etc., have been taken into account.

The counters of BUST are commonly divided into two groups: the inner counters (for search neutrino signal from supernova remnants) and the outer counters (used as an active muon veto).

We calculated the average neutron flux for external group of counters using the equation (3). After taking into account the above mentioned considerations, the total neutron flux with 28.6 to 100 MeV is

$$\Phi_n \simeq 2.33 \cdot 10^{-9} cm^{-2} \cdot s^{-1}$$

for the experimental hall of BUST detector. Due to Monte Carlo estimation of registration efficiency, we obtain a more accurate result in comparison with previous data processing [6]. According to Monte-Carlo modelations [7] the following equation predicts the muon induced neutron flux as a function of depth:

$$\Phi_{pred}(h_0) = P_0 \cdot (P_1/h_0) \cdot e^{-h_0/P_1},$$

where h_0 is the equivalent depth in km.w.e relative to a flat overburden, and P_0 , P_1 are the fitting parameters. The muon-induced neutron flux at the 0.85 km.w.e. (BUST) was obtained using a scailing method Φ_{pred} (0.85) = 15.1 · 10^{-9} cm^{-2} s^{-1} . The value Φ_{pred} (0.85) is in qualitative agreement with our results.

4. Conclusion

The experimental data collected by the BUST detector were used to estimate the neutron flux at the external counters of facility. The experimental method is based on the delayed coincidences between two signals from any of the BUST counters. It is assumed that the first signal is due to inelastic interaction of a neutron with the organic scintillator, while the second

signal comes from the decay of an unstable radioactive isotope formed when the fast neutron interacts with the ^{12}C nuclei. The experimentally found muon induced neutron flux (for neutron energies $E \geq 28.6$ MeV) is in a qualitative agreement with predictions of the Monte-Carlo (FLUKA) models.

Acknowledgements

This study is performed with a part of the instrument certified as a Unique Scientific Facility (Baksan Underground Scintillation Telescope) and at an office that is an item of the Shared Research Facilities state program (Baksan Neutrino Observatory of the Institute for Nuclear Research).

References

[1] Alekseev E N et al. 1998 Phys. Part. Nucl. 29 254

[2] Novoseltseva R V et al. 2011 Bull. Russ. Acad. Sci., Phys. 75 419

[3] Žugec P et al. 2014 Phys. Rev. C 90 021601

[4] Agafonova N Y et al. 2013 Phys. Rev. D 87 113013

[5] Bruno G 2013 Journal of Instrumentation 8 T05004

[6] Boliev M. M. et al. 2017 Bull. Russ. Acad. Sci.: Phys. 81 509

[7] Mei D-M et al. 2006 Phys. Rev. D. 73 053004

Real-time multimessenger observation system for the search of optical counterparts of the high energy events

A.N. Kurenya[1], I.M. Dzaparova[1,2], D.D. Dzhappuev[1], E.A. Gorbacheva[1], O.I. Mikhailova[1], M.A. Nalivkin[2], S.A. Naroenkov[2], V.B. Petkov[1,2], V.B. Puzin[2], I.S. Savanov[2], A.V. Sergeev[1,2], A.F. Yanin[1]

[1]Institute for Nuclear Research of the Russian Academy of Sciences,
60th October Anniversary Prospect, 7a, 117312 Moscow, Russia; kurenyaalexandr@rambler.ru

[2]Institute of Astronomy of the Russian Academy of Sciences,
48 Pyatnitskaya St., 119017, Moscow, Russia

Abstract The system for prompt search and follow-up study of transient astrophysical objects in optical and high-energy gamma ranges is under developing now. The search for the bursts of cosmic rays and cosmic gamma radiation will carry out at the complex of facilities of the Baksan Neutrino Observatory. The search and follow-up study for optical flashes accompanying high energy events will carry out at the complex of astronomical telescopes of the Terskol Peak Observatory. The universal control program of the astronomical telescopes has been developed. The program allows searching for transient phenomena in the optical range using external alerts (from BNO facilities, the GCN network, etc.).

Keywords: transient phenomena, multi-messenger observation, real-time systems

1. Introduction

Of late years the multi-messenger approach is widely applied for the study of astrophysical objects and transient phenomena. The fact of the matter is that the high-energy sky has revealed a large number of powerful astrophysical objects capable to emit radiation across the entire electromagnetic spectrum. Now it is obvious that the joint study of the different "cosmic messengers" (cosmic rays, neutrinos, photons, and gravitational waves) is necessary for the complete understanding of the most energetic phenomena in the Universe.

At present the quick search for astrophysical objects which produce both, bursts of high energy cosmic radiation and optical flashes, is carried out in the near real-time mode with the system for collecting and analyzing data from the facilities of the Baksan Neutrino Observatory (BNO) of INR RAS and a complex of astronomical telescopes at the Terskol Peak Observatory (Terskol branch of INASAN). Unique complex of BNO facilities is intended for study of cosmic rays and cosmic gamma radiation in wide range of primary energies. The complex consists of Baksan Underground Scintillation Telescope (BUST) [1, 2] and two EAS arrays: "Carpet-2" [3] and "Andyrchy" [4]. The BNO facilities work in continuous mode of operation and they are recording of cosmic rays from upper hemisphere (so called "all sky all time" mode). These apparatus allow searching for bursts of cosmic gamma radiation in wide range of primary gamma-rays energy: from 1 TeV (at the BUST) up to 80 TeV (at the EAS arrays "Carpet-2" and "Andyrchy") [5, 6]. The search for the bursts of cosmic radiation (EAS

clusters) is carried out in the near real-time mode using data of the BUST and “Carpet-2” facilities. Then the coordinate position of the burst is used for the search of possible optical counterpart. Integrated server for the data concentration is placed at the BNO. There are two communications paths. First one joins the local networks of BNO and Terskol Peak Observatory by means of radiochannel with Cisco Aironet 1410 units (Figure 1). Second one use Internet. Search for transient phenomena in the optical range is carried out using alerts from BNO facilities. For this purpose the universal control program for the astronomical telescopes has been developed.

Fig1. *Scheme of networking. The local networks of BNO and Terskol Peak Observatory are joined by means of radiochannel implemented on three Cisco Aironet 1410 modules. One module operates at Cheget peak in the access point mode. Two others modules operate in bridge mode at the «Andyrchy» EAS array and at the Terskol peak.*

2. Search for cosmic radiation bursts

Raw experimental data of the BNO facilities are accumulated in the internal memory of on-line computers of each facility during fixed time interval (15 minutes for the BUST and 20 minutes for the “Carpet-2” EAS array) and then are copied to hard disk of the file server. After this the data are analyzed at two dedicated workstations. For each of registered events the EAS arrival direction is reconstructed. A search for bursts in the sky is in fact a search for spatiotemporal clusters of events. In the past this method was applied at the BNO facilities for the searching of gamma-ray bursts [5, 6].

Since the time intervals were taken to be fairly short, the search for spatial clusters of events is performed in the horizontal coordinate system. For each event i with an absolute time t_i and arrival angles $(\theta, \varphi)_i$, we searched for a cluster of such events $i, i + 1, \ldots, i + N - 1$ that the shower arrival directions differed by less than α_r from the weighted mean direction. The maximum time difference in the cluster should not exceed 10 s. Thus, each cluster is characterized by the multiplicity N, duration Δt, absolute time T, and arrival direction (θ, φ). At the moment the size of the angular cell, α_r, was chosen in such a way that the cell contains about 96% of the events from point-like source. On the assumption of Rayleigh distribution α_r is 3º for the BUST and 5.58º for the EAS array “Carpet-2”. It should be noted that such selection conditions gives us too large number of clusters (about several thousand per day)

with the purpose to use they as alerts. Therefore in this experiment the clusters are discriminated on duration against their multiplicity. And in the issue only 0.15% of clusters are used as alerts. In the first place this discrimination allows separating clusters with large multiplicity, i.e. bursts with large energy fluxes. The clusters of short duration with small multiplicity are used as alerts, too. The discrimination used allows us to save a part of events for the search for hypothetical evaporating primordial black holes [7, 8]. In what follows at the EAS array "Carpet-2" the method of separation of showers produced by primary photons will be used [9].

3. Remote control of the astronomical telescopes complex

The work with experimental data is carried out using dedicated server which is placed at the laboratory building of BNO. Access to the experimental data of BNO facilities is realized by means of two communications paths. First one is the internetworking of the local networks of BNO and Terskol Peak Observatory. The radiochannel on base of three Cisco Aironet 1410 units is used (***Fig2***). One module operates at Cheget peak in the access point mode. Two others modules operate in bridge mode at the "Andyrchy" EAS array and at the Terskol peak. The module operated at the "Andyrchy" EAS array is connected with BNO laboratory building by optical cable.

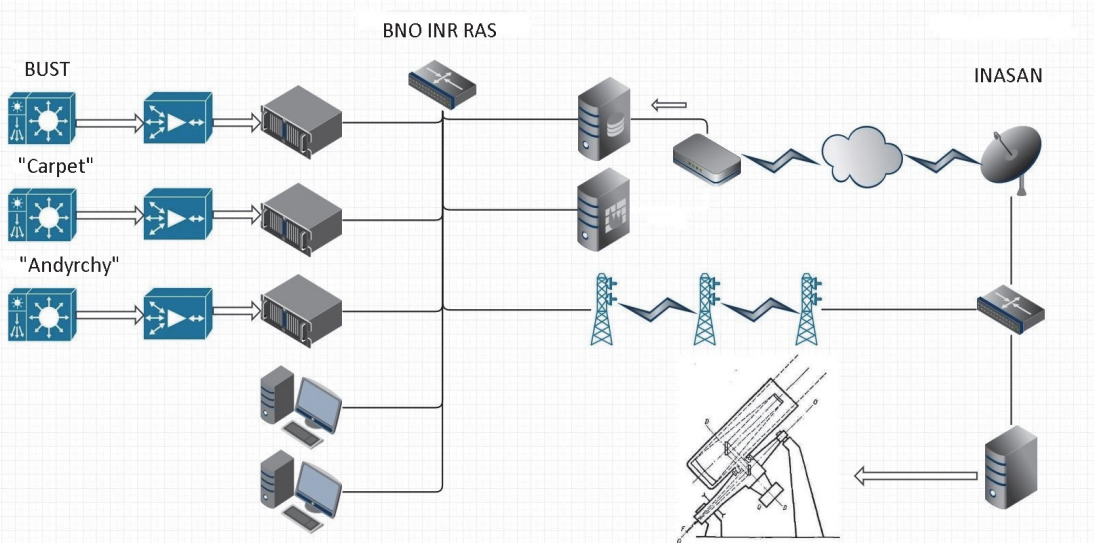

Fig2. *Block diagram of the system for the search of optical counterparts of the high energy events.*

Second one is routing through the Internet with a fixed IP address. Both communications paths allow us to connect with dedicated server via HTTP and FTP, and over the local network using the SMB protocol. The communications paths and the dedicated server are protected from the extraneous access.

The program for control of the complex of astronomical telescopes is designed to work with astronomical instruments (support-rotating device, CCD camera, wheel of light filters, dome) during observation sessions. This program uses the ASCOM standard (Astronomy Common Object Model) what allows to communicate with any equipment using this standard. Advantage of the ASCOM standard is the possibility to operate with different instrument

models, irrespective of their manufacturer. And the program for control of the complex of astronomical telescopes interplays with any software driver of astronomical instruments (***Fig3***).

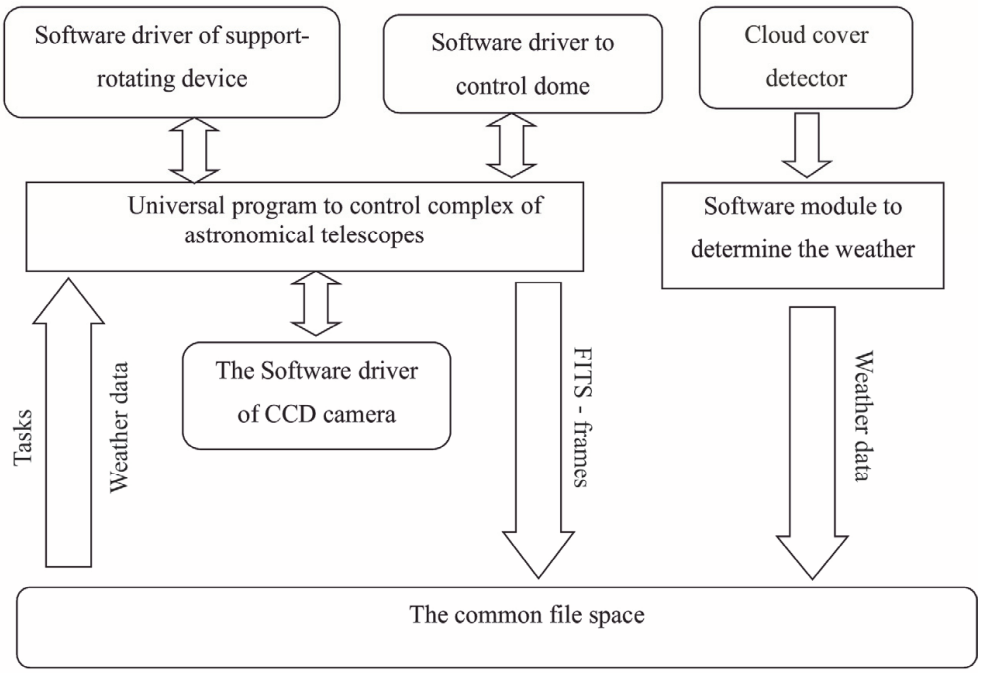

Fig3. *Scheme of intercommunications between devices drivers and universal control program of the astronomical telescopes complex*

The program has a mode of operation "robotic telescope". Weather permitting at the onset of navigational twilight the software drivers of dome, rotary support and CCD camera will be turn on. The schedule of observation session will be loaded from web-server in automatic mode. If during observation session alerts with greater priority (from BNO facilities or GCN) appear then program flow is interrupted and subsequent observations are conducted using pointing from these alerts.

The test observation sessions revealed that the observation process is under way in automatic mode without failures. But due to wide field of view of BNO facilities the wide-field optical telescopes are needed for such kind of investigations.

4. Conclusion

Prompt search for optical counterparts of high energy events, revealed by EAS arrays and neutrino telescopes, is very important for the study of cosmic transient phenomena. To date such search is carried out at the complexes of facilities of the Baksan Neutrino Observatory and astronomical telescopes at the Terskol Peak Observatory in the near real time mode.

At the moment a real time system is under development. New system will allows making essential progress in the study of transient astrophysical objects.

Acknowledgements

This study is performed with a part of the instrument certified as a Unique Scientific Facility (Baksan Underground Scintillation Telescope) and at an office that is an item of the Shared Research Facilities state program (Baksan Neutrino Observatory of the Institute for Nuclear Research). The work is supported by the Russian Foundation for Basic Research, project number 16-29-13034.

References

[1] E.N. Alekseyev et al. Baksan underground scintillation telescope. Proc. 16 ICRC, v. 10, p. 276, 1979.

[2] E.N. Alekseyev et al. The Baksan underground scintillation telescope. Phys. Part. Nucl. v. 29, p. 254, 1998.

[3] D.D. Dzhappuev et al. Modernization of the Carpet-2 array of the Baksan Neutrino Observatory. Bull. Russ. Acad. Sci. Phys., v. 71, No. 4, p.525, 2007.

[4] V.B. Petkov et al. Andyrchy Facility for Detection of Cosmic Rays. Instruments and Experimental Techniques, v. 49, No. 6, p. 785, 2006.

[5] D.V. Smirnov et al. Search for UHE gamma-ray short transients at Andyrchy EAS array. Proc. 29 ICRC, v.4, p.451, 2005.

[6] D.V. Smirnov, V.B. Petkov, and S.N. Karpov. Search for Ultrahigh-Energy Cosmic Gamma-Ray Bursts on the Baksan Underground Scintillation Telescope. Astronomy Letters, v. 32, No. 1, p. 1, 2006.

[7] V.B. Petkov et al. Searching for Very-High-Energy Gamma-Ray Bursts from Evaporating Primordial Black Holes. Astronomy Letters, v. 34, No. 8, p. 509, 2008.

[8] V.B. Petkov et al. Experimental search for gamma-ray bursts from evaporating primordial black holes. J.Exp.Theor.Phys., v. 110, p. 406, 2010.

[9] D. D. Dzhappuev et al. The Carpet-3 experiment to search for diffuse gamma rays with energies of more than 100 TeV. Bull. Russ. Acad. Sci. Phys., v. 81, No. 4, p.424, 2017.

Program of scientific researches at the BNO INR RAS – 50 years into operation

V.V. Kuzminov[1]

[1] Institute for Nuclear Research of the RAS, 60-th October Anniversary Prospect, 7a, Moscow 117312, Russia; bno_vvk@mail.ru

Abstract Brief historical information about different episodes of the Baksan Neutrino Observatory of the INR RAS creation is presented. Ground-based and underground facilities are described. A list of the main tasks solving with these facilities and some main results are given. Perspective plans of the investigations are viewed.

Keywords: Cosmic Rays, Solar Neutrino, Low Background Researches, Ground Level and Underground Installation Complex

1. Introduction

In the late 1950s, the ideas were proposed to build an underground complex of scientific facilities to carry out fundamental researches in cosmic ray physics and neutrino astrophysics. In the 1960s Academician M. A. Markov, the leading figure in this field at that time, suggested to study the weak interaction in underground experiments using neutrino from cosmic rays. The suggested technique was based on registration of muons generated in the interactions of neutrino with nucleons of matter of the Earth's interior. Theoretical calculations were performed and first evaluation of intensity of high energy neutrino flux from possible galactic sources was obtained.

Another field of research that needs underground laboratories is studying the neutrino flux coming from the Sun. The background of ground-based detectors is significantly larger than that of the underground environment, due to cosmic ray muons, and therefore completely masks the sought-for effect.

On June 19, 1963 the resolution of the Academy of Sciences of the USSR approved the construction of an underground complex of laboratories, and a new section in the P. N. Lebedev Physical Institute of the AS of the USSR called "Neutrino" with Professor G. T. Zatsepin as its Head and Professor A. E. Chudakov as his Assistant was organized. The scientific bases and a Neutrino station project were finished to the 1967 year. On June 29, 1967 Council of Ministers of the USSR enacted an order about a creation of the Station (Observatory) and building works ware started at the same year. Professor A. A. Pomansky assigned as a first director of the Station. The mentioned personalities are shown on the photos ***Fig1*** and ***Fig2***.

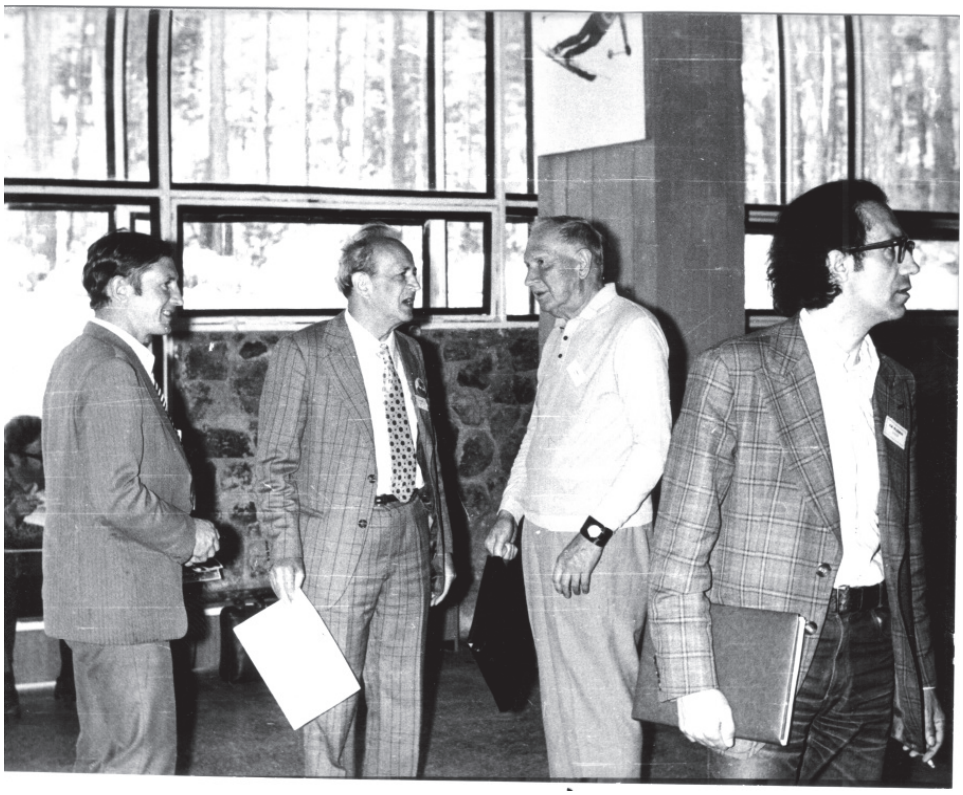

Fig1. *In the lobby of the NEUTRINO'77 conference. (from left to right): 1. Vise director of the BNO INR AS of the USSR E. N. Alexeev; 2) Academician G. T. Zatsepin; 3) Academician M. A. Markov; 4) Corresponding Member V. A. Kuzmin.*

Fig2. *Photo (1972 y.) of people involved in the Baksan Neutrino Observatory creation, (from left to right) the first Director of BNO A. A .Pomansky, the building manager, the researchers V. V. Alekseenko and V. A. Kuznetsov, the official people, Academician G. T. Zatsepin, President of the AS of the USSR Academician M. V. Keldysh, vice Director of BNO E. N. Alexeev, Director of the INR AS USSR Academician A. N. Tavhelidze, Corresponding Member of the AS of the USSR A. E. Chudakov.*

The proper place for the future observatory was found in the vicinity of Mount Elbrus, in the Baksan valley of Kabardino-Balkaria (Russia). According to the building project, two parallel horizontal mines were to be excavated under the mount Andyrchy (3937 m) to accommodate future underground laboratories. Cosmic ray flux at the end of the main tunnel (~ 4000 m from the entrance) is at least 7 orders of magnitude lower than that on the surface.

The original project was to create only two underground laboratories: for the scintillation telescope and chlorine-argon neutrino telescope. Further scientific development lead to construction of many other scientific laboratories related to cosmic ray studies and other researches that require underground shielding conditions. Necessary engineer and utility structures, apartment houses for the staff were built and finally the original project of two facilities gave rise to the Baksan Neutrino Observatory of the Institute of Nuclear Research of RAS, and a newly-born village was called Neutrino. That was the first specialized scientific underground complex built to carry out investigation into a wide spectrum of studies in cosmic ray physics, elementary particles physics, and neutrino astrophysics [1], [2]. In 1998 a group of scientists, namely E. N. Alexeyev, A. V. Voevodsky, V. N. Gavrin, G. T. Zatsepin, A. A. Pomansky, A. N. Tavhelidze and A. E. Chudakov, who had made a major contribution into the creation of the Baksan Neutrino Observatory, was awarded with State Prize. Later V. N. Gavrin and G. T. Zatsepin were awarded with B. M. Pontekorvo Prize and with D. V. Skobeltzin Gold Medal for the creation of Gallium-Germanium Neutrino Telescope and a valuable contribution into the study of solar neutrino.

2. The ground-based complex of BNO

2.1. “Carpet”

In 1973 the first facility of the Observatory came into operation. It was the ground-based detection facility “Carpet” composed of 400 standard scintillation detectors situated in the experimental hall called “Elling”[3]. Each detector is a rectangular aluminum tank (70 cm·70cm·30cm) filled with liquid scintillator on the base of white spirit (a high purity kerosene fraction of petroleum). Each tank is viewed by PMT (15 cm in diameter). In 1973 the first facility of the Observatory came into operation. It was the ground-based detection facility “Carpet” composed of 400 standard scintillation detectors situated in the experimental hall called “Elling”[3]. Each detector is a rectangular aluminum tank (70 cm·70cm·30cm) filled with liquid scintillator on the base of white spirit (a high purity kerosene fraction of petroleum). Each tank is viewed by PMT (15 cm in diameter) through a viewing port mounted on the central round hole of the larger face of the tank. This ground-based facility of 200 m^2 shown in ***Fig3*** is an exact replica of the one of the eight layers of the Baksan Underground Scintillation Telescope that came into operation later.

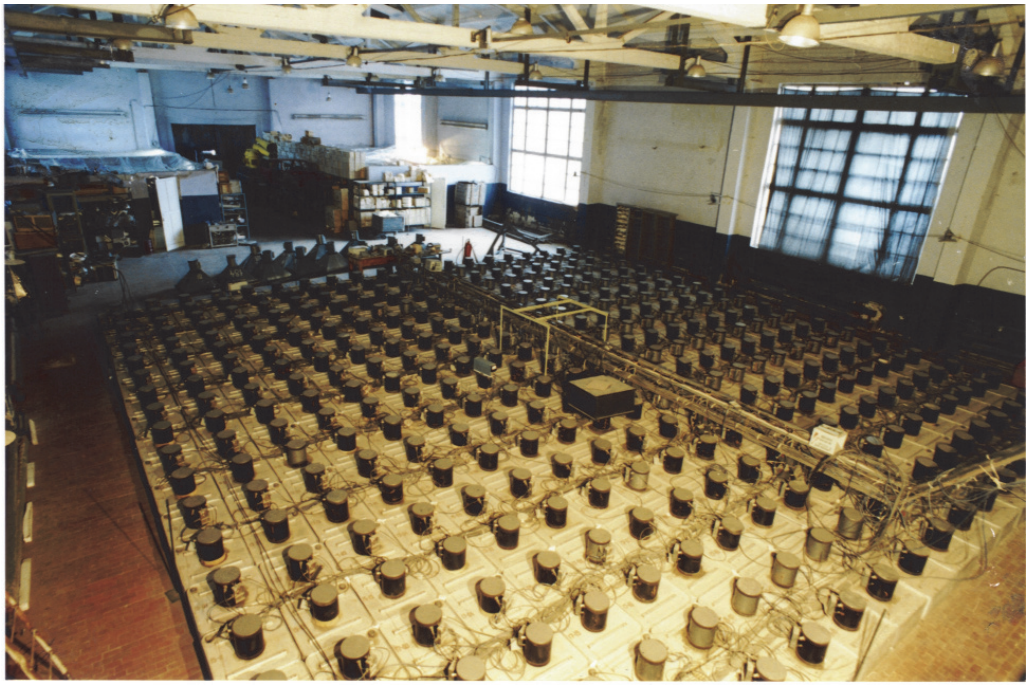

Fig3. *The overview of the "Carpet" facility.*

The "Carpet" facility was targeted to study primary cosmic rays of $5.7 \cdot 10^9 \div 10^{16}$ eV, mechanisms and characteristics of their interaction with particles of the atmosphere by registering a single secondary component together with EAS generated in such interactions.

2.1.1. Main directions of researches

1. **EAS's core.** Analysis of the obtained data allowed one to interpret the presence of multi-jets showers as a result of a generation of streams of particles with large transverse momentum, and to evaluate the cross-section of this process. This experimental result was the first one to confirm quantum chromodynamics predictions [4].
2. **Cosmic rays variations.** Large counting rate of single muons from cosmic rays ($\sim 4.3\ 10^4\ s^{-1}$) allows high statistical accuracy even for small time intervals (0.003% for 4 min), and as a consequence makes it possible to observe short-time variations (micro-variations). None of these have been found with the "Carpet" array at a confidence level of 0.001%. During this research work a new type of sporadic temporary variations characterized by small time was discovered and attributed to the meteorological effects. Their strong correlation with the electric field of the atmosphere (such variations occur only during thunderstorms) allowed one to explain this phenomenon and quantitatively describe it [5]. The gigantic increase of cosmic ray intensity during powerful solar burst on September 29, 1989 is one of the most interesting examples of temporary variations in the muon counting rate. Particles of solar origin with energies up to 10^{10} eV were observed for the first time in such an event, and it was the "Carpet" facility that provided the most evident and accurate data at that time [6].
3. **Cosmic ray anisotropy.** Studying showers of low energy corresponding to primary

cosmic rays (c.r.) of 10^{13} eV revealed anisotropy of the latter. First and second harmonics have been found in the count rate of these showers for sidereal time. C.r. anisotropy for 10^{13} eV was calculated to be (0.057 ± 0.005)% [7].

4. **Ultra-high energy gamma-astronomy.** Air showers of E ≥ 10^{14} eV are continuously registered and the data are analyzed along several lines: search for point sources of gamma-quanta of the same energy; search for signals from extended gamma-ray sources (mainly in the galactic plane); search for c.r. anisotropy at these energies; search for x-ray and gamma-ray bursts for known sources. One of the interesting results is the registration of the burst in Crab Nebula, on February 23, 1989. It was the team of scientists of "Carpet" that first published the result [8]. Later it was confirmed by teams of Kolar Gold Mine (India) and EAS Top (LNGS) facilities.
5. **Neutron flux variations in the atmosphere.** Studying air neutron flux variation involves continuous recording of neutron monitor count rate; the data obtained are sent across internet to www.nmdb.eu-nest-seach.php. Analysis of the parameters of variations presents information used in further studies of characteristics of solar bursts and their effect on the interplanetary magnetic field.

2.2. "Carpet-2(3)"

"Carpet" performance was significantly improved after coming into operation in 1998 of one section (the middle one) of the three-sectioned large underground Muon Detector facility (MD). The middle section is at ~ 40 m from the "Carpet"'s center. MD is under 2 m layer of the ground (5 m w.e.) which absorbs the soft c.r. component and is composed of 175 scintillator detectors (1 m^2 each and made of plastic scintillator of 5 cm thickness). The continuous registering area of the facility is 175 m^2 (5 m x 35 m). The new complex installation was named "Carpet-2". The "Carpet-2" facility allows studying EAS muon component. The dependence of the mean number of muons of ≥ 1GeV (N_μ) registered by MD on the total number of EAS particles (N_e) has been found as $N_\mu \sim N_e^{\alpha}$, where $\alpha = 0.8$. Analysis of the data obtained with MD and "Carpet" allowed scientists to significantly increase the sensitivity of the experiment searching for local sources of ultrahigh energy gamma-quanta, to start studying chemical composition of primary cosmic rays of $E \geq 10^{14}$ eV, and to carry out investigation of variations of muons with energies above 1 GeV [9].

The creation of "Carpet-3", the advanced version of "Carpet-2", is now in progress. Occupation of the two residual underground hall sections with the detectors is finishing. The sensitive area will increase up to 615 m^2. It is supposed to be a multipurpose facility registering cosmic rays. Its main purpose would be to study the knee of the c.r. spectrum. "Carpet-3" would register the following components of EASs: 1) electron and photon; 2) muon (with threshold of 1GeV); 3) hadron.

2.3. "Andyrchy"-array

In 1996 the "Andyrchy "array targeted to register EASs with $E_0 \geq 10^{14}$ eV came into operation. It consists of 37 standard detectors (1 m^2 each, plastic scintillator of 5 cm thickness) evenly spread over the area of 45.000 m^2 on the slope of the Andyrchy mountain with a maximum gradient of altitude of 150 m and at a distance of 40 m from each other [10]. The central detector of "Andyrchy" is located over BUST, and a vertical thickness of mountain rock separating them is 350 m.

The following researches are carried out at "Andyrchy": ultrahigh energy gamma-astronomy [11]; anisotropy of cosmic rays with $E_0 \geq 10^{14}$ eV [12]; search for gamma-ray bursts with hard energy spectrum [13].

3. The underground complex of the BNO facilities

Schematic view of a longitudinal section of the BNO adit and Andyrchy slope is shown in ***Fig4*** presenting the locations of different underground laboratories and the dependence of underground muon flux on the distance from the entrance. Descriptions of the laboratories are adduced below.

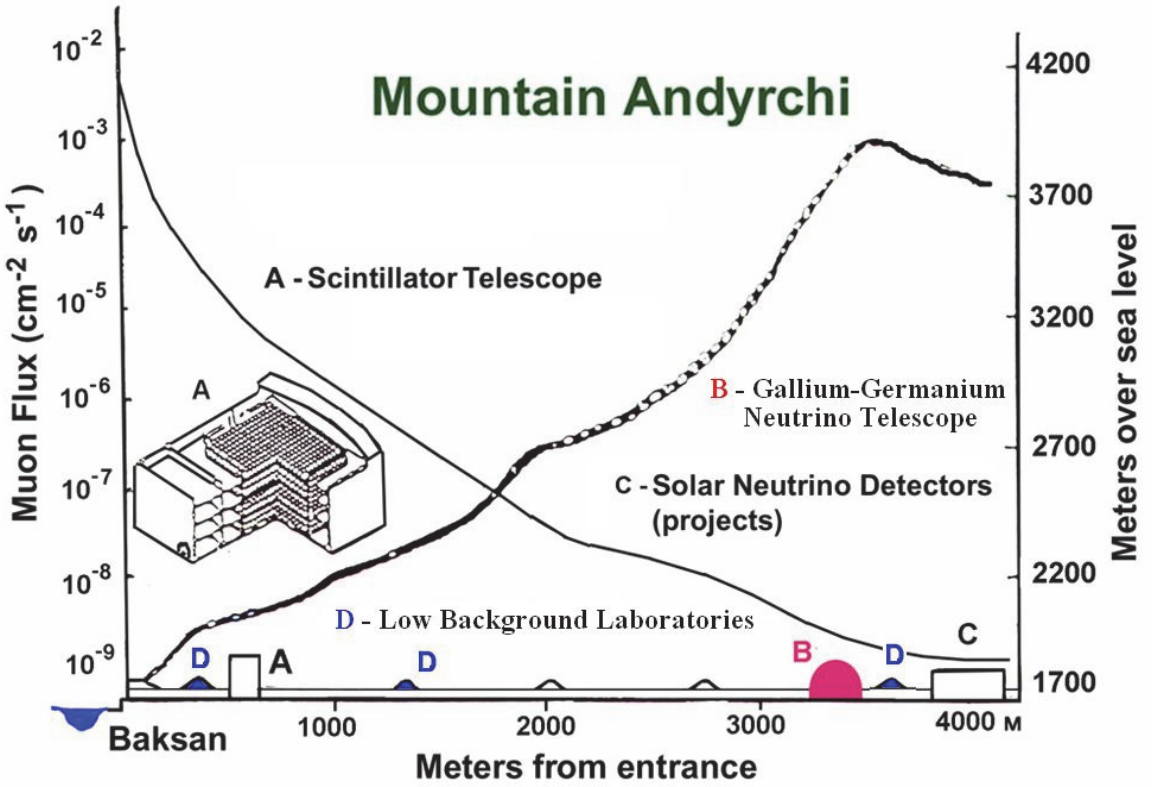

Fig4. *Schematic view of a section of the Andyrchy slope along the adit (right scale) and dependence of underground muon flux on the laboratory location depth (left scale).*

3.1. The Baksan Underground Scintillation Telescope

The Baksan Underground Scintillation Telescope (BUST) has come into operation in 1978. It was targeted to solve various tasks in astrophysics, cosmic rays physics and elementary particle physics [14]. BUST is situated in the underground hall of ~ 12.000 m^3 at a distance of 550 m from the entrance to the underground horizontal tunnel.

A view of the BUST hall at the one of the building moment is shown in ***Fig5***.

The telescope is a rectangular building of 11.1 m height and 280 m^2 base. The blocks of the building are made of low-radioactive concrete. Its four horizontal and four vertical planes are covered with standard scintillation detectors (3180 in total). The total mass of the telescope is 2500 t, that one of the scintillator is 330 t. A view of one of the horizontal planes is shown in ***Fig6***.

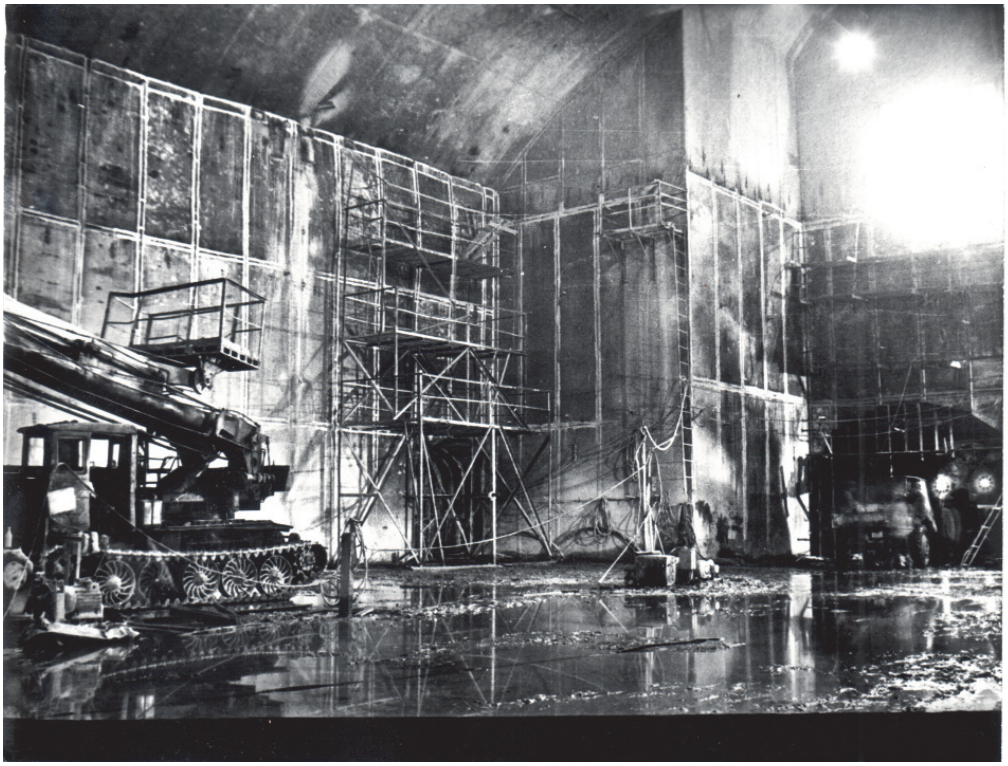

***Fig5**. Photo of the BUST hall at the one of the building* moment

***Fig6.** View of the BUST top horizontal plane.*

Though relatively small, the thickness of the mountain rock above the telescope reduces the background caused by c.r. by 3600 times in comparison with that on the surface (the count rate of single muons with $E > 0.2$ TeV is 12 s^{-1}). The reduced c.r. background allows

scientists to study problems related to rare processes registration, such as measurement of the muon flux generated by high-energy neutrino; search for neutrino bursts accompanying a star collapse in the Galaxy, and others. At the same time, the residual c. r. intensity in the underground environment allows one to carry out a research into a wide range of tasks of cosmic ray physics: anisotropy of c.r. of > 10^{12} eV, chemical composition of primary c.r. of $10^{12} \div 10^{16}$ eV, interaction of muons of > 1TeV with matter, and others.

3.1.1. Main results of the BUST experiments

Series of the important results was obtained at the BUST. Some of them are:

1. Muon flux generated by atmospheric neutrino of cosmic rays in the rock under BUST has been measured to be [$I_\mu^\nu = (2.60 \pm 0.15)\ 10^{-13}$ cm^{-2}s^{-1}sr^{-1}] [15].
2. One of the first limits obtained for the oscillation parameters of atmospheric neutrinos of $\nu_\mu \rightarrow \nu_\tau$ and $\nu_\mu \rightarrow \nu_e$ types [16].
3. A limit on high-energy neutrino flux from local sources in the galactic plane was obtained.
4. The best limit, for a time, on the slow and heavy magnetic monopoles was determined [17].
5. The amplitude [$(12.3 \pm 2)\ 10^{-4}$] and phase [1.6 ± 0.8] (in sidereal time) of the first harmonic of c.r. anisotropy have been measured [11].
6. Data accumulated during 34 years (live time 29.8 years) of monitoring the Galaxy in studying neutrino bursts from gravitational stellar collapses gave a limit on the frequency of bursts f to be f<0.077 yr^{-1}(90% C.L.) [18].
7. Neutrino flux from SN 1987 A that collapsed in the Large Magellan Cloud was registered simultaneously with USA, Italy and Japan facilities [19].

3.2. Low-background Laboratories

Low-Background Laboratories (LBL) carry out research of extremely rare reactions and decays with energy release up to 4 MeV. For these studies one needs to diminish not only the background caused by cosmic rays but also that one due to the decay of natural radioactive elements always present in the environment. The latter task has been solved by screening the experimental underground facility with a combination of layers of ultrapure shielding materials absorbing radiation, and by making sure that the facility is made of ultrapure material. The researches carried out in the LBL are search for various modes of double beta-decay of a number of isotopes; search for candidate-particles for dark matter of the Universe; test of the law of electrical charge conservation and many others.

There are three underground laboratories, situated at a different depth, where LBL researches are carried out:

1) low-background chamber at a depth of 660 m w.e, 385 m from the entrance to the tunnel;
2) chamber for precise measurements at 1000 m w.e. depth, 620 m distance from the entrance;
3) deep underground low-background laboratory (DULB-4900) at 4900 m w.e. depth, 3670 m from the entrance [20]. A view of DULB-4900 is shown in ***Fig7***.

Cosmic ray flux in these three chambers is reduced by $2 \cdot 10^3$, $8 \cdot 10^3$, and 10^7, respectively.

Fig7. *A view of DULB-4900.*

A number of low-background facilities based on semiconductor, gaseous and scintillation detectors have been designed, made and used over the years in various experiments such as:

1) Study of cosmogenic radioactive isotope distribution in the samples of moon rock brought by Automatic Interplanetary Stations Luna-16, Luna-20 and Luna-24;
2) Test of the hypothesis of cosmic ray intensity being permanent during the last several hundreds of thousands of years performed by measuring the content of cosmogenic isotope ^{81}Kr in the atmospheric air [21];
3) Experiments searching for two-neutrino and neutrinoless double beta-decay of isotopes of ^{100}Mo, ^{150}Nd. The (2β2ν)-process was obtained for the ^{150}Nd for the first time in the world [22];
4) A series of experiments to search for 2β-decay of the ^{136}Xe [23];
5) A series of experiments to search for 2K-capture in ^{78}Kr [24] and ^{124}Xe isotopes and $2\beta^+$- and $e\beta^+$-decays of ^{78}Kr;
6) Joint (Spain-Russia-USA) experiment IGEX to search for 2β-decay of the ^{76}Ge [25];
7) Search for hypothetic solar axions [26], and many others.

3.3. Gallium-Germanium Neutrino Telescope

Gallium-Germanium Neutrino Telescope (GGNT) is targeted to measure solar neutrino flux which carries unique information on thermonuclear reactions in the central regions of

the Sun as well as on neutrinos themselves. Since 1986 the experiment has been carried out within the frames of the Soviet American Gallium Experiment (SAGE) [27].

The experiment is based on the reaction ($^{71}Ga + \nu_e \rightarrow {}^{71}Ge + e^-$) that was suggested in 1965 by Dr. V. A. Kuzmin. The advantage of this reaction is its low threshold of 0.233 MeV. The pp-neutrinos, having energy up to 0.423 MeV and constituting the main portion of solar neutrino flux, can be registered through this reaction. Radioactive isotope, ^{71}Ge produced in this reaction undergoes decay by electron capture, with $T_{1/2}$=11.4 days half-life. Registering ^{71}Ge decays allows one to determine the number of interacting neutrinos and to calculate the solar neutrino flux.

The underground complex of GGNT laboratories is situated at a distance of 3.5 km from the entrance to the tunnel. A view of the GGNT hall is shown in ***Fig8***.

Fig8. *A view of the GGNT hall.*

About 50 t of metallic gallium in a melted state is placed into seven chemical reactors as a target. A unique and effective technique has been developed to extract ^{71}Ge atoms from the melted metallic gallium target containing $5 \cdot 10^{29}$ of ^{71}Ga atoms. The periodicity of this extraction procedure which is the basic technological process of the telescope is 30 days. The gas GeH_4 is synthesized on the base of the extracted stable Ge-carrier atoms added to the target to extract the generated ^{71}Ge atoms. It constitutes the main component of the gas mixture filled the proportional counter to register ^{71}Ge decays in the underground registration system of GGNT during 4 months, thereby covering $\geq$ 10 half-life periods of ^{71}Ge. Then, within the period of two months, the background is measured. The whole cycle of operations called a run includes ^{71}Ga-target exposition, extraction of ^{71}Ge, and measurement of ^{71}Ge decays.

3.3.1. The results of calibration and solar neutrino experiments

1. The analysis of data obtained in the period of January 1990 - December 2016, including 259 complete runs, yielded $64.76^{+3.5}_{-3.7}$ SNU [28] (1 SNU = 1

interaction per second in the target containing 10^{36} atoms of an active isotope). The result obtained in the SAGE experiment constitutes 51 % from the value of 127.9 ± 8.1 SNU calculated within the frames of the Standard Solar Modal (SSM) BPS08. The SSM value does not take neutrino oscillation into account. This result of SAGE experiment together with the results of other underground experiments registering solar neutrino (Homestake, USA; GALLEX/GNO, LNGS; Kamiokande/SuperK, Japan; SNO, Canada) allows to calculate estimations of : 1) pp-neutrino flux that reaches the Earth in the form of electron neutrino (electron flavor), [(3.4 ± 0.47) 10^{10} $cm^{-2}s^{-1}$]; 2) total neutrino flux produced in pp-reactions inside the Sun and reaching the Earth in various flavors (electron-, muon- and tau-neutrino) due to oscillation of original electron neutrino, [(6.0 ± 0.8) 10^{10} $cm^{-2}s^{-1}$]. The experimental value of the total neutrino flux is in good agreement with the one predicted by SSM, $(5.95 \pm 0.06)\cdot 10^{10}$ $cm^{-2}s^{-1}$.

2. To test and calibrate the techniques used in the SAGE experiment a ^{51}Cr source of $1.91\cdot 10^{16}$ s^{-1} intensity emitting neutrinos of 747 keV (90%) and 430 keV (10%) was used. In this calibration experiment the ratio of the measured rate of ^{71}Ge production to the expected one caused by a source of given activity has been found to be 0.95 ± 0.12 [29].

Another calibration experiment was made with artificial neutrino ^{37}Ar source emitting 811 keV neutrinos of $15.1\cdot 10^{15}$ s^{-1} intensity. The same ratio of the ^{71}Ge production rates has been found to be $0.79^{+0.09}_{-0.10}$ [30].

3.3.2. The experiment BEST

The experiment BEST (Baksan Experiment on Sterile Transitions) with the two concentric zones Ga-target and 3MCi artificial ^{51}Cr neutrino source is preparing at the BNO now [31]. The goals of this experiment are to search for the short-baseline neutrino oscillation and to test of sterile neutrino hypothesis. The detector preparation is finished. A method of the measurements has tested. An intensive work on the power neutrino source preparations is doing.

3.4. OGRAN facility

At a distance of 1350 m from the entrance to the main tunnel, the new laboratory is created to accommodate the Optoacoustic GRavitational ANtenna (OGRAN). The OGRAN facility has been constructed using principles of solid-state and laser interferometer gravitational antennae. Acoustic vibrations of solid-state detector (manufactured in the form of cylindrical aluminum bar with a central axial tunnel) induced by gravity wave are registered by optical resonator Fabri-Perro, whose mirrors are mounted on the far ends of the detector. Low noise of such an optical read-out system allows sensitivity of relative deformation to be of 10^{-18} for the detector of 2.5 t without any cooling procedure. This sensitivity is good enough to detect bursts of gravity wave radiation generated in relativistic cataclysms in the center of our Galaxy (~10 kpc) and its close vicinity (up to 100 kpc) according to optimistic scenarios. OGRAN is the cooperative project carried out by Institute for Nuclear Research of RAS, Institute of Laser Physics of SB RAS and Moscow State University (Sternberg Astronomical Institute- SAI MSU).

The detector would come into operation in 2018.

3.5. Underground complex of Geophysical Facilities

Environmental parameters of the underground laboratory complex are held within stable limits; vibration and acoustic noises are lowered by many times in comparison with those on the surface. Such underground environment provides necessary conditions to carry out various geophysical researches securing their high sensitivity.

There are three underground geophysical laboratories situated at a different distance from the tunnel entrance and supplied with different measuring devices and instruments:

1) laboratory of SAI MSU, at a distance of 530-610 m from the entrance to the tunnel; researches of the Earth strains are carried out with the high-sensitivity wide-band laser interferometer [32];
2) the geophysical laboratory No1, at ~1520 m; it is a nearby geophysical complex of the Schmidt Institute of Physics of the Earth RAS having tilt indicators (inclinometers), magnetic variometers, and earthquake detection station at its disposal;
3) the geophysical laboratory No2, at ~4000 m; it is a distant geophysical complex IPE RAS having tilt indicators, magnetometers, gravimeters, thermometers as well as earthquake detection stations pertaining to Geophysical Survey RAS.

Data obtained in geophysical experiments allow scientists to monitor seismic activity in the earth crust related to the sleeping volcano Elbrus which is at a distance of about 20 km from the underground geophysical complex of facilities.

3.6. Project of the Baksan Underground Large Volume Scintillation Detector

It is proposed to create in the BNO a multipurpose large volume liquid scintillator neutrino detector with a mass of 10 kt intended for the investigations of the neutrino and antineutrino fluxes from the Sun, Earth and other astrophysical sources. It is planning that the detector will placed at the 5000 m w.e. depth. The geographic features of the Observatory location allows one to suppress a background connected with the antineutrino fluxes from nuclear power plants that gives a possibility to register antineutrino flux from the Earth, which gives an information about a constitution and composition of the region earth crust [33].

4. Conclusion

Various researches at the Baksan Neutrino Observatory INR RAS are carried out in collaborations with Institutions all over Russia and the world. To name some of them, Kabardino-Balkarian State University, Federal South University, Moscow State University, National Research Nuclear University MEPHI, Schmidt Institute of Physics of the Earth RAS, Pushkov Institute of Earth magnetism, ionosphere and radiowaves propagation RAS (IZMIRAN), Polar Geophysical Institute RAS, Geophysical Survey RAS, Institute of Astronomy RAS, JINR, Kharkov National University (Ukraine), Institute of Nuclear Problems (Cosmic Ray Laboratory, Lodz, Poland), international collaborations AMoRE, GERDA, LEGEND and EMMA. All these collaborations significantly increase the efficiency of the Baksan complex of ground-based and underground facilities in solving a wide range of problems in modern science.

References

[1] A. A. Pomansky, “Baksan Neutrino Observatory of INR AS of USSR”, Atomnaya energiya, v.44, (1978), 376-383. (in Russian)

[2] V. V. Kuzminov “The Baksan Neutrino Observatory”. Eur. Phys. J. Plus (2012) 127: 113

[3] E. N. Alekseev, V. V. Alekseenko, A. V. Voevodsky et al. “Scintillation detector of 200 m^2 area for the cosmic rays registration”, Izvestiya Akademii Nauk SSSR. Seriya Fizicheskaya, v.38, (1974), 1097-1100. (in Russian)

[4] A. E. Chudakov, D. D. Dzhappuev, A. S. Lidvansky, V. A. Tizengauzen, V. P. Sulakov, G. Navarra. “Investigation of EAS with multicore structure”. Proc. of the 16th ICRC, Kyoto, v.8, (1979), 222-226.

[5] V. V. Alexeenko, N. S. Khaerdinov, A. S. Lidvansky, V. B. Petkov, "Transient variations of secondary cosmic rays due to atmospheric electric field and evidence for pre-lightning particle acceleration". Physics Letters A 301 (2002) 299-306.

[6] V. V. Alexeenko, A. B. Chernyaev, A. E .Chudakov, N. S. Khaerdinov, A. M. Semenov, A. V. Voevodsky. “29 September 1989 GLE at Baksan Air shower Array (BASA)”. Proc. of the 23th ICRC, Calgary, v.3, (1993), 163-166.

[7] Alexeyenko V. V., Chudakov A. E., Gulieva E. N., Sborshikov V.G. “Anisotropy of small EAS ($\sim 10^{13}$ eV)”. Proc. of 17th ICRC, Paris, v.2, (1981), 146-149.

[8] V. V. Alexeenko, Yu. M. Andreyev, A. E. Chudakov, A. S. Lidvasky, S. S. Ozrokov, V. V. Sklyarov, V. A. Tizengauzen, S. L. Osborn. “Burst like event observed by Baksan EAS Array from the Crab Nebule 23 Feb.1989”. Proc. of the 22th ICRC, Dublin, v.1, (1991), 293-295.

[9] D. D. Dzhappuev, A. U. Kudzhaev, V. V. Alexeenko, N. F. Klimenko, A. S. Lidvansky, O. I. Mikhailova, V. B. Petkov, Yu. V. Stenkin, A. L Tsybuk and A. B. Chernyaev. “Studying the Muon and Hadron Components of Extensive Air Showers with the Carpet-2 Array”. Bull. of the Russian Academy of Sciences, Physics, vol. 73, № 5, (2009), 642-644.

[10] E. N. Alekseev et al., "Air shower array 'Andyrchy' above the Baksan Underground Scintillation telescope", Bull. Russ.Acad.Sci. Phys 57, (1993), 668.

[11] V. A. Kozyarivsky, A. S. Lidvansky, V. B. Petkov, and T. I. Tulupova, “Mean Diurnal Variations of Cosmic Ray Intensity as Measured by Andyrchi Air Shower Array ($E \geq 100$ TeV) and Baksan Underground Scintillation Telescope ($E \geq 2.5$ TeV)”. arXiv:astro-ph/0406059v1, 2004.

[12] V. B. Petkov, A. S. Pozanenko, V. M. Loznikov, A. N. Gaponenko, M. V. Andreev, and A. V. Sergeev, "Search for high energy gamma-ray bursts". Astrophys. Space Sci. Trans, 7, (2011), 97-100.

[13] V. B. Petkov, E. V. Bugaev, P. A. Klimai, M. V. Andreev, V. I. Volchenko, G. V. Volchenko, A. N. Gaponenko, Zh. Sh. Guliev, I. M. Dzaparova, D. V. Smirnov, A. V. Sergeev, A. B. Chernyaev, A. F. Yanin, "Searching for Very-High-Energy Gamma-Ray Bursts from Evaporating Primordial Black Holes", Astronomy Letters, v. 34, No. 8, (2008), 509–514. (arXiv:0808.3093v1 [astro-ph], 2008)

[14] E. N. Alexeyev, V. V. Alexeyenko, Yu. M. Andreyev, V. N. Bakatanov, A. V. Butkevich, A. E. Chudakov, M. D. Galperin, A. A. Gitelson, V. I. Gurentsov, A. E. Danshin, V. A. Dogujaev, V. L. Dadikin, Ya. S. Elensky, V. A. Kozyarivsky, I. M. Kogai, N. F. Klimenko, A. A. Kiryushin, Yu. N. Konovalov, B. A. Makoev, V. Ya. Markov, Yu. Ya. Markov, Yu. V. Malovichko, N. A. Metlinsky, A. R. Mishelev, S. P. Miksheyev, Yu. F. Novoselsev, V. G. Sborshikov,

V. V. Sklyarov, V. I. Stepanov, Yu. V. Stenkin, Yu. R. Sulla-Petrovsky, T. I. Tulupova, A. V. Voevodsky, V. I. Volchenko, V. N. Zakideshev. “Baksan underground scintillation telescope”. Proc. of 16th ICRC, Kyoto, v.10, (1979), 276-281.

[15] M. M. Boliev, A. V. Butkevich, A. E. Chudakov, B. A. Makoev, S. P. Mikheyev, V. N. Zakideshev. “ν-flax as measured by Baksan underground telescope”. Proc. of 17th ICRC, Paris, v.7, (1981), 106-109.

[16] М. М. Болиев, А. В. Буткевич, В. Н. Закидышев, Б. А. Макоев, С. П. Михеев, А. Е. Чудаков, «Ограничения на параметры осцилляций нейтрино по данным Баксанского подземного телескопа». Ядерная физика, т.34, вып.5, стр. 1418-1421, 1981.

[17] Yu. F. Novoseltsev, M. M. Boliev, A. V. Butkevich, S. P. Mikheev and V. B. Petkov, "A search for massive magnetic monopoles at the Baksan Underground Scintillation Telescope (BUST)", Nuclear Physics B (Proc. Suppl.), v.151, N1, (2006), 337-340.

[18] Novoseltsev Yu. F., Boliev M. M., Dzaparova I. M., Kochkarov M. M., Novoseltseva R. V., Petkov V. B., Volchenko V. I., Volchenko G. V., Yanin A. F. “A search for neutrino bursts signal from supernovae at the Baksan Underground Scintillation Telescope”. Proc. of International Workshop on Quark Phase Transition in Compact Objects and Multimessenger Astronomy: Neutrino Signals, Supernovae and Gamma-Ray Bursts, (Nizhnij Arkhyz – Terskol, October 7014, 2015), Pjatigorsk, Izdatelstvo "SNEG", 2016, pp. 76-84

[19] E. N. Alexeyev, L. N. Alexeyeva, I. V. Krivosheina, V. I. Volchenko. “Detection of Neutrino Sygnal from SN1987A, using the INR Baksan underground scintillation telescope”. Proc. of the 2nd Int. Sym. UP-87, M., (1988), 85-93.

[20] Ju. M. Gavriljuk, A. M. Gangapshev, A. M. Gezhaev, V. V. Kazalov, V. V. Kuzminov, S. I. Panasenko, S. S. Ratkevich, S. P. Yakimenko. “Working characteristics of the New Low-Background Laboratory (DULB-4900, Baksan Neutrino Observatory)”arXiv: 1204.6424 [physics.ins-det] 01 May 2012 Nuclear Instruments and Methods in Physics Research A 729 (2013) 576–580.

[21] V. V. Kuzminov, A. A. Pomansky. "^{81}Kr production rate in the atmosphere". Proc. of the 18th Int. Cosmic Ray Conf., India, Bangalore, v.2, (1983), 357-360.

[22] A. A. Klimenko, S. B. Osetrov, A. A. Pomansky, A. A. Smolnikov, S. I. Vasilyev. “Search for a two-neutrino mode of double beta decay of the isotope ^{150}Nd”. Pis'ma Zh.Eksp. Teor.Fiz., 58, No.3, (1993), 177-179. (in Russian)

[23] Ju. M. Gavriljuk, A. M. Gangapshev, V. V. Kazalov, V. V. Kuzminov, S. I. Panasenko, S. S. Ratkevich, D. A. Zhantudueva, S. P. Yakimenko. “Results of a search for 2β-decay of ^{136}Xe with high pressure copper proportional counters in Baksan Neutrino Observatory INR RAS”. arXiv:1112.0859v2 [nucl-ex] 20 Dec 2011

[24] Yu. M. Gavrilyuk, A. M. Gangapshev, V. V. Kazalov, V. V. Kuzminov, S. I. Panasenko and S. S. Ratkevich. “Indications of 2ν2K capture in ^{78}Kr” Phys. Rev. C 87, 035501 (2013)

[25] C. E. Aalseth, F. T. Avignone, R. L. Brodzinski, J. I. Collar, E. Garcia, D. Gonzales, F. Hasenbalg, W. K. Hensley, I. V. Kirpichnikov, A. A. Klimenko, H. S. Miley, A. Morales, J. Morales, A. Ortis de Solorzano, S. B. Osetrov, V. S. Pogosov, J. Puimedon, J. H. Reeves, C. Saenz, A. Salinas, M. L. Sarsa, A. A. Smolnikov, A. S. Starostin, A. G. Tamanyan, A. A. Vasenko, S. I. Vasiliev, A. Villar. “Recent Results from the IGEX Double-beta Decay Experiment”. Nucl. Phys. B (Proc.Suppl.), 48, (1996), 223-225.

[26] Yu. M. Gavrilyuk, A. N. Gangapshev, A. V. Derbin, I. S. Drachnev, V. V. Kazalov, V. V. Kobychev, V. V. Kuz’minov, V. N. Muratova, S. I. Panasenko, S. S. Ratkevich, D. A. Semenov, D. A.

Tekueva, E. V. Unzhakov, S. P. Yakimenko. “New experiment on search for the resonance absorption of solar axion emitted in the M 1 transition of 83 Kr nuclei”. JETP Letters, May 2015, Volume 101, Issue 10, pp 664-669

[27] J. N. Abdurashitov, V. N. Gavrin, S. V. Girin, V. V. Gorbachev, P. P. Gurkina, T. V. Ibragimova, A. V. Kalikhov, N. G. Khairnasov, T. V. Knodel, I. N. Mirmov, A. A. Shikhin, E. P. Veretenkin, V. M. Vermul, V. E. Yants, G. T. Zatsepin et al. (SAGE Collaboration), “Measurement of the solar neutrino capture rate with gallium metal”. Phys. Rev. *C* **60** 055801 (1999); astro-ph/9907113

[28] V. N. Gavrin “Contribution of Gallium experiments to the understanding of solar physics and neutrino physics”. Physics of Atomic Nuclei, v.76, N10. (2013), 1238-1243.

[29] J. N. Abdurashitov, V. N. Gavrin, S. V. Girin, V. V. Gorbachev, P. P. Gurkina, T. V. Ibragimova, A. V. Kalikhov, N. G. Khairnasov, T. V. Knodel, I. N. Mirmov, A. A. Shikhin, E. P. Veretenkin, V. M. Vermul, V. E. Yants, G. T. Zatsepin et al. (SAGE Collaboration), et al. (SAGE Collaboration). “Measurement of the response of a gallium metal solar neutrino experiment to neutrinos from a ^{51}Cr source”. Phys. Rev. *C* 59 2246 (1999)

[30] J. N. Abdurashitov, V. N. Gavrin, S. V. Girin, V. V. Gorbachev, P. P. Gurkina, T. V. Ibragimova, A. V. Kalikhov, N. G. Khairnasov, T. V. Knodel, I. N. Mirmov, A. A. Shikhin, E. P. Veretenkin, V. M. Vermul, V. E. Yants, G. T. Zatsepin et al. (SAGE Collaboration), et al. (SAGE Collaboration). “Measurement of the response of a Ga solar neutrino experiment to neutrinos from a ^{37}Ar source”. Phys. Rev. *C* 73 045805 (2006).

[31] V. Gavrin, B. Cleveland, S. Danshin, S. Elliott, V. Gorbachev, T. Ibragimova, A. Kalikhov, T. Knodel, Yu. Kozlova, Yu. Malyshkin, V. Matveev, I. Mirmov, J. Nico, R. G. H. Robertson, A. Shikhin, D. Sinclair, E. Veretenkin, J. Wilkerson. “Current status of new SAGE project with 51Cr neutrino source”. Phys. Part. Nucl. 46 (2015) 131-137

[32] V. K. Milyukov, V. N. Rudenko, B. S. Klyachko, A. M. Kart, A. V. Myasnikov. “Wide-Band Laser Interferometer for Monitoring the Earth Strains”. In: Solid State Laser (Laser Optics’98). Proceedings of the International Society for Optical Engineering (SPIE). v.368, (1998), 116-121.

[33] I. R. Barabanov, L. B. Bezrukov, A. V. Veresnikova, Yu. M. Gavrilyuk, A. M. Gangapshev, V. Yu. Grishina, V. I. Gurentsov, V. P. Zavarzina, V. V. Kazalov, S. D. Krokhaleva, V. V. Kuz’minov, A. S. Kurlovich, B. K. Lubsandorzhiev, S. B. Lubsandorzhiev, A. K. Mezhokh, V. P. Morgalyuk, P. Yu. Naumov, G. Ya. Novikova, V. B. Petkov, A. M. Pshukov, A. Yu. Sidorenkov, V. V. Sinev, Sh. I. Umerov, E. A. Yanovich, T. Enquist, P. Kuusiniemi, J. Joutsenvaara, A. Virkajarvi. “Large-volume detector at the Baksan Neutrino Observatory for studies of natural neutrino fluxes for purposes of geo- and astrophysics”. Physics of Atomic Nuclei, Volume 80, Issue 3, May 2017, pp 446–454

A.E. Chudakov as a scientist and one of the founding fathers of underground physics

A.S. Lidvansky

Institute for Nuclear Research, Russian Academy of Sciences; Moscow; lidvansk@lebedev.ru

Abstract Professor A.E. Chudakov was one of the founders of the Baksan Neutrino Observatory, and it is quite appropriate on the day of its half-centenary to commemorate him and his many-sided research activity. A short review of his scientific achievements is given, with a special emphasis on their pioneer character.

Keywords:, Cosmic Rays, Muons and Neutrinos, Underground Physics, Gamma Ray Astronomy

1. Introduction

Alexander Chudakov started his research career under the supervision of S.N. Vernov in 1946, while still a student. His further biography is extremely simple: for twenty three years (from 1948 to 1971) he was a researcher in the Lebedev Physical Institute of the USSR Academy of Sciences, and for thirty years (1971-2001) he was the head of a laboratory in the Institute for Nuclear Research of the USSR (since 1991, Russian) Academy of Sciences. The principal dates of his scientific career are as follows: PhD degree (1953), Doctor of Science (1959), Corresponding member of the USSR Academy of Sciences (1966), Professor (1969), full member of the Academy (1987), and a member of the Presidium of RAS (1990). From 1983 until the end of his life he was a head of the Council on Cosmic Rays in the Academy of Sciences.

As far as his international activity is concerned, one should notice that he was a member of the International Academy of Astronautics (elected in 1963). Starting from 1975 he was a member of the Cosmic Ray Commission of the International Union of Pure and Applied Physics (IUPAP). Later, he became a secretary (1981-1984) and chairman (1984-1987) of this Commission. However, not his degrees and awards is the subject matter of this paper, I would like rather to consider his contributions to science and him as a scientist type.

2. Pioneer of gamma-ray astronomy and fluorescence method

It was said about one English medieval king that he was “every inch a king”. Alexander Chudakov was “every inch a scientist”, and of a rather special type: he was pioneer par excellence. ***Fig1*** shows the view of the first gamma-ray telescope constructed by Chudakov in Crimea. This was the first instrument specially designed for observations of very high energy gamma rays of cosmic origin, and because of it the Cherenkov astronomy started earlier than satellite astronomy. To confirm the recognition of this fact ***Fig1***

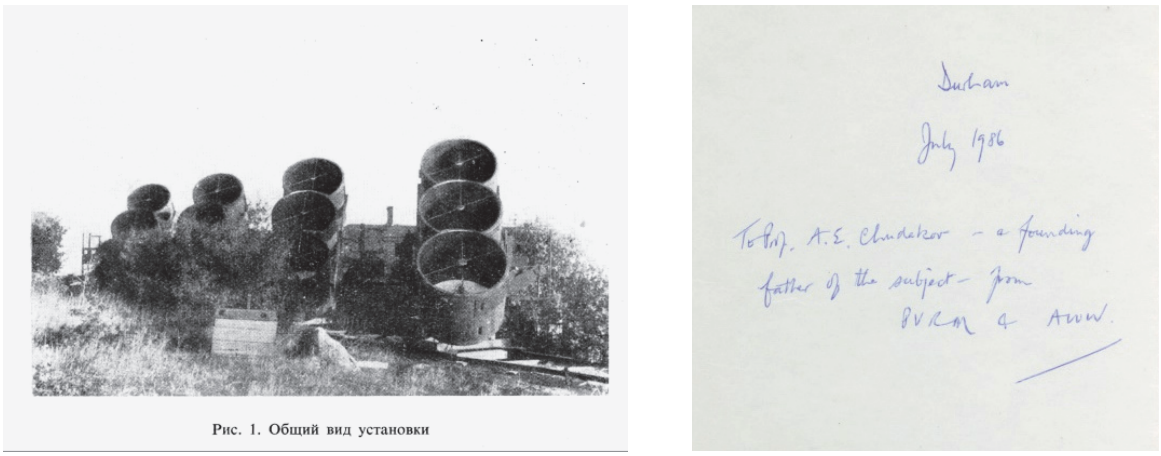

Fig1. *The first Cherenkov gamma-ray telescope constructed by Chudakov in Crimea (upper left), the inscription made by Prof. Sir Arnold Wolfendale on the copy of his monograph "Gamma ray astronomy"[1] presented to Chudakov (upper right panel), and (bottom panel) the future look of the CTA system (Southern Hemisphere site).*

demonstrate also the presentation inscription made by Prof. Sir Arnold Wolfendale, former Astronomer Royal for Britain, on his monograph [1] written together with Indian scientist P.V. Ramana Murthy: "To Prof. A.E. Chudakov – a founding father of the subject – from PVRM and AWW. Durham, July 1986". Also shown in ***Fig1*** (bottom panel) is the general view of the future CTA (Cherenkov Telescope Array) observatory, most promising and advanced project which is under construction at the moment. More exactly, ***Fig1*** presents only one part (southern) of the CTA system that is designed as two arrays constructed simultaneously in both hemispheres of the globe. CTA is planned as a first Cherenkov detector of the fourth generation, and it is not the only project of this type. The very high energy (VHE) gamma ray astronomy (or Cherenkov astronomy) is thriving branch of science, whose foundations were laid by Chudakov. He not only constructed the very first instrument of VHE gamma ray astronomy. He also (together with G.T. Zatsepin) had suggested the very idea of the method in paper [2]. When this paper was published (1961), the first stage of the air Cherenkov telescope (four mirrors), had been in operation for the season of 1960. But even before this Crimea gamma ray astronomy experiment Chudakov studied Cherenkov radiation of extensive air showers in Pamir mountains.

As a preparatory stage for future experiments with Cherenkov radiation of extensive air showers in 1953 Chudakov began to study the luminescence of air and other gases irradiated

by relativistic electrons. The experiment was made at various pressures, and, reducing pressure to zero, Chudakov discovered that some signal still existed at zero pressure. Putting additional metal foils into the beam of electrons he proved this signal to be the result of transition radiation predicted by V.L. Ginzburg and I.M. Frank in 1945. This was the first experimental observation of the transition radiation.

As for the ionization glow, it turned out to be sufficiently weak so that it could be neglected in Cherenkov observations. But Chudakov immediately understood that the isotropy of this radiation could be used in experiments of another type in order to observe extensive air showers from a large distance. This idea was realized much later in the Fly's Eye detector, and now the detectors of this type are being developed both for ground-based and for satellite experiments.

The priority of Chudakov can be supported by another famous scientist Prof. John Linsley from University of New Mexico who wrote to the author after Chudakov's departure [3]: "I tried to get clarification from Chudakov himself in his later years about an idea that *apparently came to him before it came to others*: to observe EAS by means of atmospheric scintillation. In a well-known remark of his at the 1962 Interamerican Symposium in La Paz, Bolivia, published in the Proceedings, he described his idea in some detail, dating it to

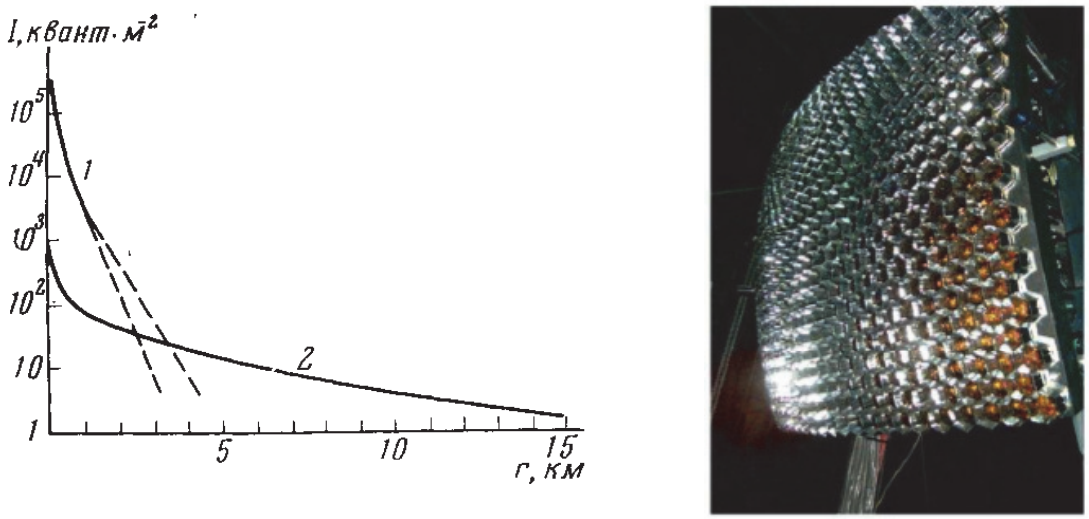

Fig2. *The lateral distribution of Cherenkov radiation and ionization glow of an EAS from paper [3], where the idea of fluorescence detection was put forward (left) and a camera of such a detector (PAO) completely assembled with all PMTs and light collectors in place.*

1955-57, the time he made pioneering measurements on atmospheric Cherenkov radiation from EAS." Several years later Chudakov with his student published this idea in a Russian journal [5]. But his *well-known remark* (to the talk presented by K. Suga [4]) was made much earlier, and still earlier (according to J. Linsley) he had understood this possibility. The left panel of ***Fig3*** presents the plot from paper [5] demonstrating lateral distributions of Cherenkov light and ionization glow. On the basis of these distributions, it was formulated in [5]: "Ionization glow… definitely dominates at distances of 5 km from the axis and more…Using pulse shape analysis at several points located at distances 5-10 km from the axis one can in principle determine not only spatial position of the axis, but the cascade curve form as well, and accordingly, the energy released in the atmosphere. It is possible to detect inclined and even almost horizontal showers". It is this suggestion that was later

implemented in many detectors. As an example, the right panel of ***Fig2*** shows the camera of one modern fluorescence detector (that of the Pierre Auger Observatory).

To finish with the topic of Chudakov and Cherenkov radiation one should recall another ingenious idea put forward by Chudakov. In 1972 he suggested a new method to measure the spectrum of giant air showers by recording their air Cherenkov radiation reflected from snow [6]. The idea was to use an optical detector mounted at the airplane flying over snowy territories, presumably during the polar night. There were some attempts to realize this idea in different modifications (to use mountain glaciers as reflectors, and balloons, tethered or in stratospheric flights, as detector carriers). However, up to the present time this idea was not properly implemented, and it waits for more successful realization.

3. Chudakov effect and the Earth's radiation belts

In 1949, Chudakov predicted the effect of the reduced total ionization of a high-energy electron-positron pair near the point of its origin due to the interference (mutual screening) of particle wave functions (as usual, he published this result much later, only in 1955 [7]. The results of his calculations are shown in ***Fig3***, where the reduction of ionization losses in

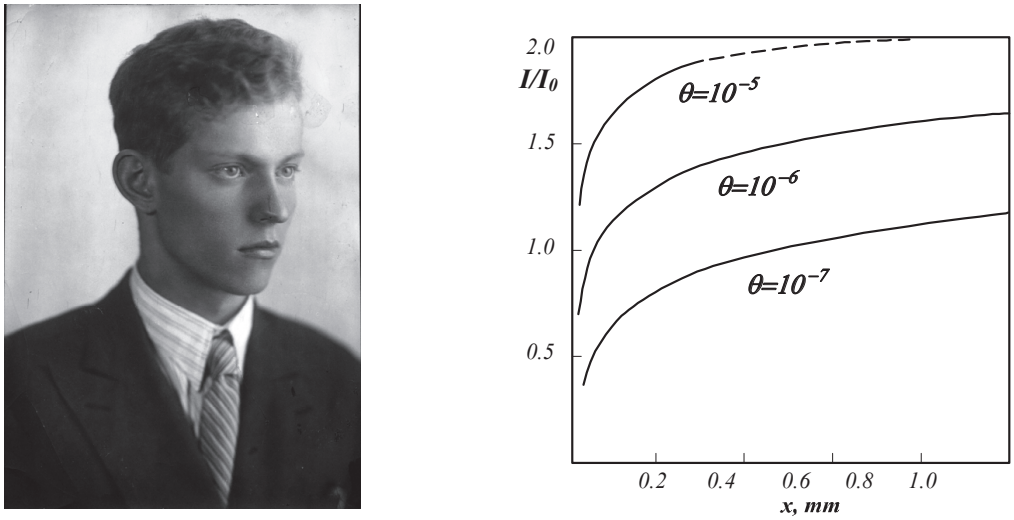

Fig3. *Young Alexander Chudakov (1946) and his calculation of ionization of an electron-positron pair as a function of the path length from the point of its origin for three values of the angle of divergence (the plot from paper [7]).*

comparison to $2I_0$ is clearly seen. ***Fig3*** present also a photo of young Alexander Chudakov. So he looked when calculating quantitatively the Chudakov effect manifestation. Since this effect depends on the energy of a pair (which determines the angle of divergence) the effect was used in some experiments with nuclear emulsions for measurements of the energy of gamma rays.

This effect was referred to by many scientists as the Chudakov effect (see for example, [8]), but it was not particularly popular. However, much later it became clear that the effect is, in fact, universal. Now the effects of the screening of color fields for narrow pairs of quarks and gluons are taken into account in QCD, and this is an obvious manifestation of the

Chudakov effect.

With the advent of satellite era, the new possibilities to study cosmic rays beyond the atmosphere have opened up. The first experiments on the first Soviet satellites were carried out by S.N. Vernov and A.E. Chudakov. The first satellite (Sputnik) launched in 1957 had no instruments for this purpose, but the second Sputnik recorded cosmic ray intensity with a Geiger counter. The lost possibility of discovering the inner radiation belt is well described in [9] by J.F. Lemaire.

"The Geiger counters of Sputnik 2 … had detected the trapped radiation near apogee over Australia with KS-5, the first orbiting instruments for cosmic ray studies. But since S.N. Vernov and A.E. Chudakov did not receive the data from the Australian receiving station they did not see the rapid rise in intensity with altitude until much later. At Sydney, Australia, the scientists with Professor H. Messel, a noted cosmic ray researcher and head of the School of Physics at the University of Sydney, recorded the telemetry signals from Sputnik 2. But they did not have the telemetry code. Asked about this during the Cosmic Ray Congress in 1959, Messel said to Singer '*They would not send us the code and we were not about to send them data*' [9].

The possibility lost by Sputnik 2 was fully used by the Explorer 1 American satellite. However, both Sputnik 2 and Explorer 1 satellites observed the inner radiation belt. The outer radiation belt was first observed by the Sputnik 3 satellite, which was the first heavily instrumented spacecraft, the laboratory in space. Explorer 4 also observed the outer radiation belt, but two months later. To summarize the instructive story of discovering the Earth's radiation belts, let us again give the floor to J.F. Lemaire.

"This piece of History re-opens the issue of who, in scientific races, are remembered as the key actor and discoverer: the pioneer who had the idea first, who designed an experiment to check this idea and prove it to be correct, or the author(s) whose paper passed the refereeing process and who, luckily, first published the results in open literature. In Geophysics it is the latter who wins this 'Guinness Book of Records' competition."

It is worthwhile to notice that, notwithstanding the discovery, Chudakov was again a pioneer in this case: "the first orbiting instruments for cosmic ray studies."

4. Large volume water Cherenkov detector

This detector was constructed by Chudakov in 1959. This facility in the form of a truncated cone contained nearly 85 t of cleared water and 16 large PM tubes (the diameter of photo-cathode 15 cm).This detector was but a short episode in the Chudakov's activity, and, as usual, he did not published anything about it. ***Fig4*** presents the top view and cross section of the Chudakov's Large Water Cherenkov detector. It is very interesting to notice on this occasion that the destiny of practically all his initiatives was a long life or fruitful development. From the modern standpoint, this detector looks like a very small prototype of Superkamiokande, less than 0.2% of it, constructed 40 years earlier, though essentially in the same design scheme. The right part of ***Fig4*** demonstrates the interior views of two largest water-Cherenkov detectors used so far by underground physics experiments: the IMB (Irwine-Michigan-Brookhaven) in the US and the Superkamiokande in Japan. The original detector was used only in a single experiment studying muon groups near the EAS axis [10], while Chudakov was already involved in quite different experiment, which made him the founding father of gamma ray astronomy.

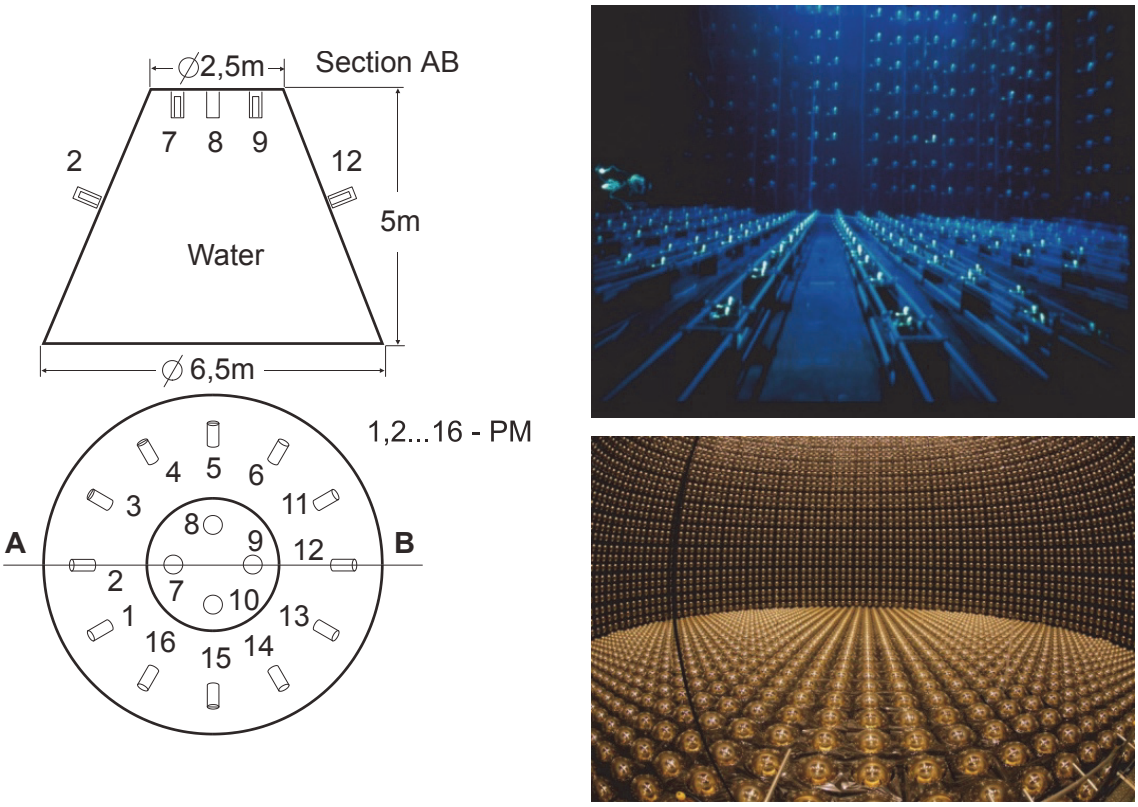

Fig4. *The first large-volume water Cherenkov detector constructed by A.E. Chudakov in 1959 (left), and two giant modern underground water Cherenkov neutrino detectors IMB (top right) and Super-Kamiokande (bottom right).*

5. Underground physics and Baksan

The very large water Cherenkov detectors (whose first prototype had been constructed by Chudakov), demonstrated in ***Fig4***, much later become instruments of the so called underground physics. But Chudakov also can be considered to be the founding father for this science due to his ideas and approach when constructing the Baksan Underground Scintillation Telescope [11]. The primary goal of this instrument, as it was planned by initiators of the project of a neutrino observatory in the governing body of USSR Academy of Sciences (academicians M.A. Markov and B.M. Pontecorvo), was to study the neutrinos generated by cosmic rays in the atmosphere. At that time only two experiments were performed to detect such neutrinos: one in India and another in South Africa. Both were located at very large depths (to suppress the muon background) in mines of conditionally natural (industrial) origin. The BNO facilities were the world-first for which special underground tunnels and cavities were constructed. Next, both previous neutrino experiments were carried with instruments recording the horizontal neutrino flux. The BUST was the first instrument aimed at detecting the vertical upward-going neutrinos having crossed the entire globe. At the same time it was placed at such a depth, where the muon background was higher than the expected neutrino signal by a factor of 10^7. This circumstance made the task of extracting the sought signal from the background extremely difficult. But on the other hand this made it possible to investigate simultaneously many problems of muon physics (to

measure the flux of muons and its variations, to study interactions of high-energy muons, their spectra, muon bundles, etc.). This multi-purpose character of the BUST allows us to call it the first instrument of underground physics. The task of detection of upward-going neutrinos was successfully solved using the time-of-flight technique, and the first neutrino from 'antipodes' was recorded by the BUST on December 14, 1978 at 08:31:10 LT. Some other important results that were obtained at Baksan by Chudakov and his team are reviewed in brief in paper [12]. More information about this outstanding scientist and his selected papers can be found on memorial web page [13].

Acknowledgments

The work is partially supported by the Russian Foundation for Basic Research, grant no. 16-02-00687.

References

[1] Ramana Murthy PV, Wolfendale AW. Gamma ray astronomy, Cambridge Astrophysics Series, (Cambridge Univ. Press, 1986).

[2] Zatsepin GT, Chudakov AE, On the methods of searching for local sources of high energy photons. J. Exp. Theor. Phys. 1961; 41: 655 (In Russian).

[3] Linsesly J, Private communication, 2001.

[4] Suga K, Methods for Observing Extremely Large Extensive Air Showers, Proc. of the Fifth Interamerican Seminar on Cosmic Rays, La Paz, 1962, vol. II, p. XLIX-1.

[5] Belyaev VA, Chudakov AE, Ionization glow of air and possibilities to use it for detection of extensive air showers, Bulletin of USSR Acad. Sci., 1966, v. 30, no. 10, p.1700.

[6] Chudakov AE, A possible method to detect EAS by the Cherenkov radiation reflected from the snowy ground surface, in "Experimental methods of studying cosmic rays of superhigh energies", Proc. All-Union Symposium, Yakutsk, 1972, p. 69 (In Russian).

[7] Chudakov AE, One ionization effect related to observation of electron-positron pairs at very high energies, Bulletin USSR Acad. Sci., Phys. Ser., vol. 19, (1955), p. 651 (In Russian).

[8] Hayakawa S, Cosmic ray physics: nuclear and astrophysical aspects, Wiley-Interscience, 1969.

[9] Lemaire JF, From the Discovery of Radiation Belts to Space Weather Perspectives. In: Daglis I.A. (eds) Space Storms and Space Weather Hazards. NATO Science Series (Series II: Mathematics, Physics and Chemistry), vol 38. Springer, Dordrecht

[10] Vavilov YuN, Pugacheva GI, Fedorov VM, On muon groups near to the axis of extensive air showers, J. Exp. Theor. Phys., 1963, vol. 44, p. 487 (In Russian).

[11] Alexeev EN, Alexeenko VV, Andreev YM, et al., Baksan Underground Scintillation Telescope, Bulletin USSR Acad. Sci., Phys. Ser., 1980, vol. 44, no. 3, pp. 609-612.

[12] Lidvansky AS, They were the first (a retrospective look at some Baksan experiments on the jubilee day), Intern. Jubilee Session-conference BNO-50, Nalchik, June 5-9, 2017. To be published in Physics of Elementary Particles and Atomic Nuclei.

[13] http://llve.inr.ac.ru/chudakov/main.htm

Neutrino from stellar collapses

L.A. Lukyanchenko[1]

[1]National Research Centre Kurchatov Institute, Moscow, Russia;
liudmila.borodikhina@lngs.infn.it

Abstract In this paper the modern results and investigation prospects of neutrino from astrophysical sources by low-background neutrino detectors are reviewed. Also results of simultaneous analysis by neutrino and gravitational waves detector are presented.

Keywords: Neutrino, Supernovae, GRB, Multimessenger astronomy;

1. Introduction

Neutrinos produced during stellar collapses carry information about collapse process because they are not influenced by the interstellar medium. Beside neutrino emission the second possible source of data about supernova explosion and gamma ray bursts mechanisms are gravitational waves that also propagate without any changes. Therefore they could bring us information about distant phenomena such as Supernovae explosions and Gamma Ray Bursts, about their origins and about processes taking place inside them. Simultaneous analysis by neutrino and gravitational waves detectors could be one of the ways to get the whole picture of these processes.

2. Neutrinos from Supernovae

It is expected that stars with masses $M_* \geq 8M_\odot$ and $M_* \leq 65M_\odot$[1] could end their lives through the Supernova explosion. All stages of the star collapse are accompanied by neutrino emission. Neutrinos carry away about 99% of binding gravitational energy [2] and provide necessary energy for supernova explosion. Neutrinos are produced through the beta- and thermal processes inside the core and star medium. During the first collapse phase neutrinos can propagate freely. But increasing of core mass leads to the formation of neutrinosphere and neutrinos are trapped inside it . Trapped neutrinos provides necessary amount of energy for the explosion through the neutrino heating process [3].

Thanks to very low interaction cross-section neutrinos emitted from Supernova could provide us with information about new neutrino physical properties and expand our knowledge about stars structure and evolution. Also the presupernova neutrino signal that preceded the explosion could help astronomical community to detect early core-collapse stages. For this aim the SuperNova Early Warning System (SNEWS) was created [4]. The SNEWS system includes modern neutrino detectors such as Super-K (Japan), LVD (Italy), Ice Cube (South Pole), KamLAND (Japan), Borexino (Italy) Daya Bay (China) and HALO (Canada). The main idea of this project is to search coincidences among neutrino candidates from different detectors during 10 second window by central computer located in Brookhaven National Lab. The time of the neutrino registration signal could help astronomers find direction to the future Supernova.

2.1. Diffuse Supernova Neutrino Signal

Neutrino signal from the individual supernova explosion is not distinguishable from the background in modern detectors when supernova distance is more than few kiloparsecs. But the neutrino flux from all supernova collapses that occurred through the existence of the Universe could be detectable. The predicted flux of such neutrinos is about ~1 cm^{-2} s^{-1} [5]. Total spectrum of these neutrino depends on Supernova rate in Universe and relative densities of ordinary matter and dark energy [5] . Therefore Diffuse Supernova Background neutrinos could provide us an information not only about supernovae explosion mechanism but also it could be independent instrument to test our knowledge of star formation rate function and constrain modern cosmological models [6,7].

Several detectors such as Super-Kamiokande [8], SNO [9] and KamLAND [10] searched for the signal from DSNB neutrinos. Although there was no DSNB-signal observed, upper limits on the neutrino fluxes were established. For electron antineutrinos the best limit on DSNB flux in energy range 13.3-31.3 MeV belongs to Super-Kamiokande collaborations. In near future Super-Kamiokande and future detector JUNO [11] are expected to be able to detect DSNB neutrino signal.

2.2. Simultaneous analysis of neutrino and gravitational waves detectors

After registration of the gravitational wave signal from the black holes merging by LIGO detector [12] several neutrino detectors including Super-Kamiokande [13], KamLAND [14] and Borexino [15] tried to find time correlation between neutrino signal and gravitational wave events. The correlation was searched upon two neutrino detection channels: through scattering on electrons in all detectors and through inverse beta decay channel in KamLAND and Borexino. No correlation was found.

Also simultaneous analysis of neutrino detectors data and gravitational waves detectors data could be performed for the search of neutrinos from distant, so-called "dark", supernovae [16]. In order to enlarge the statistics, data from several neutrino detectors such as LVD , Borexino, KamLAND, and IceCUBE will be put to common database after estimation of background for each detector. In addition to detection of neutrinos from individual distant supernovae this method could also make possible the detection of neutrinos from so-called "dark" supernovae with explosions not accompanied by light emission.

3. Neutrinos from Gamma Ray Bursts (GRB)

Gamma Ray Bursts (GRBs) are non regular bursts of gamma rays in the Universe. Their origin is not fully understood, but because of most GRBs occurring in the star formation regions of Universe they could be produced by star collapses [17]. The GRBs could be divided in two groups by the their duration. The short GRBs are bursts with total duration less than 2 seconds. The long GRBs have duration longer than 2 seconds. Beside duration short and long gamma ray bursts differ by their supposed source. Long GRBs have supernova explosion as progenitor [17].

Low background neutrino detectors Borexino [18], KamLAND [19] and Super-Kamiokande [20] searched for neutrino signal correlated with GRBs. No correlation was found and the upper limits on neutrino fluences were established. The best limit in low-energy region 2-6 MeV belongs to Borexino detector. In the higher energy range 6-15 MeV the best upper limit is established by Super-Kamiokande .

4. Conclusion

Modern detectors sensitivity is not enough to detect neutrino fluxes from the rare sources like an individual distant Supernova. More statistics and higher volume neutrino detectors are required to obtain any significant signal. But it is expected that neutrino detectors of the next generation will reach required sensitivity level.

Also simultaneous analysis based on the common data from network of the neutrino and gravitational waves detectors could allow to measure the signal from neutrinos produced inside star collapses.

References

[1] Heger et al., How Massive Single Stars End Their Life, Astrophys.J. 591 (2003) 288-300;

[2] G.Raffelt, Particle physics from stars, Ann.Rev.Nucl.Part.Sci.49:163-216,1999;

[3] H.-Th. Janka, Author version of chapter for 'Handbook of Supernovae,' edited by A. Alsabti and P. Murdin, Springer;

[4] P. Antonioli, et al, SNEWS: The SuperNova Early Warning System, New J.Phys. 6 (2004) 114;

[5] John F. Beacom, Ann.Rev.Nucl.Part.Sci.60:439-462,2010;

[6] Philipp Grothaus, Malcolm Fairbairn, Jocelyn Monroe, Phys. Rev. D 90, 055018 (2014);

[7] J. Barranco, Argelia Bernal, D. Delepine, arXiv:1706.03834 ;

[8] Super-Kamiokande Collaboration, K. Bays, T. Iida, K. Abe, Y. Hayato, K. Iyogi, J. Kameda et al., Supernova relic neutrino search at super-kamiokande, Phys. Rev. D85(Mar,2012) 052007;

[9] The SNO Collaboration, Astrophys.J.653:1545-1551,2006;

[10] The KamLAND Collaboration, Astrophys.J.745:193,2012;

[11] Fengpeng An, et al., J. Phys. G 43 (2016) 030401;

[12] The LIGO Scientific Collaboration, the Virgo Collaboration, Phys. Rev. Lett. 116, 061102 (2016);

[13] K. Abe et al. (Super-Kamiokande), Astrophys. J.830,L11 (2016), 1608.08745;

[14] A. Gando, Y. Gando, T. Hachiya, A. Hayashi,S. Hayashida, H. Ikeda, K. Inoue, K. Ishidoshiro, Y. Karino, M. Koga, et al., The Astrophys J. Lett. 829, L34 (2016);

[15] Borexino collaboration, A search for low-energy neutrinos correlated with gravitational wave events GW150914, GW151226 and GW170104 with the Borexino detector, arXiv:1706.10176 ;

[16] I. Leonor, L. Cadonati, E. Coccia, et al., Class.Quant.Grav.27:084019,2010;

[17] S.A. Colgate, Early Gamma Rays from Supernovae, Astrophys. J. 187 (1974), p. 333.

[18] The Borexino Collaboration, Astroparticle Physics, Volume 86, January 2017, Pages 11-17, ISSN 0927-6505;

[19] K. Asakura et al. (KamLAND Collaboration), Study of Electtron Anti-neutrinos Associated with Gamma-Ray Bursts Using KamLAND, Astrophys. J. 806 (2015) 87;

[20] S. Fukuda et al. (Super-Kamiokande Collaboration), Search for neutrinos from Gamma-Ray Bursts using Super-Kamiokande,Astrophys. J. 578 (2002) 317.

Mean density of matter in the Local Universe

Dmitry Makarov[1],*

[1]Special astrophysical observatory of the Russian academy of sciences,
Nizhnij Arkhyz, Russia; dim@sao.ru

Abstract The Local Supercluster is an ideal laboratory to study distribution of luminous and dark matter in the nearby Universe. In total, 54% of galaxies in the Local Universe are gathered into groups. The groups collect 82% of the K-band light. The local matter density is Ωm=0.08 within a distance of ~40 Mpc assuming H_0=73 km s^{-1} Mpc^{-1}. It is significantly smaller than the cosmic value, 0.32, in the standard ΛCDM model. The discrepancy between the global and local quantities of Ωm may be caused by the existence of a dark matter component unrelated to the virial masses of the galaxy systems.

Keywords: Local supercluster, dark matter, matter density

1. Introduction

Despite the fact that more than 80 years have passed since the first works, which found that the kinematics of galaxy systems can not be explained by visible matter, until now, the question of the nature of the dark matter, its properties and distribution remains one of the key in modern cosmology. Modern standard cosmology, according to the results of the Plank mission, considers that "dark energy" accounts for 68%, "dark matter" - 27%, and the ordinary baryonic substance is only 5% of the average density of the Universe. The ΛCDM model has achieved great success in explaining a wide range of observations, such as the formation of galaxies and parameters of the large-scale structure of the Universe. However, many problems of standard cosmology appear on small scales and small masses of objects (for example, the problem of cusps in the dark matter halos and the problem of "missing" satellites of giant galaxies).

2. The Local Volume

The sample of Local Volume galaxies gives a unique opportunity to study properties of galaxies till to very small scales, down to the absolute magnitude MB=-10 and virial mass $M=10^9 M_\odot$. In the Local Volume, conventionally limited to a radius of 10 Mpc, a large number of dwarf galaxies are detected, whose velocities and distances make it possible to investigate the Hubble flow with unprecedented accuracy compared to distant objects. The study of the stellar population of nearby galaxies allows us to restore the star formation history from the moment of their origin to the present time. In fact, the study of local Universe formed over the last 10-15 years in an independent and productive branch of observational cosmology.

Until recently, a serious obstacle in the study of the nearby Universe was the scarcity of distance estimations even for the nearest galaxies. Using the Hubble Space Telescope in combination with a new method of distance determination by the luminosity of the tip of the red giant branch (TRGB), the mass measurements of distances were preformed to about 300 nearby

galaxies with an accuracy of 5-10%. ***Fig1*** shows the Hubble diagram and the distribution of galaxies inside 10 Mpc in projection on the plane of the Local Supercluster. The different distance determination methods are color-coded. The stars correspond to the contribution of our team in the distance estimation to the nearby galaxies.

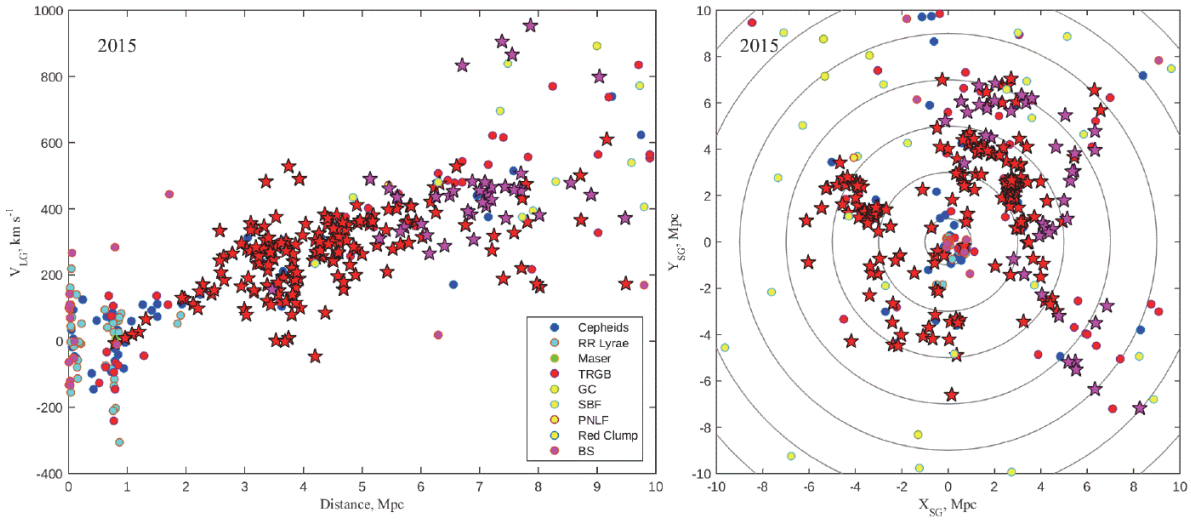

Fig1.: *The distribution of the Local Volume galaxies with redshift independent distance estimations. Different distance determination methods are code by a color. The Cepheids, RR Lyrae, Maser and TRGB methods give accuracy better that 10%. The contribution of our team is marked by stars. Left: the velocity-distance diagram of the Hubble flow. Right: the distribution of galaxies in the projection on the plane of the Local Supercluster.*

A detailed study of the motions of galaxies in the vicinity of nearby groups, including the Local Group, revealed unexpected features of the near Hubble flow. The velocity-distance diagrams outside the central regions of the groups are characterized by a small dispersion of the radial velocities about 30 km s-1. Such small chaotic motions together with high accuracy of distance determination allow us to see the deviation from the simple linear Hubble law caused by the gravitational retardation of galaxies by the mass of the group itself. The example of the Hubble flow around the Local Group is demonstrated on the ***Fig2***, where distances are measured from the center of mass of the Local Group. The zone of virial motions around our Galaxy and Andromeda galaxy is separated from the cold Hubble flow, which stars just behind the radius of a zero velocity surface of R_0=(0.96±0.03) Mpc [1]. This radius determines the total mass of the Local Group, M_{R0}=(1.9±0.2)×10^{12} $M_\odot$, which is in good agreement with virial estimation of the total mass M(MW+M31)=(1.6-2.2)×10^{12} $M_\odot$. It is necessary to note, that these estimations are obtained on different characteristic scale lengths of 1 Mpc and 0.2 Mpc respectively. Thus, we can conclude that majority of the mass in the group is concentrated inside the virial zone. Similar conclusion can be drawn from the motion of galaxies around nearby giant galaxies, Centaurus A and M 81.

3. The Local Universe

Detailed observational data on the Local Volume galaxies give a fairly complete picture of the spatial distribution of luminous and dark matter. However, the Local Volume can not be considered as a representative sample of the Universe due to large density fluctuations at 10 Mpc scales. For better representation, Makarov and Karachentsev [2] examined much bigger volume around our Galaxy, which includes Local Supercluster with its vicinities.

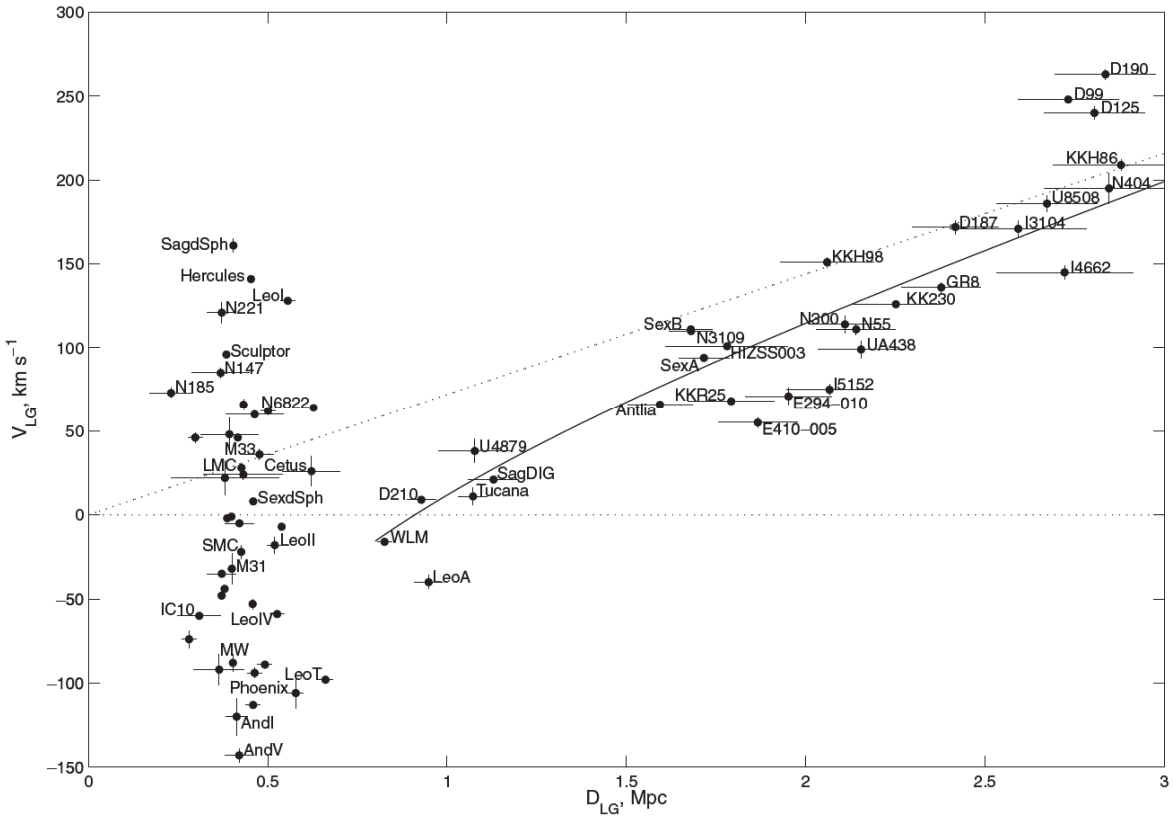

Fig2.: *The Hubble diagram in the vicinity of the Local Group. The distances and velocities of galaxies are given with respect to the centroid of the Local Group. The undistorted Hubble flow is shown by the dashed line. The solid line describes the influence of the Local Group on the motion of nearby galaxies. It allow us to estimate the mass of the Local Group of 1.9 × 10^{12} $M_{\odot}$.*

Recent huge redshift surveys like 6dF [3], SDSS [4], HIPASS [5], ALFALFA [6] significantly improved quantity and quality of the data about galaxies in the Local Universe. We gathered information on all known galaxies with radial velocities V_{LG}<3500 km s^{-1} in the rest frame of the Local Group excluding the zone of strong Galactic extinction, |b|<15º. The main efforts in our program were aimed at the systematization of data on radial velocities, apparent magnitudes and morphological types of galaxies. Moreover, we carried out a search for new dwarf galaxies and performed optical identification of HI radio sources from the HIPASS [5], ALFALFA [6] and other blind surveys. We paid special attention to cleaning the list from spurious objects and erroneous measurements. Unfortunately, because of observational specific, majority of the wrong data is dumped to the Local Universe. The most popular errors are: misclassification of star and distant galaxies as well as influence of superimposed star in optical redshift surveys, contamination of HI spectra by gas of our own Galaxy or by near galaxies because of low spatial resolution in radio observations, splitting of a galaxy on several objects in automatic image processing, as well as different kind of misprints, wrong measurements and data analysis The visual control and purification of the data was the most time consuming part of the work. The all sky distribution in equatorial coordinates of the sample of galaxies in the Local Universe is presented in ***Fig3***. The most prominent structure is the concentration of galaxies to the Supergalactic plane. Fortunately, the center of the Local Supercluster in Virgo constellation locates near the north Galactic pole, making it easy for observations and one of the most studied galaxy clusters.

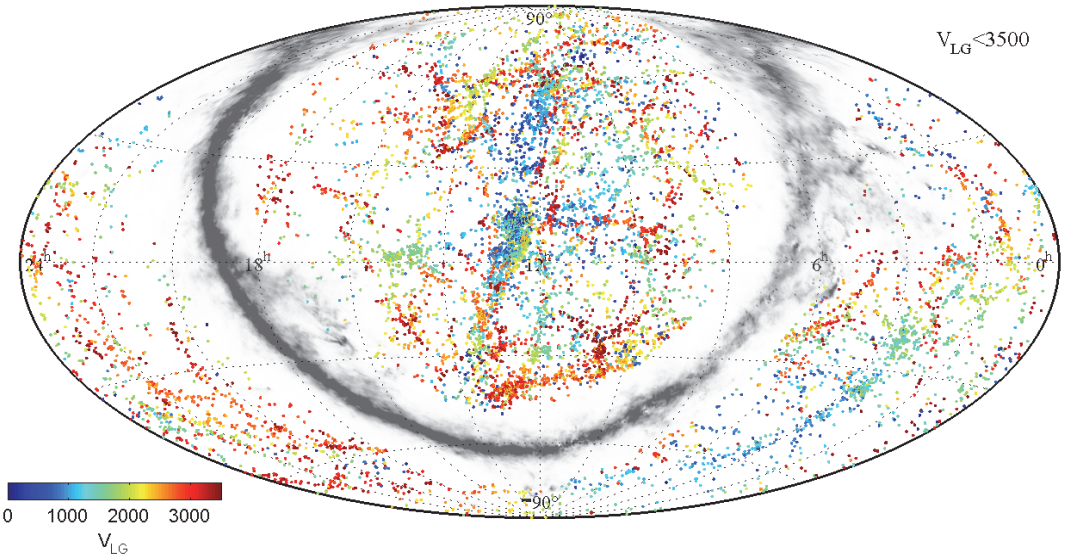

Fig3.: *All sky map of galaxies in the Local Universe. The radial velocity is color coded from the blue for nearby galaxies to the brown for distant ones. The "zone of Avoidance" in the Milky Way is shown by clumpy gray belt, which represents the extinction map in our Galaxy.*

Makarov and Karachentsev [2] have applied a new group finding algorithm to the updated and cleaned sample of 10 900 galaxies. In contrast to the simple "friends of friends" percolation algorithm, we take into account the individual luminosities of galaxies for identifying the groups of different population. Obviously, we can not consider giant and dwarf galaxies as objects with equal rights in the group. As well as bounding criteria for pair of dwarfs and for pair of giants can not be the same. Our method is based on idea that bounded system of galaxies has to have negative total energy and whole system has to reside inside a radius of zero velocity surface. Because in observations we know only brightness of the galaxy, the projection of the position of the galaxy on the sky and the projection of spatial velocity on the line of sight, we need to calibrate the grouping criteria with a standard. As such a standard, we selected nearby groups of galaxies with a well-known structure from direct measurements of photometric distances to group members. These distances were measured during our long term program on the study of 3D structure of the Local Volume.

As a result, we have created catalogs of 509 pairs [7], 168 triplets [8] and 395 more populated groups [2] as well as 520 very isolated galaxies [9]. The subsequent analysis showed that the algorithm [2] identifies groups with approximately the same characteristics for nearby as well as for distant volumes of the Local Universe. The algorithm gathers galaxies into aggregates, which are in good correspondence with the previously known systems.

In total, 54% of known galaxies reside in groups. They gather 82% of the K-band luminosity of the Local Universe. The sample of well populated groups (number of members $n \geq 4$) is characterized by the following medians parameteras: mean projected radius R=268 kpc, radial velocity dispersion σ_V=74 km s^{-1}, K-band luminosity $L_K=1.2\times10^{11}\,L_\odot$, virial and projected masses $M_{vir}=2.4\times10^{12}$ and $M_p=3.3\times10^{12}\,M_\odot$, respectively. Taking into account measurement error of radial velocities reduces the median masses by 30%. It corresponds to median mass-to-light ratio of groups, corrected for errors, $M_{pc}/L_K=22\,M_\odot\,L_\odot^{-1}$. For 97% of identified groups the crossing time does not exceed the cosmic time, 13.7 Gyr, with the median at 3.8 Gyr. This means that the algorithm forms well-evolved systems that are in the virialized state.

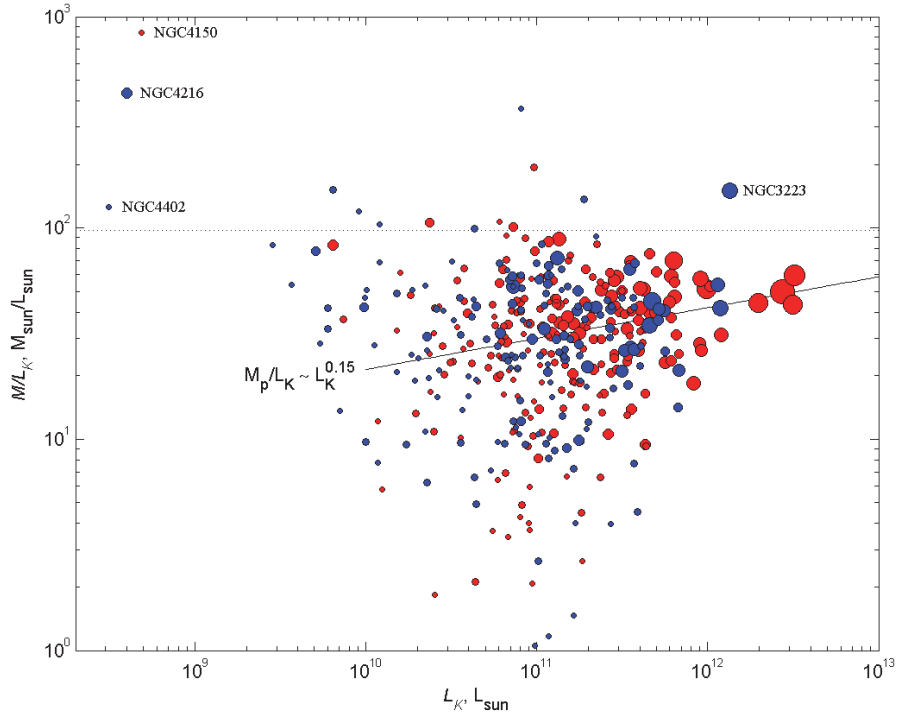

Fig4.: *Mass-to-K-light ratio of the groups as a function of K-luminosity. The groups are represented by circles scaled by population. The groups with a bulge-dominated main member are shown by red circles. The horizontal dotted line traces the global cosmic ratio, 97 $M_\odot/L_\odot$, corresponding to Ωm = 0.28. The regression (solid) line is drawn taking into account the K-luminosity as a statistical weight.*

The distribution of 395 groups by the projected mass-to-luminosity ratio versus the total K-band luminosity, L_K, is demonstrated in ***Fig4***. The groups with the bulge dominant main galaxy (T≤2) are shown with red circles, and the rest of the groups with blue ones. The size of the circles is proportional to the group population. The horizontal dotted line represents the ratio $M/L_K=97\ M_\odot/L_\odot$, which corresponds to K-luminosity density $j_K=4.28\times10^8\ L_\odot\ Mpc^{-3}$ [10] assuming a Hubble constant $H_0=73$ km s^{-1} Mpc^{-1} and the cosmic parameter of matter density Ωm=0.32 in the standard ΛCDM model. A significant spread of galactic systems in this diagram is due to the projection factors. Despite the large variations, the average ratio of virial mass to luminosity increases with the population of the system, its luminosity and correlates with the morphological type of the brightest member. All these features are well known from other catalogs of groups and clusters of galaxies.

The mean K-band luminosity density in the Local Universe inside a sphere of 40-45 Mpc is in good agreement with the global value of mean luminosity density obtained by different authors from deeper samples of galaxies. This fact supports our expectation that the sample of galaxies in the Local Universe can be considered as representative sample of the Universe. Summing the virial masses of the groups and clusters, Makarov and Karachentsev [2] mapped the distribution of the average density of dark matter around our Galaxy up to 40-45 Mpc. The shape of distribution of mass approximately repeats the shape of distribution of luminous matter. However, in almost all regions the density $\Omega m=\rho_m/\rho_c$ is below the global value Ωm=0.32 from the space CMB experiments. The mean matter density, Ωm=0.08±0.02, on the scale of 40-45 Mpc.

4. Missing dark matter problem

The observational fact that the virial masses of groups and clusters of galaxies are not able to provide the global density is not new. Similar estimates were obtained by different authors [11,12,13]. The estimation of Ωm varies from 0.05 to 0.2 for different methodologies and different samples of galaxies. The most refined methods of the virial mass estimation in the systems of different scale and population lead to the local (D≤40 Mpc) value of the mean matter density Ωm=0.08±0.02, which is 3-4 times lower than the global value Ωm=0.32 in standard ΛCDM cosmology. Various possible explanations of this contradiction were proposed:

1) Dark matter in groups and clusters extends far beyond their virial radius traced by galaxies. To reduce the Ωm discrepancy, one have to assume that the total mass of each group and cluster is about three times its virial mass. However, as was shown by the example of the Local Group, the masses of groups and clusters within the virial radius are in good agreement with the total mass inside the radius of zero velocity. Note that R_0 is ~(3.5-4.0) R_{vir}. Therefore, the existence of a large amount of dark matter at the periphery of the systems is inconsistent with the observational data.
2) There is possibility that we reside inside a giant under density region where the mean matter density is 3 to 4 times lower than the global value. However, it seems unlikely in standard ΛCDM theory to generate a giant void of 100-500 Mpc in diameter with such density contrast. Moreover, numerous K-band counts of galaxies in the range of K=12-19 mag do not show the presence of any significant cosmic lacuna around us within ~2000 Mpc.
3) The essential part of the dark matter in the Universe (about 2/3) is not associated with groups and clusters of galaxies and scattered outside the virial (and even collapsing) regions. It can be distributed in form of massive dark clumps or as a smooth dark "sea". The modern N-body simulations shows that about 2/3 of particles involved in model remain outside the dark matter halos. This number is roughly in agreement with our estimate.

5. Comparison theory and observations

Table1. *The properties of groups in different tests*

Sample	Local Universe	Best mock sample		Random mock sample	
			σ		σ
R, kpc	268	302.9	7.8	287.7	22.7
σ_V, km s^{-1}	74	61.5	2.0	65.6	4.0
M_p, $\times 10^{12}$ $M_\odot$	3.3	2.73	0.22	2.92	0.52
M_p/L_K, $M_\odot/L_\odot$	31	24.8	1.1	26.2	2.1

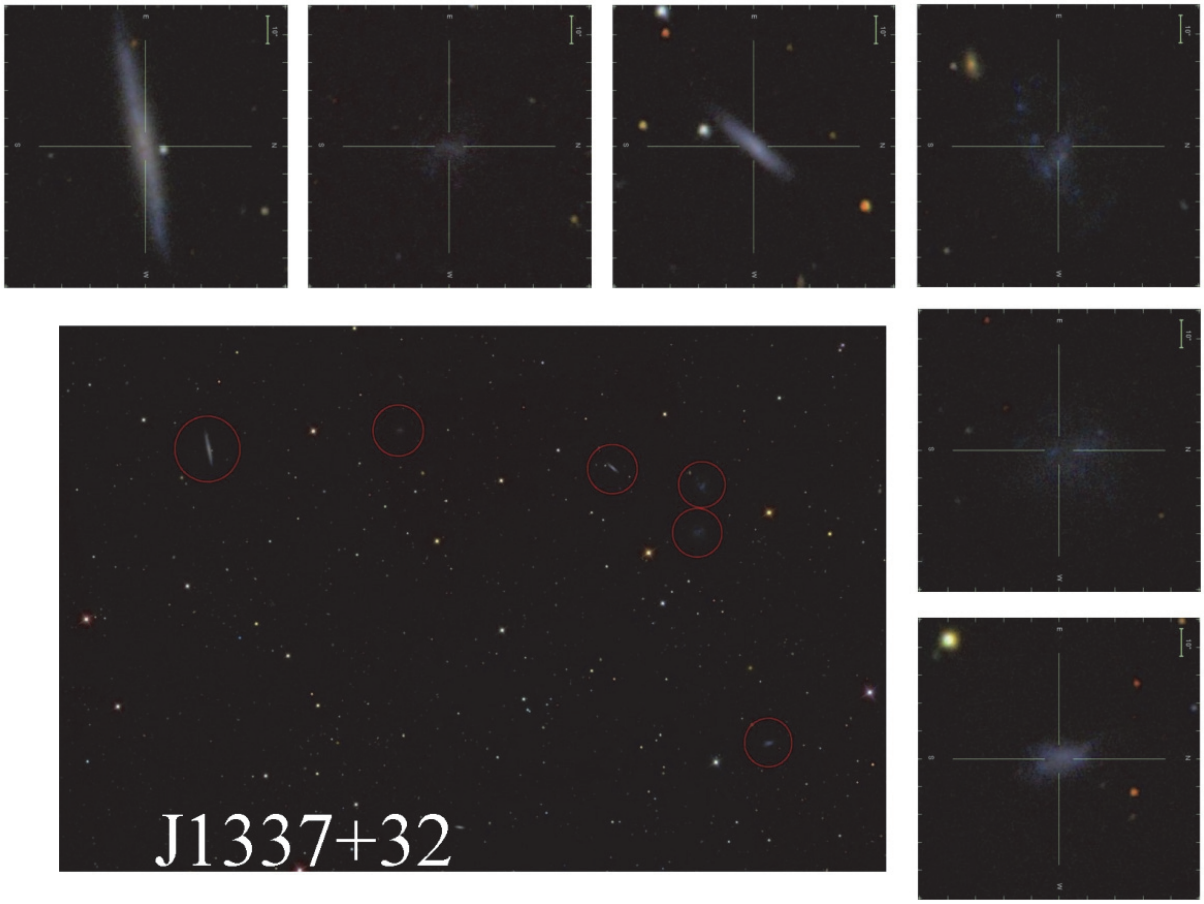

Fig5.: *Example of the most populated group of dwarf galaxies.*

We used the CLUES constrained N-body simulations [14] with 1024^3 particles of $2.554\times10^8\ h^{-1}\ M_\odot$ inside a $160\ h^{-1}$ Mpc box. We generated mock catalogs which reproduce the properties of the distribution of galaxies in the Local Universe, taking into account completeness function of the real galaxy sample and a position of an observer around nearby structures in the Universe. We have applied our group selection algorithm [2] to the mock catalogs to test the properties of groups in the N-body simulations and compare them with real groups in the Local Universe. As can be seen from ***Table1***, the properties of groups in different tests are in good agreement each other as well as in good agreement with the groups in the real sample of galaxies. It supports the idea that significant part of dark matter can be not connected with luminous matter.

6. Examples of systems with high mass-to-light ratio

In the framework of studying the three-dimensional distribution of galaxies in the Local Volume, Makarov et al. [17] measured distances to 30 galaxies in the Canes Venatici cloud I (CVn I). The system is mostly populated by dwarf galaxies and clearly differs from the other nearby galaxy groups, such as the Local Group, M81 or Centaurus A. It does not show a prominent gravitational center and looks diffuse. The high quality of distance measurements allows us to identify an area of chaotic motions around the galaxy M94 and estimate the mass

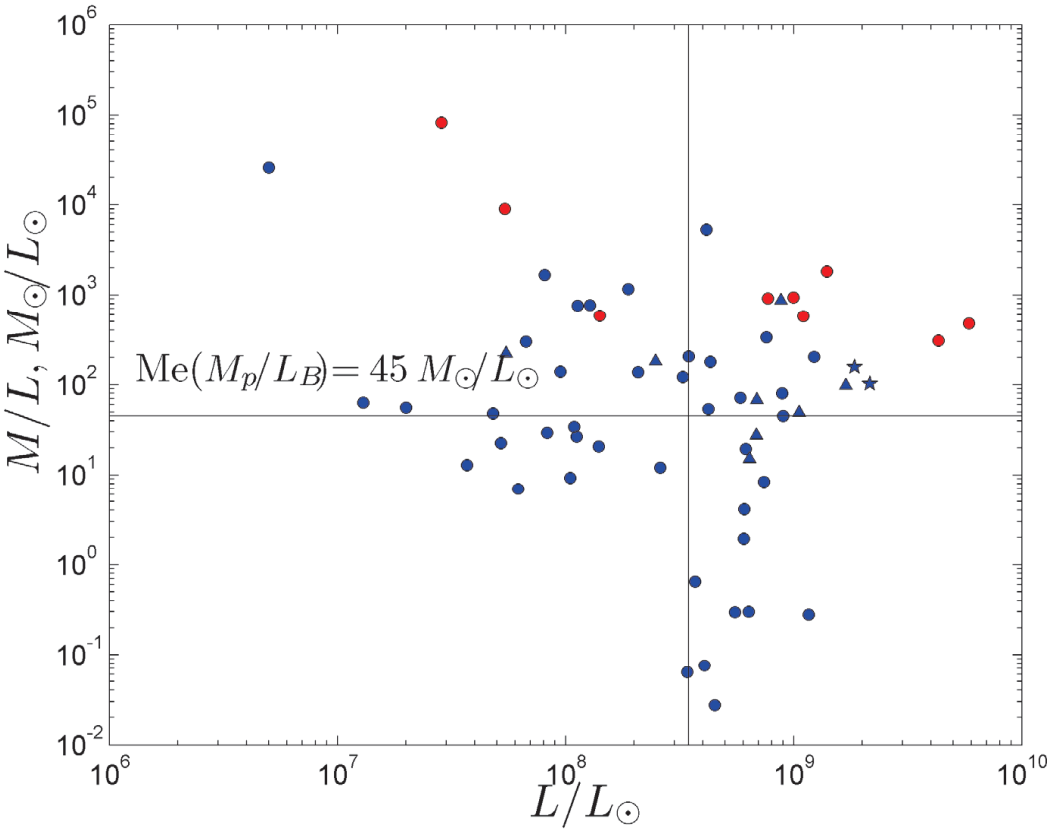

Fig6.: *Distribution of systems consisting dwarf galaxy only by their mass-to-light ration and luminosity. Red dots corresponds to the associations of Tully et al. [15] and blue ones represents the groups of dwarf galaxies found by Makarov and Uklein [16].*

of the system using virial theorem. Estimation of the mass-to-light ration, $M_p/L=159\ M_\odot/L_\odot$ for the CVn I cloud of galaxies greatly exceeds the typical ratio M/L_B~30 for the nearby groups of galaxies, such as the Local Group (M/L_B=15-20) and M81 group (M/L_B=19-32). Note that compared with the well-known nearby groups, such as the Local Group ($L_B=10.1\times10^{10}\ L_\odot$), M81 ($L_B=6.1\times10^{10}\ L_\odot$) and Centaurus A ($L_B=5.5\times10^{10}\ L_\odot$), the CVn I cloud ($L_B=1.61\times10^{10}\ L_\odot$) contains about 4-5 times less luminous matter, and M94 is at least 1 mag fainter than any other central galaxy of these groups. However, the concentration of galaxies in the Canes Venatici may have a comparable total mass.

Tully et al. [15] identified systems of dwarf galaxies in the neighborhood of the Local Group using high-precision photometric distances of nearby galaxies on the 3 Mpc scale. Such structures, which were called the associations of dwarf galaxies, have the mass-to-luminosity ratios in the range from 100 to1000 M/L and contain large amounts of dark matter. Karachentsev and Makarov [7] pointed out the existence of an unexpectedly large number of pairs consisting of dwarf galaxies. Makarov and Uklein [16] compiled the list of of groups consisting of dwarf galaxies only. The sample contains 126 objects, mainly combined in pairs. The most populated group contains six dwarf galaxies (***Fig5***). The majority of these systems reside in the low-density regions and evolve unaffected by massive galaxies. The dwarf galaxy groups forms a continuous sequence in the mass and luminosity along with the associations identified by Tully et al. [15]. The groups and associations of dwarfs have similar luminosities, however, the groups are by one order of magnitude more compact (see ***Fig6***). The median

mass-to-luminosity ratio for the groups of dwarfs is equal to 45 M/L, which indicate a greater amount of dark matter comparable to the normal groups. The systems of dwarf galaxies may contain substantial amounts of dark matter. Such “dark” aggregates may be quite numerous. They are difficult to reveal and study, and can therefore “hide” a substantial fraction of dark matter, which remains undiscovered in the studies of groups of galaxies. This may partially solve the problem of “missing” mass.

Acknowledgements

This work was supported by the Russian Science Foundation (grant 14-12-00965).

References

[1] Karachentsev I.D., Kashibadze O.G., Makarov D.I., Tully R.B. 2009; MNRAS; 393; 1265

[2] Makarov D., Karachentsev I. 2011; MNRAS; 412; 2498

[3] Jones D.H., Read M.A., Saunders W. et al. 2009; MNRAS; 399; 683

[4] Ahn C.P., Alexandroff R., Allende Prieto C. et al. 2012; ApJS; 203; 21

[5] Meyer M.J., Zwaan M.A., Webster R.L. et al. 2004; MNRAS; 350; 1195

[6] Haynes M.P., Giovanelli R., Martin A.M. et al. 2011; AJ; 142; 170

[7] Karachentsev I.D., Makarov D.I., 2008; Astrophysical Bulletin; 63; 299

[8] Makarov D.I., Karachentsev I.D., 2009; Astrophysical Bulletin; 64; 24

[9] Karachentsev I.D., Makarov D.I., Karachentseva V. E., Melnyk O.V., 2011; Astrophysical Bulletin; 66; 1

[10] Jones D.H., Peterson B.A., Colless M., Saunders W. 2006; MNRAS; 369; 25

[11] Tully R.B., 1987; AphJ; 321; 280

[12] Vennik J., 1984; Tartu Astron. Obs. Publ.; 73; 1

[13] Magtesian A., Astrofizika. 1988; 28; 150

[14] Yepes G., Martínez-Vaquero L. A., Gottlöber S., Hoffman Y., 2009, in American Institute of Physics Conference Series, Vol. 1178, American Institute of Physics Conference Series, Balazs C., Wang F., eds., pp. 64-75

[15] Tully R.B., Rizzi L., Dolphin A.E. et al. 2006; AJ; 132; 729

[16] Makarov D.I., Uklein R.I. 2012; Astrophysical Bulletin; 67; 135

[17] Makarov D.I., Makarova L.N., Uklein R.I. 2013; Astrophysical Bulletin; 68; 125

A search for neutrino bursts in the Galaxy at the Baksan Underground Scintillation Telescope; 37 years of exposure

R.V. Novoseltseva[1], M.M. Boliev[1], I.M. Dzaparova[1,2], M.M. Kochkarov[1], A.N. Kurenya[1], Yu.F. Novoseltsev[1,*], V.B. Petkov[1,2], P.S. Striganov[1], V.I. Volchenko[1], G.V. Volchenko[1], A.F. Yanin[1]

[1] Institute for Nuclear Research of the Russian Academy of Sciences, 60th October Anniversary Prospect, 7a, 117312 Moscow, Russia, novoseltsev@inr.ru

[2] Institute of Astronomy of the Russian Academy of Sciences, 48 Pyatnitskaya St., 119017, Moscow, Russia

Abstract The current status of the experiment on recording neutrino bursts is presented. As the target, we use two parts of the facility with the total mass of 240 tons. Over the period of June 30, 1980 to June, 30, 2017, the actual observational time is 31.72 years. No candidate for the stellar core collapse has been detected during the observation period. An upper bound of the mean frequency of core collapse supernovae in our Galaxy is 0.073 year^{-1} (90% CL).

Keywords: Supernova, neutrino bursts

1. Introduction

The detection of neutrinos from the supernova SN1987A experimentally proved the critical role of neutrinos in the explosion of massive stars, as it was suggested more than 50 years ago [1-3].

Neutrinos are especially important, because they reveal the physical conditions in the star core at the instant of collapse. The SN1987A event helped to establish some aspects of the theory, namely the total energy radiated, the neutrinos temperatures and the duration of the neutrino burst [4, 5].

SN 1987A was the closest supernova (SN) for hundreds of years and thus was observed with unprecedented detailedness from the earliest moments of radiation emission. This event has demonstrated that SN explosions are genericly non-spherical. It implies that three-dimensional simulations are needed to understand the nature of the phenomenon of stellar core collapse and explosion, and, in particular, of the physical mechanism that initiates the SN blast.

Large long-term neutrino detectors are the most suited ones to observe the Galaxy and search for core collapse supernovae explosions. Several neutrino detectors have been observing the Galaxy in the last decades to search for stellar collapses, namely Baksan [6,7], Super-Kamiokande [8], MACRO [9], LVD [10], AMANDA [11], SNO [12]. At present, the new generation detectors, which are capable effectively to record the neutrino burst from the next SN, are added to the facilities listed above: IceCube[13], Borexino [14,15], KamLAND [16] and some others.

The Baksan Underground Scintillation Telescope (BUST) is the multipurpose detector intended for wide range of investigations in cosmic rays and particle physics. The experiments were begun in 1978. One of the current tasks is the search for neutrino bursts. The BUST operates under this program since the mid-1980. The paper is built as follows. Section 2 is the brief description of the facility. Section 3 is devoted to the method of neutrino burst detection. Conclusion is presented in Section 4.

2. The facility

The Baksan Underground Scintillation Telescope is located in the Northern Caucasus (Russia) in the underground laboratory at the effective depth of 8.5∗104 g∗cm-2 (850 m of w.e.) [17].The facility has dimensions 17∗17∗11 m3 and consists of four horizontal scintillation planes and four vertical ones (Fig. 1).

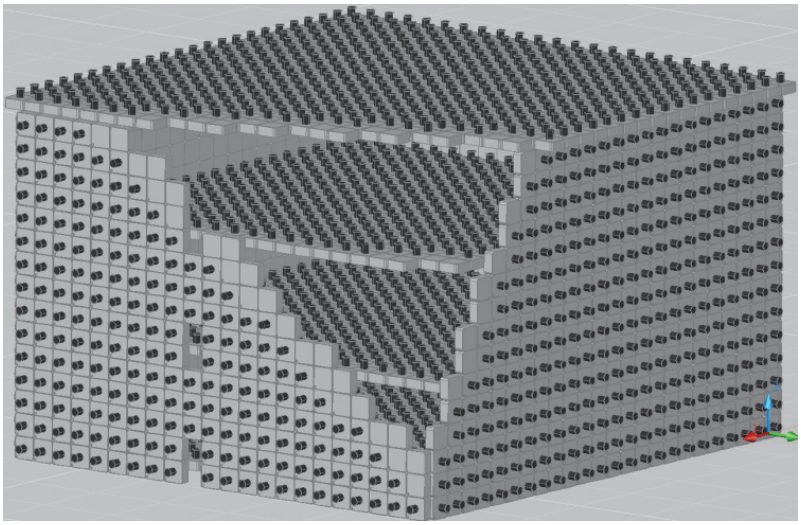

Fig1. *The Baksan underground scintillation telescope*

The upper horizontal plane consists of 576 (24∗24) liquid scintillator counters of the standard type, three lower planes have 400 (20∗20) counters each. The vertical planes have 15∗24 and 15∗22 counters. Each counter is 0.7∗0.7∗0.3 m^3 in size, filled with an organic C_nH2_{n+2} (n≈ 9) scintillator, and viewed by one photomultiplier with a photocathode diameter of 15 cm. The distance between neighboring horizontal scintillation layers is 3.6 m. The angular resolution of the facility is 2^o, time resolution is 5 ns.

The information from each counter is transmitted over three channels: an anode channel (which serves for amplitude measurements up to 2.5 GeV), a pulse channel with operation threshold 8 MeV and 10 MeV for the horizontal and vertical planes respectively (the most probable energy deposition of a muon in a counter is 50 MeV ≡ 1relativistic particle) and a logarithmic channel with a threshold 0.5 GeV. The signal from the fifth dynode of PM tube FEU-49 goes to a logarithmic channel where it is converted into a pulse whose length t is proportional to the logarithm of the amplitude of the signal [18].

The trigger is an operation of any counter pulse channel of the BUST.

The facility operates almost continuously under the program of search for neutrino bursts since the mid-1980. The total time of Galactic observation accounts for 90% of the calendar time.

3. The method of neutrino burst detection

The BUST consists of 3184 standard autonomous counters. The total scintillator mass is 330 t, and the mass enclosed in three lower horizontal layers (1200 standard counters) is 130 tons. The majority of the events recorded with the Baksan telescope from a supernova explosion will be produced in inverse beta decay (IBD) reactions

$$\bar{\nu}_e + p \rightarrow n + e^+ \quad (1)$$

If the mean antineutrino energy is $E_{\bar{\nu}_e} = 12 - 15$ MeV[19, 20], the pass of e^+ (produced in reaction (1)) will be included, as a rule, in the volume of one counter. In such case the signal from a supernova explosion will appear as a series of events from singly triggered counters (the only counter from 3184 operates; below we call such event "the single event") during the neutrino burst. The search for a neutrino burst consists in recording of single events cluster within time interval of = 20 s (according to the modern collapse models the burst duration δt does not exceed 20 s).

The expected number of neutrino interactions detected during an interval of duration δt from the beginning of the collapse can be expressed as:

$$N_{ev}^H = N_H \int_0^{\delta t} dt \int_0^{\infty} dE \times F(E,t) \times \sigma(E) \times \eta(E), \quad (2)$$

here N_H is the number of free protons, F(E,t) is the flux of electron antineutrinos, σ(E) - the IBD cross section, and η(E) - the detection efficiency. The symbol "H" in left side indicates that the hydrogen of scintillator is the target.

If one assumes the distance from the SN is 10 kpc, the total energy irradiated in neutrinos is

$$\varepsilon_{tot} = 3 \times 10^{53}\ erg \quad (3)$$

and the target mass is 130 tns (three lower horizontal layers) the expected number of single events from reaction (1) (we assume the $\bar{\nu}_e$ flux is equal to 1/6εtot) will be

$$N_{ev}^H \cong 35 \quad (4)$$

Flavor oscillations are unavoidable of course. However, it was recognized in recent years that the expected neutrino signal depends strongly on the oscillation scenario (see e.g. [21-24]. In the absence of a quantitatively reliable prediction of the flavor-dependent fluxes and spectra it is difficult to estimate the oscillation impact on ν_e– and $\bar{\nu}_e$ fluxes arriving to the Earth. Therefore we do not discuss the effects of flavor oscillations in this paper.

Background events are radioactivity (mainly from cosmogeneous isotopes) and cosmic ray muons if only one counter from 3184 hit. The total count rate from background events (averaged over the period of 2001 - 2017 years) is f1 = 0.0207 s^{-1} in internal planes (three lower horizontal layers) and ≈1.5 s^{-1} in external ones. Therefore three lower horizontal layers are used as a target; below we call this the D1 detector (the estimation (4) has been made for the D1 detector).

Background events can imitate the expected signal (k single events within sliding time interval τ) with a count rate

$$p(k) = f_1 * \exp(-f_1\tau)\frac{(f_1\tau)^{k-1}}{(k-1)!} \quad (5)$$

The treatment of experimental data (single events over a period 2001 - 2017 years; Tactual = 14.12 years) is shown by squares in Fig.2 in comparison with the expected distribution according to the expression (5) calculated at f1 = 0.0207 s^{-1}. Note there is no normalization in Fig.2.

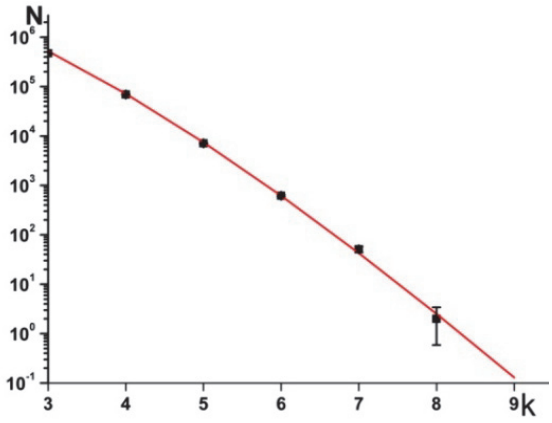

Fig2. *The number of clusters with k single events within time interval of τ = 20 s. Squares are experimental data, the curve is the expected number according to the expression (5).*

Background events create clusters with k = 8 with the rate 0.178 y^{-1}. The expected number of such clusters during the time interval T = 14.12 ys is 2.51 that we observe (2 events). The formation rate of clusters with k = 9 background events is 9.2×10-3 y^{-1}, therefore the cluster with multiplicity $k \geq k_{th}=9$ should be considered as a neutrino burst detection.

3.1. Two independent detectors

As it follows from the estimation (4) the "sensitivity radius" of the D1 detector is $R_s \cong 20$ kpc. To increase the sensitivity radius, we use those parts of external scintillator layers that have relatively low count rate of background events. The total number of counters in these parts is 1012, the scintillator mass is 110 tons. We call this array the D2 detector, it has the count rate of single events f2 = 0.12 s^{-1}. The count rates of single events in the D1 and the D2 detectors and the operating stability have been shown in Fig.3.

The joint use of D1 and D2 detectors allows us to decrease the threshold multiplicity in the D1 cluster (k_{th} =9) and, consequently, to increase R_s.

We use the following algorithm: in case of cluster detection with $k1 \geq 6$ in the D1, we check the number of single events k2 in the 10-second time frame in the D2 detector. The start of the frame coincides with the start of the cluster in the D1. Mass ratio of D2 and D1 detectors 1012/1200 = 0.843 implies that for the mean value of neutrino events k1 = 6 in the D1, the mean number of neutrino events in the D2 will be $\overline{k2}$ = 6× 0.843 ×0.8 = 4.05 (factor 0.8 takes into account that the frame duration in the D2 is 10 seconds instead of 20 seconds in the D1). Since the background adds f2×10 s = 1.2 events, we obtain finally $\overline{k2}(\overline{k1}=6)$= 4.05+1.2 = 5.25.

The D1 and the D2 detectors are independent ones therefore the imitation probability P1 of clusters with multiplicities k1 in the D1 and P2 for k2 in the D2 by background events is the product of appropriate probabilities

$$P(k1,k2) = P1(k1) \times P2(k2) \qquad (6)$$

and we obtain P(6,5) = 0.23 y^{-1}, P(6,6) = 0.045 y^{-1} (note P1 is determined according to the expression (5) and P2 is the Poisson distribution).

Therefore the events with k1≥ 6, k2≥ 6 should be considered as candidates for a neutrino burst detection (since mean values of k1 and k2 are significantly exceeded in two independent detectors simultaneously and the imitation probability of such events by background is very small). Thus we decrease the threshold value of k1 from 9 to 6 and increase the sensitivity radius up to $R_s \approx 23$ kpc.

3.2. Reactions on Carbon nuclei

There are models which predict the mean neutrino energy from SN is $\overline{E_\nu}$= 30 - 40 MeV [25, 26]. In such case the reactions on Carbon nuclei of the scintillator become effective and neutrinos can be detected in the BUST through interactions:

$$\nu_i + {}^{12}C \rightarrow {}^{12}C^* + \nu_i, \qquad E_{th}=15.1 \text{ MeV} \quad , \quad i=e,\mu,\tau, \tag{7}$$

$$C^* \rightarrow {}^{12}C + \gamma, \qquad E\gamma=15.1 \text{ MeV}$$

and

$$\nu_e + {}^{12}C \rightarrow {}^{12}N + e^-, \qquad E_{th}=17.34 \text{ MeV}$$

$$^{12}N \rightarrow {}^{12}C + e^+ + \nu_e, \qquad \tau(^{12}N) =15.9 \text{ ms} \tag{8}$$

τ is a lifetime of the nucleus ^{12}N.

If the mean energy $\overline{E_\nu}$ = 30 MeV the expected number of events in both detectors (the D1 and the D2) for reactions (7) and (8) can be estimated (under conditions (3)) by formulae

$$N_{ev2}^{C} = 25 \times \eta_2 \quad (E_\gamma = 15\ MeV) \tag{9}$$

$$N_{ev3}^{C} = 46 \times \eta_3 \quad (E_\nu = 30\ MeV) \tag{10}$$

The radiation length for our scintillator is 47 g/cm^2, therefore $\eta_2 \approx 0.2$. In reaction (6) the BUST can detect both e^- with energy (E_ν - 17) MeV and e^+ if the energy deposition from these particles is greater than 8 MeV. In the latter case, the reaction (8) will have the distinctive signature: two signals separated with (1 – 50) ms time interval (dead time of the BUST is ≈ 1 ms). In reaction (8) the sum of energies (E_{e+} + E_ν) is 17.3 MeV therefore η_3 ≈0.5 - 0.7.

It should be noticed, if $\overline{E_\nu}$ = 30 - 40 MeV a noticeable percentage of neutrino reactions will cause triggering two adjacent counters.

4. Conclusion

The Baksan Underground Scintillation Telescope operates under the program of search for neutrino bursts since June 30, 1980. As the target, we use two parts of the BUST (the D1 and D2 detectors) with the total mass of 240 tons. The "sensitivity radius" of the BUST (for a recording of neutrino bursts from supernovae) is $R_s \approx 23$ kpc.

Background events are 1) decays of cosmogeneous isotopes (which are produced in inelastic interaction of muons with the scintillator carbon and nuclei of surrounding matter) and 2) cosmic ray muons if the only counter from 3184 hits.

Over the period of June 30, 1980 to June 30, 2017, the actual observation time was 31.72 years. This is the longest observation time of our Galaxy with neutrino at the same facility. No candidate for the core collapse has been detected during the observation period. This leads to an upper bound of the mean frequency of gravitational collapses in the Galaxy

$$f_{col} < 0.73\ y^{-1}$$

at 90% CL. Recent estimations of the Galactic core-collapse SN rate give roughly the value ≈ 2-5 events per century (see e.g. [27]).

Acknowledgements

This study is performed with a part of the instrument certified as a Unique Scientific Facility (Baksan Underground Scintillation Telescope) and at an office that is an item of the Shared Research Facilities state program (Baksan Neutrino Observatory of the Institute for Nuclear Research).

References

[1] Gamow G. and Shoenberg M., The Possible Role of Neutrinos in Stellar Evolution, Phys. Rev., 58, 1117 (1940)

[2] Zeldovich Ya.B. and Guseinov O.Kh., Neutronization of matter during collapse and the neutrino spectrum, Dokl. Akad. Nauk SSSR, 162, 791,(1965)

[3] Colgate S.A. and White R.H., The hydrodynamic behavior of supernovae explosions, Astrophys. J., 143, 626 (1966)

[4] Loredo T.J., Lamb D.Q., Bayesian Analysis of Neutrinos from Supernova SN1987A, Phys.Rev.D, 65, 063002 (2002)

[5] Pagliaroli G., Vissani F., Costantini M.L., Ianni A., Improved analysis of SN1987A antineutrino events, Astropart. Phys., 31, 163 (2009)

[6] E.N. Alekseev, L.N. Alekseeva, V.I. Volchenko et al., Upper bound on the collapse rate of massive stars in the Milky Way given by neutrino observations with the Baksan underground telescope, Zh. Eksp.Teor.Fiz.,104, 2897 (1993)

[7] R.V. Novoseltseva, M.M. Boliev, I.M. Dzaparova et al., The Search for Neutrino Bursts from Core Collapse Supernovae at the Baksan Underground Scintillation Telescope, in proceedings of 31th ICRC, Lodz (2009)

[8] M. Ikeda, A. Takeda, Y. Fukuda et al., (Super-Kamiokande Collaboration) "Search for Supernova neutrino bursts at Super-Kamiokande", Astrophys.J., 669, 519 (2007)

[9] Ambrosio M. et al. (MACRO Collaboration) Search for stellar gravitational collapses with the MACRO detector, Eur.Phys.J.C, 37, 265 (2004)

[10] Aglietta M. et al. (LVD Collaboration), The most powerful scintillator supernovae detector: LVD, Nuovo Cimento A, 105, 1793 (1992)

[11] Ahrens J. et al. (AMANDA Collaboration), Search for supernova neutrino bursts with the AMANDA detector, Astropart.Phys., 16, 345 (2002)

[12] B. Aharmim, S.N. Ahmed, A.E. Anthony et al., Low Multiplicity Burst Search at the Sudbury Neutrino Observatory, Astrophys. J., 728, 83 (2011)

[13] T. Lund, A. Marek, C. Lunardini et al., Fast time variations of supernova neutrino fluxes and their detectability, Phys. Rev. D 82, 063007 (2010)

[14] Bellini G. et al.(Borexino Collaboration), First real time detection of 7Be solar neutrinos by Borexino, Phys. Lett. B 658 (4), 101 (2007)

[15] Bellini G., Novel results on low energy neutrino physics, Talk at TAUP 2011 conference, Munich, 5-9 Sept. 2011,

[16] Eguchi K. et al. (KamLAND Collaboration), First Results from KamLAND: Evidence for Reactor Antineutrino Disappearance, Phys. Rev. Lett. 90, 021802 (2003)

[17] E.N.Alexeyev, V.V.Alexeyenko, Yu.M.Andreyev et al., Baksan underground scintillation telescope, in proceedings of 16 ICRC, Kyoto, 10,276 (1979)

[18] Achkasov V.M., Bakatanov V.N., Novoseltsev Yu.F.et al., An investigation of the energy spectrum and inelastic muon interaction at the Baksan Underground scintillation telescope, Bull. Russ. Acad. Sci. Phys.,50, 2224 (1986)

[19] Imshennik V.S., Nadezhin D.K. Final stages of star evolution and supernova explosions, Itogi Nauki i Tehniki, ser. Astronomy 21, 63 (1982)

[20] Hillebrandt W., Hoish P., The supernova 1987A in the Large Magellanic Cloud, Rep. Prog. Phys. 52, 1421 (1989)

[21] Pantaleone J., Neutrino oscillations at high densities, Phys. Lett. B 287,128 (1992)

[22] Sawyer R.F., Speed-up of neutrino transformations in a supernova environment, Phys. Rev. D 72, 045003 (2005)

[23] Duan H., Fuller G.M., Carlson J. et al., Simulation of Coherent Non Linear Neutrino Flavor Transformation in the Supernova Environment I: Correlated Neutrino Trajectories, Phys. Rev. D 74, 105014 (2006)

[24] I. Tamborra, G. Raffelt, F. Hanke et al., Neutrino emission characteristics and detection opportunities based on three-dimensional supernova simulations, Phys. Rev. D 90, 045032 (2014)

[25] Imshennik V.S. Explosion Mechanism in Supernovae Collapse, Space Sci.Rev. 74, 325 (1995)

[26] Bajkov V., Suslin V.M., Chechetkin V.M. et al., Radiation of a neutrino mechanism for type II supernovae, Russ. Astronom. journal, 84 (4), 308 (2007)

[27] Adams S.M., Kochanek C.S., Beacom J.F. et al., Observing the Next Galactic Supernova, Astrophys.J., 778, 164 (2013)

The 3.6m Devasthal optical telescope and time domain astronomy

Shashi Bhushan Pandey[1],*

[1] Aryabhatta Research Institute of Observational Sciences, Manora Peak, Nainital, Uttarakhand, India, 263001; shashi@aries.res.in

Abstract: Longitudinal advantage of India is very much suitable for the time domain astronomy and particularly for time critical observations. Recently installed 3.6m Devasthal optical telescope along with back-end instruments are well suited for observations of energetic cosmic transients like Supernovae and Gamma-ray bursts. In this presentation, I summarize about the 3.6m DOT project along with proposed plans to study transients in near future.

Keywords: 3.6m Devasthal optical telescope, Imager, Transients, Supernova, Gamma-ray bursts

1. Introduction

As a part of time domain astronomy and with the help of ground/space based multi-wavelength telescopes, the astronomical community has made tremendous progress over the last hundred years to understand many aspects of our observable universe. These findings include: energetic cosmic explosions, discovery of exo-planetary systems, evidence for an accelerating universe, detailed identification and monitoring of the orbits of the asteroids and comets that may pose great dangers to the inhabitants of the Earth, and many more yet un-explored areas. With the combination of 4-10m class ground-based optical telescopes and other multi-band facilities, our understanding about Core-Collapse Supernovae (CCSNe) and Gamma-ray Bursts (GRBs) have been able to provide a great deal of information about the fate of evolution of massive stars ($> 8 - 10 M_{\odot}$) and the underlying physical mechanisms (Woosley & Bloom2006, Sokolov 2012, Kumar & Zhang 2015).

India has made several notable contributions towards optical-NIR astronomy during the latter half of the last century and had put in great efforts to set up world class observing facilities, which culminated in the indigenous building of the 2.3m Vainu Bappu Telescope (VBT) in 1987. The most recent astronomy facilities which have been set up in the country are, IIA's 2.0m Himalayan Chandra Telescope (2003) at Hanle, Ladakh and the 2.0m IUCAA Girawali telescope (2006) at Girawali, near Pune and recently the 3.6m Devasthal optical telescope (2016) at ARIES Nainital (Sagar 1999).

The Aryabhatta Research Institute of Observational Sciences (ARIES), Nainital, India has longitudinal advantage for observations of time-critical events like GRBs and other transient events as it lies in the middle of the 180 wide belt between Canary Islands (20 W) and Eastern Australia (160 E). Devasthal, the new observing station of ARIES Nainital (a mountain peak 60km away from Nainital, an altitude of 2450 m above msl, longitude 79.7E and latitude 29.4N) has advantages like dark skies, sub-arcsec seeing conditions, low extinctions and at the same time the site is easily accessible (Sagar 2000 & 2011; Stalin et al. 2000). Since 1999, ARIES has contributed significantly towards studies of afterglows of several well-known

Gamma-ray Bursts (GRBs) and Supernovae (SNe) using meter-class telescopes like 1.04m Sampurnanand Telescope and 1.3m Devasthal Fast optical telescope and the back-end instruments (Pandey 2006; Sagar & Pandey 2012).

2. The 3.6m Devasthal Optical Telescope

A modern 3.6-m Devasthal Optical Telescope (DOT) has been installed during 2015 and operational since March 2016. Deasthal is a new observing station for ARIES (see Fig1). The characterization of Devasthal site was carried out on 80 nights during 1998-1999 with a Differential Image Motion Monitor (DIMM) using a 38-cm telescope with the mirror about 2 m above the ground, and it yielded a median seeing estimate of about 1.1 arc-sec; the 10 percentile values lie between 0.7 to 0.8 arc-sec while for 35% of the time the seeing was better than 1 arc-sec (Sagar et al. 2000). The atmospheric extinction studies at Devasthal are described by Mohan et al. (2000).

Fig1*.A panoramic view of ARIES Devasthal Observatory, Nainital. The larger white dome houses 3.6m DOT whereas the smaller dome houses a 1.3m wide-field optical telescope.*

The fundamental telescope optics parameters are a primary mirror of diameter 3.6-m, f/2 primary, f/9 effective focal ratio, Ritchey-Chretien configuration with back focal distance of 2-m (see Fig2). The secondary mirror will have a diameter of about 0.9 m. The telescope performance is said to have 80% of the light encircled within 0.45 arcsec diameter in 30-arcmin field over 350-3000 nm wavelength range. The telescope has a Alt-Azimuth mounting with a zenith blind spot of less than 2 degree conical diameter. The science field of view of the DOT is 10 arcmin without corrector and 30 arcmin unvignetted field for axial port and 10 arcmin for side ports. A cylindrical space of minimum 2.5 meter below the focal plane for axial port and approximately 3.0 meter diameter around optical axis is available for the instrument envelope.

The telescope will have a pointing accuracy of less than 2 arc-sec RMS for any point in the sky with elevation greater than 10 degree and less than 0.1 arcsec RMS for 10 arcmin off-set. The tracking accuracy of DOT will be smaller than 0.1 arcsec RMS for less than one minute in open loop and smaller than 0.1 arc sec RMS for about one hour in closed loop (with auto guider). The acquisition and guiding unit is available with the telescope along with the five axis motion of secondary mirror (see Fig2). The active optics system (AOS) controls the alignment of M1 and M2 using pneumatic actuators and hexapod mechanism respectively. The corrections can also be applied in closed loop using data from the Shack-Hartmann wavefront sensing system. The vital characteristics of the telescope are given in Table1.

Table1. *Key characteristics of the 3.6m Devasthal optical telescope at ARIES Nainital.*

Parameters	**Value**
Primary Mirror clear aperture	3.6 m
Focal ratios	Primary : F/2; Effective : F/9; Plate Scale : 6:366 arc-sec /mm
Back focus distance	2.5 m
Science Field of View	10 arcmin on side ports, 30 arcmin on axial port; (35 arcmin for the AGU) in wavelength range 350 nm to 5000 nm
Mounting	Alt-azimuth
Sky coverage	15 degree to 87. 5 degree in elevation
Pointing accuracy	< 2 arc-sec RMS (Root mean squared)
Tracking accuracy	< 0.1 arc-sec RMS for 1 minute in open loop, < 0.1 arc-sec RMS for 1 hour in close loop, < 0.5 arc-sec Peak for 15 minutes in open loop.
Optical image quality	- Encircled Energy 50% (E50) < 0.3 arcsec, - Encircled Energy 80% (E80) < 0.45 arcsec, - Encircled Energy 90% (E90) < 0.6 arcsec, For the wavelength range from 350 nm to 1500 nm and without corrector for 10 arcmin Field of view.

2.1. First generation back-end instruments

For the 3.6-m DOT, Several first-generation back-end instruments were proposed for the 3.6m DOT for broad-band imaging and spectroscopy covering 350-3600 nm wavelength range i.g. (1) 4K4K CCD optical general purpose Imager for deeper photometric observations, (2) TIFR near-infrared imaging camera (TIRCAM2), (3) ARIES Devasthal Faint Object Spectrograph and Camera (ADFOSC), (4) high resolution Echelle spectrograph, (5) a TIFR-ARIES near-infrared spectrometer (TANSPEC) and (6) multi- integral field unit optical spectrograph (DOTIFS).

The ADFOSC is a focal reducer instrument and shall work both in imaging and spectroscopic modes. The instrument will have imaging capabilities with one pixel resolution of less than 0.3 arc-sec in the whole unvignetting field of view (10×10 arcmin) of the telescope and low-medium resolution spectroscopy with spectral resolution (250-5000) covering the wavelength range from 350 nm to 1000 nm. It is expected that we can image a 25 mag star in V band within an hour of exposure time. The high resolution Echelle spectrograph, capable of giving continuous spectral coverage (350 nm to 1000 nm) in a single exposure with a signal-to-noise ratio of 100 per 4 km/s bin for an integration time of one hour for a star of 14 magnitude at V

band (see Fig6). The concept of the high resolution Echelle spectrograph will be similar to many contemporary high resolution spectrometers such as HERMES (Raskin et al. 2011). A general purpose near-infrared imaging camera with limited spectroscopic capability is proposed by TIFR Mumbai for observations in the near-infrared bands between 1 and 2.5 micron. It will use a 1024× 1024 Hawaii HgCdTe detector array manufactured by Rockwell International USA and will have flexible optics and drive electronics that will permit a variety of observing configurations. The primary aim of this instrument would be to obtain broad and narrow band imaging of the fields as large as ~ 4× 4 arcmin and also to use it as a long-slit spectrometer with moderate resolving power when attached to the telescope. The proposed TANSPEC when coupled with the 3.6m telescope is expected to reach the 5 detection of 22.5 mag in J, 21.5 mag in H and 21.0 mag in K with one hour integration.

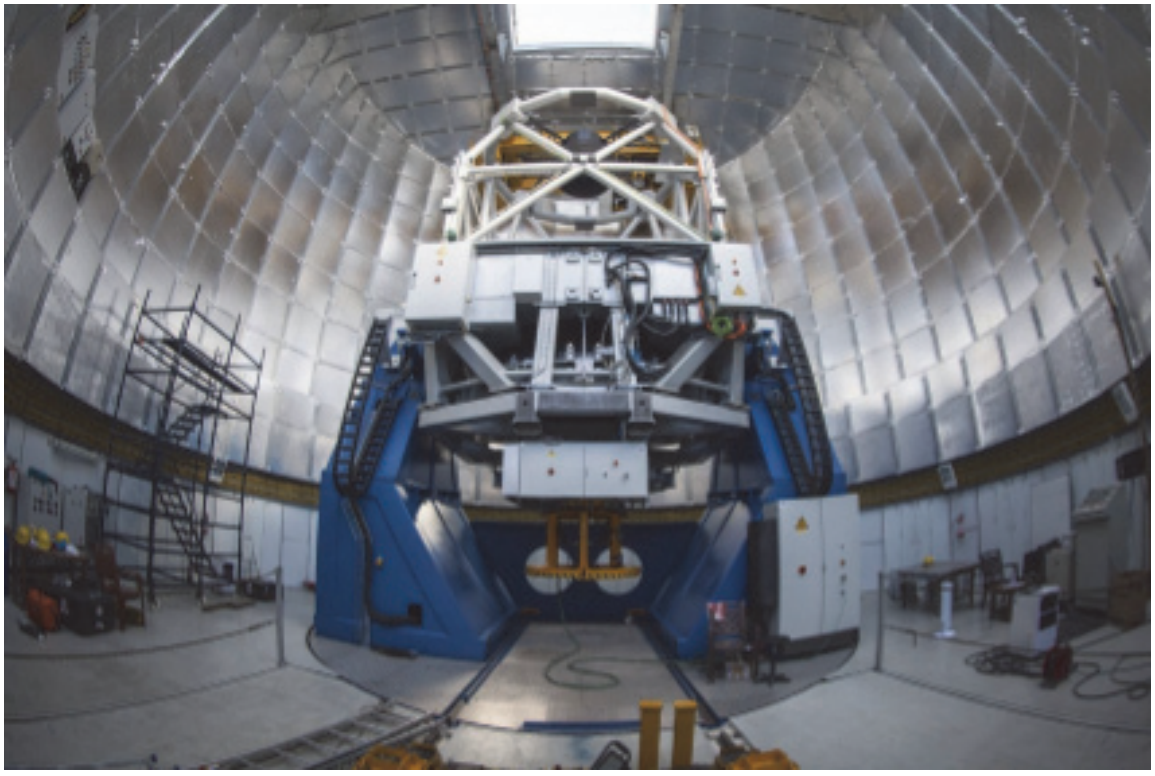

Fig2. *The 3.6m DOT as installed at Devasthal Nainital by a Belgian company AMOS (fall 2015) inside the dome build indigenous by an Indian firm. This telescope is installed at nearly 11-m height from the ground level to improve seeing.*

2.2. 4K×4K CCD Imager

The first light instrument, as an in-house developmental activity, called 4K4K CCD Imager with motorized filter-housing and camera mounting arrangements is designed to be mounted at the axial port of the 3.6m DOT. The f/9 beam of the telescope system is directly used without any focal reducer and has a plate-scale of 6.4 arcsec/mm. It is planned to use the f/9 beam directly to utilize the central unvignated 10x10 arcmin2 of the science field using appropriate filters. So, based on the scientific goals mentioned above, it was decided to purchase a blue-enhanced, back-illuminated 4K4K CCD chip with a pixel size of 15 micron in 2011 from Semiconductor Technology Associates Inc. (STA) USA (for more details about the camera and

ARCHON controller, please refer, http://www.sta-inc.net/). For the STA CCD chip, the quantum efficiency curve as a function of wavelength is also shown in Fig3a. For the given plate scale of 6.4 arc sec/mm, a 15 micron 4Kx4K CCD camera is able to image 6.5x6.5 arc min of the sky. Using the given parameters of the telescope and the CCD, throughput simulations are described in Fig3.b.

Mechanisms of the two motorized filter wheels (both software and hardware) were designed, developed and implemented in-house. The 3.6m DOT Imager instrument consists of two filter wheels. Both filter wheels have separate set of six filter positions namely U; B; V; R; I; C (Clear) and u; g; r; i; z; c (Clear), respectively. Microcontroller based control unit and GUI software are used for the positioning of two filter wheels in the Imager Instrument. Control unit consists of a PIC microcontroller having Serial Communications Interface (SCI) module USART (Universal Synchronous Asynchronous Receiver Transmitter) and a circuit that converts from RS-232 compatible signal levels to the USART's logic levels and vice-versa. Homing is achieved after powering ON using Hall Effect sensors. A detailed log of commands, status and errors are continuously generated by the GUI software. Both the control unit and the software have been successfully tested and integrated with the Imager instrument. More details about the CCD Imager are published by Pandey et al. (2017).

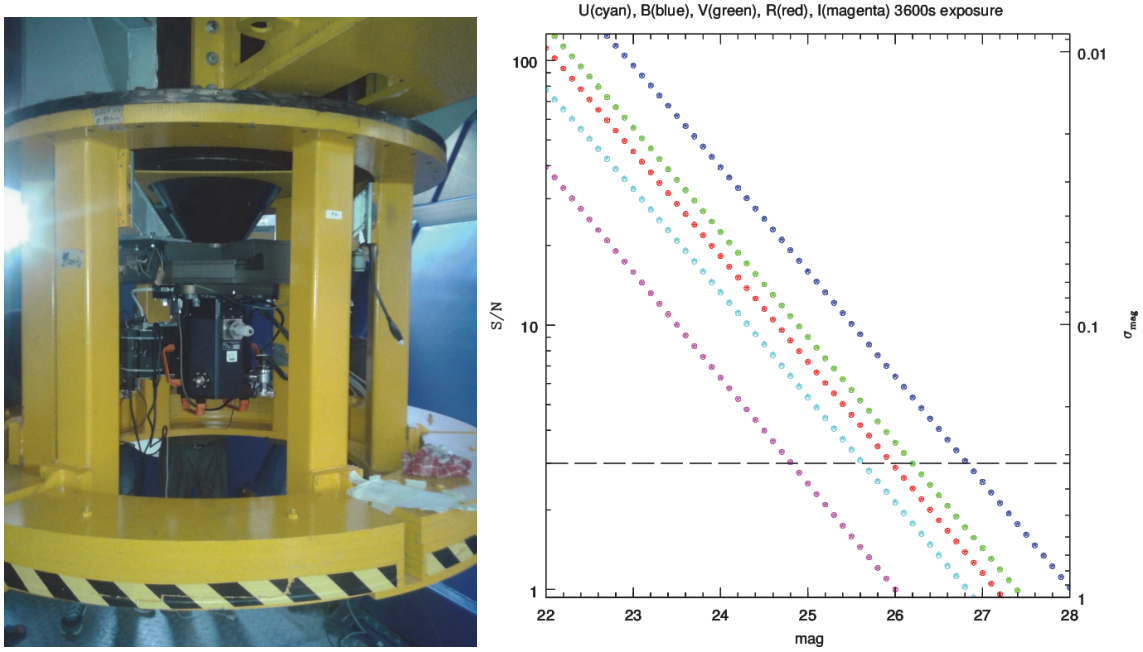

***Fig3**. (a) The fully assembled 4K×4K CCD camera along with shutter and automated filter wheels mounted at the axial port of the 3.6m DOT.*

(b) A simulated plot of magnitude (X-axis) vs. signal-to-noise ratio (Y-axis, left) and corresponding error in the magnitude determinations (Y-axis, right) based on the throughput calculations (Mayya 1991) of the 3.6m telescope with the proposed 15 micron 4K×4K CCD camera for set of Bessel UBV RI filters, for assumed equivalent exposure time of 1 hour each, seeing value of 1.5 arc-sec.

Deeper imaging of Galactic and extra-galactic point sources (B ~ 25 mag) and objects with low surface brightness could be performed using the 4K4K CCD Imager in several broad-band filters (set of Bessel UBVRI and SDSS ugriz filters) at the axial port of the 3.6m telescope. It is

also proposed that with the 3.6m DOT sources identified with GMRT and ASTROSAT would also be followed-up to a deeper limits (Pandey et al. 2017).

3. Time domain astronomy and transients

Time domain astronomy covers a very broad verity of astronomical objects and their properties at diverse times-scales as described in Fig4. Transients are usually the result of some kind of explosion or collision that leads to a change in the physical character of the source (e.g. supernovae, gamma-ray bursts, neutron star mergers), or a result of accretion of matter (nova outbursts, tidal disruption events, AGN flares). These events are unpredictable, show a temporal evolution of the physical conditions, and often fall below the detection threshold when faint. Such Target of Opportunity (ToO) transient events generally require a rapid response to a trigger of observations. Variability in sources can be intrinsic; caused by either a change in the physical conditions (e.g. Cepheid Variables, stellar flares), or accretion induced (e.g. cataclysmic variables, AGN), or extrinsic; as a result of geometry (e.g. binaries, lensed objects, transiting planets). Variability observations can be time dependent, or time critical requiring observations that are time-resolved. Photometric and spectroscopic study of some of these objects is quite crucial for the 3.6m Devasthal optical telescope available at Indian longitude during this age of multi-wavelength era.

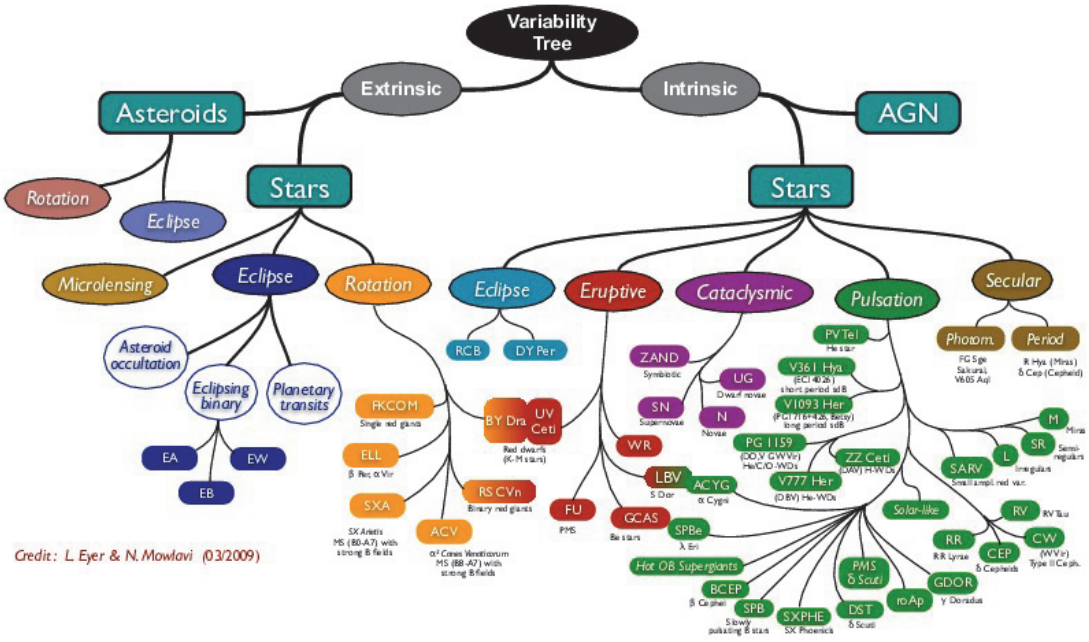

Fig4*. A variability tree showing a zoo of objects classified based on their characteristic properties and most of them are considered as a part of time domain astronomy to understand them in more detail. Cataclysmic category is particularly important to emphasize on the nature of objects showing transients due to explosions like supernovae (SNe) and gamma-ray bursts (GRBs).*

Energetic cosmic explosions under the cataclysmic category are particularly important

considering longitudinal advantage of India and availability of the 3.6m DOT and the back-end instruments. The main areas of interests are study of core-collapse supernovae and their correlation with long GRBs, short duration GRBs and study of "kilonovae" as a counterpart of Gravitation wave candidates. Tidal disruption events and candidate soft gamma-ray repeaters are also planned to be studied using this telescope. Detailed study of type Ia supernovae discovered by the upcoming 4.0m International Liquid Mirror Telescope (ILMT) are also targeted to be studied using the 3.6m DOT. Explosive transients discovered within the other multi-wavelength facilities like ASTROSAT (the first Indian multi-wavelength satellite) are also planned to be observed using this facility and other complementary observational facilities.

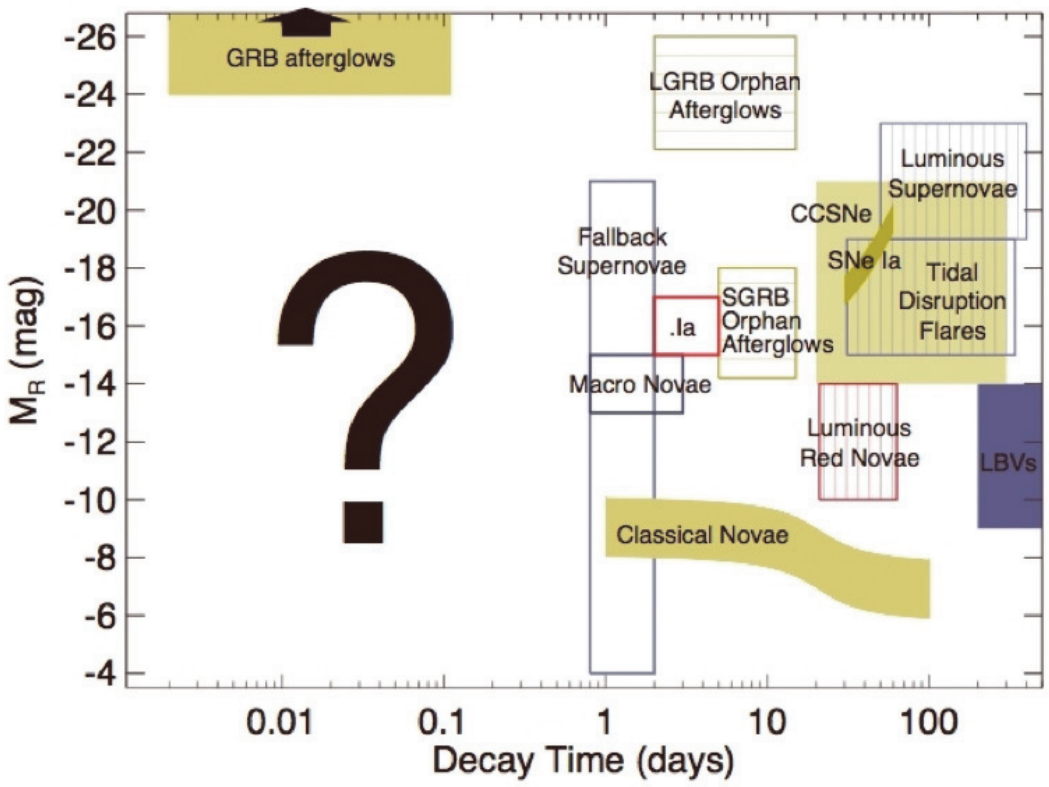

***Fig5**. This figure demonstrates the transient phase space as observed using various multi-wavelength facilities. The X-axis denotes the time in days whereas Y-axis is brightness in absolute magnitude. Various transients are shown as scatter plot. It also demonstrates the importance of upcoming facilities to search for new transients and know more about known transients)This figure has been adopted from NOAO web-site https://www.noao.edu/currents/img/time-domain.jpg and the reference is thankfully acknowledged).*

4. Early results with the 3.6m DOT and the 4Kx4K CCD Imager

The 3.6m DOT has been successfully installed at Devasthal. A rigorous on-sky performance of the telescope was tested using Test-WFS and the CCD Camera. The telescope was accepted for science observation in February 2016. The first light instruments 4Kx4K Imager and the FOSC are being tested at the moment. The telescope was technically activated jointly by the Prime Ministers of India and Belgium on 30 March 2016 in the presence of the Minister of Science and Technology, Government of India. In Fig6 below, the color magnitude diagram of the Globular cluster NGC 4147 is demonstrated showing detection of many faint point sources

(B >24 mag) whereas in Fig7 a color composite RGB image of the NGC 613 is shown with core-collapse type IIb SN 2016gkg clearly detected.

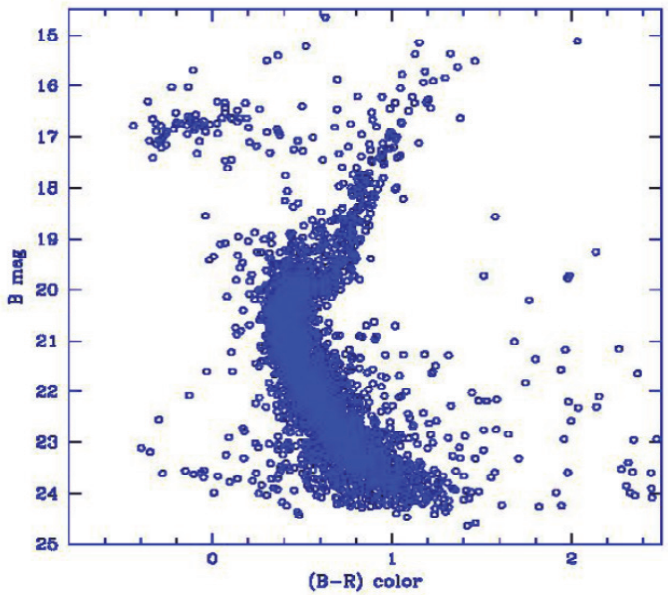

***Fig6**. The B versus (B- R) color-magnitude diagram (CMD) of the Globular cluster NGC 4147 as obtained using the present calibration data taken using the 4K4K CCD mounted at the axial port of the 3.6m DOT. The total number of common stars plotted (detected in both filters) is around 3500 with a photometric accuracy of < 0.2 mag. In this figure, the number of detected stars having B < 24 mag are around 150 (with a photometric accuracy of < 0.2 mag) in the effective exposure time of 120 sec.*

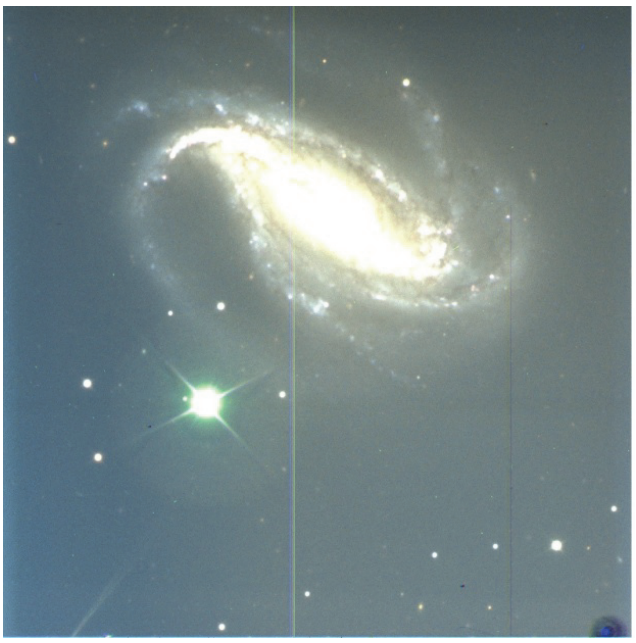

***Fig7**. A color composite RGB image (3*200 sec) of the spiral galaxy NGC 613 taken in November 2016. Supernova 2016gkg (at V ~ 17 mag) is clearly visible in the upper right quarter of the frame.*

In summary, longitudinal advantage of Indian sub-continent makes the recently installed 3.6m telescope as a novel facility for astronomical observations, specially, to study time critical

events, i.g. transients. This telescope along with the first generation back-end instruments could be efficiently used to study new transients, specially, the fainter ones with shorter time scales and the follow-up of the sources with identified gravitational wave candidates. Study of new explosive transients as a part of time domain astronomy will play a key role in near future along with the upcoming multi-wavelength facilities to explore the underlying physics behind these sources.

Acknowledgments

The author acknowledges Prof. V. V. Sokolov for the invitation to be part of Scientific organizing committee of the workshop titled "”SN 1987A, quark phase transition in compact objects and multi-messenger astronomy”" and deliver an invited talk as presented in this article.

References

[1] Kumar P., Zhang B., 2015, Physics Reports, 561, 1

[2] Raskin L. et al., 2011, A&A, 526, A69

[3] Sagar, R., Pandey, A. K., Mohan, V., et al. 1999, BASI , 27 , 3

[4] Sagar R., 2000, Current Science, Volume 78, No. 9, 1076

[5] Sagar R., Omar A., Kumar B. et al., 2011, Current Science, Volume 101, No. 8, 1020

[6] Sagar R. & Pandey S. B., 2012, Astronomical Society of India Conference Series, 5, 1

[7] Stalin C. S., Sagar R. & Pant P. et al., 2000, Bull. Astr. Soc. India, 29, 39

[8] Sokolov, V. V., 2012, ASI conference proceedings, Vol 5, 15

[9] Pandey S. B., 2006, PhD Thesis

[10] Pandey et al., 2017, arXiv:1711.05422v1, Refereed proceedings of the first BINA Workshop held in ARIES, November 2016. To appear in the Bulletin of Liege Royal Society of Sciences

[11] Mayya Y. D. 1991, JApA, 12, 319

[12] Woosley, S.E., Bloom, J.S., 2006, ARA&A , 47 , 507

Multimessenger search for evaporating primordial black holes

V.B. Petkov [1,2],*, E.V. Bugaev[1], P.A. Klimai[1]

[1]Institute for Nuclear Research of the Russian Academy of Sciences,
60th October Anniversary Prospect, 7a, 117312 Moscow, Russia; vpetkov@inr.ru

[2]Institute of Astronomy of the Russian Academy of Sciences,
48 Pyatnitskaya St., 119017, Moscow, Russia

Abstract Primordial black holes (PBHs) are black holes which may form in the early Universe through the gravitational collapse of primordial cosmological density fluctuations. Due to Hawking radiation these PBHs are supposed to evaporate by emitting particles. Recent developments in the experimental searching for evaporating PBHs in the local Universe are reviewed. The multimessenger techniques of searching for signals from evaporating PBHs are discussed.

Keywords: Primordial Black Holes, Hawking Radiation, Multimessenger Astronomy

1. Introduction

Primordial black holes can be formed in the early Universe through the gravitational collapse of primordial cosmological density fluctuations – those that give rise to the observed structure of the Universe (galaxies and clusters of galaxies) during its subsequent evolution. For an appreciable number of PBHs to be formed, it is important that significant density fluctuations on small mass scales existed in the early Universe. The curvature fluctuations and the related density fluctuations are currently believed to result from an inflationary expansion of the Universe; significantly, the power spectrum of these fluctuations is entirely determined by the parameters of the theoretical inflation model used and primarily by the form of the inflation potential. There exist quite a few models (see, e.g., [1] and references therein) in which a fluctuation spectrum that ensures the formation of a considerable number of PBHs is predicted.

The regularities of the black hole formation are determined not only by the cosmology and physics of the early Universe. Theoretical predictions of the PBH formation probability depend strongly on the theory of gravitation and the model of gravitational collapse used. Direct search for the PBHs is based on the Hawking radiation [2, 3], which leads to their evaporation on a characteristic time scale [4, 5]

$$\tau(M_{BH}) \approx 1.15 \cdot 10^{65} \left(\frac{M_{BH}}{M_{Sun}} \right)^3 y \qquad (1)$$

The critical mass for which τ equals the age of the Universe (≈ 13:7 Gyr) is ≈ 5.1×1014 g [4].

It should be noted that the evaporation of black holes has not been completely studied to date. There are several theoretical models of the evaporation process [6 – 10]. The technique of searching for the high energy photon signal from evaporating PBHs depends on temporal and energy characteristics of their gamma-ray emission. Because these characteristics differ for different evaporation models, the upper limit obtained for the number density of evaporating PBHs in a local region of space depends strongly on the specific evaporation model.

Of course the distribution of PBHs in space is important for their direct search. Because of the local increase in the density of PBHs in our Galaxy [11], the constraints on their number density imposed by a direct search can be more stringent than those imposed by diffuse extragalactic gamma-ray background measurements, which are sensitive only to the mean PBH density in the Universe.

PBHs might arguably be the most natural candidates to solve the dark matter problem: they are cold, weakly-interacting, and do not require extensions of the Standard Model of particle physics. So, experimental detection of PBHs could provide a unique probe of the early Universe, gravitational collapse, high energy physics and quantum gravity. The nondetection of PBHs at the current level of the experimental technique also carries useful information and allows further progress to be made in understanding the early Universe.

2. Search for gamma-ray bursts from evaporating PBHs

At the final PBH evaporation stage the high-energy gamma-ray burst (significant and time-localized excess of gamma radiation above the background) is generated. Different evaporation models give different temporal and energy characteristics of these bursts. Experimental search for such events has been carried out at several EAS arrays and Cherenkov telescopes for three evaporation models. In the first (best-known) model [6], the photons produced by the fragmentation of evaporated quarks are assumed to make a large contribution to the total photon spectrum from evaporating PBHs. In the other two models [7, 8], the photons produced by the interaction of evaporated quarks (and leptons) with one another are also taken into account. The interactions of evaporated particles are important if something like a photo- or chromosphere is formed around the PBH during its evaporation (as is assumed in [7, 8]). In these experiments the upper limits on the number density of evaporating PBHs in local region of the Galaxy have been obtained [12].

According to model with quark gluon phase transition [13], the gamma − ray burst occurs when in the vicinity of a black hole in the flow of its radiation the hadron-quark phase transition take place, which can happen at $T > 100$ MeV . The quark-gluon plasma, once created, absorbs the radiation of ever increasing temperature, emitted by the black hole. Then the energy accumulated in the shell of plasma is ejected for a short period of time (~ 100 ms) as a burst of ~ 100 keV photons. Their mechanism could, in principle, explain some experimentally detected rather short gamma − ray bursts [13].

The evaporation model with relativistic phase transitions predicts ultrashort (~ 10–13 s) gamma-ray bursts with the spectrum with the maximum intensities simultaneously at the photon energies of 100 MeV and 100 GeV [8]. Such ultrashort gamma-ray bursts can be detected by EAS arrays located on mountains as EASs with a uniform lateral distribution. Experimental search for PBHs in frame of this evaporation model was carried out at Andyrchy EAS array; a limit on the concentration of evaporating PBHs in a local region of the Galaxy for this evaporation model has been obtained [14].

So far the searching for very-high-energy gamma-ray bursts from evaporating PBH yields only limits on their concentration in local region of the Galaxy. Moreover, in this kind of experiments only limits on the PBH's concentration can be obtained. In order to prove that particular event is the burst from evaporating PBH the multimessenger approach is needed.

3. Multimessenger search for PBH evaporation signal with AMON [15]

Most evaporation models predict, after stage of gradual evaporation, an explosion of PBHs during the last few seconds of their lives. A burst of high energy particles is produced as a result of the explosion. Different kinds of these particles could be registered in coincidence by several detectors with large fields of view. The search for such events has been proposed within the Astrophysical Multimessenger Observatory Network (AMON) framework [15]. The discovery potential for joint detections of multimessenger bursts due to evaporating PBHs has examined for IceCube (neutrinos), HAWC(gamma rays) and Pierre Auger (gamma rays, neutrons and protons). Only model without a chromosphere [6] was considered for such search, because a PBH chromosphere [7, 8] would give steeper particle spectra making these high-energy experiments not suitable for detection of the PBH bursts [16]. It was argued that this multimessenger approach is essential to distinguish between bursts due to PBHs and other possible sources, should a positive detection occur. Both real-time and archival searches for PBH bursts are planned within the AMON framework.

4. Transient radio and optical pulses from exploding PBHs

The electromagnetic pulses can be generated during PBHs explosions due to interactions of emitted charged particles (mainly electrons and positrons) with the interstellar magnetic field. Possible radiation mechanism, proposed by Rees [17], consists in collective interaction of electrons and positrons with an ambient field. The emitted charged particles in this case are considered as a conducting sphere, expanding into a uniform magnetic field. The spectrum of radiation depends on Lorentz factor of expanding shell and strength of ambient magnetic field [18].). Calculated spectra of electromagnetic emission for field strength of 0.5 nT are presented on Fig. 1 for three values of Lorentz factor. One can see that this radiation mechanism gives us possibility to detect exploding PBHs by the use of optical and/or radio telescopes (or both, in coincidence).

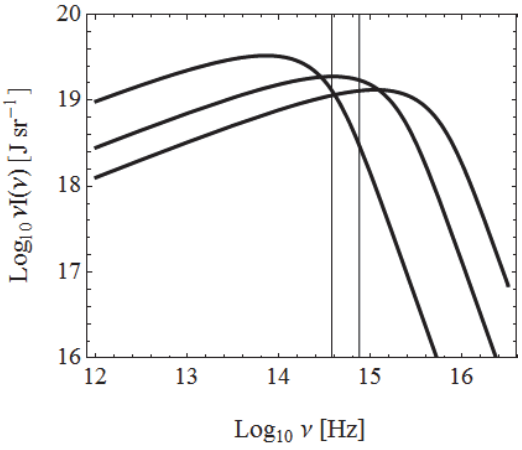

Fig1*. Radiation spectra of exploding PBH calculated for Rees – Blandford mechanism [15, 16] (see text for detais). From left to right, Lorentz factor γ= (4, 7, 10) ×106. Vertical lines bound the range of wavelength 400 – 800 nm.*

The search for radio pulses from PBH explosions was carried out using the Eight-meter-wavelength Transient Array (ETA) [19]. No compelling astrophysical signal was detected in this experiment; only upper limit on the rate of exploding PBHs was obtained for an exploding PBH with a fireball Lorentz factor of 104.3.

It should be noted that the evaporation process of black holes is essentially changed in the presence of an extra spatial dimension. The fact of the matter is that with the addition of an extra spatial dimension, black holes could exist in different phases and undergo phase transitions [20, 21]. For one toroidally compactified extra dimension, two possible phases are a black string wrapping the compactified extra dimension, and a 5-dimensional black hole smaller than the extra dimension. A topological phase transition from the black string to the black hole results in a significant release of energy by means of Rees-Blandford mechanism. The ETA observations [19] also imply an upper limit on the rate of PBH explosions in the context of certain extra dimension models as described in [21].

5. Search for very high-energy gamma-ray bursts from evaporating PBHs in coincidence with optical flashes

As was mentioned above, the multimessenger approach gives us a possibility to distinguish between bursts due to PBHs and other possible sources. The joint search for very high-energy gamma-ray bursts and optical flashes from evaporating PBHs is a kind of multimessenger approach. At present the quick search for astrophysical objects which produce both, bursts of high energy cosmic radiation and optical flashes, is carried out in the near real-time mode with the facilities of the Baksan Neutrino Observatory (BNO) of INR RAS and a complex of astronomical telescopes at the Terskol Peak Observatory (Terskol branch of INASAN) [22].

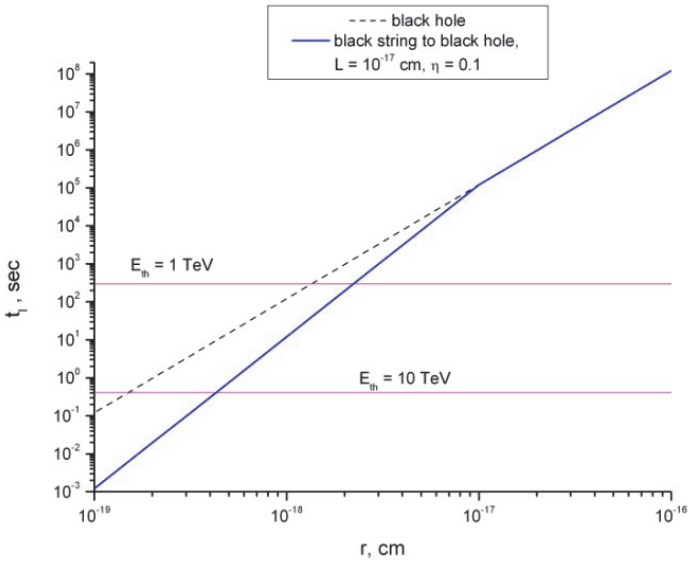

Fig2. *The dependence of the time until the end of PBH evaporation tl on black hole radius r. Dashed line – for usual space, solid line – for space with one toroidally compactified extra dimension with L = 10-19 m, where a topological phase transition from the black string to the black hole is happened. Horizontal lines show values of tl for two threshold energies of gamma-rays, 1 TeV and 10 TeV, for the model without a chromosphere.*

Unique complex of BNO facilities consists of Baksan Underground Scintillation Telescope (BUST) [23, 24] and two EAS arrays: "Carpet-2" [25] and "Andyrchy" [26]. The BNO facilities work in continuous mode of operation and they are recording of cosmic rays from upper hemisphere (so called "all sky all time" mode). These apparatus allow searching for bursts of cosmic gamma radiation in wide range of primary gamma-rays energy: from 1 TeV (at the BUST) up to 80 TeV (at the EAS arrays "Carpet-2" and "Andyrchy") [27 – 29].

The search for very high-energy gamma-ray bursts from evaporating PBHs can be performed at EAS arrays only in frame of model without a chromosphere, because a PBH chromosphere would give steeper particle spectra making these high-energy experiments not suitable for detection of the PBH bursts [16]. But even in this model the burst duration is very short ($\leq$ 40 ms) for the EAS arrays "Carpet-2" and "Andyrchy", due to their high energy thresholds [29]. Therefore the burst of very high-energy gamma-rays and optical flash from the final black hole explosion happens in usual space practically simultaneously. However the burst of gamma-rays can be registered prior to optical flash at the BUST, with its lower threshold energy (see Fig2).

In the model with one toroidally compactified extra dimension, after topological phase transition from the black string to the black hole, a 5d black hole continues to evaporate with a different rate (Fig. 2). In principle two optical signals could be expected in this model: first one due to a topological phase transition from the black string to the black hole (when $L \sim r$) and second one from the final 5d black hole explosion, with delay between two successive signals depending on size of an extra dimension L. But second signal is expected to be weaker than that first one, with much smaller total emitted energy [20]. In any case "all sky" optical telescopes are needed, both for the successful search of the evaporating PBHs and for distinction of the evaporation models.

Acknowledgements

This study is performed with a part of the instrument certified as a Unique Scientific Facility (Baksan Underground Scintillation Telescope) and at an office that is an item of the Shared Research Facilities state program (Baksan Neutrino Observatory of the Institute for Nuclear Research). The work is supported by the Russian Foundation for Basic Research, project number 16-29-13034.

References

[1] E. Bugaev and P. Klimai. Large curvature perturbations near horizon crossing in single-field inflation models. Phys. Rev. D 78, 063515, 2008.

[2] S.W. Hawking. Black hole explosions? Nature, 30, 248, 1974.

[3] S.W. Hawking. Particle creation by black holes Comm. Math. Phys., 43, 199, 1975.

[4] B.J. Carr. Primordial Black Holes and Quantum Effects. In: Nicolini P., Kaminski M., Mureika J., Bleicher M. (eds), Proceedings of 1st Karl Schwarzschild Meeting on Gravitational Physics. Springer Proceedings in Physics, v. 170, p.23. Springer, Cham, 2016. arXiv:1402.1437.

[5] T. N. Ukwatta et al. Primordial Black Holes: Observational characteristics of the final evaporation. Astroparticle Physics, 80, 90, 2016. arXiv:1510.04372.

[6] J.H. MacGibbon and B.R. Webber. Quark- and gluon-jet emission from primordial black holes: The instantaneous spectra. Phys. Rev. D 41, 3052, 1990.

[7] A.F. Heckler. Calculation of the emergent spectrum and observation of primordial black holes. Phys. Rev. Lett., 78, 3430, 1997.

[8] R.G. Daghigh and J.I. Kapusta. High temperature matter and gamma ray spectra from microscopic black holes. Phys. Rev. D, 65, 064028, 2002.

[9] D.B. Cline, D.A. Sanders, W.P. Hong. Further evidence for some gamma-ray bursts consistent with primordial black hole evaporation. The Astrophysical Journal, 486:169, 1997.

[10] O.D. Lalakulich, V.B. Petkov and G.M. Vereshkov. Relativistic phase transitions in the radiation flow of primordial black holes and high-energy gamma bursts. ASP Conference Series, 312, 453, 2004.

[11] J.R. Chisholm. Clustering of Primordial Black Holes: Basic Results. Phys. Rev. D 73, 083504, 2006.

[12] V.B. Petkov. Experimental Search for Evaporating Primordial Black Holes. Physics of Particles and Nuclei, 46, 205, 2015.

[13] D.B. Cline, D.A. Sanders, W. Hong. Further evidence for some gamma-ray bursts consistent with primordial black hole evaporation. ApJ, 486, 169, 1997.

[14] G. M. Vereshkov, V. B. Petkov. Search for Ultrashort Gamma-Ray Bursts from Evaporating Primordial Black Holes. JETP Letters, 101, 146, 2015.

[15] G. Tešić. Searching for primordial black hole evaporation signal with AMON. PoS(ICRC2015)328.

[16] V.B. Petkov, E.V. Bugaev, P.A. Klimai et al. Experimental Search for Gamma-Ray Bursts from Evaporating Primordial Black Holes. JETP, 110, 406, 2010.

[17] M.J. Rees. A better way of searching for black-hole explosions? Nature, 266, 333, 1977.

[18] R.D. Blanford. Spectrum of a radio pulse from an exploding black hole. MNRAS, 181, 489, 1977.

[19] S.E. Cutchin et al. Constraining the Rate of Primordial Black-Hole Explosions and Extra Dimension Scale using a Low-Frequency Radio Antenna Array. PASP, 127, 1269, 2015. arXiv:1608.01945

[20] B. Kol. Explosive black hole fission and fusion in large extra dimensions. arXiv:hep-ph/0207037.

[21] M. Kavic et al. Transient Pulses from Exploding Primordial Black Holes as a Signature of an Extra Dimension. JCAP11(2008)017. arXiv:0801.4023

[22] A.N. Kurenya et al. Real-time multimessenger observation system for the search of optical counterparts of the high energy events. Proceedings of The International Conference “SN 1987A, Quark Phase Transition in Compact Objects and Multimessenger Astronomy”, Russia, Terskol (BNO INR RAS), Nizhnij Arkhyz (SAO RAS), 2-8 July 2017, INR RAS, Moscow, 2018 (this issue).

[24] E.N. Alekseyev et al. The Baksan underground scintillation telescope. Phys. Part. Nucl., 29, 254, 1998.

[25] D.D. Dzhappuev et al. Modernization of the Carpet-2 array of the Baksan Neutrino Observatory. Bull. Russ. Acad. Sci. Phys., 71, 525, 2007.

[26] V.B. Petkov et al. Andyrchy Facility for Detection of Cosmic Rays. Instruments and Experimental Techniques, 49, 785, 2006.

[27] D.V. Smirnov et al. Search for UHE gamma-ray short transients at Andyrchy EAS array. Proc. 29 ICRC, 4, 451, 2005.

[28] D.V. Smirnov, V.B. Petkov, and S.N. Karpov. Search for Ultrahigh-Energy Cosmic Gamma-Ray Bursts on the Baksan Underground Scintillation Telescope. Astronomy Letters, 32, 1, 2006.

[29] V.B. Petkov, E.V. Bugaev, P.A. Klimai et al. Searching for Very-High-Energy Gamma-Ray Bursts from Evaporating Primordial Black Holes. Astronomy Letters, 34, 509, 2008.

Galileo Versus Aristotle: the Case of Supernova 1987A#

P. Galeotti[1], G. Pizzella[2],*

[1] Dipartimento di Fisica dell'Università, INFN and OATO-INAF, Torino, I-10133 Italy

[2] Istituto Nazionale di Fisica Nucleare, Laboratori Nazionali di Frascati, Rome, I-00044 Italy; Guido. Pizzella@lnf.infn.it

Abstract Most current supernova theories state that this phenomenon lasts a few seconds and ends with a big final explosion. However, these theories do not take into account several experimental results obtained with neutrino and gravitational wave detectors during the explosion of SN1987A, the only supernova observed in a nearby galaxy in modern age. According to these experimental results the phenomenon is much more complex that envisaged by current theories, and has duration of several hours. Indeed, SN1987A exploded on February 23, 1987, and two neutrino bursts, separated by 4.7 hours were detected: the first one at 2^h 52^m UT and the second one at 7^h 35^m UT. Furthermore, correlations between the neutrino and two gravitational wave detectors, ignored by most of the scientific community, were observed during the longer collapse time. Since the current *standard* theories, based on some rough simplifications, are a clear example of an Aristotelian attitude, still present in our days, we believe that a more Galilean attitude is necessary, being the only correct way for the progress of science.

Keywords: Supernovae, Individual: 1987a, Neutrinos, Gravitational Waves

1. Introduction

On August 21, 1609, Galileo Galilei showed to the people in Venice the wonders of his new telescope: ships in the sea which were hard to see at naked eyes, the Moon craters, the Jupiter satellites, the Sun dark spots.

A few months later he went to Florence to show to the Grand Duke Cosimo de Medici the four satellites of Jupiter, which he named Medicei. He did not bother at all the desertion of some university professors who, although invited, did not show up to the appointment: no envy, but simply because they had remained loyal to the Aristotelian view of the Universe and they did not see anything that would have forced them to change their own advanced opinions.

Even intelligent people had hard time in convincing themselves that what they could see with the telescope was real, especially for things they could not touch with their hands, like the celestial bodies. It seemed that human nature is made so as not to accept any news that leads off the already marked road, and this characteristics of the human nature has not changed during the centuries.

In this paper we wish to argue that many scientists, in the attempt to explain what

The paper was published in Astrophysical Bulletin, 2017, Vol. 72, No. 3, pp. 251–256, DOI: 10.1134/S1990341317030142

happened with SN1987A, follow a sort of Aristotelian point of view, ignoring or pretending to ignore facts based on observations.

SN1987A was a unique event during our time, because modern instrumentation was available for measuring phenomena generated by this event. We recall that the first observation of a neutrino burst was real-time detected on February 23, 1987, at $2^h\,52^m$ UT in the very deep underground Liquid Scintillation neutrino detector (hereafter LSD) inside the Mont Blanc laboratory. This event was immediately communicated (IAU Circular n. 4323 of February 28, 1987) after the information of a visual supernova was available, and soon after was discussed, on March 2, during the Rencontres de Physique de la Valle d'Aoste.

Several days later it was announced that neutrino bursts were also observed in coincidence in the Kamiokande and the IMB detectors, very soon followed by the Baksan experiment. Nevertheless, some important experimental data were, and still are, ignored by many scientists who developed models of supernova explosion. In the following, we draw the attention to three of these observations, which have not been taken into proper consideration even if they are among the most important ones:

- the long duration of the Kamiokande neutrino burst;
- the coincidences between the LSD and Baksan detectors;
- the correlation between neutrino and gravitational wave detectors.

2. Two Neutrino Bursts Detected in Kamiokande

We have received by the Kamiokande collaboration the list of observed events reporting, for each event, the time and the N_{hit}, being N_{hit} the number of photo-multipliers hit in the trigger at each event time. For example, an event with energy 10~MeV gives $N_{hit} = 26$ and with energy 30 MeV gives $N_{hit} = 73$; the Kamiokande collaboration has put a threshold at $N_{hit} = 20$, corresponding roughly to an energy of 7.5 MeV. In total this list contains 1937 triggers, detected during the full day February 23 above $N_{hit} = 20$, giving a rate of about 0.024 pulses per second.

It is well known that Kamiokande (KND in the following) observed a burst of eleven neutrino interactions at 7^h35^m UT with a duration of 12.4 s, with a very low imitation rate from the background, and in coincidence, even if with a poor timing, with the eight neutrino burst observed by the IMB detector [1, 2]. A careful search for bursts [3], however, shows a second cluster of seven pulses in KND at about 20~minutes after the first one, starting at 7^h54^m and with a duration of 6.2 s, with energies $22 < N_{hit} < 33$ and with an imitation rate from the background of one event every 669 years. One can find an indication of this second cluster in ***Fig4*** of [2] from which, however, one does not realize that the cluster consists of seven pulses well above the background in just six seconds, as shown here in ***Table 1***. We believe that this second pulse, shown in ***Fig1***, escaped to the attention of the Kamiokande collaboration.

Since the IMB detector had an energy threshold above 20 MeV, this detector observed clustered pulses in coincidence with the first KND cluster at 7^h35^m UT made by several high energy pulses, but it did not have the sensitivity to observe clustered pulses in coincidence with the second KND cluster at 7^h54^m, made of pulses with energy of the order or less than 15 MeV.

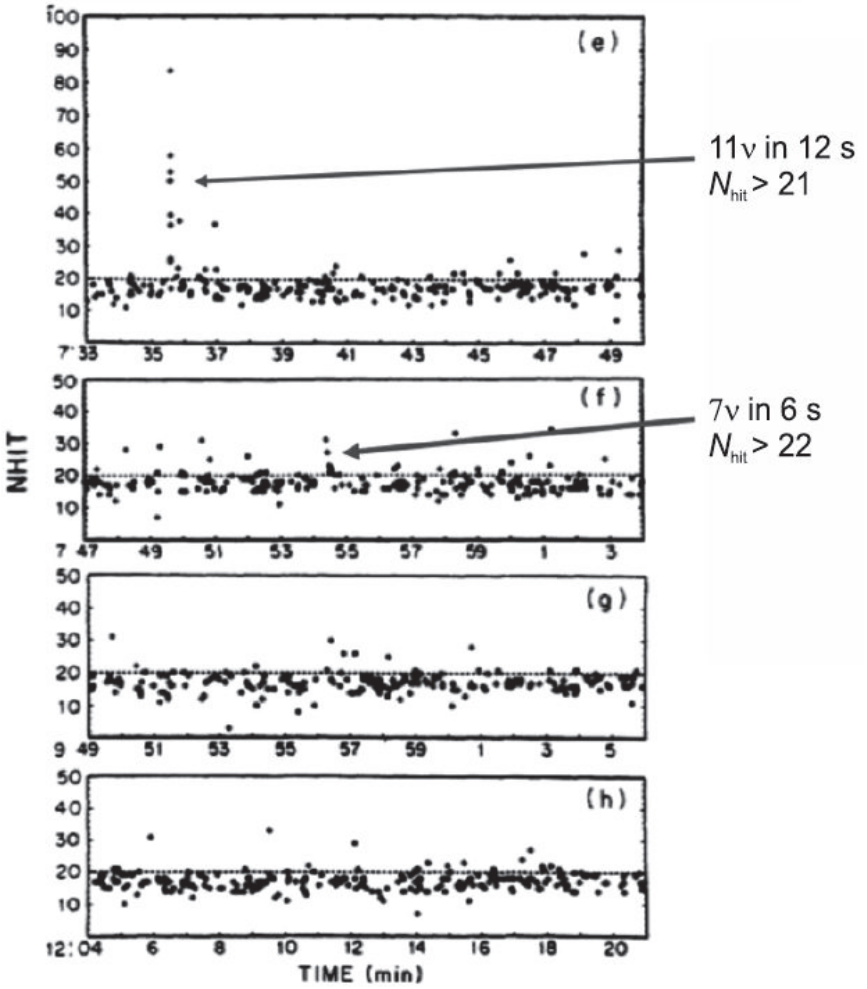

Fig1. *Scatter plot of N_{hit} versus time, as shown in* ***Fig4*** *of [2]. The second pulse is barely visible, but it stems out clearly if one process the data.*

Table1. *UT time and N_{hit} of the seven pulses in the Kamiokande second burst. This cluster has duration of 6.2 s and an imitation rate from the background of 669 years*

Hour	min	sec	N_{hit}
7	54	22.26	33
7	54	24.11	29
7	54	25.33	28
7	54	25.34	27
7	54	27.13	22
7	54	28.37	22
7	54	28.46	22

3. Coincidences between LSD and Baksan Neutrino Detectors

Among all neutrino detectors, LSD and Baksan Scintillation Telescope (BST in the following) have very similar characteristics. The data recorded by these two detectors show an extraordinary correlation [4–6] at the time of the LSD burst.

We start by remarking that the Baksan event times, as recorded on the magnetic tapes, have an error of +2 s, −54 s with respect to the UT. Also we recall that the Baksan telescope has recorded a burst of neutrinos, the first of which occurs at the recorded time of $7^h36^m1^s.8$. Comparing with IMB, we find that we must correct the Baksan recorded times by −30.4 s.

In ***Fig2*** we show the number of coincidences between LSD and BST during a one-hour time period versus the correction time t_c for three values of the coincidence window $\delta t = \pm 0.5$, 1.5, 2.5 s.

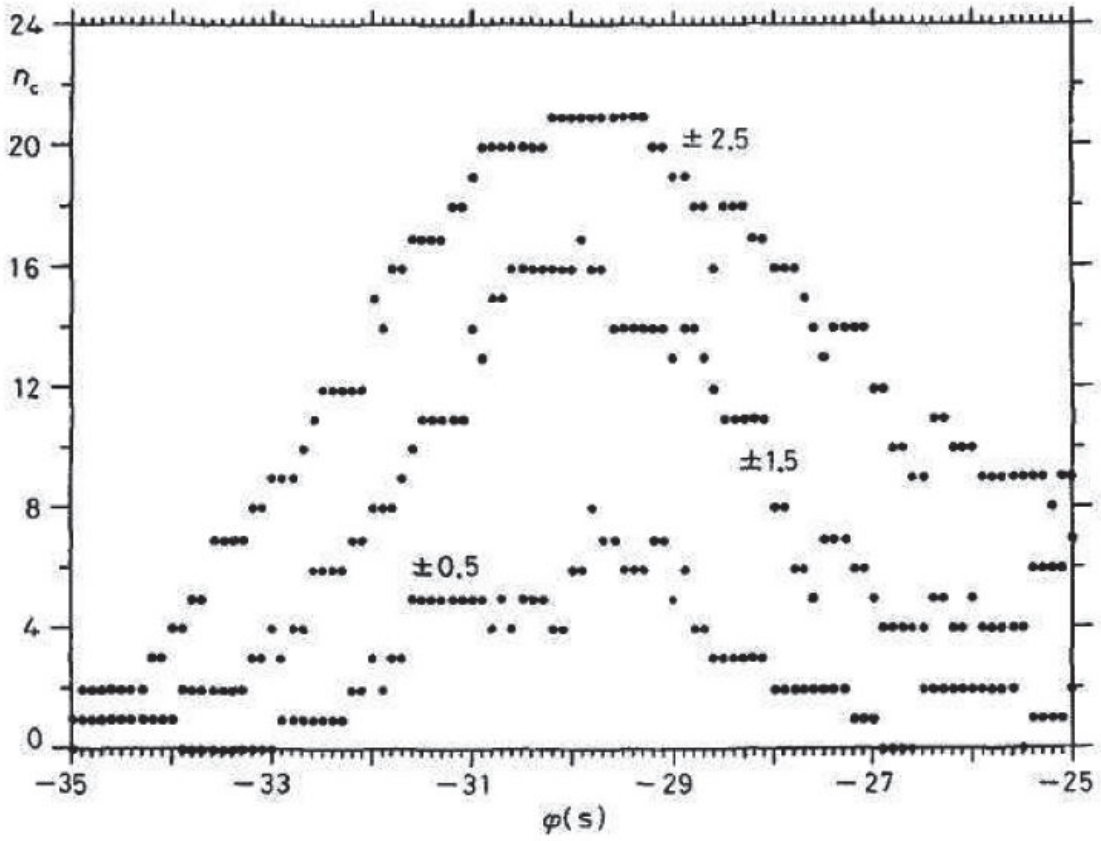

Fig2. *LSD–BST coincidences for various coincidence windows δt = ±0.5, 1.5, 2.5 s vs. the Baksan correction time. One-hour period, 2^h to 3^h. Figure 11 from [12].*

We notice a striking excess of coincidences[1] for t_c in the interval that agrees with the IMB burst at $7^h35^m41^s.4$.

[1] Prof. A. E. Chudakov was very surprised for this unexpected result, and decided to perform by himself the analysis of the LSD and BST data. The result of his independent analysis confirms the same coincidence excess at the Mont Blanc time [6]. Chudakov even wrote a letter to F. Reines [7] asking to discuss this "crazy" fact of events in coincidence between LSD and Baksan.

For calculating the probability that the observed coincidence excess has been obtained by chance, we estimate the background with the well-known formula

$$n_{bk} = \frac{N_1 N_2 \delta t}{one\ hour}$$

where N_1 and N_2 indicate the neutrino events from LSD and BST in the one hour period. The results are shown in ***Table2***.

Table2. *Probability p to obtain n_c coincidences by chance for the three coincidence windows*

δt	$\overline{n}$	n_c	p
0.5	1.52	8	4.4×10^{-3}
1.5	4.56	17	7.6×10^{-5}
2.5	7.6	21	1.4×10^{-4}

4. Correlation between Neutrino and Gravitational Wave Detectors

The gravitational wave (GW) detectors in Rome and in Maryland recorded several signals in time coincidence between them and with the LSD experiment, for a long time duration that includes the time of the LSD event: 2^h52^mUT. The GW signals preceded the LSD signals by 1.1 – 1.2 s, with an absolute systematic error in timing of the order of 0.5 s [8–10]. The probability that the correlation had occurred by chance was estimated to be very small, of order of 10^{-6} [11]. A summary of the correlations among neutrino and gravitational wave detectors can be found, for example, in reference [12].

This observation was unexpected, because the sensitivity of the detectors seemed to be too small for detecting gravitational waves presumably produced by this extragalactic supernova. Indeed the classical cross-section for the interaction of gravitational waves with matter is far below that needed to detect GW [13–15].

The correlations were studied making use of an algorithm[2], called the *net excitation method* and described in detail in [11, 16], based on the idea to make use of *all available data* in underground detectors, and not only those considered to be produced by neutrino interactions.

The algorithm consist in taking

$$E_{RM}(t) = E_R(t) + E_M(t),$$

where E_R and E_M are the measured energies (also called energy innovations, in Kelvins) of the *events* obtained with the Rome (RO) and the Maryland (MA) detectors at the same time t, 3600 values $E_{RM}(t)$ per hour.

Then the sum $E(t) = \Sigma_i E_{RM}(t_i)$ is computed, where t_i is the time of the i event of the LSD neutrino detector. The summation is extended over a given time interval (say one hour) in which N_v events of the neutrino detector (most of them certainly due to background) are present.

[2] Suggested by Sergio Frasca.

The background for this algorithm is obtained by calculating $E(t_1, t_2) = \Sigma_j(E_R(t_{1j}) + E_M(t_{2j}))$ at $2N_v$ times t_{1j} and t_{2j} chosen randomly within the time interval. In one hour we have many more than 3600 × 3600 independent values of $E(t_1, t_2)$.

The analysis consisted in comparing the value $E(t)$ with the very large number of background values determined by considering non coincident signals RO and MA, observed at times uncorrelated with the neutrino events. In absence of any real signal we expect that $E(t)$ be just one of the many $E(t_1, t_2)$ background values and, on average, we expect that half of the background values be larger than $E(t)$ and half be smaller.

We apply now this algorithm to the data of RO, MA and LSD. We find the result shown in ***Fig. 3a***, where we compare our *signal* $E(t)$ with one million determinations of the background. The algorithm is applied to moving periods of one-hour stepped by 0.1 hour[3].

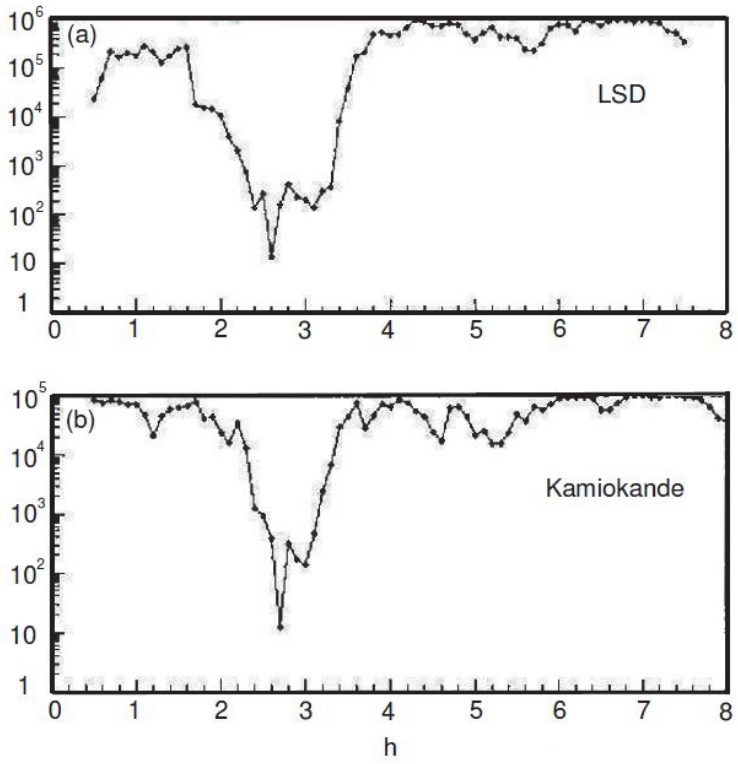

Fig3. (a)*: the n values for N = 1 000 000 obtained for the correlations of Maryland + Rome with LSD during periods of one hour from 0h to 7h. 5 of February 23.* ***(b)****: the same algorithm, for N = 100 000, is applied for the correlation RO, MA and Kamiokande. We notice that all the best correlations occur both at the LSD time. The two correlations are independent, because we make use, in the two cases, of different data for RO and MA.*

When an experimental unexpected result, as that of ***Fig. 3a***, is obtained, usually one repeats the experiment with different data, but in our case we have only one supernova. However, we have different, independent data, namely those obtained by the Kamiokande experiment. Thus, while waiting for the next galactic supernova, we asked Prof. Masatoshi Koshiba to provide the Kamiokande data for a new analysis.

Koshiba was very cooperative and immediately supplied the data which we received on

[3] See also ref. [17].

January 27, 1988. We repeated the analysis applying the same procedure as with the Mont Blanc data and, incredibly, we found just the same correlation at the same time, as shown in ***Fig. 3b***.

At last, in order to estimate the overall probability that the result shown in ***Fig3*** be accidental, we have repeated the same correlation analysis for four independent files of data: RO, MA, LSD and KND [16]. To have a better time resolution, in this new quadruple analysis we have used one-half hour periods stepped by 0.1 hour, and we have obtained the result shown in ***Fig4***. During the period from $2^h\ 36^m$ UT to 3h 6m UT, that includes the LSD five-neutrino event at 2.87 hour UT, we have in total 83 independent triggers (32 in LSD and 51 in KND). The sum of the corresponding 83 energy innovations in RO plus the 83 energy innovation in MA in coincidence with the 83 neutrino events, divided by 83, was 74.349 K, while the average background (computed by choosing randomly 83 energy innovations in RO plus 83 in MA, not in coincidence with the LSD and KND data) was 51.771 K during that half an hour period.

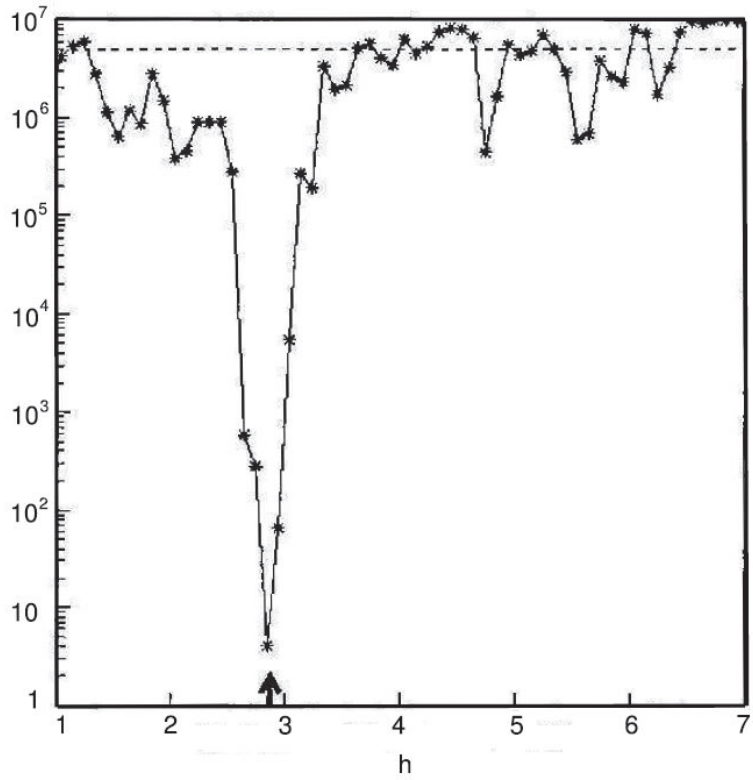

Fig4. *The* net excitation method *is applied on 30-minutes time periods moved in steps of 0.1 hour from 0 to 8 hours UT of February 23, shown on the abscissa scale. As in our previous analysis [4, 11] we have introduced a delay of 1.1 s between the neutrino and the GW signals. On the ordinate scale we show the number of times N, out of 10^7, the GW background determinations are greater or equal than the GW energy innovation obtained in correspondence of the neutrino* events *that includes both the LSD and the KND data. At the LSD time we have N = 4, corresponding to a probability of 4×10^{-7} that the correlation is accidental. The dashed line indicates the expected value in the case of absence of correlation.*

The difference between the signal and the average background is equal to 74.349 − 51.771 = 5.5σ, giving a probability of 1.9×10^{-8} that this result be due to chance, in the case of a normal distribution of the noise. If the data distribution is not exactly Gaussian [16] the probability that this results is accidental is a little bit higher: 4×10^{-7}.

5. Conclusion

One major problem associated with a supernova explosion is the duration of the inner core collapse. According to most theories of supernova explosion, the collapse develops in a few seconds but all the experimental data from supernova 1987A, as shown in this paper, indicate a duration of order of hours. The discrepancies between data and theories could be due, in our opinion, to the fact that most theories do not take into account core rotation and magnetic fields, even if pulsars, i.e. a possible final result of the collapse have the strongest magnetic field and the fastest rotation in the Universe. Furthermore these theories ignore several experimental results, some of them have been described here.

Some unconventional models based on fast rotation and fragmentation of the collapsing core have been suggested soon after the explosion to explain the experimental data from neutrino and gravitational waves detectors [18–21]. These models are supported by the recent observations of the remnant of SN1987A made by NuSTAR (Nuclear Spectroscopic Telescope Array, a satellite launched by NASA on June 2012 to study the X-ray sky) that show a clear evidence of an asymmetric collapse [22]. The asymmetry of the explosion is an essential requirement in support of a collapse in two stages and, eventually, of the emission of gravitational waves.

A typical theory for explaining the long duration of the phenomenon is, for example, that described in [21], where a rotational mechanism of the explosion of a supernova is considered, that leads to a two-stage collapse with a phase difference of about 5 h. It remains, however, no explanation for the signals detected in gravitational wave detectors.

Among the possibilities, if not due to gravitational waves produced by the asymmetric collapse and injected in the direction of the Earth, one should consider the signals due to exotic particles.

But, in any case, we believe that no data should be ignored if they stem out clearly from the observations, as suggested about 400 years ago by Galileo in a world still dominated by Aristotelian views while, in our modern world, a Galilean approach must be considered the only scientific one.

Acknowledgements

We thank the Kamiokande, the LSD and the Rome Collaborations for having supplied to us their data.

References

[1] K. Hirata, T. Kajita, M. Koshiba, et al., Phys. Rev. Lett. **58**, 1490 (1987).

[2] K. S.Hirata, T. Kajita,M. Koshiba, et al., Phys.Rev.D **38**, 448 (1988).

[3] P. Galeotti and G. Pizzella, arXiv:0706.2235 (2007).

[4] M. Aglietta, A. Castellina, W. Fulgione, et al., Nuovo Cimento C Geophys. Space Phys. C **14**, 171 (1991).

[5] E. Amaldi, M. Bassan, E. Coccia, et al., Annals New York Academy Sci. **571**, 561 (1989).

[6] A. E. Chudakov, Annals New York Academy Sci. **571**, 577 (1989).

[7] Private communication. letter by Chudakov to Reins on 15March 1990.

[8] E. Amaldi, P. Bonifazi, M. G. Castellano, et al., in Results and Perspectives in Particle Physics (1987), pp. 59–68.

[9] E. Amaldi, P. Bonifazi, M. G. Castellano, et al., Europhysics Lett. **3**, 1325 (1987).

[10] M. Aglietta, G. Badino, G. Bologna, et al., Europhysics Lett. **3**, 1315 (1987).

[11] M. Aglietta, G. Badino, G. Bologna, et al., Nuovo Cimento C Geophys. Space Phys. C **12**, 75 (1989).

[12] G. Pizzella, Nuovo Cimento B Ser. **105**, 993 (1990).

[13] R. Ruffini and S. Bonazzola, Phys. Rev. **187**, 1767 (1969).

[14] S. Weinberg, *Gravitation and Cosmology: Principles and Applications of the General Theory of Relativity* (Wiley-VCH, New York, 1972).

[15] G. Pizzella, Nuovo Cimento Rivista Ser. **5**, 369 (1975).

[16] P. Galeotti and G. Pizzella, Europ. Phys. J. C **76**, 426 (2016).

[17] G. Pizzella, Italian Phys. Soc. Proc. **100**, 31 (2010).

[18] A. de Ru´ jula, Phys. Lett. B **193**, 514 (1987).

[19] L. Stella and A. Treves, Astron. and Astrophys. **185**, L5 (1987).

[20] V. S. Berezinskii, C. Castagnoli, V. I. Dokuchaev, and P. Galeotti, Nuovo Cimento C Geophys. Space Phys. C **11**, 287 (1988).

[21] V. S. Imshennik and O. G. Ryazhskaya, Astronomy Letters **30**, 14 (2004).

[22] S. E. Boggs, F. A. Harrison, H. Miyasaka, et al., Science **348**, 670 (2015).

Neutrino interaction with nuclei

S.V. Semenov[1]

[1] National Research Centre "Kurchatov Institute", Moscow, Russia; Semenov_SV@nrcki.ru

Abstract Cross section of neutrino-nucleus interaction is calculated for a number of nuclei, used in neutrino detectors. The calculations are performed by the means of the model-independent method, based on the experimental data on nuclear reactions. The obtained theoretical values coincide with the existing experimental results.

Keywords: Neutrino Detection, Charge Current and Neutral Current Interaction, Charge Exchange Reactions, Nuclear Resonance Fluorescence

1. Introduction

Theoretical investigation of neutrino-nucleus interaction has many applications, such as neutrino detection, neutrino oscillations study, nucleosynthesis processes examination. The expressions for cross sections contain nuclear matrix elements, which are the goal of calculations for a variety of nuclear models. For there is a certain spread of results of these estimations it is reasonable to obtain nuclear matrix elements by the model-dependent approach, which use experimental data on nuclear reactions. These are beta decay processes, charge exchange reactions, nuclear resonance fluorescence, which can give direct information on nuclear structure. Below the corresponding model-independent cross section calculations are produced and compared with existing experimental data on neutrino-nucleus interaction.

2. Charged Channel

In neutrino interaction with nucleus, caused by charged current, the following transition takes place:

$$\nu_l + (A,Z) \rightarrow (A,Z+1) + l^- \qquad (1)$$

The final nucleus *(A,Z + 1)* can be in ground or excited state. There are experimental data for cross section of reaction (1) for two nuclei: ^{12}C with ν_e and ν_μ beams and ^{56}Fe with ν_e beam, obtained by KARMEN and LSND Collaborations. The exclusive reaction k - j k k – j

$$\nu_e + {}^{12}C \rightarrow {}^{12}N_{g.s.} + e^- \qquad (2)$$

was investigated both at KARMEN [1,2] and LSND [3]. The neutrino source is the positive muon decay at rest (DAR), $\mu^+ \rightarrow e^+ + \nu_e + \bar{\nu}_\mu$. The corresponding spectra of ν_e and $\bar{\nu}_\mu$, the Michel spectra, have the form.

$$S_M(E_{\nu_e}) = \frac{96E^2_{\nu_e}}{m^4_{\mu}}(m_{\mu} - 2E_{\nu_e}),$$
$$S_M(E_{\overline{\nu}_{\mu}}) = \frac{32E^2_{\overline{\nu}_{\mu}}}{m^4_{\mu}}(\frac{3}{2}m_{\mu} - 2E_{\overline{\nu}_{\mu}}) \quad (3)$$

The maximal neutrino energy is mμ/2=52.8 MeV. The monoenergetic muon neutrino flux with $E_{\nu_\mu} = 29.8$ MeV, originating from stopped positive pion decay, $\pi^+ \rightarrow \mu^+ + \nu_\mu$, is also present.

The values of cross section of $^{12}C(\nu_e, e^-)^{12}N_{g.s.}$, averaged over electron neutrino spectrum (3) are the following:

$$<\sigma> = (8.1 \pm 0.9_{stat} \pm 0.75_{syst}) \cdot 10^{-42} \text{ cm}^2 \text{ [1]},$$
$$<\sigma> = (9.1 \pm 0.5_{stat} \pm 0.8_{syst}) \cdot 10^{-42} \text{ cm}^2 \text{ [2]},$$
$$<\sigma> = (9.1 \pm 0.4_{stat} \pm 0.9_{syst}) \cdot 10^{-42} \text{ cm}^2 \text{ [3]}.$$

Theoretical calculations of type (2) reaction cross section can be performed on the base of experimental data on log *ft* value of β-transition from the final to the initial nucleus [4]. The corresponding expression is:

$$\sigma(\varepsilon_\nu) = \frac{2\ln 2(2J_f + 1)\pi^2}{m_e^3 \cdot 10^{\log(ft_{\beta^+, EC})}} \pi_r \varepsilon_r F(Z_f, \varepsilon_r)$$
$$= \frac{0.264(2J_f + 1)}{10^{\log(ft_{\beta^+, EC})}} \pi_r \varepsilon_r F(Z_f, \varepsilon_r) \cdot 10^{-40} \text{ cm}^2 \quad (4)$$

Here J_f is the total momentum of the final nucleus, J_f=1 for $^{12}N_{g.s}$; $\log(ft_{\beta^+, EC})$ is related to the β transition from the final to initial nucleus; ε_ν, π_r, ε_r are the neutrino energy, momentum and energy of outgoing electron in units of electron mass m_e respectively; $\varepsilon_r = \varepsilon_\nu - M_f + M_i$, where M_i and M_f are the masses of the initial and final nuclei in units of electron mass; and $F(Z_f, \varepsilon_r)$ is the Coulomb correction function. The method of calculation of $F(Z_f, \varepsilon_r)$ is presented in [5]. The neutrino threshold energy is $\varepsilon_{\nu,thr} = M_i - M_f + 1$. For $^{12}C(\nu_e, e^-)^{12}N_{g.s.}$ reaction $E_{\nu,thr}$=17.3 MeV. For $^{12}N(\beta+)^{12}C$ transition $\log ft_{\beta^+}$ =4.12±0.03 [6]. As a result the cross section (4) averaged over νe spectrum (3) equals $9.1 \cdot 10^{-42}$ cm^2, and coincides with experiment.

The $^{12}C(\nu_\mu, \mu^-)^{12}N_{g.s.}$ reaction cross section was measured in LSND experiment. The ν_μ beam is produced by the π^+ decay in flight (DIF). The muon neutrino spectrum has its maximum at E_ν ~70 MeV and extends to ~300 MeV. The flux-averaged cross section is $(6.6 \pm 1.0_{stat} \pm 1.0_{syst}) \cdot 10^{-41}$ cm^2. Theoretical expression for cross section of $\nu_\mu + ^{12}C \rightarrow ^{12}N_{g.s.} + \mu^-$ is determined by the formula, similar to (4)

$$\sigma(\varepsilon_\nu) = \left(\frac{m_\mu}{m_e}\right)^2 \frac{2\ln 2(2J_f + 1)\pi^2}{m_e^3 \cdot 10^{\log ft_{\beta^+}}} \pi_r \varepsilon_r F(Z_f, \varepsilon_r) \quad (5)$$

Here neutrino energy, momentum and energy of outgoing electron are scaled by muon

mass m_μ. The muon neutrino threshold energy equals $E_{\nu,thr}$=122.4 MeV. Theoretical value of cross section (5), averaged over muon neutrino DIF spectrum, $<\sigma(\varepsilon_\nu)>=8.6\cdot10^{-41}$ cm^2 and is in agreement with experimental result.

For there is reasonable accord between theoretical estimations and experimental measurements of neutrino-^{12}C interaction in charged channel, the expression (4) can be used for analysis of neutrino signal, registered with the help of liquid scintillator, which contain large quantity of carbon-12 nuclei. Particularly, for $^{12}C(\nu_e, e^-)^{12}N_{g.s.}$, $E_{\nu_e} = 40$ MeV, $\sigma(E_{\nu_e}) = 14.4\cdot10^{-42}$ cm^2.

Investigation of neutrino-^{56}Fe interaction is an actual problem, due to the presence of large amounts of iron as a shielding material in scintillator detectors, such as LSD and LVD. Electrons and gamma quanta would be produced under the exposure of supernova neutrino radiation in the reaction with iron nuclei and they could be recorded by the detector [7]. Charge current reaction is the following:

$$\nu_e + {}^{56}Fe \rightarrow {}^{56}Co^* + e^- \qquad (6)$$

In reaction (6) cobalt nucleus is in the excited state, for the ground state of cobalt-56 nucleus has quantum numbers 4^+, so the corresponding cross section for ^{56}Fe(ν_e,e$^-$)^{56}Co$_{g.s.}$ is small, compared to the cross section of giant resonances excitation. These resonances are: analog 0^+ resonance (AR), caused by Fermi transition, and Gamow-Teller 1^+ (GT) resonances. The cross sections (6) can be calculated by the means of the expressions:

$$\sigma_F(E_\nu) = \frac{G_\beta^2 m_e^2}{\pi} M_F^2 \pi_e \varepsilon_e F(Z_f, \varepsilon_e)$$

$$\sigma_{GT}(E_\nu) = \frac{G_\beta^2 m_e^2}{\pi} g_A^2 M_{GT}^2 \pi_e \varepsilon_e F(Z_f, \varepsilon_e)$$

Here M_F and M_{GT} are nuclear matrix elements, g_A is the is the axial-vector interaction constant, g_A=1.2761, ε_e and π_e are the energy and momentum of outgoing electron in units of m_e, $\varepsilon_e=(E_\nu-\Delta)/m_e$, Δ is the mass difference of the ^{56}Co* and ^{56}Fe nuclei. For AR nuclear matrix element can be written as follows: M_F^2=(N-Z). Gamow-Teller matrix elements obey sum rule, which in application to neutron-rich nuclei can be expressed as $\sum_i M_{GT_i}^2 = 3(N-Z)e_q^2$, where e_q is the effective GT charge, e_q=0.8. Thus nuclei with large neutron excess (N-Z) are preferable for neutrino detection. In [8] a number of 1^+-states and the appropriate matrix elements were found for the reaction (6) on the base of theory of Gamow-Teller resonance [9]. Excitation of AR and GT-resonances in ^{56}Co produces 5-10 MeV gamma quanta accompanied by electron emission. For the test of the nuclear model the total ^{56}Fe(ν_e, e$^-$)^{56}Co* reaction cross section, averaged over muon DAR neutrino spectrum was calculated. It gives the value $2.62\cdot10^{-40}$ cm^2, which is in agreement with results, obtained in KARMEN experiment, $(2.56 \pm 1.08(stat) \pm 0.43(syst))\cdot10^{-40}$ cm^2 [10].

The obtained cross section is used for estimation of number of neutrino signals from SN1987a, observed in LSD [11], which correspond to the first stage of rotating mechanism of Supernova explosion scenario [12]. The neutrino flux during the first burst consists of electron neutrinos with a total energy $W_{\nu_e} = 8.9 \times10^{52}$ erg. The neutrino energy spectrum is hard with an average energy of ~30–40 MeV. The second neutrino burst [13] corresponds to

the standard collapse theory without rotation with the formation of the neutrino sphere and with an equal energy distribution between all types of neutrinos [14].The calculated event number [8,15] coincides with the observed number of signals, registered in LSD.

Distribution of Gamow-Teller strength B(GT) for transition (6), $B(GT) = M_{GT}^2$, can be deduced from the experiments on charge exchange ^{56}Fe(p,n)^{56}Co reaction [16]. Several 1^+ states below excitation energy E_x ~4 MeV were observed and a broad maximum with great density of GT-states in the E_x region 8-15 MeV was found. The total GT-strength is $\Sigma B(GT) = 9.9 \pm 2.4$ [16]. This leads to reaction (6) averaged cross section $<\sigma> = (3.08 \pm 0.5)\cdot 10^{-40}$ cm^2, which agrees with KARMEN experiment. For E_ν=40 MeV cross section of ^{56}Fe(ν_e, e$^-$)^{56}Co, calculated on the base of charge-exchange reaction results [16], equals $4.8\cdot 10^{-40}$ cm^2.

Charge-exchange reaction on ^{71}Ga [1] can be used for calculation of solar-neutrino absorption cross section for the Gallium-Germanium experiment [18].

3. Neutral Channel

Calculation of inelastic neutrino scattering cross section on nuclei, caused by neutral current is valuable to investigation of neutrino oscillations, processes during Supernova explosions and to neutrino detectors construction. These reactions are equally sensitive to all neutrino flavors:

$$\nu_x + (A,Z) \rightarrow \nu_x^{'} + (A,Z)^* \tag{6}$$

where x=e,μ,τ. In the energy range under consideration the inelastic scattering is determined, in the main, by allowed transitions. For the ground state of the initial nucleus the cross section of (6) is expressed as follows:

$$\sigma^{NC}(E_\nu) = \frac{G_F^2 g_A^2}{\pi(2J_i+1)}(E_\nu - E_x)^2 \left| \left\langle f \left\| \sum_k \boldsymbol{\sigma}(k) t_0(k) \right\| i \right\rangle \right|^2 \tag{7}$$

Here E_ν is the incident neutrino energy, E_x is the excitation energy of nucleus $(A,Z)^*$. The Gamow-Teller strength $B(GT_0)$ handles the dependence of cross section on nuclear structure.

$$B(GT_0) = \frac{g_A^2 \left| \left\langle f \left\| \sum_k \boldsymbol{\sigma}(k) t_0(k) \right\| f \right\rangle \right|^2}{2J_i + 1} \tag{8}$$

In (8) t_0 is the zero component of isospin operator and summation is performed over all nucleons of the nucleus.

The magnitude of $B(GT_0)$ can be obtained by the model independent way on the base of experimental data. For allowed GT-transitions ΔJ=1, $\Delta\pi$=0, so electromagnetic B(M1) strengths can give information on nuclear matrix elements, which govern neutral current neutrino-nucleus interaction [20]. Electromagnetic dipole transitions in ^{56}Fe [21] and in ^{208}Pb [22] were measured in photon-scattering experiments with linearly polarized photon beam, which give the possibility to determine the parity quantum numbers of excited dipole states and corresponding magnetic dipole M1 strength. These results were used in [15, 23] for calculation of cross section of inelastic neutrino scattering on ^{56}Fe and ^{208}Pb. In the case of

^{208}Pb the experiment on investigation of resonance structure of ^{207}Pb+n system [24] was also taken into account.

For M1 transitions the width of the excited 1^+-state relative to the transition of the nucleus to the ground state is determined by the expression [25]

$$\Gamma_0 = \frac{16\pi}{27}\frac{E_x^3}{\hbar^3 c^3} B(MI) \quad , \tag{9}$$

where E_x is the excitation energy and B(M1) is the reduced probability. It can be shown, that isovector contribution dominates in B(M1) [20] and $B(GT_0)$ and B)M1) are connected by the following relation:

$$B(GT_0) = \frac{4\pi g_A^2}{3\mu_v^2}\frac{B(M1)}{\mu_N^2} \tag{10}$$

Here μ_v is the isovestor nucleon magnetic moment, μ_v=4.706.

It follows from (9), (10), that

$$\frac{B(M1)}{\mu_N^2} = 0.2592\frac{\Gamma_0}{E_x^3} ,$$

where excited state width Γ_0 is measured in meV and E_x in MeV and

$$B(GT_0) = 0.308\frac{B(M1)}{\mu_N^2} .$$

Thus $B(GT_0)$ can be obtained from the values of excitation energy and width of 1^+-state and cross section of inelastic neutrino scattering can be obtained according to the following expression:

$$\sigma^{NC}(E_\nu) = 1.6862\cdot 10^{-44}(E_\nu - E_x)^2 B(GT_0) \tag{11}$$

Here E_ν, E_x are measured in MeV.

Cross section of inelastic neutrino-nucleus interaction, governed by a neutral current was measured for excitation of (1^+, 1; 15.11 MeV) state in ^{12}C nucleus in the KARMEN experiment. The results of flux averaged cross sections for electron neutrino and muon antineutrino spectrum (3) are:

$$< \sigma^{NC}(\nu_e + \bar{\nu}_\mu) > = (10.8 \pm 5.1_{stat} \pm 1.1_{syst})\cdot 10^{-42} \text{ cm}^2 \text{ [26]};$$

$$< \sigma^{NC}(\nu_e + \bar{\nu}_\mu) > = (10.4 \pm 1.0_{stat} \pm 0.9_{syst})\cdot 10^{-42} \text{ cm}^2 \text{ [2]}.$$

The experimental value of (1^+, 1; 15.11 MeV) state width equals, Γ_0=38.5±0.8 eV [27]. So, from (9)-(11) the value of σ^{NC} can be calculated, $< \sigma_{th}^{NC}(\nu_e + \bar{\nu}_\mu) > = 14.7\cdot 10^{-42}$ cm^2. The measured cross section for monoenergetic ν_μ from π^+-decay at rest, E_{ν_μ}=29.8 MeV, is: $\sigma^{NC} = (3.2 \pm 0.5_{stat} \pm 0.4_{syst})\cdot 10^{-42}$ cm^2 [28]. Theoretical value of this cross section, based on intensity of M1 γ-transition [27], according to (9)-(11), equals $3.2\cdot 10^{-42}$ cm^2. Consequently, the addressed approach leads to satisfactory agreement with experimental data for inelastic neutrino scattering on ^{12}C. The calculated magnitude of $^{12}C(\nu,\nu')^{12}C^*(1^+,1;15.1$ MeV) cross section for E_ν=40 MeV is $9.3\cdot 10^{-42}$ cm^2.

4. Conclusion

The model-independent approach, based on nuclear reactions investigation, gives the possibility to determine nuclear matrix elements and estimate cross sections of neutrino-nucleus interaction. The calculated values coincide with the results of KARMEN and LSND experiments for and ^{12}Fe ^{12}C nuclei. The extension of this experimental work for a more wide set of nuclei, both in neutral and charge channels is a valuable problem for elementary particle physics. High-precision experiments on charge-exchange reactions for a number of nuclei of interest are desirable for exact determination of nuclear excitation characteristics. The method under consideration can be used for calculation of neutrino-nuclei interaction cross section in application to different problems of neutrino physics.

References

[1] Bodman B., Booth N.E., Burtak F. et al. Cross section of the charged current reaction $^{12}C(\nu_e,e^-)^{12}N_{g.s.}$. Phys. Lett. B, 1992, **280**, 198-203.

[2] Bodman B, Booth N.E., Drexlin G. et al. Neutrino interactions with carbon: recent measurements and a new test of ν_e , ν_μ universality. Phys. Lett. B, 1994, 332, 252-7.

[3] Imlay R. New results on electron-neutrino carbon scattering and muon-neutrino scattering at LSND, Nucl. Phys. A, 1998, **629**, 531c-7c.

[4] S.V. Semenov, Yu. V. Gaponov, F. Šimkovic, and P. Domin. Analysis of solar-neutrno induced ββ processes for several nuclei. Yad. Fiz., 2002, **65,** 2247-50 ;

P. Domin, F. Simkovic, S.V. Šemenov, Yu. V. Gaponov, Phenomenological Study of Solar-Neutrino Induced Double Beta Decay of Mo100. Czech. J. Phys., 2002, **52**, 451-8.

[5] S.V. Semenov, F. Šimkovic, V.V. Khruschev, P. Domin. Contribution of the lowest 1^+-intermediate state to the 2νββ-decay amplitude. Yad. Fiz., 2000, **63,** 1271-3.

[6] F. Ajzenberg-Selove. Energy levels of light nuclei A=11-12. Nucl. Phys. A, 1990, **506**:1-158.

[7] V.S. Imshennik, O.G. Ryazhskaya, Rotating collapsar and possible interpretation of LSD neutrino signal from SN 1987A. Astron. Lett. 2004, 30: 14-30.

[8] Yu. V. Gaponov, O.G. Ryazhskaya, S.V. Semenov, Interaction of Electron Neutrinos with ^{56}Fe in the LSD for *Eve* ≤ 50 MeV. Physics of Atomic Nuclei 2004; **67**, No. 11:1969–1973.

[9] B. Zenitz, KARMEN: Neutrino physics at ISIS. Prog. Part. Nucl. Phys., 1994; **32**: 351-3.

[10] Yu. V. Gaponov, Yu.S. Lutostansky Possible Existence of I^+ Resonance in Charge Exchange Reactions of Spherical Nuclei, JETP Letters 1972; **15**: 120-2; Yu. V. Gaponov, Yu.S. Lutostansky, Gamow-Teller resonance and Wigner multiplet scheme. , JETP L etters 1973; **18**: 75-7.

[11] V.L.Dadykin et al. Detection of a rare event on 23 February 1987 by the neutrino radiation detector under Mont Blanc. JETP Letters 1987; 45, Iss10:.593-5;

Aglietta M., Badino G., Bologna G. et al. On the Event Observed in the Mont Blanc Underground Neutrino Observatory during the Occurrence of Supernova 1987A . Europhys. Lett. 1987; 3(12):1315-7.

[12] Nadyozhin D.K. The gravitational collapse of iron-oxygen stars with masses of 2 and 10 solar masses. II.. Astrophys. and Space Sci. 1977; 51:283; Imshennik V.S., Nadezhin D.K., The gravitational collapse of iron-oxygene stars. Pis'ma Astron. Zh. 1997, 3: 353 (in Russian);

Imshennik V.S. Rotational explosion mechanism for collapsing supernovae and the two-stage neutrino signal from supernova 1987A in the Large Magellanic Cloud. UFN 2010; 53:1081-1092.

[13] Hirata K., Kajita T., Koshiba M. et al. Observation of a Neutrino Burst from Supernova 1987A. Phys.Rev. Lett. 1987; 58:1490-3;

Bionta R.M., Blewitt G., Brattor C.B. et al.. Observation of a Neutrino Burst in Coincidence with Supernova 1987A in the Large Magellanic Cloud. Phys. Rev. Lett. 1987; 58: 1494-6.

[14] Imshennik V.S., Nadezhin D.K. Final stages of stars evolution and supernovae bursts. Itogi Nauki Tech., Ser. Asrtron. VINITI AN USSR. M. 1982, **21**: 1-63 (In Russian).

[15] O.G. Ryazhskaya, S.V. Semenov. Interaction of electron neutrino with LSD detector. Proc. Int. Workshop on Quark Phase Transition in Compact Objects and Multimessenger Astronomy: Neutrino Signals, Supernovae and Gamma-Ray Bursts, Russia, Nizhnij Arkhyz (SAO RAS), Terskol (BNO INR RAS), October, 7-14, 2015 (Publishing Hause Sneg, Pyatigorsk, 2016).P.105-110.

[16] J. Rapaport,T. Taddeucci, T.P. Welch et al. Excitation of giant spin-isospin multipole vibrations in ^{54,56}Fe and ^{58,60}Ni. Nucl. Phys. A, 1983, **410**: 371-398.

[17] D.Frekers, T. Adachi, H. Akimune et al. Precision evalkuation of the ^{71}Ga(ν_e,e^-) solar neutrino capture rate from the (^{3}He,t) charge exchange reaction. Phys. Rev. C, 2015, **91**: 034608.

[18] V. Barinov, V. Cleveland, V. Gavrin, D. Gorbunov, T. Ibragimova. Revised neutrino-gallium cross section and prospects of BEST in resolving of Gallium anomaly. arXiv:1710.06326v1 [hep-ph], 2017.

[19] T.W. Donnelly and R.P. Peccei, Nuclear structure effects in nuclei, Phys. Rep., 1979, **50**: 1-85.

[20] H.C. Lee, Neutral current and the nuclear scattering of reactor antineitrinois, Nucl. Phys.A , 1978; **294**, 473-491;

K. Langanke, G. Martinez-Pinedo, P. von Neumann-Cosel, and A. Richter, Supernova Inelastic Neutrino-Nucleus Cross Sections from High-Resolution Electron Scattering Experiments and Shell-Model Calculations, Phys. Rev. Lett., 2004, **93**, 202501, 1-4.

[21] T. Shizuma, T. Hayakawa, H. Ohgaki et al, Dipole strength distribution in ^{56}Fe, Phys. Rev. C 2013; **87**: 024301, 1-7.

[22] T. Shizuma, T.Hayakawa, H. Ohgaki et al, Fine structure of magnetic-dipole-strength distribution in ^{208}Pb. Phys. Rev. C 2008, **78**:061303,1-4.

[23] S.V. Semenov, Inelastic neutrino scattering on nuclei. Bull. of the Russian Acad. Sci.: Physics 2017, **81**:735-8.

[24] R. Kohler, J.A. Wartena, H. Weigmann et al, Nuclear structure of ^{208}Pb from ^{207}Pb+n resonances. Phys. Rev. C 1987, **35**:1646-60.

[25] John M. Blatt and Victor F. Weisskopf, Theoretical Nuclear Physics. New York: Springer, 1979.

[26] B. Bodman, N.E. Booth, F. Burtak et al, First observation of the neutral current nuclear excitation ^{12}C(ν,ν')^{12}C*(1^+,1). Phys. Lett. B 1991, **267**:321-4.

[27] F. Ajzenberg-Selove, Energy levels of light nuclei A=11-12. Nucl. Phys. A, 1985, **433**:1-157.

[28] B. Armbruster, I. Blair, B.A. Bodman et al, Measurement of the weak neutral current excitation ^{12}C(ν_μ,ν_μ) ^{12}C* (1^+,1;15.1 MeV) at E_{ν_μ} =29.8 MeV. Phys. Lett. B, 1998, **423**:15-20.

Spatial Distribution of GRBs with Known Redshifts

Stanislav Shirokov[1],*, Alexander Raikov[2]

[1]Saint Petersburg State University, Saint Petersburg, Russia,
arhath.sis@yandex.ru

[2]Pulkovo Observatory, Saint Petersburg, Russia

Abstract The conditional density method and the pairwise distances method to study gamma-ray bursts spatial distribution are used. The GRB sample is based on Swift program and includes 364 objects with measured redshifts and fluences. The main sample is divided into two cases. In both cases entire celestial sphere up to 8 Gpc is taken, but in the second case without Galactic belt. As a reference sample we use comparison of the real sample with the uniform distributions within the same geometry and the same number of points. Also we perform modeling of the luminosity function and Malmquist bias which allows to consider total sample without additional cuts such as volume limited subsamples. Our statistical analysis shows that the fractal dimension of the GRB sample, D, is about 2.6 on the range from 2 to 6 Gpc.

Keywords: gamma-ray bursts, large-scale structure of the Universe, fractal dimension.

1. Introduction

It is known that gamma-ray bursts (GRB) are the result of massive supernovae explosions and the neutron stars coalescence. Thus the GRB large scale distribution reflects large scale distribution of visible matter (galaxies). The nature of matter distribution on large scales is actual problem for cosmology and fundamental science ([1], [2]). The GRB extreme luminosity allows registering sources at large redshift (today up to 10 Gpc), which makes it possible the study of spatial distribution of galaxies on super large scales.

The correlation function method according to [3] gave correlation length of the Swift GRB space distribution $r_0 = 388\ h^{-1}$, index of correlation function $\gamma = 1.57 \pm 0.65$ (at 1σ level), and uniformity scale $r > 7700\ h^{-1}$ Mpc. The pairwise distances method was first applied in [4] to study of 201 GRB with known redshifts and angle coordinates, so the estimation of the fractal dimension was $D = 2.2 \div 2.5$. In [5] the giant ring of GRB with diameter 1720 Mpc was observed at $0.78 < z < 0.86$. The analysis of 352 Swift GRB in [6] gave at small scales the fractal dimension $D = 2.3 \pm 0.1$ in the ΛCDM frameworks, and $D = 2.5$ in other models.

However all these studies were performed without taking into account selection and distortion effects. In our work we study influence of the selection effects on the derived value of the fractal dimension. Also we get estimation of the fractal dimension for very large scales.

2. Data and Methods

We use the Swift GRB sample [7] which includes 364 objects with measured redshifts and fluences. The statistical analysis is based on determination of the fractal dimension of the GRB space distribution. Both the conditional density method ([1], [2], [8]) and pairwise distances method [9] are applied.

Since spatial distribution of 400 objects is poor to correct the determine of fractal dimension, it is necessary to modify the considered methods. First, ratio of distribution curves of non-uniform set to uniform set with the same number of points is should be regarded. This allows one to see the differences from the uniform distribution on all scales without considering the boundary effect. The slope of the graph is equal to D - 3. If a set is uniform then the graph will lie on the horizontal axis. Second, known sets is can be compared with real distribution. The three-dimensional Cantor's sets is selected for D = 2 and D = 2.5. In order to move from mathematical fractal to a model GRB catalog it is necessary take into account selection effects of the observations. The absorption in the galactic belt is approximated by cutting out points with a galactic latitude of more than 10 degrees in both hemispheres. Luminosity distribution of a model catalog together with the Swift catalog is shown on Fig1.

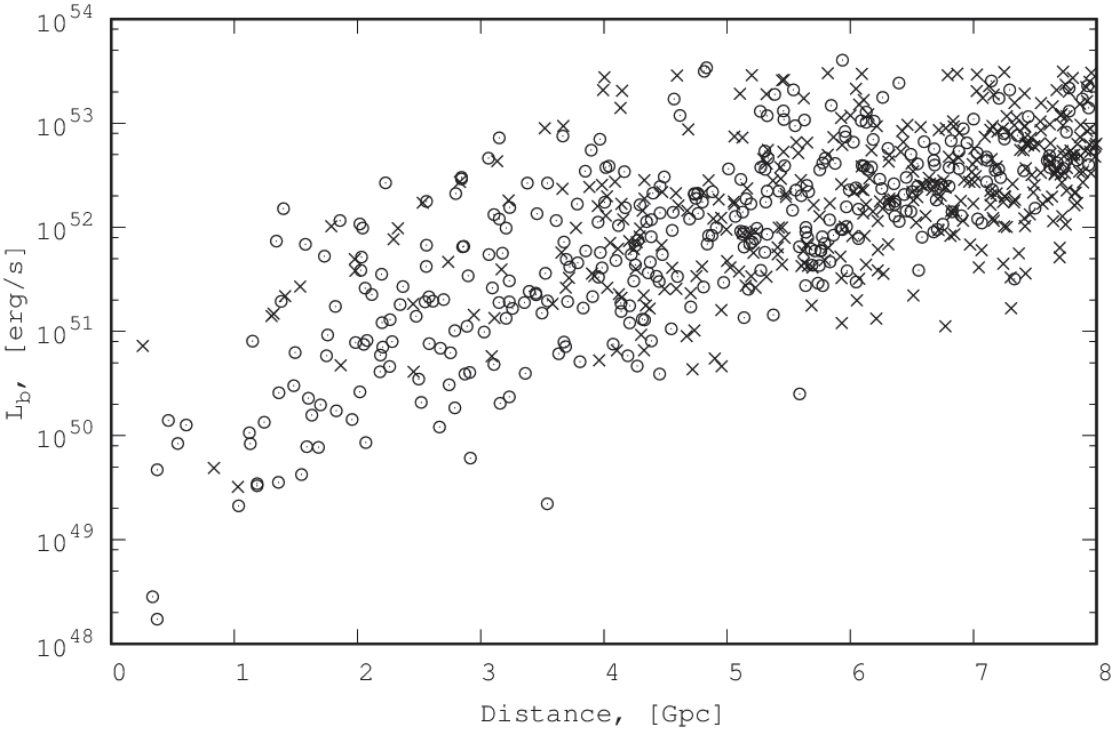

Fig1. *Luminosity distributions of the Swift GRB catalog (circles) and model catalog (crosses).*

The results of the methods are presented in Fig2 for the conditional density and in Fig3 for the pairwise distances. The model fractal catalogs are marked with the unfilled squares for D = 2 and circles for D = 2.5. The GRB Swift catalog is marked with the filled circles. An average distance between points is ~ 1 Gpc taken for the left border of the graphs. Since fractal dimension is given by graph slope in a log scale, it is necessary to consider the ratio of measured density to uniform distribution.

It can bee seen, that the behavior of the GRB curve looks like the fractal curve on the scale from 1.5 Gpc to 5 Gpc in both cases. At the same times, the GRB slope corresponding to D = 2.5 is clearly visible on the scale from 2.5 Gpc to 7 Gpc for the conditional density and from 1.5 to 7 Gpc for the pairwise distances. The directly approximated slope corresponds to D = 2.6, thus an accuracy of the fractal dimension estimation of this approach is ± 0.1.

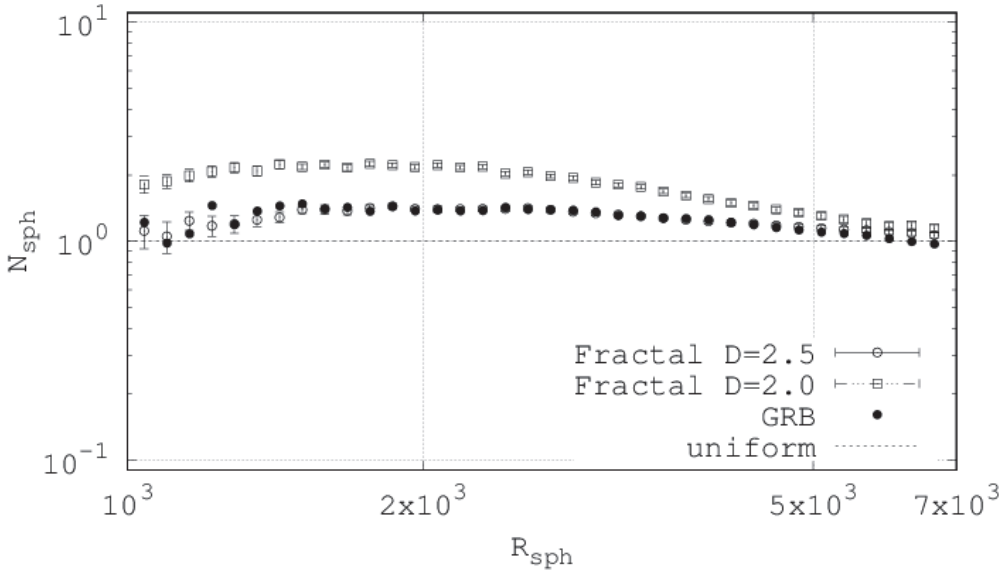

***Fig2**. The conditional density distributions of the Swift GRB catalog and the model catalogs.*

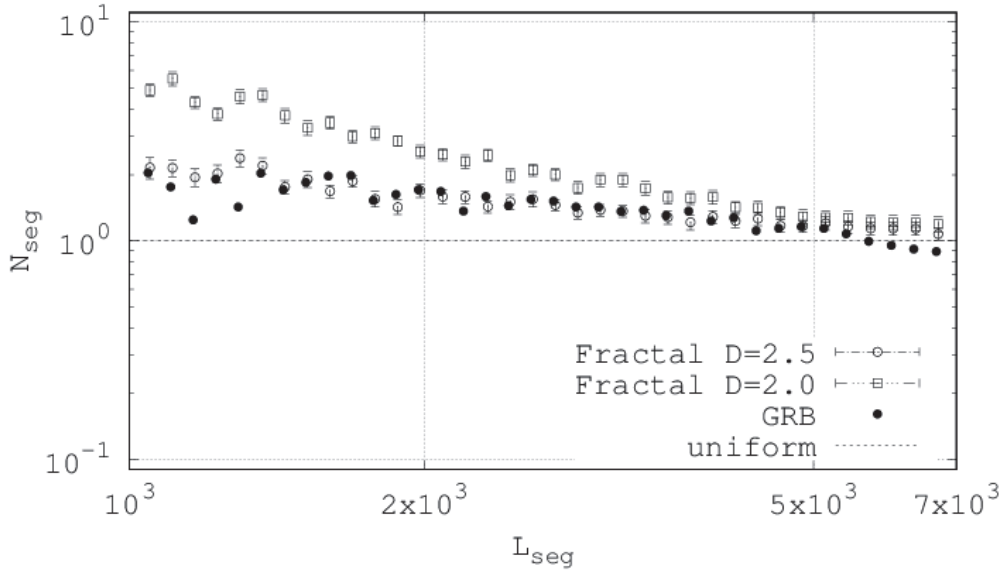

***Fig3.** The pairwise distances distributions of the Swift GRB catalog and the model catalogs.*

3. Conclusion

At first time, the conditional density is successful calculated for GRB at scales up to 7 Gpc. The similarity of slopes for different methods allows to conclude that the fractal dimension of the spatial GRB distribution from Swift GRB catalog is 2.6 ± 0.1. The GRB graph slope is saved from 2.5 Gpc for the conditional density and from 1.5 Gpc for the pairwise distances up to 7 Gpc. This result is obtained due to the consideration of ratio fractal curves to uniform curves.

References

[1] A. Gabrielli, F. Sylos Labini, M. Joice, and L. Pietronero, Statistical Physics for Cosmic Structures (Springer, Berlin, 2005).

[2] Yu. V. Baryshev and P. Teerikorpi, Fundamental Questions of Practical Cosmology, Astrophysics and Space Science Library, 383 (Springer Science, Dordrecht, 2012).

[3] Ming-Hua Li and Hai-Nan Lin, 2015, A&A 582, A111.

[4] A. A. Raikov, V. V. Orlov, and O. B. Beketov, 2010, Astrophysics, 53, 396.

[5] L. G. Balázs, Z. Bagoly, J. E. Hakkila, I. Horváth, J. Kóbori, I. I. Rácz, L. V. Tóth, 2015, MNRAS, 452, 2236.

[6] R. V. Gerasim, V. V. Orlov, and A. A. Raikov, 2015, Astrophysics, 58, 204.

[7] https://swift.gsfc.nasa.gov/archive/grb_table/

[8] F. Sylos Labini, M. Montuori, L. Pietronero, 1998, Phys. Rept., 293, 61.

[9] A. A. Raikov and V. V. Orlov, MNRAS, 2011, 418, 2558.

Measuring of the ^{14}C low abundance in liquid scintillator samples using small volume detector in low background chamber at Baksan

I.R. Barabanov[1], L.B. Bezrukov[1], A.V. Veresnikova[1], Yu.M. Gavrilyuk[1], A.M. Gangapshev[1], V.Yu. Grishina[1], V.I. Gurentsov[1], V.V. Kazalov[1], S.D. Krokhaleva[1,2], V.V. Kuz'minov[1], A.S. Kurlovich[1], B.K. Lubsandorzhiev[1], S.B. Lubsandorzhiev[1], A.K. Mezhokh[1], V.P. Morgalyuk[2], P.Yu. Naumov[4], G.Ya. Novikova[1], V.B. Petkov[1], A.M. Pshukov[1], A.Yu. Sidorenkov[1], V.V. Sinev[1],*, Sh.I. Umerov[1], E.A. Yanovich[1], T. Enqvist[5], P. Kuusiniemi[5], J. Joutsenvaara[5], A. Virkajarvi[5] and V.P. Zavarzina[1]

[1] Institute for Nuclear Researche of Russian Academy of Sciences, Prospekt 60-letia Oktyabrya 7a, 115409 Moscow, Russia, vsinev@inr.ac.ru

[2] Moscow Institute for Physics and Technology (State University), Vavilova 10, 115409 Moscow, Russia

[3] A.N. Nesmeyanov Institute of Organoelement Compounds of Russian Academy of Sciences, Vavilova 28, 115409 Moscow, Russia

[4] National Research Nuclear University (MEPHI), Kashirskoe shosse 31, 115409 Moscow, Russia

[5] Oulu University, CUPP Pyhäsalmi, Finland

Abstract The scintillation detector was constructed to research ultralow concentrations of ^{14}C in liquid scintillator samples. The detector is placed in the low background Laboratory BNO INR RAS at a depth of 4900 m.w.e. Measurements of ^{14}C abundance was done for the samples of liquid scintillator on base of linear alkylbenzene. The detector counting rate was measured and the ratio $^{14}C/^{12}C$ was extracted from the experimental spectrum the LAB sample. The background model was developed and applied for ^{14}C abundance analysis. The value obtained is $^{14}C/^{12}C$ $(9.1 \pm 1.0) \times 10^{-16}$.

Keywords: Scintillator, radiocarbon, detector, radioactivity

1. Introduction

To study natural neutrino fluxes, a scintillation detector with a mass of at least 10 kt is required. To determine the component of the geo-neutrino flux from ^{40}K, the scintillator should be several orders of magnitude cleaner than that used to measure the flux of solar neutrinos [2]. In addition, it is necessary to get rid of the ^{14}C isotope contained in the scintillator, which prevents the study of solar neutrinos from the pp cycle and the geo-neutrino flux from ^{40}K.

A program for the search for a liquid scintillator with a reduced content of ^{14}C is proposed in the Institute for Nuclear Research. For this purpose, an installation with a small scintillation detector for the study of liquid scintillator samples was created in the underground low-background laboratory of the Baksan Neutrino Observatory of the Institute of Nuclear Research of the Russian Academy of Sciences. The possibility of using a small volume detector for measuring the concentrations of ^{14}C is indicated in [3], where a 1.5-liter detector was used.

The bench can also be used to study the background of a liquid scintillator loaded with neodymium (^{150}Nd), which is intended to be used to study double beta decay.

2. Low background detector

The detector is located in the underground low-background laboratory of the BNO of the Institute of Nuclear Research of the Russian Academy of Sciences [5] and is intended for measurements of ultralow concentrations of the ^{14}C isotope in samples of a liquid organic scintillator. The laboratory is located inside the mountain (3,700 m from the entrance to the tunnel), at a depth of 4900 m.w.e., where the muon flux is ~ 0.1 m^{-2} hr^{-1} [6]. To suppress the background from neutrons and gamma quanta of the surrounding rocks, the walls, floor and ceiling of the room where the scintillation detector is installed are consistently made of layers of polyethylene (25 cm), cadmium (1 mm) and lead (15 cm). The detector itself is placed in a box of plexiglass 14.5 × 14.5 × 120 cm^3 and is surrounded on all sides by a protection from extremely pure copper 15 cm thick and lead 10 cm thick. The principle diagram of the detector is shown in Fig. 1. The detector includes a quartz cell with a diameter of 100 mm and a length of 200 mm made of quartz glass 3 mm thick (a full volume of about 1.5 L) filled with a sample of liquid organic scintillator, two cylindrical optical fibers made of organic glass (PMMA) with a diameter of 90 mm and length 50 mm, and two low-background photomultipliers (PMT) ET9302B (3"). To increase the light collection, the quartz cell and lightguides are wrapped in a mirror reflective film of VM2000. For better optical contact between the quartz cell, light guides and PMT, a silicone lubricant was used. The sealed polyethylene cover surrounding the detector from the outside, served to protect against radon. From the internal volume, radon was removed by purging with nitrogen gas.

The conditions for measuring ultralow concentrations of radiocarbon make it necessary to use materials with a low content of radioactive impurities in the detector construction. Using a low-background semiconductor detector from HPGe high-purity germanium, measurements were made of the intensity of gamma quanta of a quartz cell and a photomultiplier ET9302B. According to the measurements, calculations were made of the content of radioactive impurities (Bq/kg) in the cell and the photomultiplier in Fig. 1.

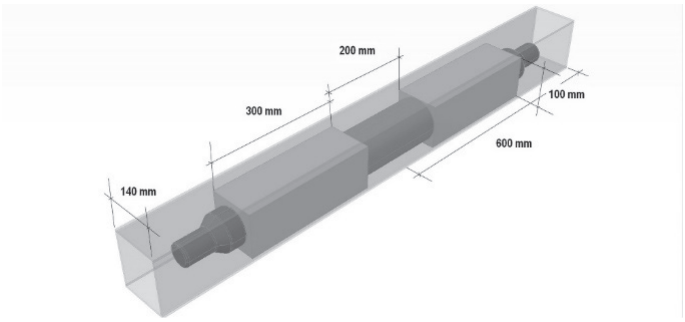

***Fig1**. Low background detector scheme.*

To further improve the background characteristics of the scintillation detector, it is planned to use more low-background photomultipliers and optimize the protection of the cell from the radiation from the voltage dividers of the photomultiplier.

3. Scintillator samples

The linear alkyl benzene (LAB) obtained from China was studied. A sample of a liquid

scintillator with an additive of 4 g/l PPO was prepared.

LAB is a mixture of hydrocarbons with the general formula C_nH_{2n-6}, density 0.856 g/l and a flash point of 143° C [8, 9]. LAB has the average formula $C_{17.73}H_{29.46}$ and is a mixture of four isomeric alkylbenzenes with the content: $C_{16}H_{26}$ – 0.125, $C_{17}H_{28}$ – 0.293, $C_{18}H_{30}$ – 0.315, C1 $C_{19}H_{32}$ – 0.267, each of which is present as a mixture of isomers of linear structure differing in the position of the phenyl residue in the hydrocarbon chain.

The light yield for a liquid scintillator based on a LAB (~ 8000 photons/MeV) and a coefficient of attenuation of a parallel light beam (15 m at a wavelength of light 420 nm) was obtained. The values obtained allow measurements in the low-energy (<50 keV) region of the beta-spectrum of radiocarbon.

For the measurements we used samples of a scintillator with a volume of 1360 ml, which are completely placed in a 1.5-liter cell.

4. Energy calibration

For the energy calibration of the detector, gamma-ray sources were used: ^{241}Am, ^{133}Ba, ^{137}Cs, ^{60}Co, ^{22}Na and ^{232}Th (^{208}Tl). The recoil energy of the recoil electron is also presented here for the backward scattering of the gamma quantum and the energy at the full absorption peak (FAP) for low-energy quanta. The energy for the maxima in the experimental distributions, which was used for calibration, is given.

5. Detector background

Solvent and copper protection of the detector passed special purification from radioactivity. Therefore, the equilibrium in the decay products of the natural radioactive chains of uranium and thorium is disrupted. If we assume that after the purification only the uranium and thorium isotopes remained, and the products of their decay were removed, then in 5 years, the thorium will again be in equilibrium with its products, and the uranium will have an equilibrium only of the ^{234}U isotope whose half-life is 2.45×10^5 years. Then the radon background will become independent, which can penetrate into the protection slots and fall into the sample of the scintillator during overflow. There is a background of ^{40}K, present in the glass and voltage divider faux. Cherenkov radiation from recoil electrons in the detector's optical fibers, caused by Compton scattering of energetic gamma quanta, can contribute.

Thus, we represent the background of the detector consisting of the following components:

1. Internal background from ^{238}U to ^{234}U,
2. The same external background, coming from the copper shield,
3. Internal background from ^{232}Th,
4. The same external background, coming from the copper shield,
5. Internal background from ^{222}Rn,
6. The same external background, coming from the copper shield,
7. External background of glass and faucet dividers from 40K,
8. The background of the Cherenkov light from the light guides together with the background of the pmt itself.

6. Determination of the contribution of ^{14}C decays to the number of scintillation cell events

The measurement of the ^{14}C content in the scintillator volume was carried out for 322.9 hours.

A digital oscilloscope National Instruments NI5105 was used to record the charge in the pulse from each photomultiplier. Trigger was the signal from one of the photomultiplier. The measurements were carried out in series, each of which was accompanied by two calibrations: one before the measurement, the other after.

The charge spectrum in the pulse of each series was transferred to the energy spectrum using its average calibration. Then the spectra were added with a weight equal to the measurement time.

The measured spectrum was fitted with simulated background spectra. The remaining part was assigned to the spectrum from ^{14}C.

At this stage, the scintillator was not blown with nitrogen to saturate it with carbon dioxide containing ^{14}C in a larger proportion. The figure shows the experimental spectrum, fitted with simulated backgrounds.

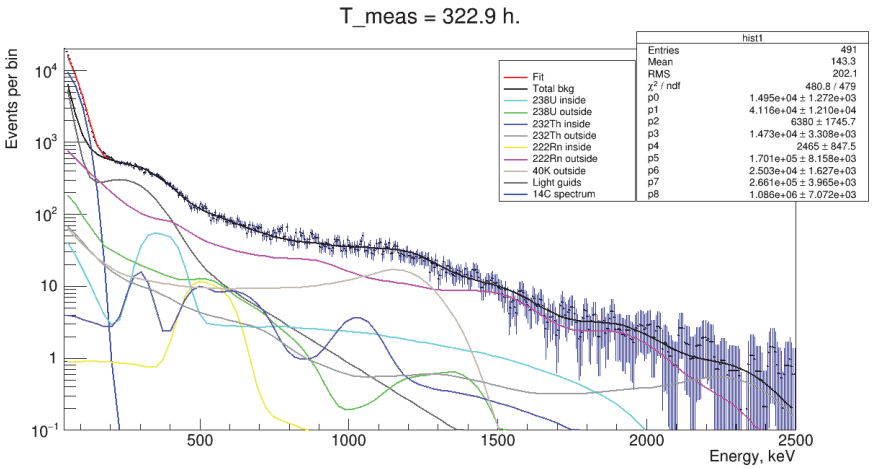

***Fig2**. Experimental spectrum from low background detector. Components of background are shown.*

Taking into account the volume of the scintillator (1360 ml), the value $^{14}C/^{12}C = (9 \pm 1) \times 10^{-16}$ for this LAB sample was obtained. Earlier, for the same sample, a value of $(5.5 \pm 1.0) \times 10^{-16}$ was obtained, and an even earlier measurement yielded a value $(3 \pm 1) \times 10^{-17}$. One can see the effect of saturation of the scintillator with carbon dioxide. Taking into account the limiting solubility of CO_2 1.18 of the scintillator volume [10], it is possible to estimate the ^{14}C content in the scintillator itself. In our case, we did not saturate the scintillator to the limit, so we take the amount of CO_2 in half of the limit, that is, 0.5 volume. We get here $^{14}C/^{12}C < 4 \times 10^{-16}$.

7. Conclusion

An installation for measuring its own background and the content of radiocarbon ^{14}C in samples of a liquid scintillator was created.

In our work, it is proposed to study samples of a scintillator with a base of a solvent obtained from various petroleum feedstocks to determine the effect of the deposit on the ^{14}C content. Solvents obtained from coal will also be investigated.

The background of the detector is analyzed in order to be able to further suppress it and lower the detector threshold for more confident separation of the ^{14}C beta spectrum. A model of the total detector background was created and successfully applied to the description of the experimental spectrum.

The setup will be used to measure the background of the scintillator with dissolved Nd for testing the methods of scintillator purification from natural radioactivity.

Acknowledgments

Authors are grateful to the organization committee of The International Conference SN 1987A, Quark Phase Transition in Compact Objects and Multimessenger Astronomy (held at 2-8 July of 2017, KBR, Terskol (BNO INR); KChR, Nizhnij Arkhyz (SAO)) for their kind invitation to present the talk.

5. References

[1] *I. R. Barabanov, L. B. Bezrukov, A. V. Veresnikova et al.* Large-Volume Detector at the Baksan Neutrino Observatory for Studies of Natural Neutrino Fluxes for Purposes of Geo- and Astrophysics // Phys. At. Nuc., 80, 446, 2017.

[2] *Bellini G., et al.* (Borexino coll.) // Phys. Rev. Lett. 107, 141302 (2011); *O. Yu. Smirnov et al.* // arXiv:1507.02432 [hep-ex].

[3] *C. Buck at al.* // Instrum. Exp. Tech., 55, 34 (2012).

[4] *B. S. Dzhelepov and L. N. Zyrianova* Influence of Atom electromagnetic field on beta-decay. // USSR Academy of Sciences, Moscow 1956.

[5] *Ju. M. Gavriljuk, A. M. Gangapshev, A. M. Gezhaev et al*. // arXiv: 1204.6424 [physics.ins-det].

[6] *V. N. Gavrin, V. I. Gurentsov, V. N. Kornoukhovet et al.* // Preprint INR-698 Moscow 1991 (rus).

[7] *I. R. Barabanov, G. Ya. Novikova, V. V. Sinev, E. A. Yanovich // arXiv: 0908.1466 [hep-ph]*.

[8] *I. R, Barabanov, L. B. Bezrukov, N. A. Danilov et al. //* Journal of Applied Chemistry 84, 385, 2011.

[9] *L. B. Bezrukov, N. I. Bakulina, N. S. Ikonnikov et al.* // Preprint INR-1382 Moscow 2014 (rus).

[10] *I. R, Barabanov, L. B. Bezrukov, B. K. Lubsandorzhiev, V. P. Morgalyuk, G. Ya. Novikova, E. A. Yanovich //* Preprint INR-1339 Moscow 2012 (rus).

The core collapse supernovae, gamma-ray bursts and SN 1987A

Vladimir V. Sokolov[1],*, Alberto J. Castro-Tirado[2,3], Tatyana N. Sokolova[1]

[1] Special Astrophysical Observatory of RAS, Nizhnij Arkhyz, Russia; sokolov@sao.ru

[2] Instituto de Astrofísica de Andalucía (IAA-CSIC), P.O. Box 03004, E-18080 Granada, Spain

[3] Departmento de Ingeniería de Sistemas y Automática (Unidad Asociada al CSIC), Escuela de Ingeniería Industrial, Universidad de Málaga, Spain

Abstract If all long gamma-ray bursts (GRBs) are related to supernovae core-collapse supernovae (SNe) explosions indeed, then a long GRB is the collapse of a massive star core or the beginning of an axially symmetric explosion of SN, and the long GRBs must always be accompanied by an SN explosion (of Ib/c type or other types of core-collapse SNe). Then the total energy release of a burst source in gamma rays is in any case not higher that the total electromagnetic energy radiated by the SN (< or ~ 10^{49} erg). Within the context of the model of asymmetric explosion of such SNe it is discussed when the relation GRB-SN is observed and when it is not observed. The accumulated statistics of GRB + SN coincidences will confirm the GRB compact model more and more. And we tell about the study of GRBs in SAO RAS, about optical identification of the first ten of GRBs.

Keywords: Afterglows, Localization, Supernovae, Asymmetric explosions, Collapse, Quark stars, Cosmology

1. Introduction

Gamma-ray bursts (GRBs) discovered in 1967 by *VELA* spacecraft, are the most violent explosions in the universe [1,2]. It can be divided into two groups, short (~ 0.2s, 25%) GRBs and long (~/> 30s, 75%) GRBs, with a separation at about 2 seconds [3]. The counterparts for all GRBs can be observed in all wavelengths (X, UV, opt, IR, radio), + gravitational waves (GWs) and neutrino (may be).

Detected as brief (0.01−100 s), intense flashes of γ–rays (mostly sub–MeV), GRBs are the brightest electromagnetic explosions in the Universe. The power emitted by GRBs in electromagnetic form can reach luminosities up to L ~ 10^{52} − 10^{53} erg s^{-1}, while active galactic nuclei (AGNs) can have L ~ 10^{48} erg s^{-1} (but for long times), and supernovae (SNe) can have L ~ 10^{45} erg s^{-1} *for the first hundreds of seconds after the explosion*. And the short variability timescales of the γ−ray emission suggest already very small dimensions for the sources, of the order of tens of kilometers, typical of massive compact stellar objects…

Below we tell about the study of GRBs in SAO RAS, about optical identification of the first ten of GRBs and the study of pulsars in the localization areas of the "old" GRB 790418 and GRB 790613. The deepest images of localizations areas of these bright *short* GRBs were first obtained by us with the 6m BTA telescope in 1994. At that time this was the first optical

study with a large telescope up to the limit ~25 st.magn. In both cases, faint blue stellar-like objects (with V about 24.5m, and B – V < 0m) were detected in localization areas. Then, in 1994, from the observed brightness and color it was supposed that these can be compact objects of type of neutron stars in our Galaxy with a surface temperature of about 100000 K, located at a distance of about 40 pc.

In those times (before 1997) the prevailing concept of GRB sources was that they are compact objects of NS type (see "Physics of Space, small encyclopedia", pp.206-209 [4]). Then we dedicated a lot of time to the study of our nearest neutron pulsar-stars also, though the galactic origin of GRBs was not confirmed afterwards. But we managed to obtain necessary experience both in observations and processing of data for faint (sometimes extremely faint) objects related to GRBs. Then, at last, the era of optical identification of new GRBs started – the *BeppoSAX* era (it seems that now the same is occurring with electromagnetic identification of sources of gravitational waves (GW) related to short GRBs, see in detail in Section 8).

So, the main ideas of this review paper are as follows:

1) Long GRBs are explosions of massive SNe; light curves of these SNe (SN1987a as a standard) and GRB afterglows are very similar (collected in this review); the model of SNe and GRBs-SNe is an asymmetric explosion and collapse of a massive core; what is the remnant?
2) Short GRBs, merging of compact objects, the problem of identification of GWs [5].
3) GRBs and superluminous SNe, also known as a hypernovae, is a type of stellar explosion with luminosity of 10 or more times higher than that of standard SN (https://en.wikipedia.org/wiki/Superluminous_supernova) – these hypernovae can produce long GRBs (which range from 2 seconds to over a minute in duration).
4) Identification of neutrino and gravitational events related to SNe in the model of asymmetric explosion of SNe, quark stars.

We would like to draw attention to the review [7] addressing to close topics and presenting a large comprehensive catalogue of 70 GRBs with multi-wavelength optical transient data on which a systematic study was performed to find the temporal evolution of color indices. In this review a special study was dedicated to the late GRB-SN bump in GRB afterglow light curves for GRBs related to SNe. See also the review [50].

2. GRBs and their localization

Now GRBs are considered as new cosmological beacons:

1) Long GRBs are the brightest electromagnetic explosions in the Universe, associated to the death of massive stars.
2) GRBs are potential tracers of the evolution of the cosmic massive star formation history (SFH), metallicity, etc.
3) GRBs also proved to be appealing cosmological distance indicators. This is a unique opportunity to constrain the Universe history to redshifts ~ 10 and may be more... The idea prevailing currently is shown in Fig1a.

We specially draw attention to the fact that what is presented in Fig.1b is not evolution of GRBs. The shaded region approximates an *effective threshold* for detection. Only! Demarcated are the GRB subsamples used to estimate the SFR. Because weak low-redshift GRBs cannot be seen at high redshifts, so we can only use *high luminosity GRBs*. (The same is said in Section 7 and in discussion of observed asymmetric explosions of SNe associated

with GRBs.)

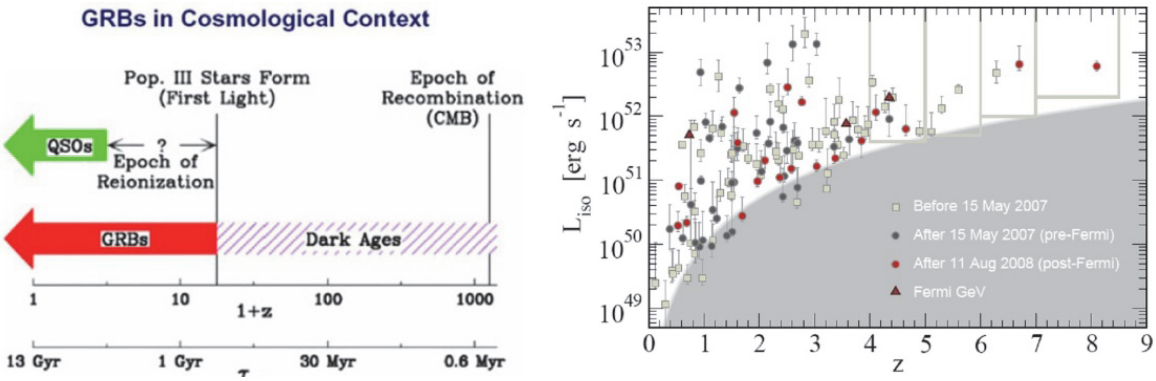

Fig1. ***a)*** *GRBs in cosmological context,* ***b)*** *from [6] — The L_{iso} luminosity-redshift distribution of 119 Swift GRBs. Squares represent the 63 GRBs used in Y¨uksel et al. (2008), with 56 found subsequently: before (grey circles) and after (red circles) the start of Fermi. Three Fermi-LAT GeV bursts (triangles) are shown (but not used in our analysis).*

On localization of GRB sources: The search and localization of the counterparts for GRBs in all wavelengths (X, UV, opt, IR, radio) started since the launch of the *Swift* satellite more than ten years ago (see in [8]), with many ground-based optical telescopes with increasing sensitivity have accumulated a rich collection of optical afterglows. This international experiment (which still goes on) for detection and localization of GRBs is shown in Fig1a. The Gamma-ray burst Coordinates Network (GCN) was created especially for that. The GCN is a system that distributes information about the location of a GRB, called notices, when a burst is detected by various spacecraft. (This experience is now used in electromagnetic identification of GW sources.)

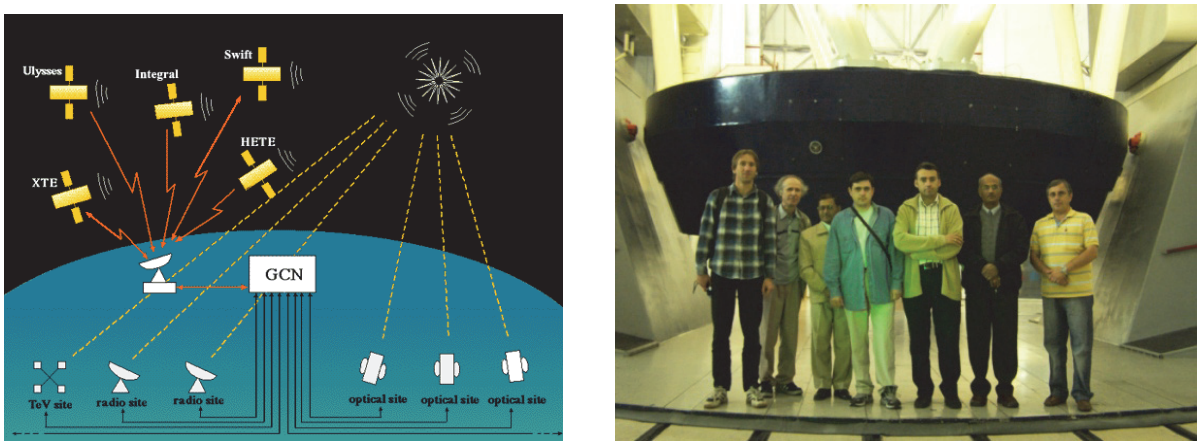

Fig2. a) *Localization of GRBs in all accessible ranges.* ***b)*** *Participants of our international team for optical identification of RBs near BTA at the international workshop in SAO on July 11, 2006. From left to right: Petr Kubanek (Czechia, Prague, Observatory), V.V.Sokolov (SAO RAS), Ballabh Sanwal (India, Nainital, Manora Peak, ARIES), Alexander Bogdanov(Ukraine, Nikolaev Astronomical Observatory), Alberto Castro-Tirado (Instituto de Astrofisica de Andalucia, Granada, Spain), Ram Sagar (India, Nainital, Manora Peak, ARIES), Sergei Guzij(Ukraine, Nikolaev Astronomical Observatory)*

3. Optical identification of the GRBs in SAO RAS from 1997

On identification of gamma-ray burst in SAO, the optical identification of the first ten GRBs: from 1997, at last, the era of optical identification of new GRBs started – the *BeppoSAX* era [8]. Our BTA observations were continued in collaboration with other teams. Participants of joint observational programs met at international workshops in 2006 ("GRB mini-workshop 2006" on 9 - 11 July 2006, www.sao.ru/hq/grb/workshop/index.html, see Fig2b), the workshop in 2009 [9] and in 2011 at the Indo-Russian workshop "Gamma-Ray Bursts, Evolution of Massive Stars and Star Formation at High Red Shifts" in India [10].

In SAO the optical identification of the first ten started with GRB 970508 – the second GRB detected by *BeppoSAX*. In 1997 our BTA observations simultaneously in 5 photometric bands (*UBVRcIc*) resulted in the most detailed (at that time) light curve of an optical stellar-like source corresponding to a GRB of May 5, 1997 (GRB 970508) registered with the space satellite *BeppoSAX*, which made a breakthrough in the problem of identification existing from the moment of registration of first bursts in 1965. Now, more than 200 gamma-ray bursts have been identified already (see [7] and references therein).

In February 1997, the Dutch-Italian satellite *BeppoSAX* was able to trace GRB 970508 to a faint galaxy roughly 6 billion light years away [11]. From analyzing the spectroscopic data for both the burst and the galaxy, Bloom et al. concluded that a hypernova was the likely cause.

So, GRB-afterglow observations for long GRBs led to the discovery of the first optical afterglows [12] (see also [50]). Finally, this GRB 970508 at z = 0.8349 turned out to be a source of cosmological origin. In the maximum brightness of a variable optical object corresponding to GRB 970508 and after the maximum, the slope of continuum spectrum was measured with BTA. The change of object colors was traced up to the 200th day after GRB. Now this GRB 970508 is at the beginning of the above-mentioned new Large Catalogue of Multi-wavelength GRB Afterglows [7], or the sample of 70 GRBs with *multi-wavelength* optical transient data (see Table 1 in [7], "Properties of the GRB Sample with Multi-color Light Curves" and references therein).

During our multi-wavelength observations of the GRB 970508 optical transient the brightness weakening rate and color indexes were changing. Beside the temporal evolution

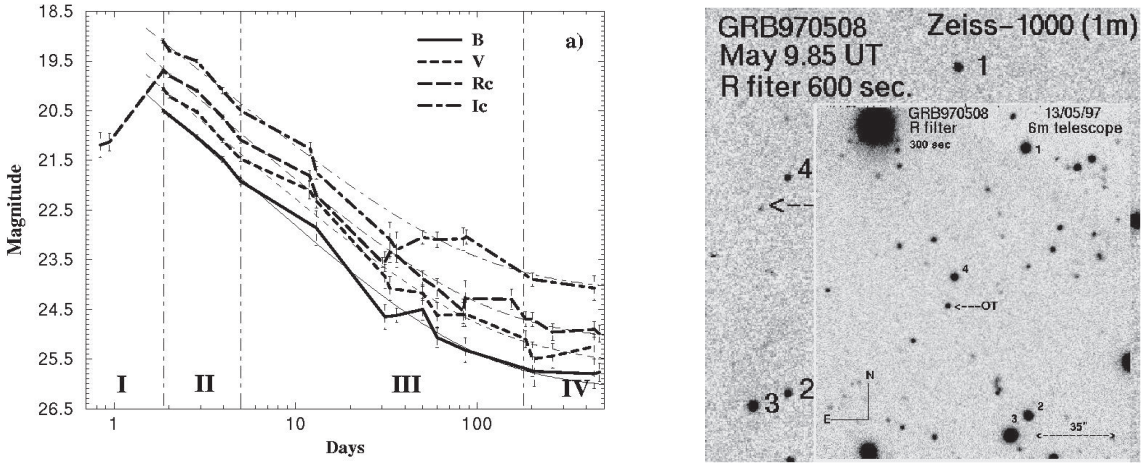

Fig3. a) *The combined light curve of the source GRB 970508 in the B, V, Rc, Ic bands obtained from data of the 1-m telescope Zeiss-1000 and the BTA telescope.* ***b)*** *Images of optical afterglow of the gamma-ray burst GRB 970508 obtained with the 1-meter telescope Zeiss-1000 at the moment of discovery and with the BTA telescope 5 days later (in the inset). Both images were obtained in the Rc band [13].*

of color indices, we noticed (with BTA) the effect of sharp slowdown of brightness weakening in infrared (~8000Å) in 36 days after the burst – the late GRB-SN bump (see below on the rebrightening effect). These new facts affected considerably the then-formed notions of the physical nature of GRBs.

The host galaxy of this GRB (an object of ~25 st.magn.) and other galaxies in the field of this GRB were also studied with BTA later. GRB 970508 was the second gamma-ray burst identified in optical, in observations of which SAO actively participated in collaboration with observers from other observatories and with the team of the famous specialized satellite *BeppoSAX*. The reddening of the optical transient (OT) of GRB 970508 in several weeks after the burst (as later in 7 other GRB OTs with z<1) was interpreted by us as the effect *directly confirming the relation between long GRBs and evolution of massive stars and SNe explosions.*

The next ***Fig3*** presents results of joint photometry of this transient source fulfilled at both telescopes: the brightest phase was studied at the 1-m telescope; the fainter stages were accessible, naturally, only for BTA [13]. Light curves of the optical transient of GRB 970508 in B, V, Rc and Ic bands were taken from [13]. The light curve (with a peak at about 2 days and slowdown in ~40 days) was observed in the R band by Garcia et al. [14] also.

So, from our data of ~40 days after the GRB, the flattening in Ic band (see in ***Fig3***) in late-time GRB 970508 optical afterglow (z = 0.835) was first detected, and then the host galaxy was also studied (see ***Fig4***).

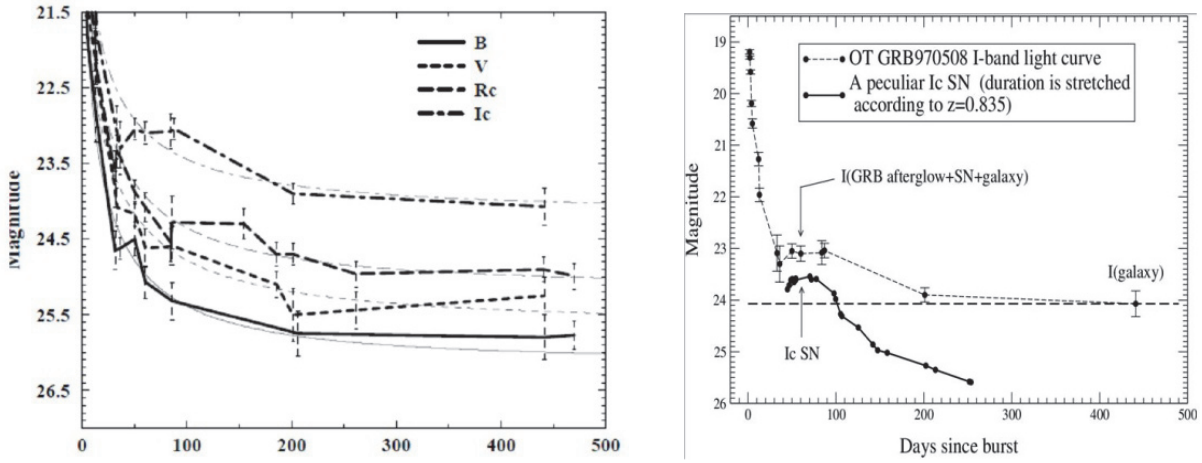

Fig 4. a) *The recent BVR_cI_c light-curve behavior of the OT + host galaxy of GRB 970508 up to ~470 days from the time of the GRB. Four independent BVR_cI_c power-law fits ($F = F_0 \times t^{\alpha} + F_c$, see Table 2) with different α are indicated by the thin lines.* ***b)*** *For comparison, the light curve of the Type Ic SN is shown.*

On the relation with CCSNe: Is the Type Ic core-collapse SN (CCSNe) in the light curve of the optical transient of GRB970508? ***Fig4b*** (without the very first point from ***Fig3a***) shows a typical light curve of such a CCSN. Thus, nonmonotonicities of type of the second burst (rebrightening) of GRB 970508 OT in 30-40 days after the GRB can be a direct consequence of the evolution scenario for a GRB source: "a massive star → a Wolf-Rayet star → a pre-supernova = a pre-GRB → GRB and explosion of a type Ib/c supernova".

So, in February 1997, the Dutch-Italian satellite *BeppoSAX* was able to trace GRB 970508 to a faint galaxy roughly 6 billion light years away [15]. (See the last points in Figs4.) From analyzing the spectroscopic data for both the burst and the galaxy, Bloom et al. concluded that a hypernova was the likely cause.

4. GRBs & core-collapse SNe, on the rebrightening effect, the late GRB-SN bump, SN 1998bw and GRB 030329

The first hypernova observed was SN 1998bw, with a luminosity 100 times higher than a standard Type Ib [16]. But the first confirmed superluminous SN connected to GRB wasn't found until 2003, when GRB 030329 illuminated the Leo constellation [17].

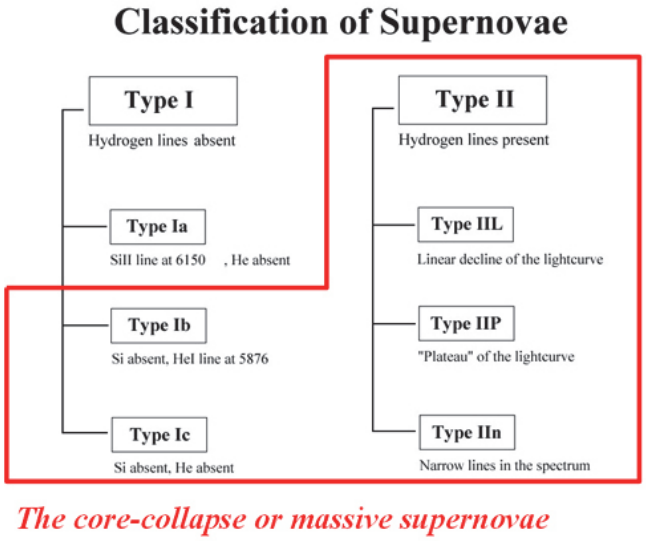

Fig 5. *SNe are the most violent explosions at the end of the star's life, and SNe are classified according to their spectra and light curve.*

Fig5 shows the Classification of SNe. Today, it is believed that stars with $M \geq 40M_{\odot}$ produce superluminous SNe [18]. *The core-collapse or massive supernovae:* according the (formal) definition, the Type Ic and Ib SNe don't have conspicuous lines of hydrogen in their optical spectra.

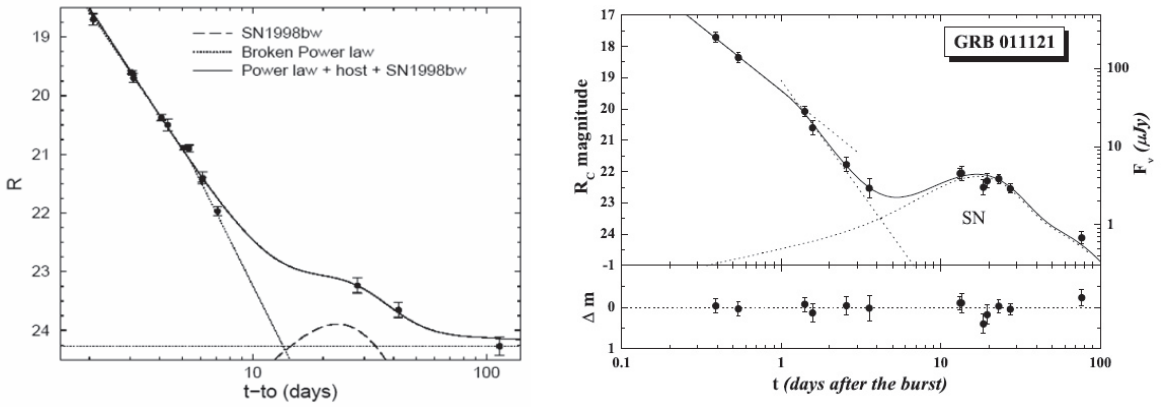

Fig6. *a) The GRB 991208 R-band light curve (the solid line) fitted with a SN1998bw-like component at z = 0.706 (the long dashed line) superposed to the broken power-law OA light curve displaying the second break at $t_{break} \sim 5$ d (with $\alpha_1 = -2.3$ and $\alpha_2 = -3.2$, the short dotted lines) and the constant contribution of the host galaxy (R = 24.27 ± 0.15, the dotted line). b), from Zeh, Klose, Hartmann paper [21]: The afterglow of GRB 011121 (z = 0.362) showed a very clear signature of the SN 1998bw-like late-time bump rising some days after the GRB*

On the rebrightening effect in light curves: Some GRBs have shown the rebrightening effect (or the late GRB-SN bump) and flattening in their late optical afterglows, which have been interpreted as emergence of the underlying SN light curve. But a systematic study on the GRB afterglows with this approach made us supposing *that all long-duration GRBs are associated with CCSNe* [19]. Below other cases with identical rebrightening of afterglow (see Figs6), typical for such *hypernovas* [20](see also [50]) are shown. It is this rebrightening that was observed for GRB 970508 afterglows (see ***Figs 3*** and ***4***) and subsequently also for many other GRB afterglows [7].

See also in A.Zeh, S.Klose, D.Hartmann paper [21] and all references therein: **"**The key finding is photometric evidence of a late-time bump in *all* afterglows with a redshift </~ 0.7, including those of the year 2003 (GRBs 030329 and 031203) and 2004 (GRB 021006; [42]). For larger redshifts the data are usually not of sufficiently quality, or the SN is simply too faint, in order to search for such a feature in the late-time afterglow light curve. This extra light is modeled well by a SN component, peaking (1+*z*)(15…20) days after a burst. This, together with the spectral confirmation of SN light in the afterglows of GRB 021211, 030329 and 031203 further supports the view that in fact *all long-duration GRBs show SN bumps in their late-time optical afterglows*. Given the fact that a strong late-time bump was also found for XRF 030723 [10] and a less strong bump for XRF 020903 (but with spectroscopic confirmation of underlying SN light [39]) might indicate that this conclusion holds also for X-ray flashes (even though the finding of XRF-SNe might be more difficult; see [39])**"**.

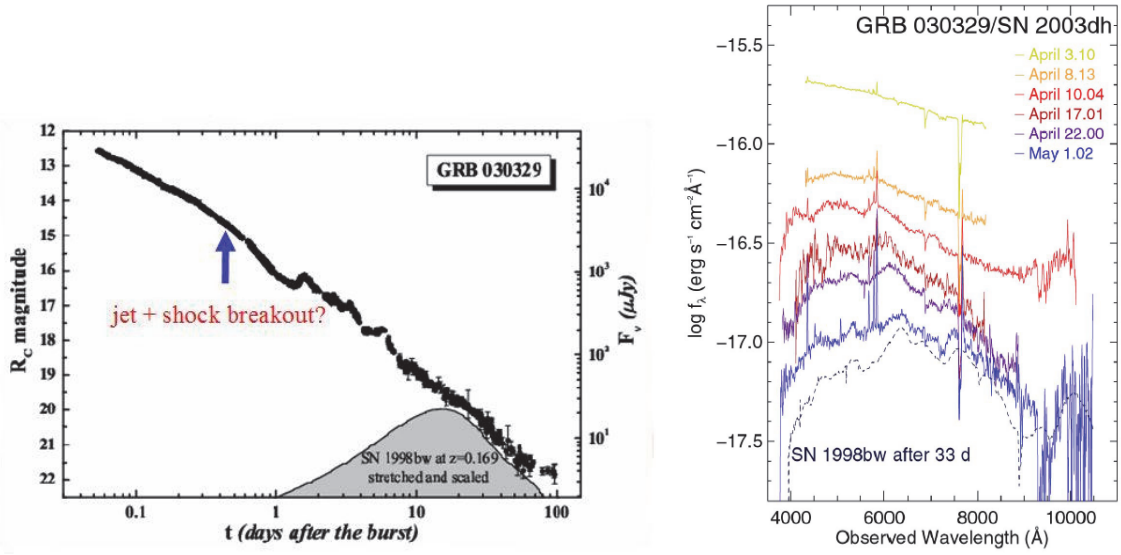

Fig7. a) *Presumably, if there were no spectroscopic evidences at hand, the SN had easily been missed in the data.* ***b)*** *Sketch of the hidden SN bump in the afterglow of GRB 030329. Various re-brightening episodes of the genuine afterglow, in combination with a relatively late break-time of the light curve, made the photometric signature for the underlying SN explosion very small.*

In particular, for the above-mentioned GRB 030329 (z=0,169), in 33 days a characteristic of the same spectrum of SN 1998bw was finally observed [22], see Figs7.

Fig7a shows interpretation of the light curve of GRB 030329/SN 2003dh with a blue arrow pointing to the на jet + shock breakout effects [19].

On early BTA spectroscopy of the GRB 030329 afterglow:

In 2003, the earliest spectra of Optical Transient were obtained for this burst with BTA (see Fig8). Characteristic broad details available already in these early spectra indicate the direct connection between the gamma-ray burst and CCSN explosion. Our spectra agree with the Nature-spectrum Hjorth, J., et al. [22].

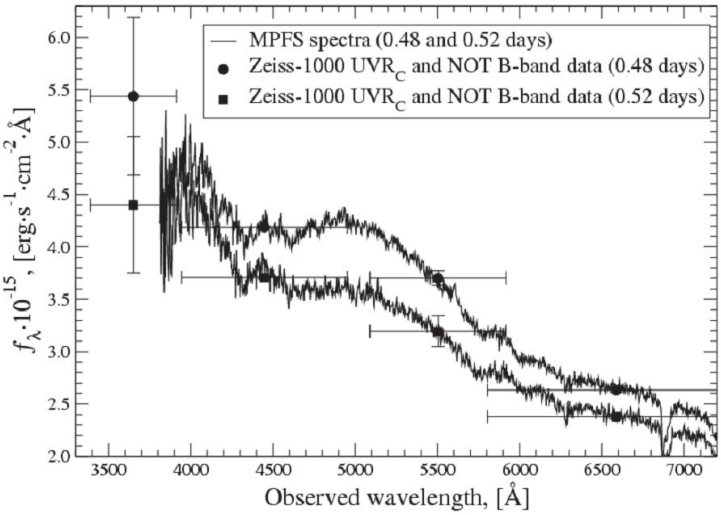

Fig8. *Early spectra and photometry of GRB 030329 OT from BTA & Zeiss-1000 & NOT [23].*

The spectrum of GRB 030329 OT in the first hours (see Fig8) can be a mixture of a GRB afterglow spectrum and early spectrum of type Ib/c CCSN. This can be a crucial argument in favor of the idea that, indeed, (long) cosmic GRBs can be the beginning of explosion of distant massive CCSNe and are observed during collapse of massive stellar cores at the end of their evolution (this result was accepted as one of the most important achievements of SAO RAS in 2003).

So, many people were speaking about a relation between GRBs and massive SNe (CCSNe), but a question of principle still remains: are long GRBs always related to this SNe type? That is why the obtaining of *the earliest spectra* of GRB OTs for (relatively!) close and rare (in comparison with other GRBs) events of type of GRB 030329 (z=0.1685) still remains topical.

5. GRB/XRF 060218/SN2006aj and interpretation of early spectra

In February 2006, the BTA spectra of GRB 060218/SN 2006aj afterglow were obtained under a joint program with the Institute of Astrophysics of Andalucia (Spain). As well as for the object GRB 030329/SN 2003dh (z = 0.1685), our observations turned out again to be among the earliest spectra of the two GRB/SN bursts.

The observational results showed that considerable changes in “standard”/popular scenarios describing both the GRB phenomenon itself and the explosion of a (massive) CCSN are inevitable. The observed UV excesses in these early spectra directly indicate to interaction between shock wave and stellar wind of a massive progenitor star (so-called “the SN Ic shock break-out effect”).

The results of SAO's observations of early spectra of these two GRBs, which are reliably identified with type Ib CCSNe, can considerably specify both the nature of a GRB source and the explosion mechanism of SNe of this type. This is an old problem, whose solution is reduced to the understanding of how the relativistic collapse of an evolving massive stellar cores occurs and what is the final result – a quark star of a singularity – black hole?

SN 2006aj UBVRIJ light curves [24]:

The light curve of GRB 060218 afterglow in Fig9 also showed the effects identical to ones described above – a peak with L_{max} ~/> 10^{45} erg/s and subsequent rebrightening [25]. So, the light curves showed non-monotonic behavior with the two maxima. The same first maximum was observed in SN1987A and SN1993J and attributed to shock break-out. The arrow in Fig9a points to the end of the shock break-out phase, as for SN1987A and SN1993J.

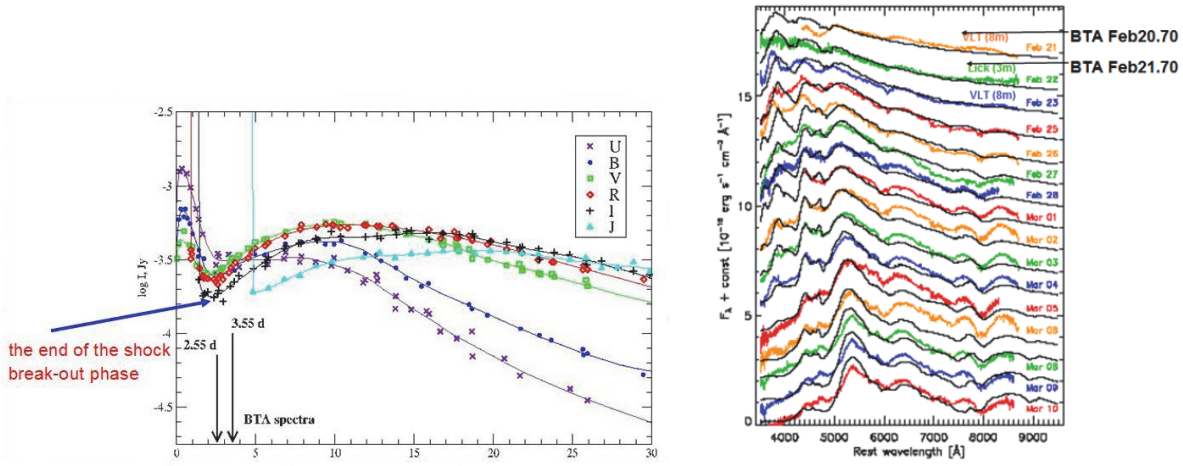

Fig9 a,b *– the light curve of GRB 060218 afterglow and spectra obtained with VLT (8 m) and Lick (3m). The arrows point also the BTA spectra. The black lines are for theoretical spectra, color lines denote real observations.*

In Fig9b and Table1 one can see also the spectra [25] obtained with BTA relative to other telescopes. Black lines are for theoretical spectra, color lines denote real observations.

Table1*. The early spectra of GRB 060218 OT before Feb 23.*

Telescope	**Tfirst Sp**	**astro-ph**
MDM (2.4m)	1.95 days (20.097 UT)	0603686 (Mirabal et al.)
BTA (6m)	**2.55 days (20.70 UT)**	
ESO VLT (8m)	**2.89 days (21.041 UT)**	0603530 (Pian et al.)
BTA (6m)	**3.55 days (21.70 UT)**	
NOT (2.56m)	3.78 days	0603495 (Sollerman et al.)
ESO Lick (3m)	4.01 days (22.159 UT)	0603530 (Pian et al.)
ESO VLT (8m)	**4.876 days (23.026 UT)**	0603530 (Pian et al.)

GRB/XRF 060218 and SN 2006aj : *Swift* (Feb. 18.149, 2006 UT) detected a peculiar GRB/XRF [28] X-ray emission was prevailing in the GRB spectrum, the GRB is also

classified as XRF (X-Ray Flash) redshift z=0.0331 (can be compared to GRB 030329/SN 2003dh, z=0.1683, Ic SN).

In the Table1 Tfirst Sp is a time after GRB 060218. These are spectra with the high S/N ratio. The 6100A absorption reaches the maximal depth and width at the moment UT Feb ~ 23. (Here we do not take into account the early spectrum of their paper Modjaz et al. [27], obtained with the low S/N ratio at the FLWO 1.5m telescope 3.97 days after the burst.)

So, we managed [25] to obtain spectra between the peak and the phase of this rebrightening – see the BTA spectra in Fig10 (a,b): 2 broad absorption details (5900 - 6300A) in both spectra were interpreted as hydrogen lines (sign of stellar-wind envelope around a massive progenitor star of the γ-ray burst). The fitting [25] by synthetic SYNOW [29] spectra with the velocity of the photosphere (V_{phot}), all elements and their ions equal to 33,000 km s^{-1} is shown by smooth lines differing only in the blue range of the spectrum at λ < 4000 Å. HI denotes the Hα PCyg profile at V_{phot} = 33,000 km s^{-1}. The model spectrum for the photosphere velocity 8000 km s^{-1} is shown for example by the dashed line as an example of the Hα PCyg profile.

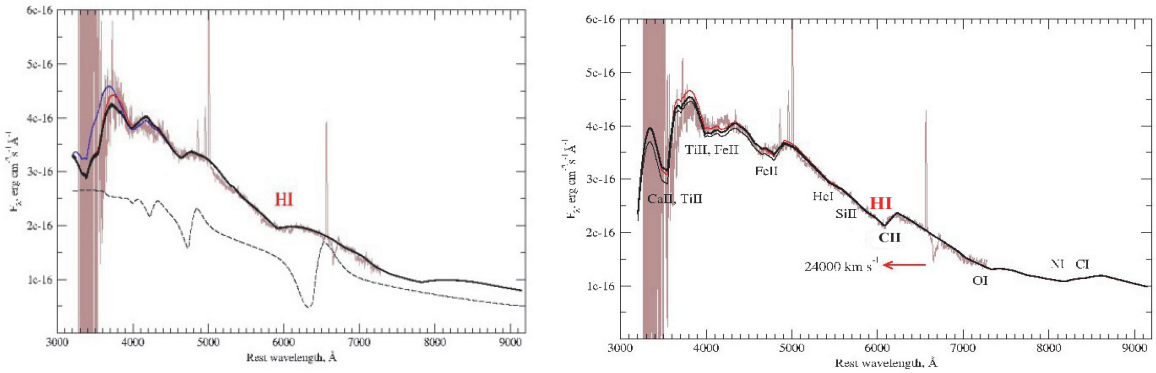

Fig. 10. *a), The SN 2006aj spectrum in rest wavelengths obtained with BTA in 2.55 days after XRF/GRB 060218. SN 2006aj/ GRB 060218, 2006 Feb. 20.7 UT, Δt = 2.55 d. The* ***undetached case****: v = 33,000 km s^{-1} (v ~ r).*
b) SN2006aj/GRB060218, 2006 Feb. 21.7UT, Δt = 3.55 d. The ***detached case****: 18000 km s^{-1} ≤ V ≤ 24000 km s^{-1} (v ~ r).*

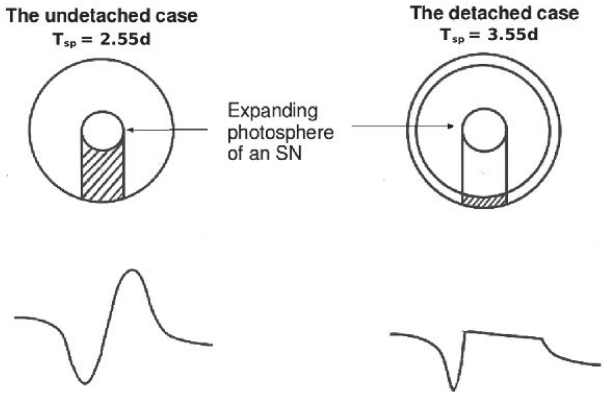

Fig. 11*. Line profiles corresponding to the cases when envelope layers (i.e. layers over the photosphere) detach or do not detach from the expanding photosphere, when the gas expansion velocity increases proportionally to distance to the center (v ~ r, see the text). The shaded regions form the absorption component of the PCyg profile. The time of BTA spectra is shown: Δt = 2.55 d and Δt = 3.55 d.*

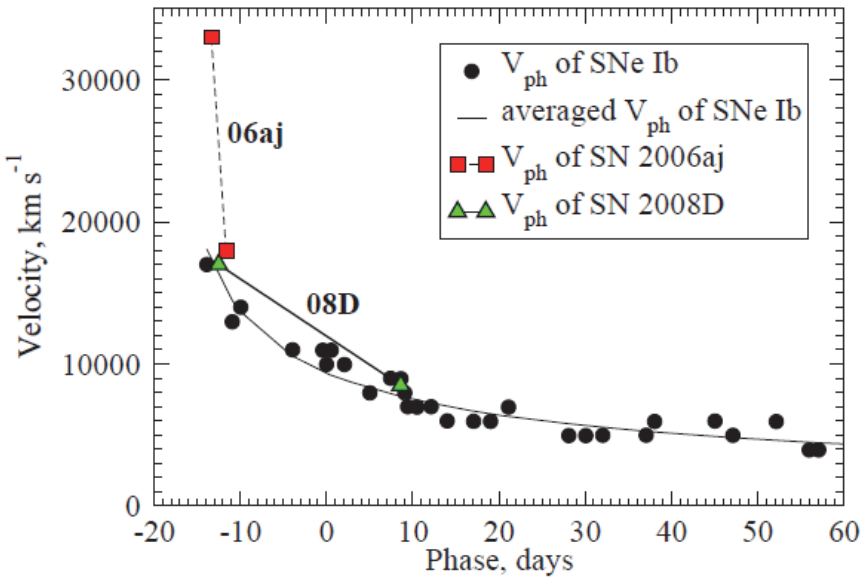

Fig12. *Velocity at the photosphere, the photosphere, as inferred from Fe II lines, is plotted against time after maximum light. The line is a power-law fit to the data, with SN 1998dt at 32 days (open circle) excluded Figure 22 from [29]. Squares (SN 2006aj) and diamonds (SN 2008D) are photosphere velocities, inferred from our spectra.*

In Fig11 the velocity of expansion is proportional to radius [25,29]. The expanding photosphere of an SN – the round in center for two cases is shown: the undetached case and the detached case (see details in [25]). In order to produce a peaked rather than a flat H-alpha emission component the hydrogen would have to be present down to the photosphere, rather than being confined to a detached high–velocity shell such as we have invoked for the absorption component.

What is "the Core-collapse SNe" in view of these results? See in Fig5 the scheme on the classification of SNe: SNe with the undetached hydrogen lines have obvious hydrogen lines and are classified as Type II. SNe with *detached* (see Fig11) hydrogen lines are classified as Type Ib because the presence of hydrogen is not immediately obvious. Type IIb SNe are those that have *undetached* hydrogen lines, when they are first observed. In some cases, whether an event is classified as Ib or IIb may depend on *how early the first spectrum is obtained*... Type Ic supernovae (SNe Ic) are very similar to SNe Ib, but they lack conspicuous He I lines.

Once more about Fig9 from [26]. The result is as follows: it is not surprising that at so huge expansion velocities as in our Fig10a (33000 km s^{-1}) nobody paid attention to broad details in the first observed spectra – see Fig8b where the smooth black lines denote the interpretation of spectra up to Feb 23 (the third spectrum), with no mention of hydrogen yet. Though by that time one could obviously see a wide absorption near 6100Å, which we interpreted [26] as the *detached* case with 18000 km s^{-1} – see our diagram velocity vs time in Fig12.

6. XRF 080109/SN2008D and others GRB/XRF/SNe

For XRF 080109/SN2008D (z=0.0065): two early BTA spectra with their SYNOW interpretation are shown in Fig13a and b. Fig12 presents location of the object (see the caption).

In total, in the period 1998-2010 in SAO RAS we investigated 6 such bursts – GRBs and SNe with spectroscopically confirmed connection:

GRB 980425/SN 1998bw (z=0.0085),
GRB 030329/SN 2003dh (z=0.1687),
GRB 031203/SN 2003lw (z=0.1055),
GRB/XRF 060218/SN2006aj (z=0.0335)
XRF 080109/SN2008D (z=0.0065)
GRB 100316D/SN2010bh (z=0.059)
+ the numerous phot. Confirmations

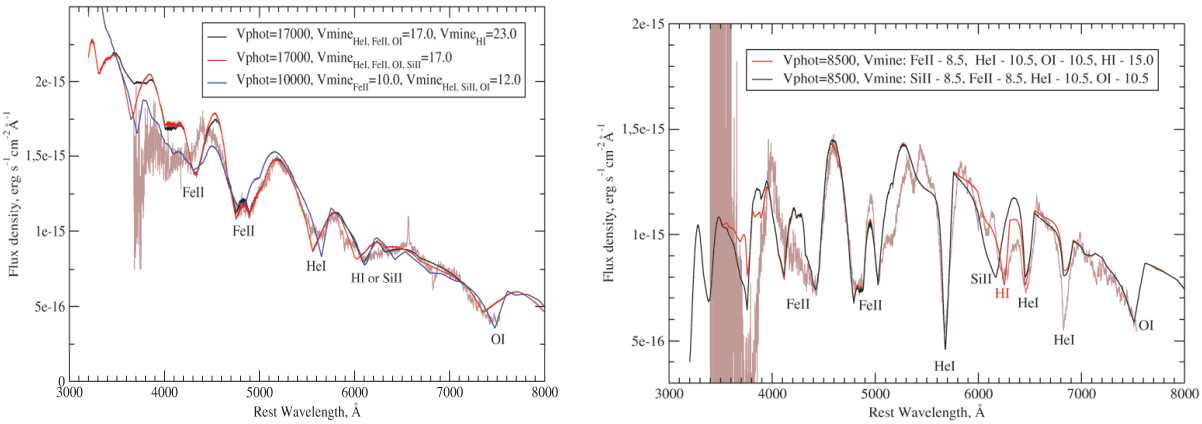

Fig13. a) *Spectrum of SN 2008D(XRF080109), Jan. 16. Physical conditions in the envelope of this SN were modeled with the SYNOW code.* ***b)*** *Spectrum of SN 2008D, Feb. 6, and SYNOW modeling.*

The searching for more spectrally confirmed pairs of GRBs (XRFs) and SNe in future observations is very important for understanding the nature of the GRB-SN connection, the nature of GRBs, and the mechanism of core-collapse SNe explosion.

The same is discussed in the paper "Gamma Ray Bursts in the *Swift-Fermi* Era" [30] and see references therein. Ibid. Table II (Nearby GRBs and Supernova Detections or Limit) gives one of the first lists of 24 cases of such coincidences GRB/SN up to z = 0.606 (for GRB 050525A). **"**On 19 February 2006 *Swift* detected the remarkable burst GRB 060218 that provided considerable new information on the connection between SNe and GRBs. It was longer (35 min) and softer than any previous burst, and was associated with SN2006aj at only z = 0.033. SN2006aj was a (core-collapse) SN Ib/c with an isotropic energy equivalent of a few 10^{49} erg, thus underluminous compared to the overall energy distribution for long GRBs. The spectral peak in prompt emission at ~5 keV places GRB 060218 in the X-ray flash category of GRBs [31], the first such association of a GRB-SN event. Combined BAT-XRT-UVOT observations provided the first direct observation of shock-breakout in a SN [28]. This is inferred from the evolution of a soft thermal component in the X-ray and UV spectra, and early-time luminosity variations. Concerning the SN, SN 2006aj was dimmer by a factor ~2 than the previous SNe associated with GRBs, but still ~2-3 times brighter than normal SN Ic not associated with GRBs [32, 26]. GRB060218 was an underluminous burst, as were two of the other three previous cases."

See also a new list of 70 GRBs with multi-wavelength optical transient data (and GRBs and Supernova Detections) in the above-mentioned paper by Liang et al. [7] dedicated to the study of the Properties of the GRB Sample with Multi-color Light Curves.

7. GRBs & CCSNe – the models

So, GRBs were identified with quite a definite class of supernovae – the core-collapse supernovae (CCSNe) or massive supernovae. It is a new era in the study of GRBs and CCSNe indeed. Thanks to GRBs, these SNe can be observed from the very beginning. Starting from the study of this SN1998bw, the astronomy of GRBs, their afterglows and host galaxies with the BTA telescope is now organized in the following way:

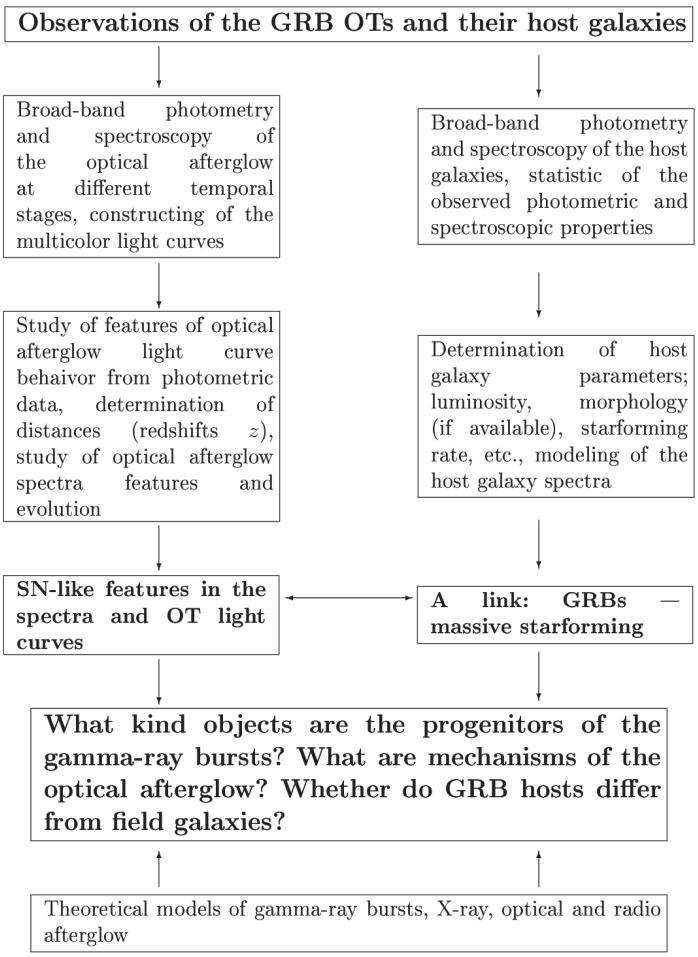

The closer GRB has the more features of SN (from 2000)... [46,25,30,7]**.** So, GRB may be the beginning of core-collapse SN explosion, and GRB is a signal allowing us to catch a SN at the very beginning of the exploding – right after collapse of a massive core.

The general belief is that core collapse supernovae connected with XRF/GRBs event can be naturally explained by the *aspherical axially-symmetrical* explosion of massive SNe. The common assumption is that in the case of an XRF type flash the observer is located outside the cone where for some reasons the bulk of gamma-ray radiation is concentrated. The asphericity is generally observed in a nebular phase. This nebular phase is shown in Fig15a from [34]. This figure explains why GRB and CCSNe cannot be observed always.

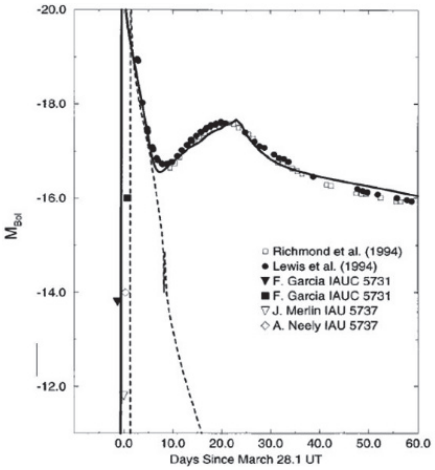

Fig14. *Earliest observations for SN1993J (II → I b) taken together with the bolometric light curve provide constrains on the initial radius of the progenitor stars. The model calculations have initial progenitor radii, R = 2.0 × 10^{13} cm (the dashed line) and R = 4.0 × 10^{13} cm (the solid line). The triangles are upper limits and no bolometric corrections have been applied to the early observations.*

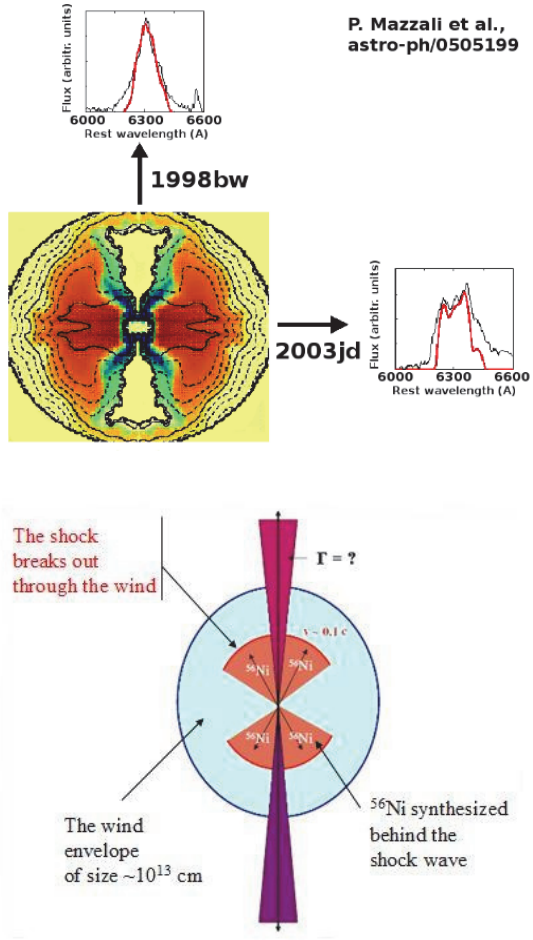

Figure 15.a) *The doubled peaked of [OI] emission must be observed for SNe which were not accompanied with GRBs, like SN2003jd e.g. And the single peak of the emission is observed in the nebular phase of SNe, which are accompanied with GRBs, like GRB 980425/SN 1998bw.* ***b)*** *Schematic model of asymmetric explosion of a GRB/SN progenitor.*

Why we cannot see any GRB event connected with SNe?

On close and distant GRBs and SNe:

Thus, the doubled peaked [OI] emission must be observed for SNe which were not accompanied with GRBs, like SN2003jd, SN2008D, and so on. And the single peak of [OI] emission is observed in the ***nebular phase*** of SNe which are accompanied with GRBs, as in the cases of GRB 980425/SN 1998bw, GRB060218/SN2006aj and others.

Fig15b shows the popular conception of the relation between long-duration GRBs and core-collapse SNe (the picture from [35]). One can see the shock breaks out through the wind envelope of size ~10^{13} cm, the characteristic expansion velocity of the shock wave and ^{56}Ni synthesized behind the shock.

A strongly non-spherical explosion may be a generic feature of CCSNe of all types. Though while it is not clear that the same mechanism that generates the GRB is also responsible for exploding the star [36]. Here it should be noticed that though the GRB phenomenon is unusual, but the object-source (SN) is not too unique. Another fact is that the more distant a GRB is, the less/smaller features of a SN are.

So, this is the second result of identification of GRBs:

Now long-duration GRBs are identified with (may be) ordinary massive CCSNe. The Core-collapse SNe explosions arise from the death of massive stars and hence are closely related to the cosmic star-formation rate and to massive-star evolution, and are responsible for the energy and baryonic feedback of the environment [37].

On the Core-collapse SN 1987A and GRBs:

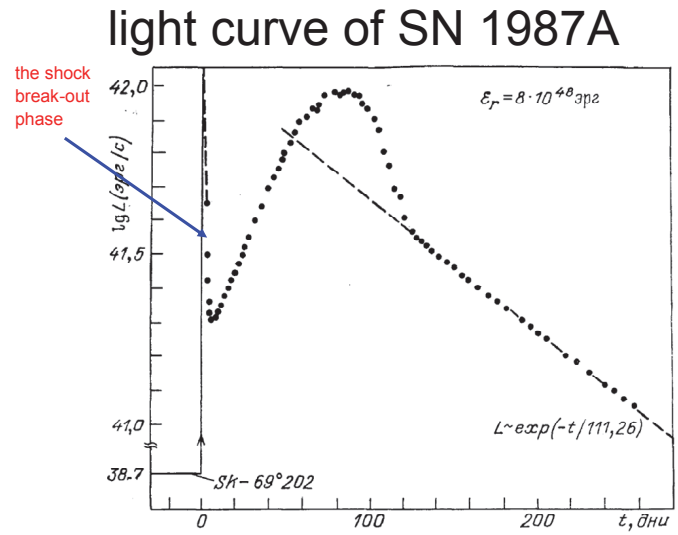

Imshennik & Nadyozhiin, UFN, **156**, 261, (1988), fig.16

Fig. 16. *The bolometric light curve of SN 1987A from the review* [38].

This Fig16 should be compared with the above Fig14 для SN1993J II → Ib, where the maximum luminosity was L_{max} ~ 10^{45} erg/s, and the same features in the light curve were observed (see Fig9a), as were observed also for GRB/XRF 060218/SN2006aj**.**

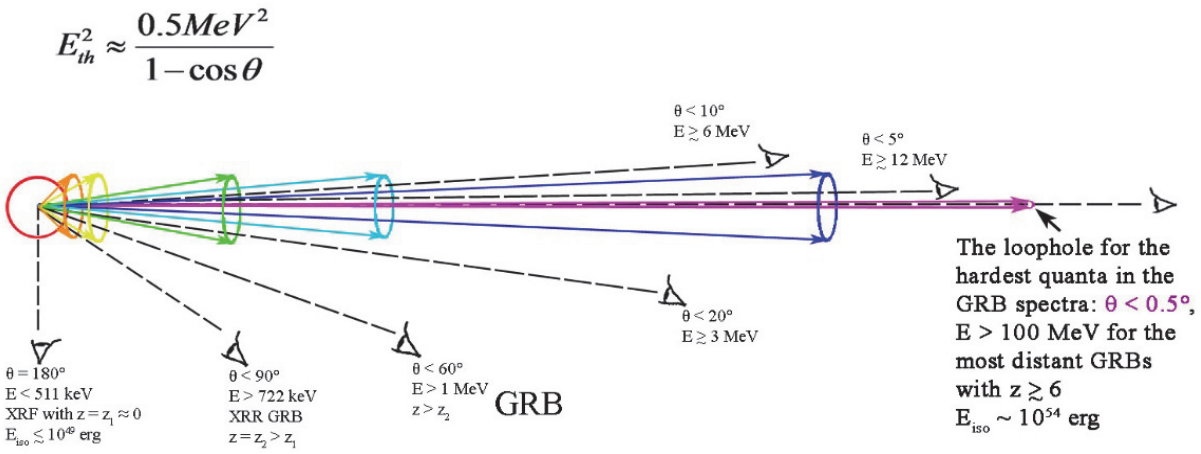

Fig17. *Collimated gamma-ray emission from GRBs – see the text.*

And on the GRBs, asymmetric explosion and so on:

If γ-rays are collimated *right in a GRB source* (with a size $c\,\delta T$ < 3000 km), then it is possible to interpret gamma-ray and X-ray emissions as is shown in Fig17. The cones (with the opening angle θ) contains the more and more hard radiation (as θ decreases) along some selected direction (or a selected axis in GRB source) with energy of quanta $E > E_{th}$. The length of arrows is proportional to the threshold energy E_{th}. The circle denotes the isotropic and the softest component of radiation with total energy of ~/<10^{49} erg. The hardest quanta of a GRB spectrum are concentrated in the *narrowest* cone, since the threshold of e^-e^+ pair creation E_{th} depends a lot on the angle θ. So, GRBs are observable only along the axis of a GRB/SN explosion, i.e. at sufficiently small θ.

The farther is an observer from the SN explosion axis, the more of X-ray radiation and the less gamma-ray quanta are in the spectrum of the flash — GRBs transform to X-ray Rich GRBs (like GRB030329) and become X-ray Flashes [39, 23]. When observing at an angle close to 90◦ to the SN explosion axis, no GRB is seen; one observes *only* an XRF (X-ray Flash) and then a powerful UV flash caused by interaction in the shock and the envelope surrounding the pre-SN as was in the case of SN1993J.

One way or another, but it must be much less than for classical GRBs observed close to the SN explosion axis (the least probable situation). The substantially asymmetric explosion can be a genetic feature of core-collapse SNe of *all* types, though it is not clear yet if the mechanism generating the GRB is also responsible for the star explosion [40].

So, if all long GRBs are related to SNe explosions indeed, then a long burst is the collapse of a massive star core or the beginning of an axially symmetric explosion of SN, and the long GRBs must always be accompanied by an SN explosion (of Ib/c type or other types of core-collapse SNe). Then the total energy release of a burst source in gamma rays is in any case not higher that the total electromagnetic energy radiated by the SN (< or ~ 10^{49} erg). And the accumulated statistics of GRB + SN coincidences [7] will confirm the GRB compact model more and more.

8. Core-collapse SN 1987A and Conclusions

The Hubble Space Telescope was pointed at the SN 1987A remnant in 1994 (see Fig18b). Explanation: What's causing those odd rings in SN 1987A? In 1987, the brightest SN in

recent history occurred in the Large Magellanic Clouds. In the center of the picture there is an object central to the remains of the violent stellar explosion. When the Hubble Space Telescope was pointed to the SN remnant in 1994, however, the existence of curious rings was confirmed. The origins of these rings still remains a mystery.

Speculation about the cause of the rings includes beamed jets emanating from a dense star left over from the SN, and a superposition of two stellar winds ionized by the SN explosion.

But see the model (in Fig17) of an asymmetric explosion of a GRB/SN progenitor…

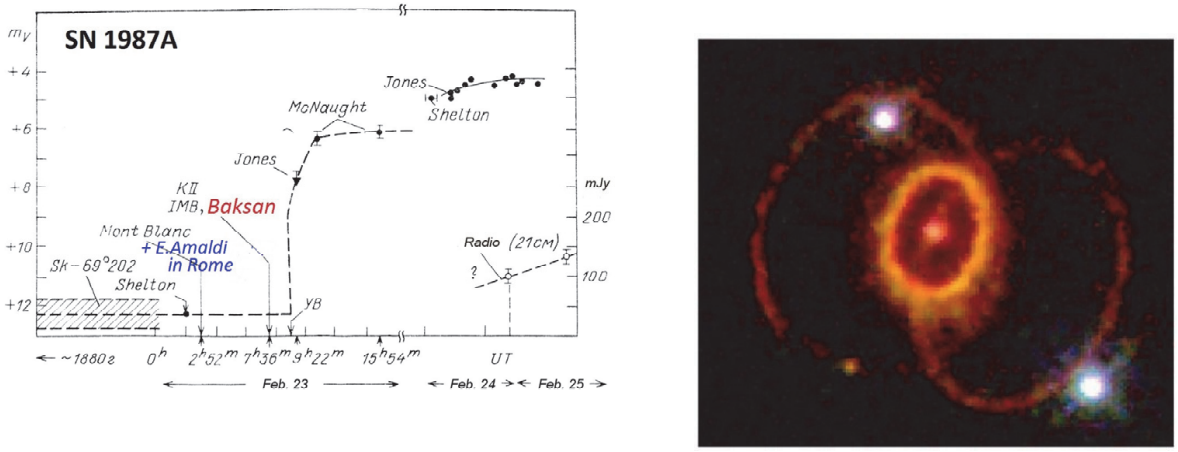

Fig18. a) *Observations of SN 1987A* ***before*** *and in the first days after its discovery (from [38]).*
b) *The SN 1987A remnant in 1994.*

So, GRBs and their afterglows are of great interest for studies related to stellar astrophysics, the interstellar and intergalactic medium, and most important, they reveal themselves as unique probes of the high redshift Universe.

Discovery of the relation between long-duration GRBs and CCSNe is the most important progress in this domain during recent 30 years. Now the search for SN signs in photometry and spectra of GRB afterglows became the main observational direction both for large ground-based telescopes and space platforms. In particular, in the process of study, a new branch of observational cosmology has arisen as a result of investigations of GRB host galaxies. The GRBs themselves are already considered as a tool for studying processes of star-forming at cosmological distances up to redshifts z~10.

Irrespective of specific models of this phenomenon, it might be said now that when observing GRBs we observe the most distant SN explosions which, probably, are *always* connected to the relativistic collapse of massive stellar cores in very distant galaxies. The connection is that GRBs may serve as a guideline to better understand the mechanism, and possibly solve the long-standing problem of the core-collapse SN explosion, since in the GRBs we have additional information related to the core-collapse.

On the quark-gluon plasma in the compact stars, GRBs, Neutrino signals, and Gravitational Wave emission:

Short GRBs can be connected with compact objects of stellar mass and a burst near (or on) their surface. The equation of state of these objects (maybe, quark stars) can be tested by studying them in all wavelength ranges. Professional astronomers and physicists investigating matter with supernuclear density understand well already that the modern science is standing at the threshold of discovery of quite a new state – quark-gluon plasma,

quark stars (see in [41] a report of the Special Commission: The summary of the EMMI Rapid Reaction Task Force on "Quark Matter in Compact Stars", October 7-10, 2013, FIAS, Goethe University, Frankfurt, Germany).

Quark gluon plasma is now a new direction both in high energy physics and in the study of compact objects of neutron star type [45]. The phase transition to the quark-gluon plasma state is surely connected with the mechanism itself of core-collapse supernova explosion, and energy of such a transition can be a source of GRBs. Neutrinos which are observed with modern detectors (including Russian ones, e.g. Baksan Underground Neutrino Telescope) can serve as signals of the transition of matter to purely quark matter. Equipment of gravitational detectors (LIGO, VIRGO) is also developed for such signals.

Participation of astronomers in programs for the study of localization boxes of neutrino (and, possibly, gravitational) events is being discussed already in detail (see https://wikispaces.psu.edu/display/AMON). The recent measurement of 2ʘ pulsars has initiated an intense discussion on its impact on our understanding of the high-density matter in the cores of NSs. During this meeting, the recent observational astrophysical data were reviewed. The possibility of pure quark stars, hybrid stars and the nature of the QCD phase transition were discussed and their observational signals delineated + SNe & GRBs.

A task force meeting was held from October 7-10, 2013 at the Frankfurt Institute for Advanced Studies to address the presence of quark matter in these massive stars [41]. In this paper, in connection with observations of SN1987A ***before*** and in the first days after its discovery (see Fig18a) it was specially noted:

"The time-delay between the moment of SN explosion and the moment of the quark phase transition could explain a few observed features of Gamma-Ray Bursts, as e.g. the existence of very long quiescent times seen in a few bursts [43] and the possible existence of Gamma-Ray Bursts for which no associated SN explosion is observed [44]."

In connection with this remark, here it should be remembered also the first detection of GWs by the team of *Edoardo Amaldi* – see in Fig18a. The data recorded by the Rome room temperature gravitational-wave antenna during the Supernova SN 1987*a* [42] have been analyzed in connection with the Mont Blanc neutrino event. An energy innovation is observed which precedes by (1.4 ± 0.5) s the first observed neutrino arrival time with the probability of being accidental of 3 per cent. But an estimation of the energy emitted as GW *distributed over* 4π and a frequency bandwidth of 1 kHz gives the figure of 2400 $M_{\odot}$, which is abnormal according to standard views on GW…

Later on, the work on identification and studying the nature of GRBs has been fulfilled (up to the present time) in a wide international collaboration. The participants of the program, beside the SAO team, are the researchers from Spain (the 10.4-m GTC, the 4.2-m Calar Alto, etc.), France (the submm Observatory at Plateau de Bure), New Zealand, India (the 2.34-m VBT Kavalur, the 2.01-m HCT IAO, the 1.04-m ST Naini Tal).

At present, the software was elaborated in SAO which provides the on-line translation of alerts about GRBs and other transients discovered by the space missions *Swift*, *Fermi*, *MAXI*, *INTEGRAL*, etc., and with ground-based facilities. (See also [47] and references therein.) When there is an alert, an observer sees a dialog box in the monitor which, in case of the positive decision, permits to start immediate pointing to the object's coordinates. So, the reaction time of the complex is reduced to minimum.

From the aforesaid, the *main result* of the many-year program on identification of GRBs in SAO can be formulated as follows:

Since (long) GRBs are the beginning of CCSNe explosion and, most probably, during the gamma-ray burst we do see (as V.F.. Shvartsman was guessing it in the old days) the relativistic collapse of a stellar core and the birth of a very dense compact object – a remnant of the SN explosion. (Judging from the new paper [7], many people already understand it...) But here new problems arise related with new cosmological tests.

Since GRBs are at very far cosmological distances (with redshifts more than 10) this poses additional questions which are of outmost importance for *observational* cosmology:

- What are redshifts at which the sky distribution of GRBs becomes homogeneous [48,49] ?
- What are the redshifts where such bursts (which are related now with collapse of compact objects of stellar mass) are unobservable already?
- And so on...

Acknowledgements

In conclusion we would like to thank all participants of identification of the first ten of gamma-ray bursts in SAO: S.V. Zharikov, S.N. Mitronova, T.A. Fatkhullin, V.L. Afanasiev, V.V. Vlasyuk, S.N. Dodonov, astronomers and administration of SAO and all colleagues who contributed to obtaining the above results with BTA and Zeiss-1000.

References

[1] Kumar, P., & Zhang, B., 2015, Physics Reports, 561, 1

[2] Wang, F. Y., Dai, Z. G., & Liang, E. W., 2015, New Astro. Rev., 67, 1

[3] Kouveliotou, C., Meegan, C. A., Fishman, G. J., et al. 1993, ApJ, 413, L101

[4] R.A. Syunyaev, “Physics of Space. Small Enciclopedia”, Moscow, 1986, pp. 206-209 (in Russian)

[5] L. Fesik, “Localization of gravitational waves as a test of gravitation theory”, “ GW170104 optical counterpart and possible scenarios of gravitational waves generation”, in Proceedings of The International Conference “SN 1987A, Quark Phase Transition in Compact Objects and Multimessenger Astronomy”, Russia, Terskol (BNO INR RAS), Nizhnij Arkhyz (SAO RAS), 2-8 July 2017, INR RAS, Moscow, 2018.

[6] “The Star Formation Rate in the Reionization Era as Indicated by Gamma-ray Bursts”, Matthew D. Kistler, Hasan Yuksel, John F. Beacom, Andrew M. Hopkins, J. Stuart B. Wyithe Astrophys.J.705:L104-L108,2009 arXiv:0906.0590

[7] Liang Li, Yu Wang, Lang Shao, Xue-Feng Wu, Yong-Feng Huang, Bing Zhang, Felix Ryde, Hoi-Fung Yu “A Large Catalogue of Multi-wavelength GRB Afterglows I: Color Evolution And Its Physical Implication”, arXiv:1712.03704, Accepted for publication in ApJS

[8] Neil Gehrels and Soebur Razzaque, “Gamma Ray Bursts in the *Swift-Fermi* Era”, arXiv:1301.0840

[9] SAO workshop в 2009 (www.sao.ru/hq/grb/workshop_2009/index.html)

[10] Proceedings of the Indo-Russian workshop “Gamma-Ray Bursts, Evolution of Massive Stars and Star Formation at High Red Shifts”, 2011 ARIES Nainital, ASI Conference Series, Vol.5.

[11] Bloom (1998). “THE HOST GALAXY OF GRB 970508”. The Astrophysical Journal (507): L25–28. arXiv:astro-ph/9807315

[12] Castro-Tirado et al. 1998, Science 279, 1011

[13] Zharikov S.V., Sokolov V.V., Baryshev Yu.V., A&Ap, 1998, v.337, p.356

[14] Garcia et al. ApJ, 500, L105-L108 (1998)

[15] Bloom (1998). “THE HOST GALAXY OF GRB 970508”. The Astrophysical Journal (507): L25–28. arXiv:astro-ph/9807315

[16] Woosley (1998). “Gamma-Ray Bursts and Type Ic Supernovae: SN 1998bw”. The Astrophysical Journal. 516 (2): 788. arXiv:astro-ph/9806299

[17] Dado (2003). “The Supernova associated with GRB 030329”. Astrophysical Journal. 594 (2): L89–92. arXiv:astro-ph/0304106

[18] Heger (2002). “How Massive Stars End Their Life”. Astrophysical Journal. 591: 288. arXiv:astro-ph/0212469

[19] A. Zeh, S. Klose, D.H. Hartmann 2004

[20] Castro-Tirado A.J., et al. 2001, for GRB 991208 (z = 0.706)

[21] A.Zeh, S.Klose, D.Hartmann 2004

[22] Hjorth, J., et al. 2003, Nature, 395 (astro-ph/0306347)

[23] Sokolov et al., Bull. Spec. Astrophys. Obs. 2003, 56, 5-14 and in astro-ph/0505535

[24] Jelínek et al., 2008, in preparation

[25] Sonbas et al., SN 2006aj, UBVRIJ light curves, arXiv:0805.2657

[26] P. A. Mazzali, et al., Nature, 442, 1018 (2006)

[27] Modjaz et al., arXiv:0603377

[28] Campana, et al., Nature 476, 421 (2006)

[29] SYNOW: D.Branch et al., 2001, A.Elmhamdi et al., 2006

[30] arXiv:1301.0840 Gamma Ray Bursts in the *Swift-Fermi* Era Neil Gehrels, Soebur Razzaque

[31] B. E. Robertson & R. S. Ellis, Astrophys. J. 744, 95 (2012)

[32] Pian, et al., Nature, 442, 1011 (2006)

[33] ApJ 449, L51-54, 1995 Young, Baron, and Branch.]

[34] P. Mazzali et al., arXiv:0505199

[35] Woosley and Heger , 2006

[36] astro-ph/0603297, Leonard, Filippenko et al.

[37] Madau et al. 1998

[38] Imshennik & Nadyozhiin, UFN, 156, 261, (1988)

[39] Sokolov et al. Bull. Spec. Astrophys. Obs., 2006, 59, 5

[40] A. Filippenko et al. (astro-ph/0603297)

[41] Michael Buballa et al., EMMI Rapid Reaction Task Force on "Quark Matter in Compact Stars" arXiv:1402.6911

[42] E. Amaldi 1,3, P. Bonifazi3,4, M. G. Castellano3,4, E. Coccia2,3, C. Cosmelli1,3, S. Frasca1,3, M. Gabellieri1, I. Modena2,3, G. V. Pallottino1,3, G. Pizzella1,3, P. Rapagnani1,3, F. Ricci1,3 and G. Vannaroni3,4 EPL (Europhysics Letters), 1987, Volume 3,Number 12 , The Data Recordered by the Rome Room Temperature Gravitational Wave Antenna, during the Supernova SN 1987a in the Large Magellanic Cloud

[43] A. Drago and G. Pagliara Astrophys. J. 665 (2007) 1227–1234, astro-ph/0512602.

[44] C. D. Dermer Astrophys.J. 684 (2008) 430, arXiv:astro-ph/0703223

[45] Ignazio Bombaci, Domenico Logoteta, Isaac Vidana, Constanca Providencia, Quark matter nucleation in neutron stars and astrophysical implications, arXiv:1601.04559

[46] V.V. Sokolov et al. 2006, Bull. Spec. Astrophys. Obs., 59, 5

[47] THESEUS: a key space mission for Multi-Messenger Astrophysics G. Stratta, R. Ciolfi, L. Amati, G. Ghirlanda, N. Tanvir et al., ArXiv:1712.08153

[48] Khabibullina, M.L., Verkhodanov, O.V., Sokolov, V.V., Astrophysical Bulletin 69, 472 (2014).

[49] G. Stratta, et al., 2017, THESEUS: a key space mission for Multi-Messenger Astrophysics, arXiv:1712.08153

[50] Castro-Tirado A.J., Sokolov, V.V. and Guziy S.S. 2018, Gamma-ray bursts: Historical afterglows and early-time observations, These Proceedings

Future Fast Radio Bursts (FRB) search with the RATAN-600 radio telescope at 4.7 GHz

S.A. Trushkin[1], S.N. Fabrika[2], P.G. Tsybulev[3], N.A. Nizhelskij[3]

[1] Radio Astrophysics lab, SAO RAS, Nizhnij Arkhyz, Russia; satr@sao.ru

[2] Star physics lab, SAO RAS, Nizhnij Arkhyz, Russia

[3] Radio continuum lab, SAO RAS, Nizhnij Arkhyz, Russia

Abstract We have started the search program of the mysterious and rare fast radio bursts (FRB) with the RATAN-600 radio telescope. We have prepared the special antenna - the Western Sector and the secondary mirror (SM5) named by Type-5. The measured effective area of the antenna will be near 1100 meter in square. The three from four new high sensitivity receivers at 4.7 GHz have been already established in the focal plane of SM5. The total frequency band of 600 MHz of each receiver was divided by the microwave filters on four sub-bands of 150 MHz and signals of 12 (16) channels of back-end are recorded with the maximal temporal resolution 0.49 ms. We develop online routine on the powerful PC, analyzing the coming signals in order to find the fast bursts, shifted in time due to the interstellar (or intergalactic) dispersion (DM ~ 100-1000 pc/cm3) in dependence on the sub-band frequencies. Alerts of the such distant (out of the Solar system) events with expected fluences ~1-30 Jy ms and error box of coordinates will be sent to the robotic optical wide-angular small telescopes array constructed in SAO RAS. The relatively big field of view of the four-beam system in the 24-hours survey allows us to detect up to 10 FRB per year. In June 2017 we have carried out the pilot observations of the bright and close pulsar PSR B0329+54 at 2.3 and 4.7 GHz with the wide-bands (120 and 600 MHz, respectively). We have detected the 10-30 pulses with the known spin period P=0.71452s getting in the antenna beams, recorded with time interval 0.49ms. The width of the average pulse is equal to W50=10 ms at 4.7 GHz. Such measurements are well test for the FRB search. We have started of the survey in September 2017.

Keywords: Radio Astronomy, Radiometers, Fast Radio Bursts, Blind Radio Surveys, Dispersion Measure, Pulsars

1. Introduction

The first FRB was discovered [1] in 2007 in archived pulsar data from Parkes telescope. It was a 5-millisecond single radio frequency burst which undergoes the high interstellar (or intergalactic) dispersion. Since the current catalog has ~25 FRBs, lasting no more than a few of milliseconds. They seem to come from sources beyond our Galaxy. Some last longer than others, and the light from a few is polarized. In 2012 [2] had found a repeating FRB121102, meanwhile all the other signals had been single. It was identified: a faint, distant dwarf galaxy around 780 Mpc away, in a star-forming region that is a steady radio source. Many telescopes are looking for FRBs. We have decided to begin in such search with RATAN-600 radio telescope in continuous survey observations with the special antenna and the innovative radiometric four-beam complex with division of each wide-band to four narrow-bands at 4.7 GHz and rapid data-sampling up-to 0.49 ms.

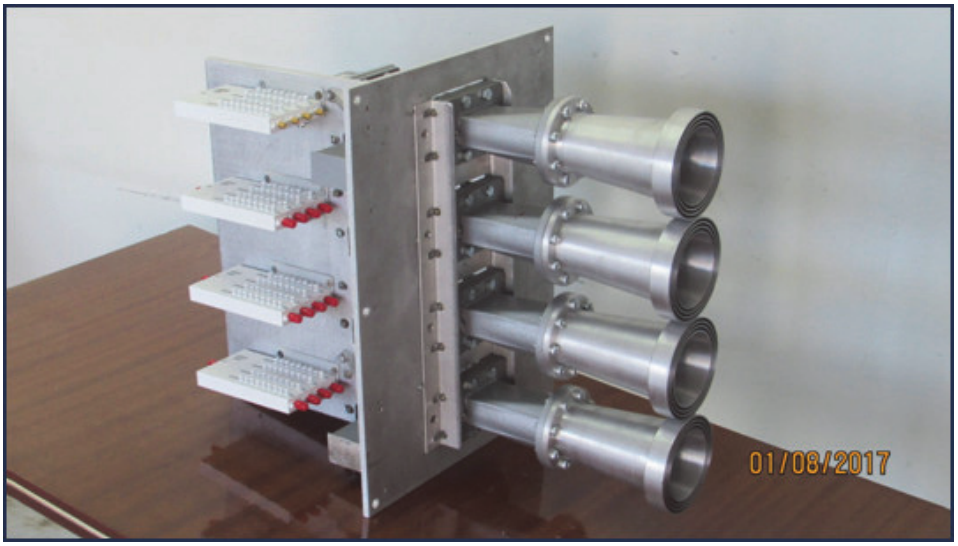

Fig1. *Four-beam radiometer at 4.7 GHz in the test mode in lab.*

2. The current survey

2.1. Receivers

We have used the low-noise radiometer at 4.7 GHz with wide-band 600 MHz and the calculated sensitivity near 3 mK per a second. The four-beam complex with microwave filters, dividing the wide band for four sub-bands, 150 MHz each is shown in ***Fig1***.

2.2. Antenna

The main mirror antenna is the Western sector (WS) of the RATAN-600 radio telescope.

In the WS focus is placed effective secondary mirror SM5 with an enhanced field of small aberrations in the focal plane. We have established WS at elevation of the known calibrator source 3C48 (0137+33), that is very close to the repeated FRB 121102 (0529+33). For search for the new FRB we need a big field of view (FOV). For example FOV of the 13-beams system at Parkes 64m telescope is equal 13* 3.14*13’ *13’/4 = 1724 arc min in square for each time slice. For WS and four beams at 4.4-5.0 GHz (a total band 600 MHz) we can calculate the FOV: 4* 3.14*2’*32’/4 = 200 arcmin in square. The cross-section of sky motion will be under the positional angle ~60 deg. Three beams of antenna WS in the angular scale 8’*25’ for each are given in ***Fig2.***

We observe a strip of the sky (~600 degrees in sq.) due to the Earth motion per day. The strip of the survey is shown in the Galactic coordinates in ***Fig3***. The strip reaches the Galactic North pole regions at RA=12–13h.

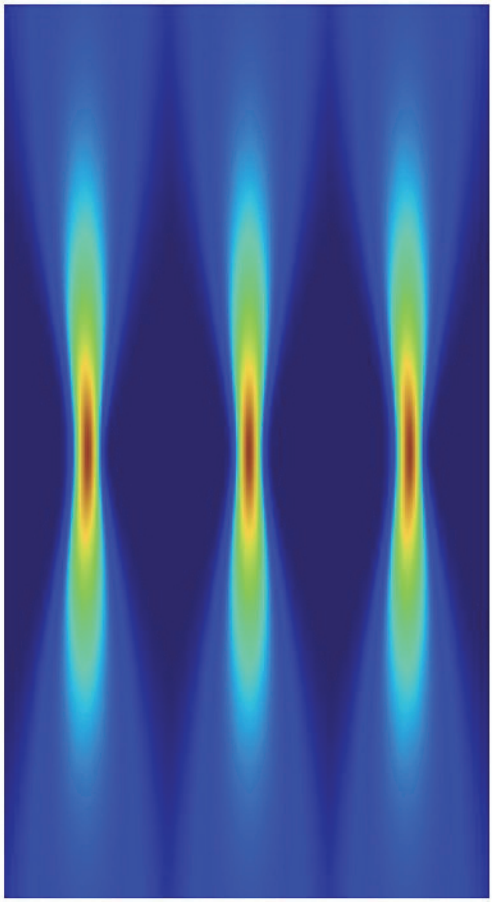

Fig2. *Three beams of the current survey, calculated with real parameters of antenna (h=52.36deg) and the secondary mirror N5 at wavelength 6.7 cm of the multi-channel radiometers.*

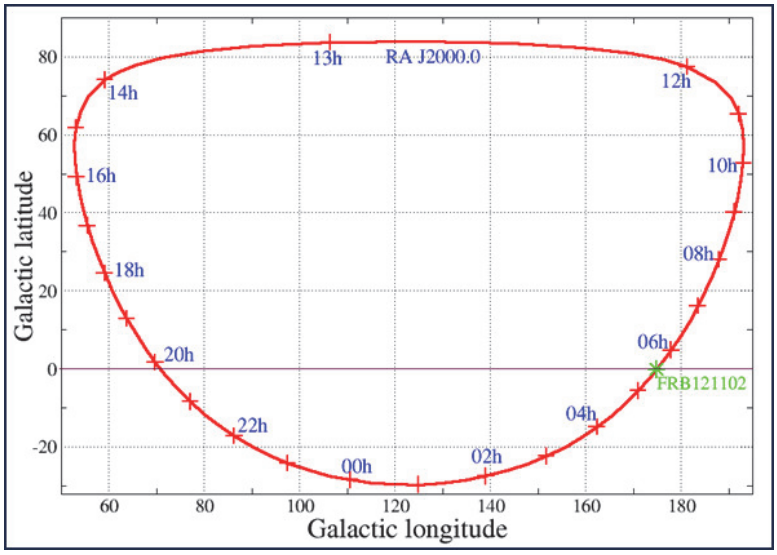

Fig3. *The strip of the pilot survey with the West sector of RATAN-600*

2.3. Some test results

In order to check the rapid data-sampling of the telescope data we carried out ten pilot observations of the bright pulsar PSR0329+54 (P=0.714s) with other wide-band radiometers (2.3, 4.6 and 11.2 GHz) on the "Southern Sector" antenna during the lower culmination of the source (***Fig4***). In each observation we have detected the 5-30 single pulses from pulsar at 2.3 and 4.6 GHz (***Fig5***) and even once at 11.2 GHz. We did not use any following for the source because the antenna was unmoved.

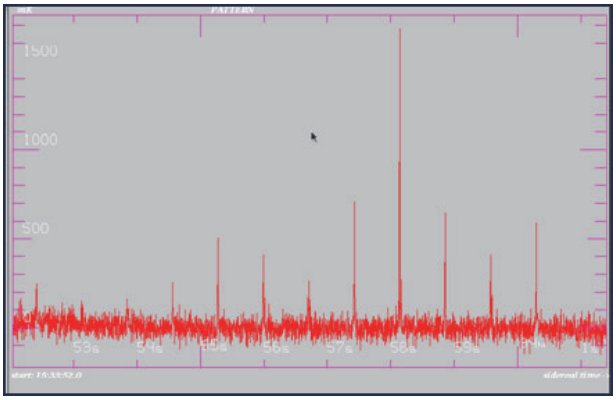

Fig4. *Drift scan of PSR0329+54 at 4.7 GHz*

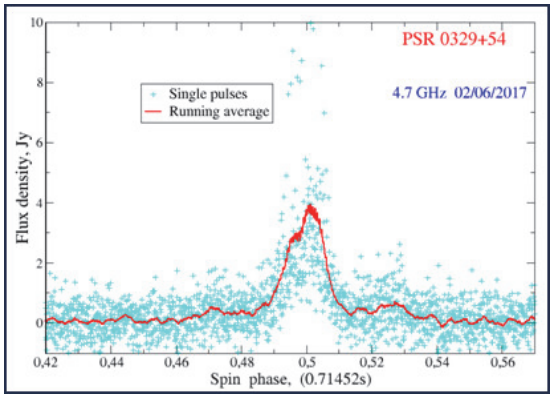

Fig5. *The mean pulse profile of PSR0329+54 at 4.7 GHz*

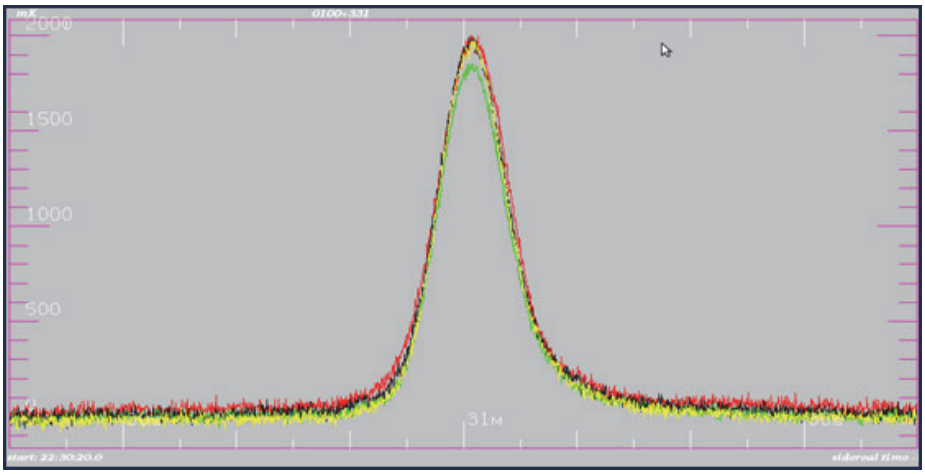

Fig6. *Scans of 3C48 (0137+33) at 4 subbands with sampling 50 ms*

We have detected very variable series of pulses day by day. Sometimes the fluxes in a pulse reached ~10 Jy at 4.6 GHz. We summed all detected pulsed to obtain the mean (from ~50) profile and they are in good accordance with the studies of the PSR0329+54. De-dispersion could be provided by the analysis of the arrival times of a pulse at four narrow subbans. Using the usual formula for $\mathrm{deltaT} = 4.15 \cdot 10^6 \, (1/f_1^2 - 1/f_2^2)$ DM we can estimate the delectability of the dispersed signals. For MD = 300 pc/cc the dt will be about 3-4 ms, what could be measured with given complex. Sure we consider signals with deltaT =0 as a local interference or satellites on the Earth orbits.

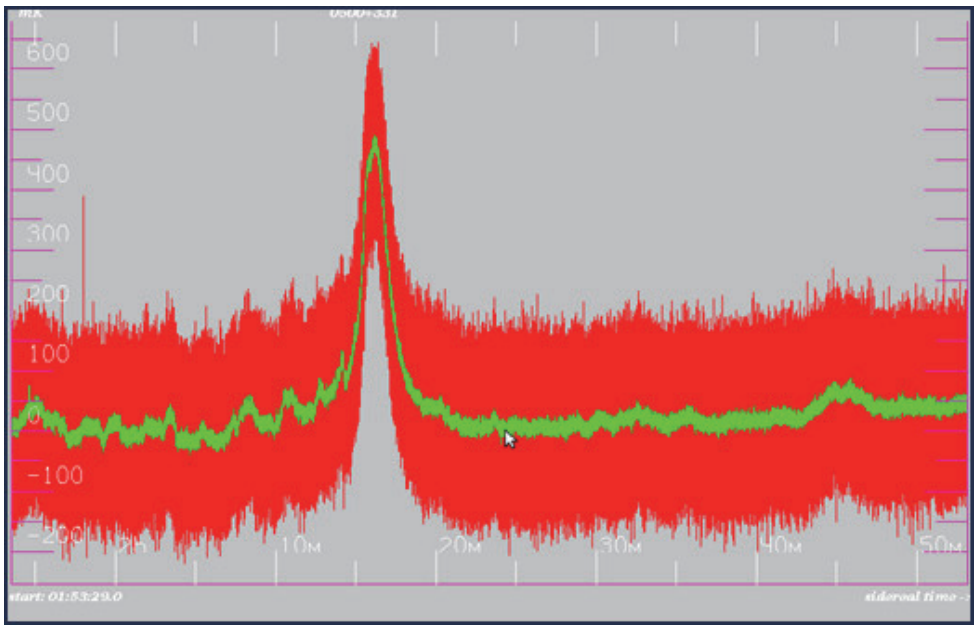

Fig7. *Mean (from 9) scan of the RA:5th hour of the survey. This is a cross-section of the Galactic plane. The pointer is shown the location FRB121102.*

During September - November 2017 we have done more than 70 full daily scans with the three-beam system. The post-data-reduction showed that the night time is most favorable in terms of absence of interference. Most of day-time interference could be easy recognize in the multi-channel observations. The realized sensitivity of the complex is close to 0.6 Jy per a sub-channel for the sampling dt =0.49 ms. For flux density calibration and antenna pointing we have used the known source 0137+33 (3C48) (***Fig6***). We did not detect any signals with high dispersion. The mean scan of during RA (J2000) =5h for 9 the sequential days in November 2017 with original sampling 0.49 ms and compressed to 4.9 ms are shown in ***Fig7***.

3. Conclusion

The search of the FRBs with RATAN-600 radio telescope could be important new field of the rapid radio photometry. We carry out the continuing survey and prepare the real-time data-processing in order to announce about FRB just after its detection. In 2018 we will use new robotic optical telescope near of BTA telescope in order to search for any association with FRB, because the coordinate errors of the RATAN detection will be compatible with beam sizes or about 2x30 arc min. While we concede Parkes telescope in FOV we hope to detect a few of FRB per year. The higher frequency (4.7 GHz vs 1.4 GHz) could be important feature of the current survey, because probably some FRB (FRB121102) has the maximal fluxes at frequency higher 6 GHz [5]. On other side if results of the project will be positive, we will strive to increase the number of the beams or the operating frequencies.

Acknowledgements

We are grateful for the financial support of the project by the Russian Scientific Foundation (grant N 14-50-00043) and from the stuff of the radio astronomical department of SAO RAS.

References

[1] Lorimer, D. R., Bailes, M., McLaughlin, M. A., Narkevic, D. J., Crawford, F. Science 318, 777–780 (2007)

[2] Spitler, L. G. et al. Nature 531, 202–205 (2016)

[3] Chatterjee, S. et al. Nature 541, 58–61 (2017)

[4] Petroff, E., Barr, E. D. et al. 2016 FRBCAT: The Fast Radio Burst Catalogue

[5] Gajjar, V. et al FRB 121102: Detection at 4 - 8 GHz band with Breakthrough Listen backend at Green Bank Atel , 10675, 1

Russian optical telescopes: facilities for follow-up observations of sources of gamma-ray bursts and supernovae, identification of neutrino and gravitational-wave signals

V.V. Vlasyuk[1]

[1]Special Astrophysical Observatory of RAS, Nizhnij Arkhyz, Russia; vvlas@sao.ru

Abstract New challenges for the ground-based astronomy (mainly, for the Russian one) are discussed. All instrumental facilities – both current and prospective – of Special Astrophysical Observatory are briefly described. Some proposals on alert events observational strategy for Russian telescopes are presented.

Keywords: Ground-Based Astronomy, Alert Events, Gamma-Ray Bursts, Astronomical Instrumentation.

1. Introduction

The first years of the 21-st century in the modern astronomy were marked, among other things, by detection of astrophysical signals of a principally new type. They include neutrino events, fast radio bursts and, finally, gravitational-wave signals. The statement about the beginning of era of so-called Multimessenger Astronomy has become a commonplace already. The main challenge of the modern astronomy is to reliably detect these signals, to identify them as soon as possible in other, already "classical" ranges and to understand the physical nature of phenomena generating these signals. We give a brief description of available facilities of optical telescopes of Special Astrophysical Observatory of RAS and other Russian observatories, which are able to solve such tasks. The details of promising projects developed in SAO are presented. An important aspect of the problem is the fulfilling the earliest possible observations with equipment installed in the telescope focuses in the standby mode – spectrographs, cameras for direct imaging and high temporal resolution systems. The systems monitoring the celestial hemisphere in SAO are themselves capable to generate the alert signals for subsequent studying. The available experience of scientific integration obtained by us during recent decades in the process of studying optical afterglow of gamma-ray bursts permits us to hope for successful implementation of scientific tasks of this kind.

2. New challenges for the ground-based astronomy at the early XXI century

2.1. Gamma-ray bursts

Strictly speaking, the era of studying powerful bursts of emission in the gamma-ray range (Gamma Ray Burst – GRB) started almost 50 years ago, when, within the framework of the USA space program of monitoring nuclear explosion, in 1967 the data about first events of this kind were obtained. Three years later the astronomical community was informed about discovery of the burst GRB700822 registered by three Vela satellites simultaneously.

The next 25 years were dedicated to the intense study, the building of different model of burst origin, attempts to identify them in spite of big errors in coordinates. Only 1997 – the first year of operation of the BeppoSAX mission, which permitted to considerably enhance precision of burst location – was successful in the first optical identification (February 28), determination of distance to the gamma-ray burst (May 8) and, finally, discovery of a burst at a cosmological distance of $z=3.42$ (December 14).

This was the beginning of a new era in the research. Of course, the detailed picture of the gamma-ray burst phenomenon is not built yet, in spite of the subsequent 20 years. But it became indisputable that this phenomenon is accompanied by enormous energy release never met by researchers before. The launch of new missions – HETE-2, SWIFT, INTEGRAL – in combination with quasi-simultaneous ground-based research using robotic systems and the largest telescopes made it possible to get new data shedding light to nature of the phenomenon, to establish relation between the bursts and supernovae explosions and, finally, to determine that gamma-ray burst are the most distant objects in the Universe for today. A remarkable review of the gamma-ray burst problem is presented in [1].

2.2. Gravitational-Wave Signals

In the field of gravitational-wave astronomy we are now approximately in the situation similar to that with gamma-ray burst research before operation of BeppoSAX: the researchers have already learnt to register them, but their position precision is still far for that necessary for reliable identification.

The era of direct registration of gravitational waves has begun right in front of our eyes, when at 9:15 on 14 September 2015 two detectors of gravitational waves built in the framework of the LIGO collaboration in Hanford and Livingston (USA) have got signals with a time lag of 7 milliseconds between them, as was predicted theoretically. It was denominated as GW150914. The theoretical apparatus developed long ago has permitted to explain the observed picture as the merging of two black holes of 36 and 29 Solar masses, the arising black hole is to have mass equal to 62 masses of the Sun. Energy released in the process of merging during tenths of a second is equivalent to about 3 Solar masses. Distance to the system where this phenomenon occurred is estimated as 1.3 billion light years. Since this event was detected only by two installations, there is no question of precise localization of the system – the GW150914 error box is about one thousand square degrees. There are some theoretical problems also: first of all, it is difficult to explain how a pair system of massive black holes could origin and live till our days.

By now, several other responses of gravitational-wave detectors were registered, which are already interpreted as a more acceptable scenario, when neutron stars are merging, but not black holes. Apparently, the situation will become clearer with a better localization of source

of gravitational waves, when several other similar detectors will come into operation. This will enable to get error boxes of several degrees and minutes, which will considerably accelerate their subsequent identification.

2.3. Neutrino Astronomy

As before, the neutrino astronomy counts the "caught" neutrinos by units, which also does not facilitate the further identification of their sources. It can be said that by now there is only one event (of course, beside generation of neutrinos in the interior of the Sun), which gave a noticeable signal. This is our nearest explosion of a supernova in the Large Magellanic Cloud galaxy at a distance of only 50 kpc from us, which is quite a small distance on an intergalactic scale.

The progress in construction of new neutrino telescopes is enormous, but, nevertheless, for the present the researchers can reliably get a significant neutrino signal only within a sphere of approximately identical size. Astrophysicists are inspired optimism that we will surely know when a supernova will explode in our Galaxy by getting neutrino signals from many underground, underwater and under-ice installations. We are separated from the most recent such explosion already by more than 400 years, so, it is time to fulfill the statistical law of supernovae burst rate.

The researchers are not only waiting for a supernova in our Galaxy, but also create more and more powerful installations with the hope to detect supernovae events in other galaxies also. The international neutrino observatories ANTARES, SuperKAMIOKANDE and especially ICECUBE keep enhancing their precision parameters achieving error boxes of several degrees. This allows us to hope for success in identification of such events due to joint efforts of the whole astronomical community. Baksan Neutrino Observatory can also give alert signals for optical identification, but, due to specific character of such investigations, this information is most often useful for observatories of the southern hemisphere, and we can only hope for targeting from, first of all, the ICECUBE installation operating at the southern pole of the Earth.

2.4. Fast Radio Bursts

The phenomenon of fast radio bursts (FRB), as well as sources of gravitational waves, is a discovery of the new century already. During several years (before 2013) the powerful millisecond pulses of radio emission (the flux of more than 1 Jy during less than 10 milliseconds) were considered to be of the terrestrial origin, but the experiment with the 64m radio telescope in Parks (Australia) has shown their not only extraterrestrial, but extragalactic nature. Due to the measured lag in the arrival of a pulse at different wavelengths, it is possible to estimate distance to a FRB source, which is hundreds and thousands megaparsecs (now the list includes more than 20 such bursts).

The fact that FRBs are still counted by unites is a consequence of small field of view of large radio telescopes. Allowing for their sizes, the expected number of fast radio bursts in the sky can be from 1000 to 10000 per day. Creation of new telescopes with large field of view equipped with multichannel radiometers will permit increasing their number many times, simultaneously enhancing their coordinate precision. So, in this field also, the united effort of astrophysicists-observers will be needed soon to identify such events quickly.

Speaking about a possible interpretation of such phenomenon, a good suggestion can be from the fact that the expected rate of fast radio bursts (about 0.001 per galaxy per year) coincides (or close with accuracy of one order) with the core-collapse supernovae explosion rate, which is about 0.01 per galaxy per year.

3. What Should Be Observed and with What Equipment?

As the multiyear experience of astrophysical research shows, the most complete information about phenomena under study is obtained from combination of data in the maximum wide spectral range. For all enumerated types of phenomena this means a required demand of optical identification.

So, the rate of expected events:

1. Gamma-ray bursts – 2-3 per week.
2. Gravitational events – several ones during recent 2 years.
3. Neutrino events – several ones per year.
4. Fast radio burst – less than 10 per year so far.

Apparently, we cannot hope for radical increase of the event number in the nearest years (maybe, except FRBs). The author still remembers enthusiasm among the researchers of gamma-ray bursts about multiple increasing of events after new missions HETE-2 and SWIFT were launched. Alas! The nature does not indulge us… So, the most probably, we will have to be satisfied with rare alerts, seeking to get maximum information about each event as soon as possible with available observational facilities in the so-called Target-of-Opportunity (ToO) mode.

What can the Russian ground-based astronomy answer to indicated challenges? At present, its armory includes mainly the long-time optical telescopes with nowadays-modest fields of view often with not too high-tech equipment.

Fig1. *General view of the complex MiniMegaTORTORA created jointly by a team of SAO RAS headed by G.M. Beskin, and specialists of OOO "Parallaks" (Kazan) with the financial support of Kazan (Privolzhsky) Federal University.*

So, at present, to study transient events in Russian observatories, the following research complexes in the shared-use mode are proposed (items 1-3 refer to SAO RAS):

1. The 6m telescope BTA equipped with complexes for spectroscopy and photometry with the field of view of 6 angular minutes, the method of fast photopolarimetry in a small field, but with a possibility of analysis at milliseconds times and better;

2. the 1m telescope Zeiss-1000 equipped with a CCD photometer with a set of wide-band filters with the field of view of 7′ and a low-resolution spectrograph with low penetrating power for such tasks;
3. a multi-channel wide-angle complex of subsecond temporal resolution MiniMegaTORTORA having the field of view of 900 sq.degrees and the limit stellar magnitude about 11.5 during exposure of 0.1 sec. The general view of the complex is presented in Fig1.
4. the 2m Russian-Ukrainian telescope Zeiss-2000 of the Terskol Branch of Institute of Astronomy of RAS equipped with a CCD photometer with the field of view of 11′ and a moderate-resolution spectrograph;
5. the 2.6m Shajn telescope of the Crimean Astrophysical Observatory equipped with CCD photometers with the fields of view of 9′ and 20′.

Observational time of these telescopes is allocated by the Russian Telescope Time Allocation Committee, and the details description of instruments is given in Circulars of the Committee [2]. Beside these telescopes in Russia there are a number of optical telescopes of the class of 1-2 m, which are under the authority of scientific and educational organizations.

Among promising projects of the nearest future useful for solution of the indicated tasks, we can mark out a complex of small telescopes of 0.5 m diameter with field of view of several degrees (the perspective view of the site area is shown in Fig2, now the construction of the first telescope with the observing hut-outhouse is being carried out), a photopolarimeter of the 1m telescope and a fast photopolarimeter of “hot reserve” of the Nasmith-1 focus of the 6m telescope. These projects are being conducted in SAO RAS and are close to their implementation.

Fig2. *The design view of a complex of small 0.5m telescopes after completion of construction. The authors of the project are a team of SAO RAS researchers headed by S.N. Fabrika and G.G. Valyavin, OOO “Parallaks” (Kazan).*
Financial support is from a grant of Russian Scientific foundation №14-50-00043.

4. The project of a survey wide-field telescope

Among new infrastructure projects, which are urgent for successful operation in the framework of alert programs, one should mark out a project of a large-aperture telescope of the 4m class equipped with gigapixel mosaic detectors.

Since there is no proper project we give here a brief description of initial technical requirements of such a telescope.

The main tasks for the instrument are supposed to be the study of transient sources: gamma-ray bursts, supernovae explosions, neutrino events, fast radio bursts, the fulfilling of deep surveys with a set of medium-band filters for studying samples of active galactic nuclei, massive identification of sources, which will be detected by the cosmic mission SRG, the mapping of the Galaxy plane in emission lines of ionized gas, the surveys of the sky in polarized light, etc.

The main characteristics of the telescope:

- altazimuth mounting;
- the optical scheme – quasi- Ritchey-Chrétiens;
- diameter of the main mirror – about 3.5 (4) m;
- the mirror material – sitall CO-115M (Zerodur);
- focuses – Cassegrain, 2(4) Nasmiths;
- the operational spectral range: 0.35 – 1.7 (2.5) microns;
- angular resolution – not worse than 0″.5;
- the operational field – 2º (it is desirable up to 3 º).

An important feature of the project is the system of adaptive optics, a system of adaptation of wave front in a small field. Among other things, the effective operation of the telescope supposes introduction of technology of high-performance reflecting coatings with the reflectance factor up to 97% in a wide range.

The supposed equipment: in the Cassegrain focus – a mosaic of 20k×20k el (optics) and 8k×8k (IR) for photometry in wide fields; in the Nasmith focus it is supposed to install an integral field spectrograph and a scanning Fabry-Perot interferometer; the creation of a multi-object spectrograph for 300-500 objects is also possible.

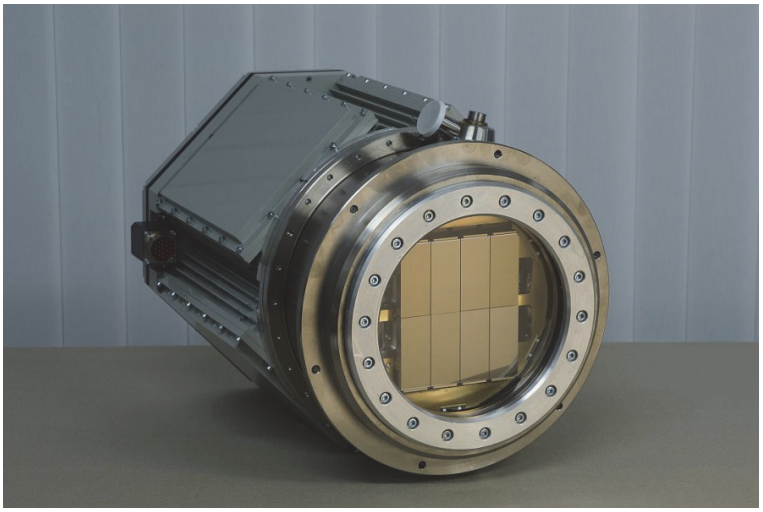

Fig3. *A prototype of the large-format mosaic detector created in SAO RAS by the Advanced Design Laboratory under the direction of Cand.Sc.(Engineering) S.V. Markelov.*

Among possible prototypes of such an instrument there is the 4.1-m telescope VISTA operating in the European Southern Observatory. The time of its creation is estimated as 2018-2023. The cost will about 3.5-4 billion roubles based on current prices.

Among technical facilities already available in SAO RAS one can mark out the available groundwork for creation of large-format mosaic detectors of optical emission. One of specimens of such systems is shown in Fig3.

5. Methodology for studying alert events

We consider the space missions Swift, Fermi, INTEGRAL, Lomonosov and others as a source of alert information. The alerts from the MiniMegaTORTORA system are quite possible. In addition to that we also aim at the search for optical components of source of neutrinos and gravitational waves (GW events) detected with neutrino observatories and with detectors of LIGO (Laser Interferometer Gravitational-wave Observatory) and Virgo.

The fulfilling of research is a part of the program carried out by an international observational collaboration including the observatories обсерваторий Calar Alto (Spain, 2.2 and 3.5 m for direct imaging and spectroscopy), La Palma (Spain, the telescopes of the 1-2m class for photometry, the 4.2m and 10.4m GTC for photometry and spectroscopy), Nainital (India, the 1.0m and 1.3m optical telescopes for direct imaging), Campo-Imperatore (MAO RAS, Italy), AZT-24 for photometry in the near IR.

Execution of work supposes 3 stages of the research involving different telescopes and instruments:

Stage 1: identification and improvement of coordinates with the 1m and 2m telescopes in the photometric mode, for very rough error boxes – identification with MiniMegaTORTORA, which results in prompt transfer of coordinate information to BTA and other large telescopes.

Stage 2: the study: photometry in the BVRcIc bands with the 1-2m telescopes up to R~22, BTA – the spectroscopy of objects brighter than R~22 in the range 350-950 nm for determination of red shift of a source and obtaining absorptions in the line of sight, resolution depends on the source brightness, the fast photometry and polarimetry with complexes of fast variability in the first minutes and hours after a burst, then – the photometry with the deep limit up to R~25.

A CRITICAL MOMENT: photopolarimetry for determination of the collapse geometry, the polarization value is expected to be of order of 10%.

Stage 3: Photometry and low-resolution spectroscopy with BTA and GTC of different phases of the source evolution – the appearance of the secondary maximum brightness, spectral peculiarities of supernovae.

Unfortunately, this strategy is good for identification of sources with good error boxes, which are gamma-ray bursts now. Her our advantage is a fast reaction to alerts of different types and our geographical position. In case of sources of othe types the coordinate precision is not sufficient yet; the telescopes with large fields and good limit are necessary.

6. Conclusion

1. For reliable identification of transients (from gamma-ray, radio, neutrino and gravitational sources) the coordinated optical observations are necessary.

2. In whole, equipment of SAO and other Russian observatories is ready to observations of transient sources of a new class.

3. The successful realization of the projects demands a wide international cooperation and implementation of plans for development of instrument basis, what we are going to do all together.

References

[1] Vedrenne G. and Atteia J.-L., Gamma-Ray Bursts The Brightest Explosions in the Universe, Praxis Publishing Ltd., Chichester, UK, 2009

[2] The web-resource www.sao.ru/hq/Komitet/circ.html

Formation scenarios of strange quark stars

Grzegorz Wiktorowicz[1],*, A. Drago[2], G. Pagliara[2], and S. Popov[3]

[1]Astronomical Observatory, University of Warsaw, Al. Ujazdowskie 4, 00-478 Warsaw, Poland;
gwiktoro@astrouw.edu.pl

[2]Dipartimento di Fisica e Scienze della Terra dell'Università di Ferrara
and INFN Sezione di Ferrara, Via Saragat 1, I-44100 Ferrara, Italy

[3]Sternberg Astronomical Institute, Lomonosov Moscow State University,
Universitetsky prospekt 13, 119234, Moscow, Russia

Abstract The first sentence of the Abstract should follow the word "Abstract". The abstract should be clear, descriptive, self-explanatory and no longer than 400 words. It should also be suitable for publication in abstracting services. Do not include references or formulae or special character in the abstract.

Keywords: methods: statistical – stars: neutron – stars: peculiar – X-rays: binaries

1. Introduction

Strange quark stars (QS) are defined as being composed of strange quark matter, i.e. built of three quarks: up, down, and strange. A neutron star (NS) built of hadronic matter may be perceived as metastable object which converts into a QS when a significant number of hyperons form in its interior. According to the two-families scenario (Drago et al. 2015), when a NS reaches a threshold internal density a deconfinement process occurs, which may have a duration of only 10 seconds. As a result, entire stars becomes a QS and a gravitational mass is significantly lowered (by about 10%), although the barionic mass is conserved.

The two-families scenario therefore predicts that NSs and QSs may coexist in stellar populations. Below a minimal QS mass compact object may be only a NS, whereas above maximal NS mass, only QSs are possible. Between these two limiting values, both Nss and Qss may be present (coexistence range).

A QS in this scenario may form either directly after a supernova explosion (SN), or as a result of a mass accretion onto a NS. In both cases a QS may accrete additional matter and obtain mass significantly above 2 $M_{\odot}$. In the coexistence range we expect more objects in the two-families scenario, then in the one-family scenario, i.e. case in which only NSs exist and QSs are never formed.

In this study, we analyze QS formation routes in the two-families scenario on the base of the results obtained by Wiktorowicz et al. (2017; hereafter W17). Sec. 2 concentrates on theoretical formation scenarios. Sec. 3 briefly describes the methods. Sec. 4 contains results. In Sec. 5 we summarize the paper.

2. Formation scenarios

According to the two-families scenario, a NS becomes a QS when a central density reaches values high enough for hyperons' formation. However, the exact value depends on the applied physics. Therefore, in W17 it was assumed that a NS converts immediately into a QS when a mass threshold is reached. An exemplary conversion is presented in Fig. 1. Two values for deconfinement mass were tested: 1.5 $M_{\odot}$ and 1.6 $M_{\odot}$, which correspond to the non-rotating and strongly rotating NS, respectively.

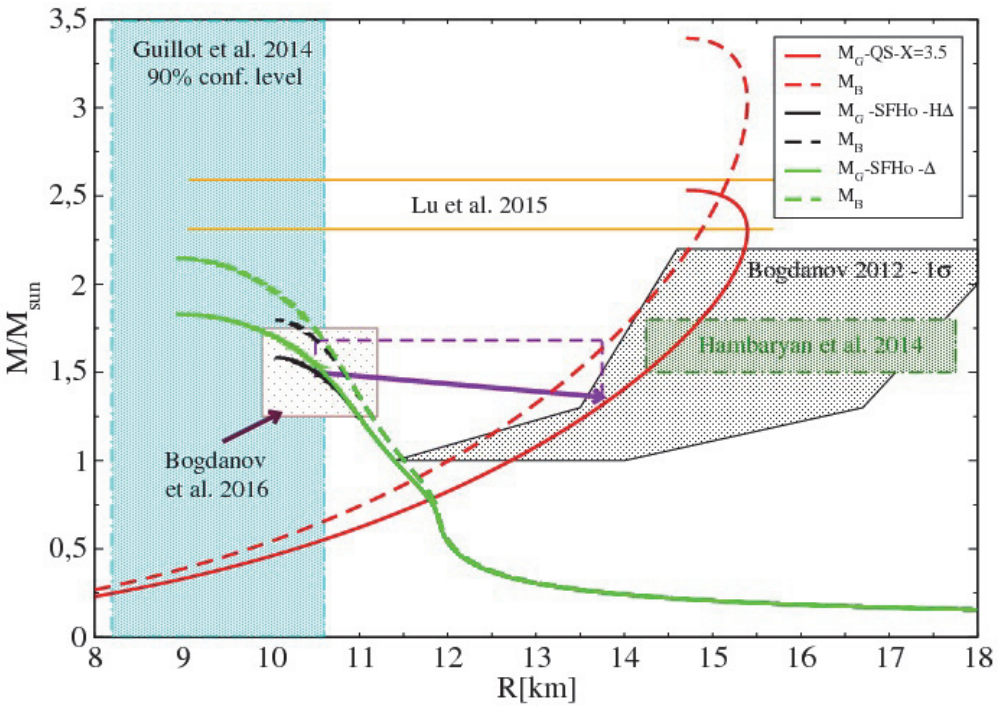

Fig1. *Equation of state for barionic matter (green) and strange quark matter (red). Masses of barions are marked with dashed lines and gravitational masses with continuous lines. A purple line shows an exemplary transition for a star which reached a limiting mass of 1.5 $M_{\odot}$. Figure from Wiktorowicz et al. (2017).*

In such a scheme, QSs in binary systems may form in three ways:

1. QS may form without any interaction,
2. one of the stars in a binary may at first form a NS and later, due to mass accretion, become a QS, or
3. a massive star may lost mass and instead of becoming a black hole, become a QS.

A very important aspect is the natal kick, which may disrupt a binary during supernova (SN) explosion. It is important only during the NS formation, as during the conversion into a QS, only the Blaauw kick (Blaauw, 1961), connected with the change of gravitational mass, is present. An exception is the situation when the post-SN mass of a NS is already above the threshold and a QS forms without additional mass accretion. Recent observations show that the binary fraction for massive stars (>10 $M_{\odot}$) is reaching nearly 100%. As QS may form only from such massive objects, probably all single Qss, if they exist, originate from disrupted binaries.

The natal kick is also extremely important for the formation of double QS, which are a probable source of strangelets. Two SNs can easily disrupt the binary, so a strong interactions between the stars are necessary in order to form a double QS. Indeed, W17 found a small amount of such objects for moderate metallicity only.

3. Modeling

In W17 a population synthesis study using the startrack code (Belczynski et al. 2002,2008) was performed. The aim of it was to investigate a population of QSs in different types of environments and see if it is possible to detect the existence of the two-families of compact objects in the coexistence zone.

For every model a population of 2 million binaries was simulated from the initial parameter space of X-ray binaries (see W17 for details). Calculations were performed with a use of Universe@Home distributed computing project.

4. Results

QSs may form as well in solar metallicity environment, as in 1% solar. The fraction of QSs never exceeds 5% of all compact objects with masses below 2.5 $M_{\odot}$. A significantly larger fraction, reaching 26% in some models, was observed in results for low-mass X-ray binaries (LMXB). Such accreting systems may efficiently increase mass of accreting NSs bringing them to the threshold for QS formation. It must be noted, however, that after the formation of a QS, a mass transfer may stop due to change in orbit resulting from the rapid change of gravitational mass of the accretor.

A typical route leading to the formation of a QS in a binary system is presented in Fig. 2. The initial parameters are similar to these for X-ray binary (XRB) progenitors. The primary is 7.2 $M_{\odot}$ on zero-age main-sequence (ZAMS), whereas the companion is about the solar mass. The primary evolves quicker and expands, fills its Roche lobe (RL), and commences a common envelope (CE) phase after about 50 Myr. The post-CE mass is too small to for a Nss, so a primary becomes a heavy white dwrf (WD; ~1.3 $M_{\odot}$). The secondary evolves longer but after about 5 Gyr being a RG fills its RL and starts a mass transfer (MT) onto a WD, which shortly after collapses to a NS. The companion refills the RL and restarts the MT. As only the NS reaches the deconfinement mass, it converts into a QS. A blaauw kick widens the orbit and typically no additional MT occurs.

Actually, most of the system (>90%) will be disrupted during the QS formation. It may be a consequence either of the NS formation, or the QS formation. A predicted formation rate of QSs in the Milky Way (MW) galaxy is between 11.6 and 23.9 per Myr. It is important to note the the general scheme of the QS formation is the same for all metallicities and two deconfinement masses.

In order to form a LMXB with a QS, i.e. system with a QS which accretes matter from the companion, the initial configuration needs to be different (Fig. 3). In such a case, the secondary is more massive (~4 $M_{\odot}$). As a result, the first MT from the secondary is unstable and leads to a second CE. Afterwards, a WD - helium star (HeS) system forms on a very short orbit of about 0.6 $R_{\odot}$. Companion fills the RL due to expansion on Helium MS and, after a phase of M, the WD forms a NS. HeS refills the RL and restarts the MT. After 20 Myr, the NS becomes a QS and the HeS becomes a WD. The orbit is short enough for the emission of gravitational waves to decrease the separation to the value in which a WD fills the RL. As a result, a MT onto a QS commences. We obtain a typical LMXB with a QS accretor.

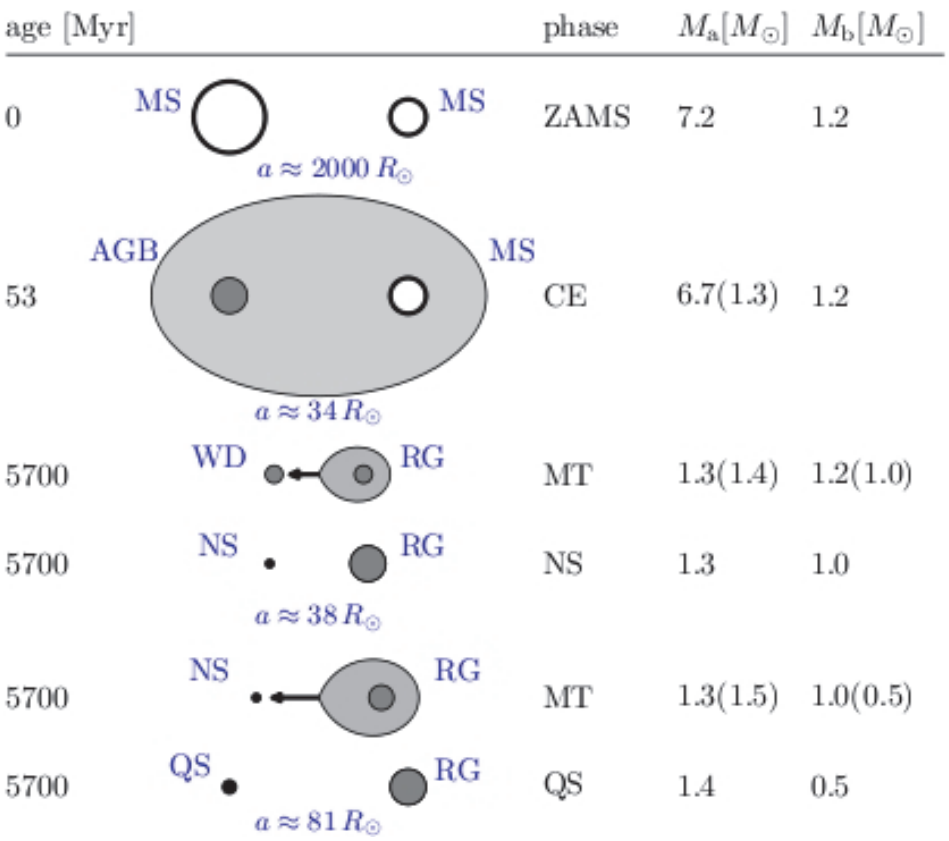

Fig2. *Typical binary evolution leading to the formation of a quark star. Abbreviations stay for: ZAMS – Zero Age Main Sequence; MS – Main Sequence; AGB – Asymptotic Giant Branch; CE – Common Envelope; WD – White Dwarf; RG – Red Giant; MT – Mass Transfer; NS – Neutron Star; QS – Quark Star. Time (left column) is provided in million years and masses (right columns) are provided in solar mass unit. See Sec. 3.2 for further details. Figure from Wiktorowicz et al. (2017).*

Despite some similarities, the formation route for QSs in LMXBs is different than the one for QSs in general. However, QSs in LMXBs are relatively more frequent than QSs in binaries in general. About 3-18% of QSs were found to reside in LMXBs according to the results of W17.

A very interesting result was presented in W17 for double QSs. Such systems may be formed only in moderate metallicity (10% $Z_\odot$) environment. What is more, the predicted merger rate for these objects is too small to trigger the strangelets pollution in the MW. It was estimated to be about 12 per Myr for the galaxy.

Typically, a double QS will form from a massive binary consisting of a 24 $M_\odot$ and 23 $M_\odot$ stars on ZAMS. The primary will evolve and expand while being on core Helium burning (CHeB) and start a MT. It will quickly lose the envelope and form a HeS. Shortly afterwards, the secondary expands on CHeB and fills its RL. However, this time the other star is to light and a CE occurs. As a result, the separation shrinks significantly. Afterwards, both stars undergo a SN and form directly QSs. The binding energy is high enough to keep the remnants bound. A typical time to merger is 8.6 Gyr.

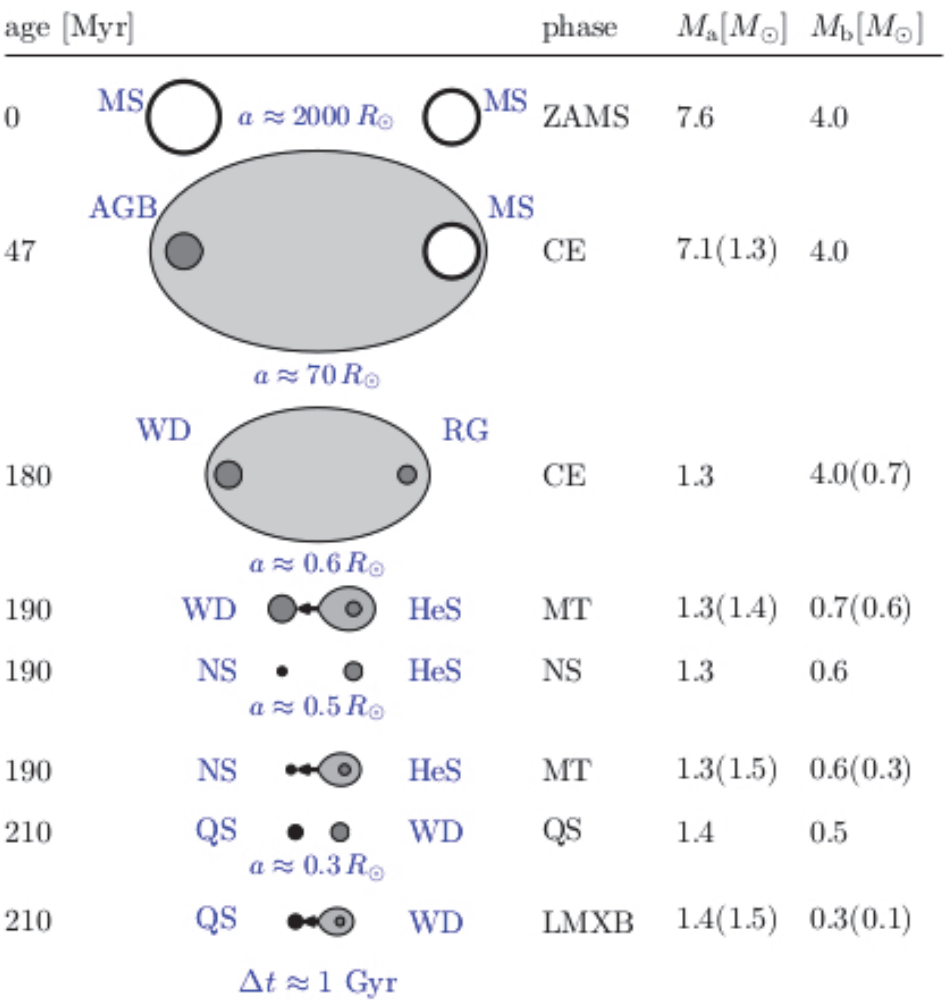

Fig3. *Typical evolution leading to the formation of a low-mass X-ray binary with a quark star accretor. The abbreviations and columns are as in Fig. 2 with additionally: LMXB – Low Mass X-ray Binary.*

5. Conclusion

A population synthesis is a very powerful tool for investigation of QSs in stellar systems. The most important results of Wiktorowicz et al. (2017) presented in this paper may be summarized as follows:

- Quark stars form typically through accretion onto a neutron stars.
- Most of quark stars are single, even though all of them probably originate from binary stars.
- Measurements of compact objects' masses are too few to reject or prove the two-families scenario.
- The rate of double quark star mergers in the Milky Way galaxy are too low to trigger deconfinement in all neutron stars.

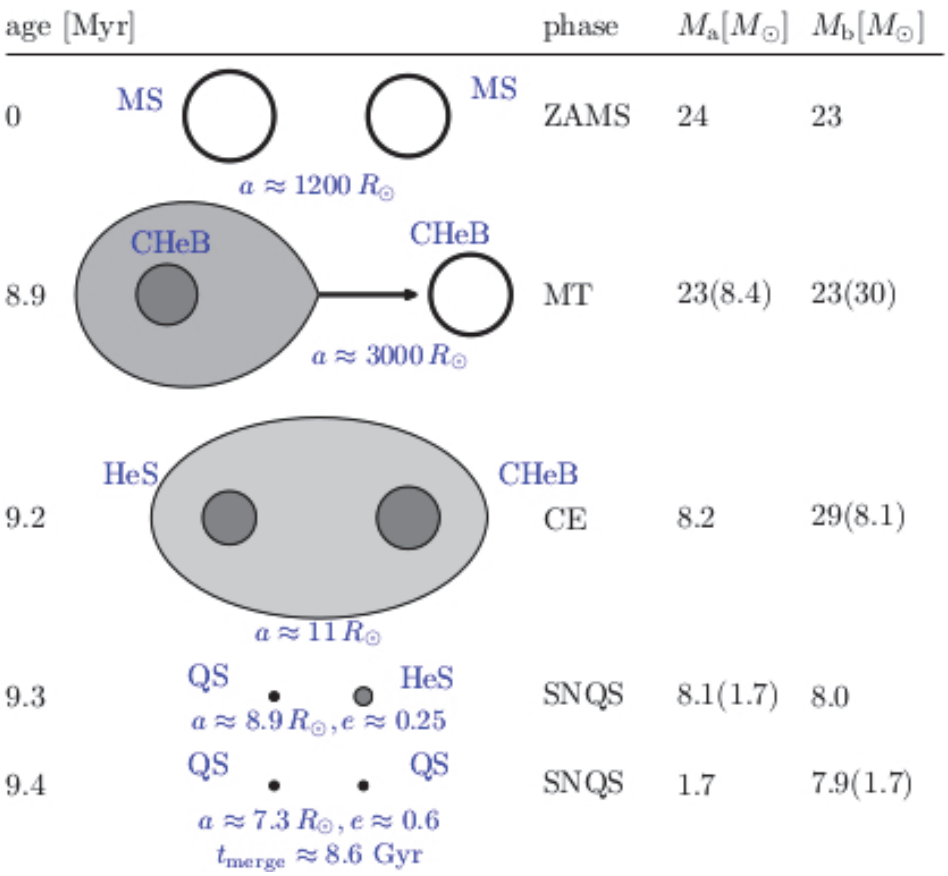

Fig4. *Typical evolution leading to the formation of a double quark star. The abbreviations and columns are as in Fig. 2 with additionally: CHeB – Core Helium Burning; HeS – Helium Star; SNQS – Quark Star formed directly in SuperNova explosion.*

References

[1] Belczyski et al. (2002) http://adsabs.harvard.edu/abs/2002ApJ...567L..63B

[2] Belczynski et al. (2008) http://adsabs.harvard.edu/abs/2008ApJS..174..223B

[3] Drago et al. (2015) http://adsabs.harvard.edu/abs/2015PhRvC..92d5801D

[4] Wiktorowicz et al. (2017; W17) http://adsabs.harvard.edu/abs/2017ApJ...846..163W

[5] Blaauw (1961) http://adsabs.harvard.edu/abs/1961BAN....15..265B

Development of a scintillation detectors based on the SiPM matrices: current status and prospects for the large volume neutrino detectors

A.F. Yanin[1], I.M. Dzaparova[1,2], E.A. Gorbacheva[1], A.N. Kurenya[1], V.B. Petkov[1,2], A.V. Sergeev[1,2]

[1] Baksan Neutrino Observatory, Institute for Nuclear Research of the RAS, Neutrino, Russia; yanin@yandex.ru

[2] Institute of Astronomy of RAS, 119017, Moscow, Russia, Pyatnitskaya str., 48

Abstract The matrices of silicon photomultipliers (SiPM) are promising multichannel photosensors for scintillation detectors. They can be used to reconstruct tracks of relativistic particles inside the detectors. The paper presents the first developments of detectors with direct contact of the SiPM matrices with the surface of a scintillation detector and with the use of Fresnel lenses, and also promising variants for large detectors of neutrino astrophysics and geophysics are proposed.

Keywords: matrices of silicon photomultipliers, charge-digital converters, VME standard, Fresnel lenses.

1. Introduction

In many areas of experimental physics, related to the collection of information in multichannel systems, silicon photoelectron multipliers (SiPM) are used instead of traditional vacuum photomultipliers. Silicon photomultipliers have many advantages over vacuum: insensitivity to magnetic field; high efficiency photon; compactness and mechanical strength [1-4]. The low power supply and the high gain of the SiPM (10^5-10^7) can greatly simplify electronic data readers. Performance and affordable cost make it possible to widely use SiPM in high-energy physics when creating detectors with a large number of photodetectors. An example of the mass application of the SiPM is the neutrino experiment T2K. In this experiment in the scintillation counters of various detectors, about 60,000 SiPMs are used as photodetectors [5]. For such large-scale projects, specialized multi-channel data acquisition systems based on special programmable microcircuits are being developed [5,6].

The development of production technologies for silicon photodetectors of increased area led to the creation of monolithic matrices of SiPM, which are used in positron emission tomography [7, 8]. Currently, SiPM and the matrices of them are widely used in nuclear medicine. Compared with the data collection systems used in high-energy physics, in nuclear medicine, in spite of the relatively small number of channels, data collection systems based on specially developed microcircuits also are used to read information [9].

In recent years, the matrices of SiPM have been widely implemented in gamma astronomy of superhigh energies [10]. When designing new telescopes of the camera (matrix) from vacuum photomultipliers, on which the Vavilov-Cerenkov light radiation is focused from the

particle flux, they are replaced by matrices from the SiPM For experiments, both monolithic matrices and individual SiPMs are used. For example, the matrix of the Cherenkov telescope FACT is made of 1,440 separate Hamanatsu MPPC S10362-33-50C [11]. The camera of the telescope of ASTRI is assembled of 16 monolithic matrices of Hamamatsu S11828-3344m, each of which consists of 16 individual SiPM [12]. For each experiment, specialized multi-channel data acquisition systems based on the developed microcircuits have been created. The matrices of the SiPM are promising multichannel photodetectors of scintillators. Using such matrices, it is possible to select and study events in different parts of the scintillator [13]. For this purpose, the authors propose to use ArrayC-60035-64P-PCB (SensL, Ireland) consisting of 64 single SiPM C-series [14]. The substrate of such a matrix made of fiberglass. Board ABL-ARRAY64P-HDR [15], with 64 channels, is designed to amplify and read the signals from each of SiPM matrix.

2. The characteristics of scintillation detector with SiPM matrices

2.1. Objectives and results

At the Baksan neutrino observatory, a detailed study of this matrix and the development of prototypes for small detectors were carried out: with direct contact of the matrices with the surface of the plastic detector and using Fresnel lenses (***Fig 1***). Before the developers, the task was to build tracks of muons through detectors. For the realization of task was preliminarily developed and created the multichannel measuring system for the data collection from the matrices from the silicon photomultipliers into standard VME, which is in detail presented in [16]. A part of the electronics was developed and assembled on its own (128-channel delay line, master pulse generation circuit, plastic detector, etc.), and the main electronic units were

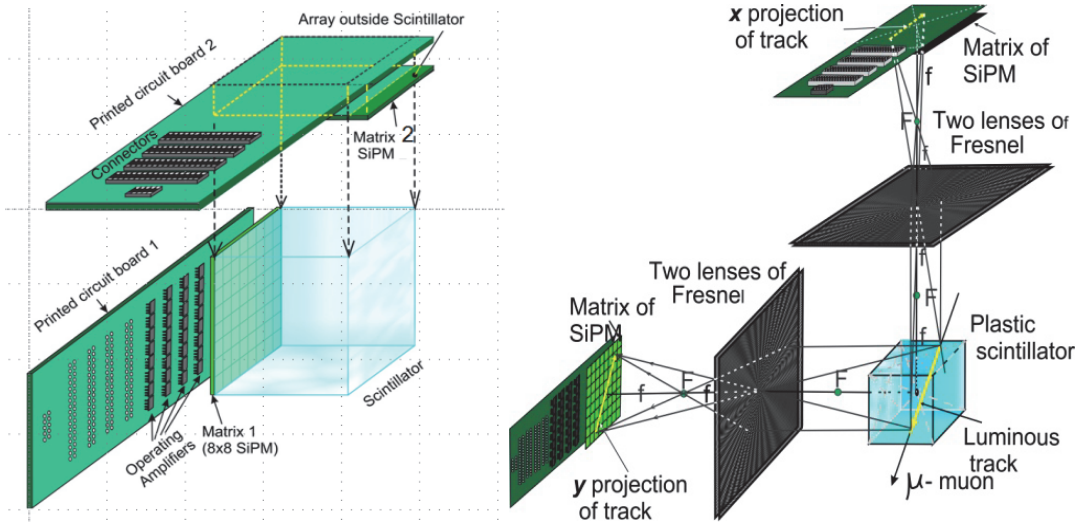

Fig1. *Left: scheme of experiment with direct contact of matrices with a scintillator. Right: working variant of a prototype of a scintillation detector with silicon photomultipliers using Fresnel lenses.*

purchased (industrial computer, VME crate, two SiPM matrices, charge-sensitive converters (QDC) and etc.). For the experiment with direct contact of the matrices with the scintillator (***Fig1, left***), the resulting tracks are shown in ***Fig2 a, b, c***. For an experiment using Fresnel lenses (***Fig1, right***), the tracks are shown in ***Fig2 d, e, f***. Width of tracks for the first case, generally, wider since there is no focusing of photons.

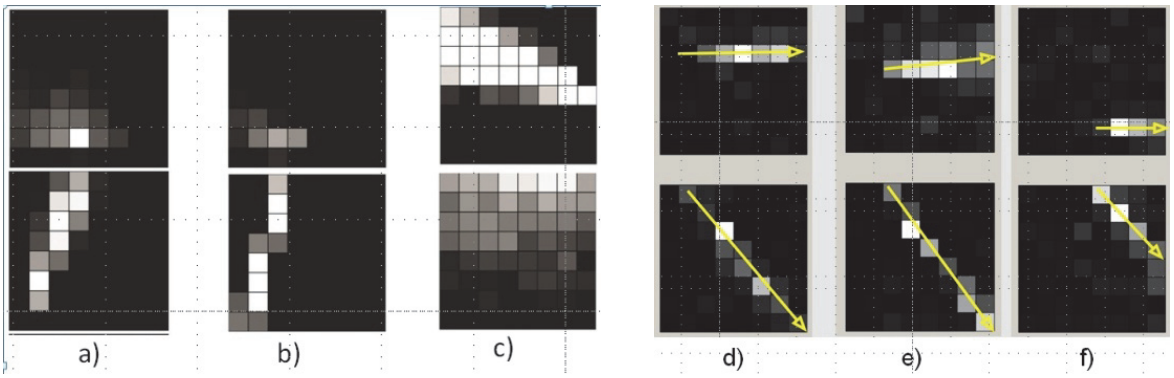

Fig2 a,b,c. *- tracks obtained for the experiment with direct contact of the matrix with the detector.* ***d,e,f*** *- tracks obtained for the variant with the use of Fresnel lenses.*

When placing an object (in this case a detector) at a distance of more than 2 focal lengths from the lens, the image size is reduced (Fig3). For this reason, the size of the detector can significantly exceed the size of the matrix. The most sharp parts of the object can be focused only on a certain distance. But since the object has extended geometric dimensions, then the focusing deteriorates to the near and far edge of the detector. For example, in Fig3 the defocusing for near edge of the detector of 118x118x118 mm^3 in size will be equal to 3.86 mm, that it is much less than the SiPM size (for the far edge the defocusing will be less – 3.06 mm). The size of the detector with Fresnel lenses can be reduced by lowering the focus requirements, because even with poor focusing, the center of the track can be determined by mathematical processing.

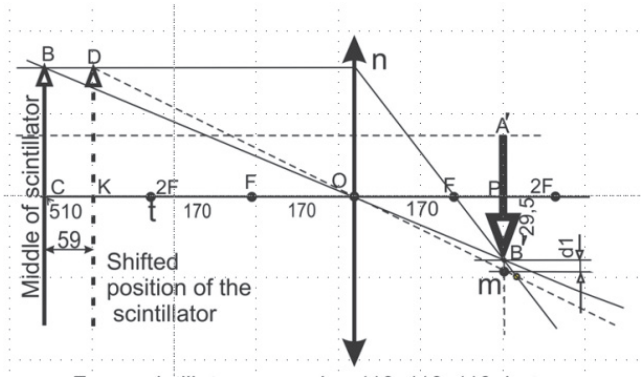

Fig3. *Depth of focus for scintillator size 118x118x118 mm.*

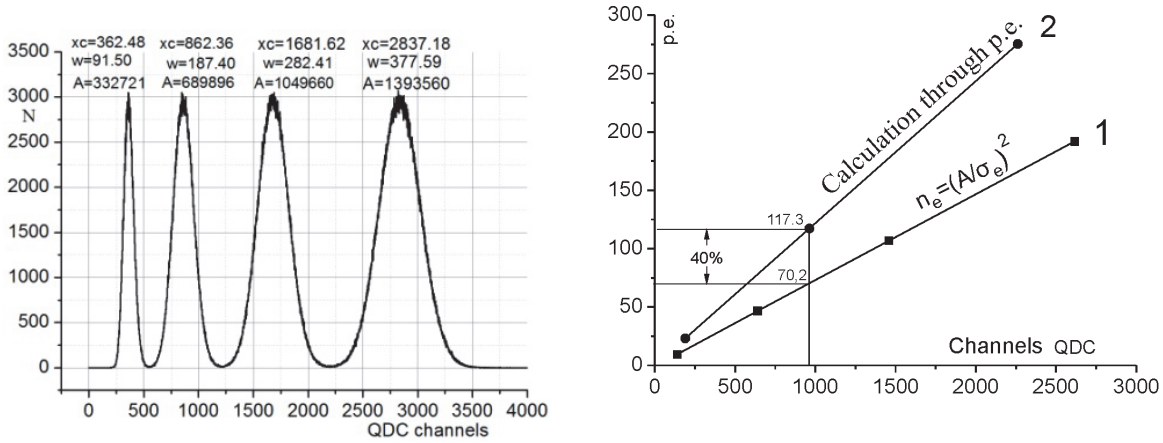

Fig4. *Left: the spectrum of SiPM with the fixed flows of the photons. Right: calibration of SiPM. 1-calibration by method 1, 2 - calibration by method 2.*

2.2. Calibration

Two methods of calibration were used.

1) Using a blue LED emitting light with a wavelength of 430 nm (which agrees well with the wavelength emitted by the scintillator used), stable fluxes of photons (but different in intensity) were fed to the SiPM matrix. Data was processed using QDC (***Fig4, left***). The QDC was run during the duration of the trigger signal for 225 ns, which is slightly longer than the pulse duration coming from the SiPM matrix. The formula (1) was applied to the obtained data and plotted 1 (***Fig4, right, line 1***).

$$n_e=(\bar{A}/\sigma_e)^2 \tag{1}$$

n_e – is the average number of photoelectrons, $\bar{A}$ – is the mean value of the charge obtained with a constant flux of photons, σ_e – is the root-mean-square deviation of charges depending on several parameters.

$$\sigma_e^2 = \sigma_s^2 + \sigma_{led}^2 + \sigma_{q.e.}^2 + \sigma_{i.\text{-}p.g}^2 \tag{2}$$

where σ_s –mean-square deviation caused by the variation of the photon density in *space* in the direction investigated SiPM. This option is basic and will occur even for the case where the led emits a stable number of photons in each pulse generator; σ_{led} - root-mean-square deviation caused by the variation in the number of photons emitted by the *LED*; $\sigma_{q.e.}$- the root-mean-square deviation due to the *quantum efficiency* of the SiPM; $\sigma_{i.\text{-}p.g}$ - root-mean-square deviation due to the presence of inter-pixel gaps (not all the photons moving in the direction investigated SiPM reach the active zone – part of the photons falls in the– *inter-pixel gaps*). The parameters σ_s and σ_{led} are the main.

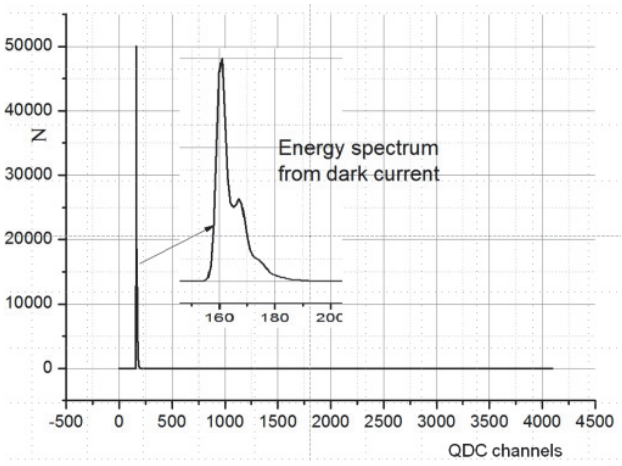

Fig5. *Spectrum of SiPM in the absence of photons.*

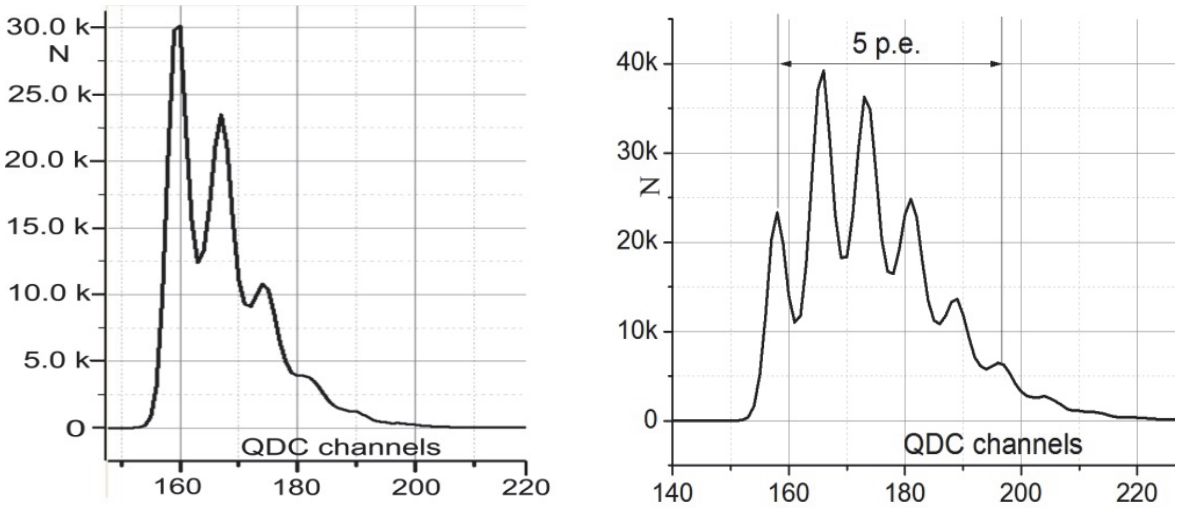

Fig6. *Dependence of the number of photoelectrons on the charge upon additional irradiation with photons. Left: - in addition to the dark current a small amount of photons (n) is added. Right: the number of photons is n + m*

2) The second method is more complex, but it is more precise. It was noticed, that in the energy spectrum of SiPM in the conditions of only dark current the weakly expressed photon maximums appear (***Fig5***). If additionally the matrix of SiPM irradiated by photons, then maximums appear much clearer (***Fig6, left***). If the photon flux still slightly increases, the peaks appear even better, but the relative number of low-electronic events (for example, one-electron or two-electron events) may decrease. (***Fig6, right***). From this figure it is possible to find how many channels QDC in the single photoelectron. ***Fig7*** shows the number of photoelectrons as a function of the number of channels for all SiPMs of both matrices. Channel 6 (SiPM 6) of matrix 2 is defective. And in ***Fig4, right*** curve 2 shows the dependence of the number of photoelectrons on the charge for SiPM 65. The sensitivity is approximately 40% higher than for the first method. The difference can be explained as follows.

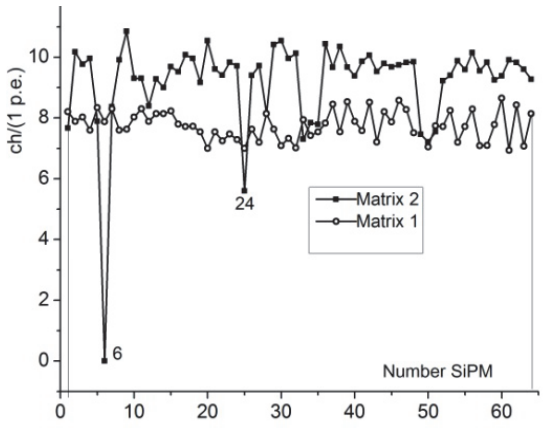

Fig7. *Dependence of the number of QDC channels per 1 p.e. for each SiPM of both matrices.*

If we eliminate at least one parameter from the total root-mean-square deviation σ_e, for example, σ_{led}, then the width of the peaks for both ***Fig4, left*** and for ***Fig6, right*** decreases, and the number of photoelectrons, according to formula 3, increases. Thus, the slope of line 1 from ***Fig4, right*** will increase. For ***Fig6, right***, the width of the peaks will also decrease, but the inter-peak spacing will not change, ie the sensitivity in photoelectrons is always the maximum.

$$n_e = \vec{A}^2/(\sigma_e^2 - \sigma_{led}^2) \quad (3)$$

But because the σ_{led} parameter is unknown, formula 1 is applied as an estimate. It is also useful in a relatively large flux of photons when individual peaks in the spectrum are no longer distinguishable.

2.3. Prospects

A large detector for the Baksan neutrino observatory is also being developed at the Institute for Nuclear Research of the Russian Academy of Sciences in order to study natural neutrino fluxes in geo- and astrophysics (Fig8). The estimated volume of the detector is 5-20 kt. Our theoretical calculations [17] allow us to conclude that it is possible to register short tracks. For example, for a detector with a scintillator mass of 5 kt with a lens aperture of 2000 cm^2 and a track length of 1.2 cm, one photoelectron can be registered at the center of the detector (the sensitivity of our data collection system is not worse than 6 channels per 1 photon (see Fig7), which should allow to record such events even taking into account optical losses). In practice, it is problematic to use Fresnel lenses for obtaining a large aperture due to of the large dimensions of the optical system. Initially, it was planned to collect photons using a truncated cone with a reflective inner surface. But as can be seen from Fig9, most of the photons do not reach the exit hole of the cone because with each reflection from the walls of the cone the angle of reflection increases (up to the unfolding of the photons in the opposite direction). For some photons, the angle $\alpha < \beta < \gamma$. To solve this problem, it is proposed to place a Fresnel lens with a focal length F at the beginning of the cone. At the point of focus place a fiber bundle with a polished end or a special matching optical adapter (Fig10). Not only photons moving parallel to the axis of the cone, but also at some angle to the axis, will enter the optical fiber entry zone.

Depending on the direction of arrival of photons, the point of their focusing will be slightly closer or slightly farther than the point F. This is because the photons in the inner walls of the truncuted cone near the exit hole will be reflected directly in the fiber. For large apertures you can take a relatively small cones and cascade them with the optional cone with fiber. In Fig10 shows how 4 truncated cones are combined along the Y coordinate and the total signal is transmitted to one of the silicon PMT matrices. The summing cone can be placed in a convenient place (even at a great distance) because of signal attenuation in the optical fiber at a distance of tens of meters virtually no. The same applies to the SiPM matrix. Thus, it is possible to generate almost any aperture with small dimensions of the cones. The response time of a silicon photomultiplier subnanosecond, so with proper electronics it is possible to obtain a temporal resolution of detectors better than 1 ns.

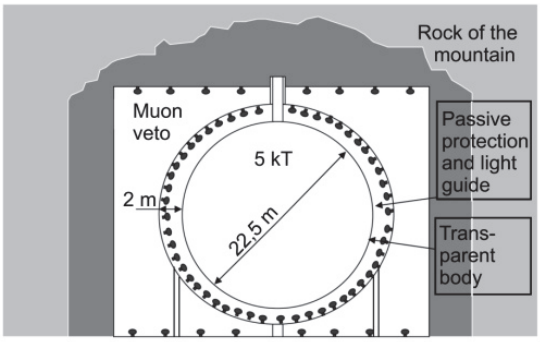

Fig8. *The large detector for the Baksan neutrino observatory with the aim of studying the fluxes of natural neutrinos in geo- and astrophysics.*

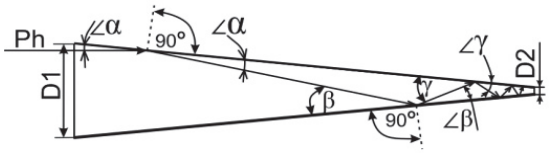

Fig9. *Passage of a photon inside a truncated cone with a reflective inner surface.*

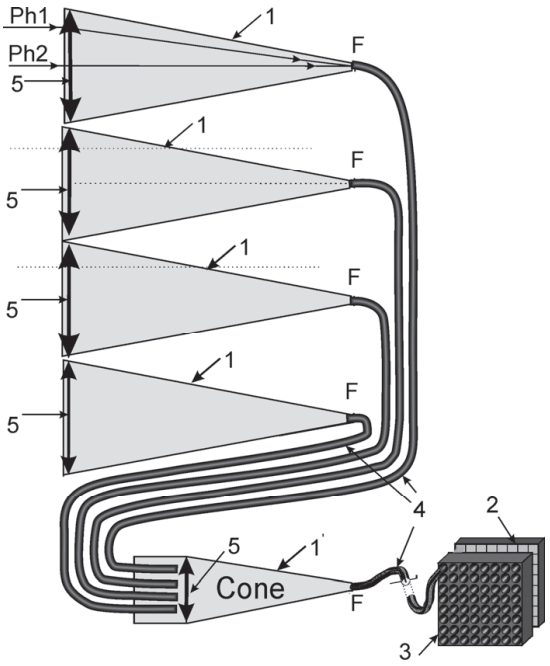

Fig10. *Cascading truncated cones to obtain a large aperture: Ph - photon, 1 - truncated cone, 1 '- summation cone, 2 - SiPM matrix, 3 - mechanical interface matrix, 4 - fiber bundles, 5 - Fresnel lens, F - focal length.*

3. Conclusion

- By direct contact of the matrices with the scintillator, there is a limit on the size of the detector. The use of the optical system removes this restriction. This improves the ratio signal/noise.
- We used a Fresnel lens made of optical acrylic with a threefold increase with the size of A4. Such mass production of lenses are available, inexpensive, and can have a large size.

- The depth of sharpness of the optical system suffices, that light track on a matrix had a width less size one SiPM, that confirm the brought pictures over with the use of the optical system.
- The experiments with optic were performed with a detector the size of 50x59x59 mm^3. We plan to increase the size of the scintillator to 500x500x500 mm^3.
- There are good opportunities for using cascaded truncated cones with Fresnel lenses for detectors of a kiloton class.
- It is possible to use 3-D printers to manufacture of cones. Additionally, in a single process can produce all needed fixing.

Acknowledgements

This study is performed with a part of the instrument certified as a Unique Scientific Facility (Baksan Underground Scintillation Telescope) and at an office that is an item of the Shared Research Facilities state program (Baksan Neutrino Observatory of the Institute for Nuclear Research). The work was carried out at the Center for Collective Use of Baksan Neutrino Observatory of the within the framework RFBR grant 14-22-03075 of the project "Development and Creation of an Experimental Scintillation Detector with a Photodetector Based on Matrixes from Silicon Photomultipliers."

References

[1] Buzhan P., Dolgoshein B., Filatov L., Ilyin A., Kantzerov V., Kaplin V., Karakash A., Kaumov F., Klemin S., Popova E., Smirnov S. Silicon photomultiplier and its possible applications // Nucl. Instrum. and Methods A. 2003. V. 504. P. 48–52.S.M. Metev and V.P. Veiko, Laser Assisted Microtechnology, 2nd ed., R.M. Osgood, Jr., Ed. Berlin, Germany: Springer-Verlag, 1998.

[2] Мусиенко Ю.В., Ахрамеев Е.В., Афанасьев А.Ю., Бондаренко Г.Б., Головин В.М., Гущин Е.Н., Ершов Н.В., Измайлов А.О., Куденко Ю.Г., Лубсандоржиев Б.К., Маяцкий В.А., Минеев О.В., Хабибуллин М.М, Хотянцев А.Н., Шайбонов Б.А.М. Высокочувствительные микропиксельные лавинные фотодиоды для сцинтилляционных счётчиков нейтринного эксперимента T2K // ПТЭ. 2008. № 1. С. 111–118. R. E. Sorace, V.S. Reinhardt, and S.A. Vaughn, “High-speed digital-to-RF converter,” U.S. Patent 5 668 842, Sept. 16, 1997.

[3] Danilov M. Novel Photo-Detectors and Photo-Detector Systems // Nucl. Instrum. and Methods A. 2009. V. 604. P. 183–189.

[4] Garutti E. Silicon photomultipliers for high energy physics detectors // J. Instrumentation. 2011. V.6. C10003

[5] Abe K., Abgrall N. Aihara and the T2K Collaboration. Application of Hamamatsu MPPC to T2K Neutrino Detectors // Nucl. Instrum. and Methods A. 2011. V. 659. P. 106–135.

[6] Vacheret A., Noy M., Raymond M., Weber A. First results of the Trip-t based T2K front end electronics performance with GM-APD. [Офиц. сайт] https://pos.sissa.it/archive/conferences/051/027/PD07_027.

[7] Zorzi N., Melchiorri M., Piazza A., Piemonte C., Tarolli A. Development of large-area silicon photomultiplier detectors for PET applications at FBK // Nucl. Instrum. and Methods A. 2011. V. 636. P. S208–213.

[8] Roncali E., Cherry S.R. Application of Silicon Photomultipliers to Positron Emission Tomography // Annals of Biomedical Engineering. 2011. V. 39. P. 1358–1377.

[9] 9. Vandenberghe S., Marsden P.K. PET-MRI: a review of challenges and solutions in the development of integrated multimodality imaging // Phys. Med. Biol. 2015. V. 60. P. 115–154.

[10] 10. Holder J. TeV gamma-ray astronomy: A summary // Astroparticle Physics. 2012. V. 39–40, P. 61–75.

[11] Anderhub H., Backes M., Biland A., Boccone V., Braun I., Bretz T., Buss J., Cadoux F., Commichau V., Djambazov Boccone L., Dorner D., Einecke S., Eisenacher D., Gendotti A., Grimm O., von Gunten H., Haller C., Hildebrand D., Horisberger U., Huber B., Kim K.-S., Knoetig M.L., Köhne J.H., Krähenbühl T., Krumm B., Lee M., Lorenz E., Lustermann W., Lyard E., Mannheim K., Meharga M., Meier K., Montaruli T., Neise D., Nessi-Tedaldi F., Overkemping A.-K., Paravac A., Pauss F., Renker D., Rhode W., Ribordy M., Röser U., Stucki J.-P., Schneider J., Steinbring T., Temme F., Thaele J., Tobler S., Viertel G., Vogler P., Walter R., Warda K., Weitzel Q., Zänglein M. Design and operation of FACT – the first G-APD Cherenkov telescope // J. Instrumentation. 2013. V. 8. P. 06008.

[12] Impiombato D., Giarrusso S., Mineo T., Catalano O, Gargano C., La Rosa G., Russo F., Sottile G., Billotta S., Bonanno G., Garozzo S., Grillo A., Marano D., Romeo G. Characterization of EASIROC as Front-End for the readout of the SiPM at the focal plane of the Cherenkov telescope ASTRI // Nucl. Instrum. and Methods A. 2013. V. 729. P. 484–490.

[13] Masek P., Jakubek J., Uher J., Preston R. Directional detection of fast neutrons by the Timepix pixel detector coupled to plastic scintillator with silicon photomultiplier array // JINST. 2013. V. 8. P. 01021.

[14] Матрица ArrayC-60035-64P-PCB http://sensl.com/estore/arrayc-60035-64p-pcb.

[15] Плата ABL-ARRAY64P-HDR. http://azimp.ru/catalogue/readout+boards/418/

[16] А.Ф. Янин, И.М. Дзапарова, В.И. Волченко, Е.А. Горбачева, А.Н. Куреня, В.Б. Петков. Многоканальная измерительная система для сбора данных с матриц из кремниевых фотоумножителей // Измерительная техника, № 3, 2017, с. 8-11.

[17] V.B. Petkov. Prospects of the Search for Neutrino Bursts from Supernovae with Baksan Large Volume Scintillation Detector// Physics of Particles and Nuclei, 2016, Vol. 47, No. 6, pp. 975–979. © Pleiades Publishing, Ltd., 2016.

On the possible consequences of multiple phase transitions inside hybrid stars

A. Yudin[1], T. Razinkova[1], D. Nadyozhin[1]

[1]Institute for Theoretical and Experimental Physics, Moscow, Russia; yudin@itep.ru

Abstract The phase transition from hadron to quark matter can be not a single strong event, but rather a series of weaker phase transitions through intermediate phases (multi-quark states). We perform a phenomenological exploration of this possibility concerning the problem of maximum mass and stability of hybrid stars.

Keywords: Hybrid Stars, Phase Transition, Quark Matter, Stellar Structure

1. Introduction

The density of matter in the central regions of neutron stars can reach more than few times of nuclear density value $\rho_n \approx 2.6 \times 10^{14}$ *g/ccm*. Hence, a phase transition from hadron matter to quark matter can occur. If this happens, such a star will contain the core, made of quarks, surrounded by ordinary hadron matter envelope. Such stars are called hybrid stars; see review in [1]. These objects have very interesting properties: they can, for example, imitate the properties of ordinary neutron stars. However, they have specific mass-radius diagram peculiarity [2] and they can be a part of the solution for long-standing problem of supernova explosion [3]. Beside this, their properties (if they exist) or their non-existence fact, have a direct connection to maximum neutron (hybrid?) star's mass problem.

With all this topics in mind, we want to refer here to another interesting possibility: in principle, phase transition from hadron to quark matter can proceed in different ways. The ordinary approach considers the single phase transition (Maxwellian or Gibbs type) from hadrons to uniform quark "sea". We want to explore here another "two-steps" opportunity: transition through some intermediate phase, made of multi-quark states [4]. Because of our current lack of knowledge about the properties of such a state, we will work in the frameworks of phenomenological approach which permits to consider the general aspects of the problem without getting too deep into the details.

2. Equation of State

For low-density hadron equation of state (EoS) we use parameterized description from [5] supplied with useful for applications FORTRAN subroutines [6]. This EoS gives for a maximum mass of pure neutron star value well above $2M_\odot$. For a quark EoS we use so-called "constant speed of sound" approximation from [7] (see also discussion in [8]). In this approximation the pressure P of matter is a linear function of its energy-density ε: $P=c_s^2(\varepsilon-\varepsilon_0)$, where ε_0 and c_s are constants, the latter has the meaning of speed of sound in speed of light units. This EoS can easily be connected to the well-known Bag model for quark matter [9]. We use standard value $c_s^2=1/3$ for uniform quark "sea" phase and value $c_s^2=2/3$ for

multi-quark phase. The higher value of c_s for intermediate phase is a consequence of general requirement: EoS must become softer with phase transition at growing density. The values of constant ε_0 determine the densities at which phase transitions occur. We assume the simplest Maxwellian type phase transition i.e. constant pressure at coexistence (mixed) phase region.

3. One Phase Transition

Let's start from the standard case of one phase transition (PT). We fix nuclear low-density EoS and sound speed in quark matter to the value $c_s^2=1/3$, and let ε_0 to vary. The change in ε_0 causes the corresponding changes in pressure P_{12} of phase coexistence and, of course, in energy-densities of phases at coexistence ε_1 and ε_2, where index 1 stands for nuclear and 2 for quark matter. It is known that density jump at phase's boundary $\lambda=\rho_2/\rho_1$ is crucial for the stability of a star with a small core of second phase: if λ is greater than critical value *3/2,* the star is dynamically unstable [10]–[11]. This is true for Newtonian gravity. For the case of General Relativity this criterion was generalized by Seidov [12], who showed that here one must use $\lambda=\varepsilon_2/\varepsilon_1$ value for the instability condition and the critical value of λ is now determined as:

$$\lambda_{cr} = \frac{3}{2}\left(1 + \frac{P_{12}}{\varepsilon_1}\right) \tag{1}$$

This expression suggests [13] the use of P_{12}/ε_1 and $\Delta\varepsilon/\varepsilon_1$, where $\Delta\varepsilon=\varepsilon_2-\varepsilon_1$, as coordinates for global exploration of mass-radius curves of hybrid stars with different EoSes. Here x-coordinate, $P_{12}/\varepsilon_1 = P_1(\varepsilon_1)/\varepsilon_1$ is directly connected with the density of the phase transition beginning, while y-coordinate, $\Delta\varepsilon/\varepsilon_1=\lambda-1$, characterizes energy-density jump. The example of calculation is shown on the ***Fig1.***

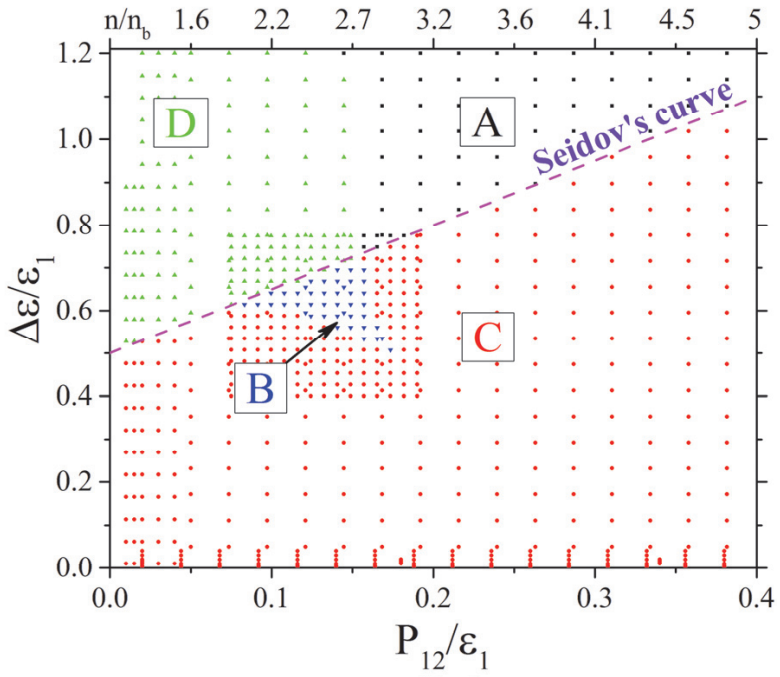

Fig1. *Topology diagram for mass-radius curves of hybrid stars. Upper axis shows the value of baryon density at the beginning of phase transition in units of nuclear baryon density $n_b \approx 0.16\ fm^{-3}$.*

The most interesting fact about this graph is that all its space is subdivided onto four zones with different hybrid star's mass-radius relation topology (see more details in [13] and [8]). The A (Absent) type is in the upper-right part of the diagram (colored black), above the Seidov's curve (the line of critical λ according to Eq. (1)). In this domain of parameters stable hybrid stars are absent. Below Seidov's curve there is a region of topology type C (Connected, colored red): stable are the hybrid stars with $0 \le M_q \le M^{max}$, where M_q is the mass of quark core of a star, and M^{max}– some maximum value, which depends on the point of the diagram. Upper-left region – type D (Disconnected, green) is characterized by the stability of hybrid stars with mass of quark core $0 < M^{min} \le M_q \le M^{max}$ i.e. there are maximum and minimum values for M_q. And last type B (Both, blue) – is a mixture of types C and D, i.e. on the mass-radius diagram there exist the stable hybrid stars with small quark cores and with big quark cores, but there is an unstable gap between. This diagram is very useful for the exploration of the ranges of EoS parameters and hybrid star properties. ***Fig2*** below shows two examples.

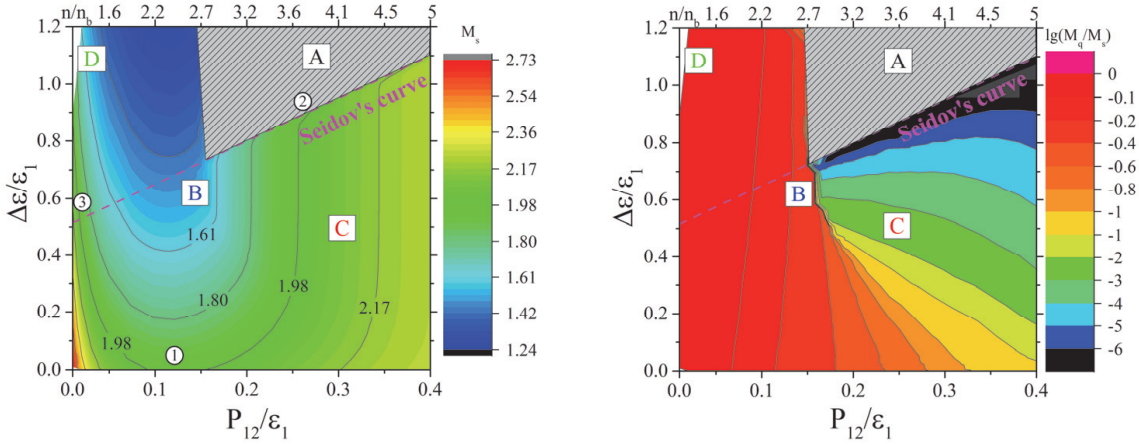

Fig2. *Left: level lines of maximum mass of hybrid star M_s. Right: level lines of $lg(M_q/M_s)$, where M_q is the mass of quark core in maximum mass stellar configuration. Area of type topology A left empty.*

On the left panel we plot level lines of maximum mass of hybrid star M_s. Area for A type topology left empty. Lines of constant mass have a quasi-parabolic structure. Now the most precisely measured value of neutron star mass is $1.97 \pm 0.04 M_\odot$ [14]. In view of this restriction we see a few allowable domains on the diagram. First, this is almost a full range of M_s at low x-coordinate (i.e. low densities of PT beginning). In addition, in lower left corner of the diagram there is a domain with very high masses of hybrid stars (see also [8]). Next, the region with $\Delta\varepsilon/\varepsilon_1 \approx 0$ is also favorable for high maximum mass. This is a natural result, because low $\Delta\varepsilon/\varepsilon_1$ means a weak phase transition. Second, there is a high P_{12}/ε_1 area of type C topology. In addition, three points marked by numbers 1, 2, 3 inside of small circles are shown and discussed below in subsection 4.2.

Now let's take a look at the right panel of ***Fig2***. Here we plot level lines of $lg(M_q/M_s)$, where M_q is the mass of quark core in maximum mass stellar configuration. One can see that unfortunately all the high-x region of type C topology has very low relative quark core mass. This means that the stability of high-mass hybrid stars here is illusive in some sense: only tiny part of the star can persist in quark matter state and the star is almost pure neutron one.

4. Two Phase Transitions

4.1. The splitting concept

Our work on multiple phase transitions was first motivated by the conclusion steamed from variational principle for the stars with PT [15]. In the cited paper we showed that the weak "splitting" of one phase transition into two parts is always favorable for stability of the star, assuming the total energy-density jump $\lambda_{tot}=\lambda_1\lambda_2$ remains the same. Now we present here the results of our numerical calculations of PT splitting for various conditions and splitting strength.

First, we fix the parameters of base EoS, i.e. the properties of uniform "quark sea" phase (the parameters of low-density nuclear EoS are the same for all cases). Thus we choose the concrete point on our base topology diagram (***Fig1***). Next we start to split this EoS by inserting intermediate quark phase with $c_s^2=2/3$ between original phases. This process is illustrated by ***Fig 3***, where solid line shows pressure-density dependence for one-PT case, while dashed line shows split EoS. Outside the splitting region this two EoSes coincide. The parameters of intermediate EoS is convenient to fix with the aid of two multipliers μ_1 and μ_2:

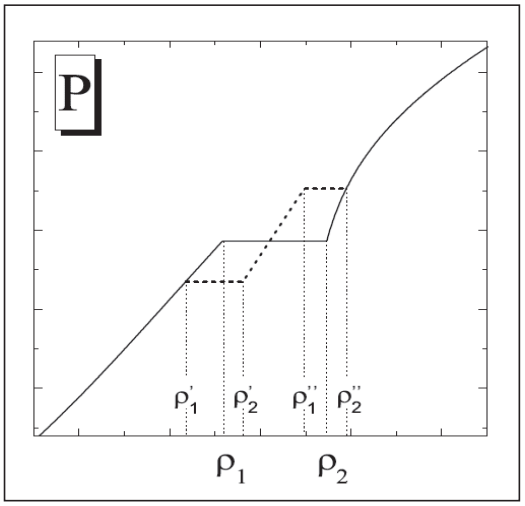

Fig3. *Pressure-density dependence for original (solid line) and split (dashed) EoS.*

$$\rho_1^{'} = \mu_1\rho_1,\ \mu_1 \le 1, \quad (2)$$

$$\rho_2^{''} = \mu_2\rho_2,\ \mu_2 \ge 1. \quad (3)$$

With multipliers μ_1 and μ_2 in hand, other parameters, such as $\rho_2^{'}$ and $\rho_1^{''}$ (see ***Fig3***) are calculated automatically from the phase coexistence equations. This is also true for intrinsic EoS parameters of the inserted phase.

4.2. Examples of calculation

Now we present a few examples of calculations for different initial conditions. First, we take a point with coordinates *(0.12,0.05)* on the topology diagram (topology type C). This point is shown by rounded number "1" on the left panel of ***Fig2***. It has the value of maximum mass $1.91M_\odot$ for stable hybrid star with one PT. The original phase transition is weak here, but still enough to lower the maximum mass value below $2M_\odot$ mass limit.

The results of our splitting procedure are shown on the combined ***Fig4***. The left panel of it shows multipliers $(\mu_1\text{-}\mu_2)$ diagram with color map for maximum mass of hybrid star with corresponding splitting (see color bar on the right). One can see that yellow, orange and red domains of $(\mu_1\text{-}\mu_2)$ diagram satisfy the observational restriction for maximum mass [14]. On the right panel of ***Fig4*** we plot Mass-Radius curves for selected cases (the values of split parameters are shown on the curves). Central density of a star increases when moving along

a curve from right to left (and, correspondingly, from bottom to top). Rightmost line corresponds to one-PT case. Black line corresponds to nuclear (hadron) phase inside the center of a star, red – to original "quark sea" phase, and blue color – to the inserted quark phase. It's clear that, from one hand, splitting can increase the maximum mass well above its critical value. But from the other hand, right panel of ***Fig4*** shows that the hybrid stars with mass above limit consist mostly of inserted quark phase, with small original quark phase core and tiny hadron envelope. This result is in some sense negative. To end with this case, we mention the specific peculiarity of *M-R* diagram that clearly can be seen on the right panel of ***Fig4***: all the *M-R* curves pass through the same small region at $R \approx 11$ km and $M \approx 1.9 M_{\odot}$. We explained this remarkable fact in [2].

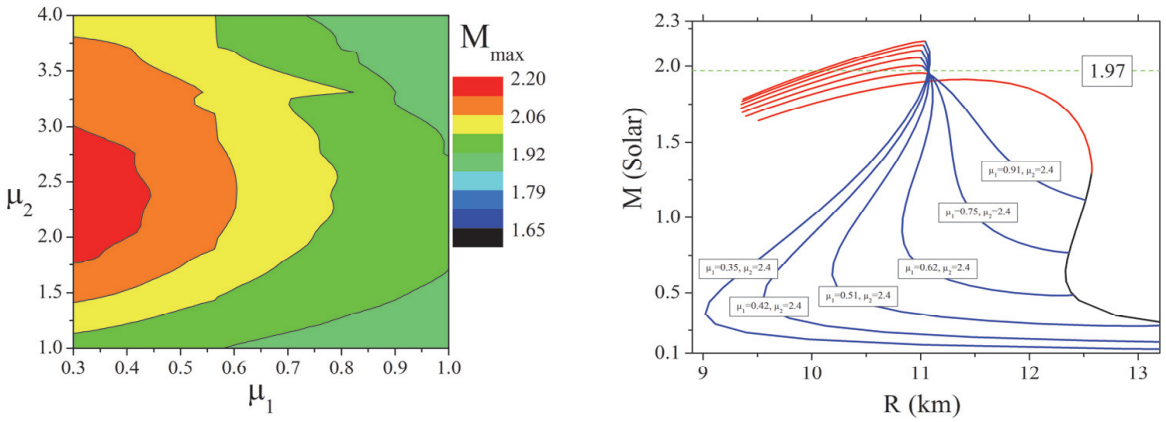

Fig4. *Left: the multipliers (μ_1-μ_2) diagram for (0.12, 0.05) point. The color map shows maximum mass of hybrid star with corresponding splitting. Right: Mass-Radius curves for selected cases, the values of split parameters are shown on the curves. Green horizontal line shows observational limit [14]. Rightmost curve corresponds to one-PT case.*

Now we can move to two other interesting cases, marked by rounded numbers "2" (topology type **A**) and "3" (type **D**) on the left panel of ***Fig2***. The first one corresponds to "Absent" topology, i.e. no stable hybrid configuration for one-PT case. ***Fig5*** (left panel) shows the *(μ_1-μ_2)* diagram for this case. We see that not only stable hybrid stars appear, but there exist *(μ_1,μ_2)* combinations which even fulfill $1.97 M_{\odot}$ observational constraint. The empty domains of diagram correspond to forbidden multiplier combinations, for which no PT can be found. But again only tiny cores of original phase are exists inside the stable configurations.

Third example, point "3", corresponds to low density of one-PT beginning and energy-density jump exceeded the Seidov's limit. Maximum stable mass here is $1.9 M_{\odot}$. The *(μ_1-μ_2)* diagram for this case is on the right side of ***Fig5***. We see here a different topology of M_{max} level lines, compared to the previous cases. And again the area of consistent with observations masses and correspondent multipliers is rather wide. But now the core of original phase here can be not so small: its maximum relative value $M_q/M_s \approx 0.3$ for the stable hybrid configuration with maximum mass $1.97 M_{\odot}$. But the hadron envelope is very small here anyway.

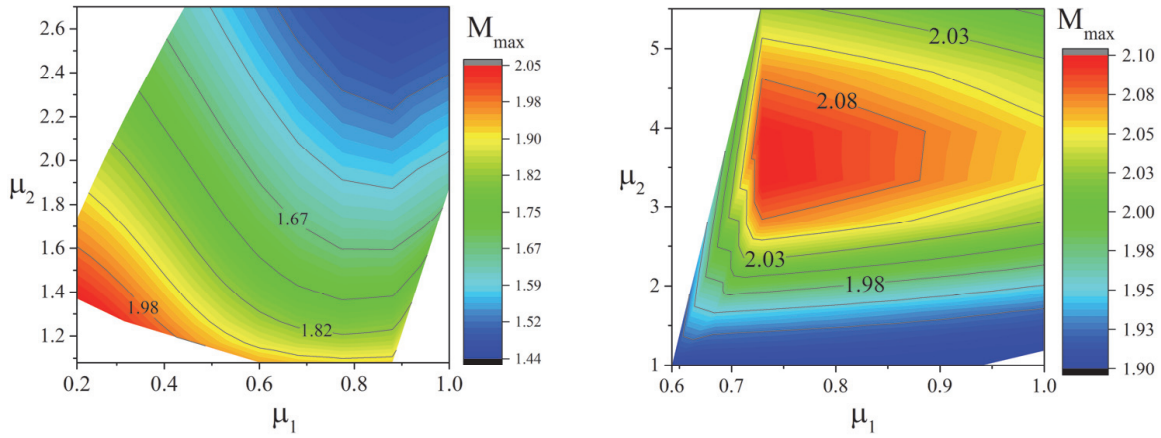

Fig5. *Multipliers (μ_1-μ_2) diagram for (0.26, 0.9) point (left) and (0.02, 0.58) point (right). The position of these points on the topology diagram is shown on the left panel of* ***Fig2*** *as points "2" and "3" correspondingly.*

5. Conclusion

In this work we explore the idea of multiple phase transitions inside hybrid stars. Our main purpose was to answer the question: can the insertion of intermediate quark states stabilize the star against collapse to black hole and thereby to increase the maximum stellar mass. Because of our current lack of knowledge about the properties of matter at very high densities, we choose the phenomenological approach (and more specifically, the constant speed of sound approximation for EoS of quark matter) as a method of investigation. The results of our research are twofold. The good news is that we really can reach and even overcome the observational $1.97M_O$ limit. Even the domain of original EoS parameters without any stable hybrid branch (type **A** topology) can be converted by specific splitting to stable hybrid configuration. But the bad side of this is that our new multi-phase configurations with observationally acceptable properties are, as a rule, almost pure quark stars with only a tiny envelope, made of hadron matter. Now is hard to decide if this is a generic property of any possible phase transition scenario or the result of our simplified approach. We plan to investigate this in close future with the aid of additional EoS parameters variation, what can be done by easy generalization of constant speed of sound approximation.

Acknowledgements

A.Y. thanks RFFI grant 16-02-00228 for financial support.

References

[1] P. Haensel, A.Y. Potekhin, and D.G. Yakovlev, "Neutron Stars 1. Equation of State and Structure". Springer, 619 (2007).

[2] A.V. Yudin, T.L. Razinkova, D.K. Nadyozhin, and A.D. Dolgov. Astron. Lett., 40, 4, pp. 201–211 (2014)

[3] I. Sagert, T. Fischer, M. Hempel, G. Pagliara, J. Schaffner-Bielich, A. Mezzacappa, F.-K. Thielemann, M. Liebendoerfer. Phys. Rev. Lett. 102, 081101 (2009)

[4] M.I. Krivoruchenko, D.K. Nadyozhin, T.L. Rasinkova, Yu.A. Simonov, M.A. Trusov, A.V. Yudin. Physics of Atomic Nuclei, 74, 3, pp. 371-412 (2011)

[5] P.Haensel & A.Y. Potekhin, Astron. Astrophys., 428, 191 (2004)

[6] http://www.ioffe.ru/astro/NSG/nseoslist.html

[7] M.G. Alford, G.F. Burgio, S. Han, G. Taranto, D. Zappala. Phys. Rev. D, 92, 8 (2015)

[8] O. Heinimann, M. Hempel, F.-K. Thielemann. Phys. Rev. D, 94, 10 (2016)

[9] J. Cleymans, R.V. Gavai, and E. Suhonen. Phys.Rep. 130, 217 (1986)

[10] M.J. Lighthill. MNRAS, 110, 339 (1950)

[11] W.H. Ramsey. MNRAS 110, 325 (1950)

[12] Z.F. Seidov. Sov. Astron. 15, 347 (1971)

[13] M.G. Alford, S. Han, M. Prakash. Phys. Rev. D, 88, 8 (2013)

[14] P.B. Demorest, T. Pennucci, S.M. Ransom, M.S.E. Roberts, J.W.T. Hessels. Nature 467, 1081–1083 (2010).

[15] A.V. Yudin, T.L. Razinkova and D.K. Nadyozhin. Astron. Lett., 43, 1, pp. 50–60 (2017)

Multi range study of the radio sources of the RATAN-600 surveys

O.P. Zhelenkova[1,2]*, E.K. Majorova[1]

[1] Informatics Laboratory, SAO RAS, Nizhnij Arkhyz, Russia; zhe@sao.ru

[2] Department of Astro Instrumentation, ITMO University, Saint-Petersburg, Russia

Abstract We present the results of the search of variable sources and transient events in the archive data of the sky surveys conducted on 3.9 GHz on the RATAN-600 radio telescope of the Special Astrophysical Observatory of the Russian Academy of Sciences (SAO RAS) in 1980-2000. 17% of the total studied sources can be attributed to the long-term variables in radio range. About half of them has significant variations in optical brightness according to the data of the optical and infra-red catalogs. Variability in the radio range is accompanied by variability in the optical range for the quite bright host objects ($R < 18^m$).

At a level of 3-5 r.m.s. we found three transient events. Using the data from radio and optical surveys and VizieR, SIMBAD, and NED databases, we made assumptions on the possible nature of these events. The first transient is probably associated with AGN activity, the second one — with a cataclysmic GRB event or with a supernova, the origin of the third is not determined. The inference on the possibility of search for variable sources and transients using the data from the RATAN-600 blind surveys was drawn. According to our estimation the surface density of radio transients is 0.03 on one square angular degree with the detection level 8–11 mJy on 3.94 GHz.

Keywords: Keyword One, Keyword Two, Keyword Three, Keyword Four, Keyword Five, Keyword Six

1. Introduction

Many radio sources exhibit flux density variations when observed at different epochs. This variability is due to both external (scintillations) and internal factors, which are associated with the radiation generation processes in the source itself. Variable radio sources are associated with different classes of objects, and their variability has different characteristic time scales. Variable radio emission is observed in active galactic nuclei (AGN), micro quasars, pulsars, and stars. Some AGNs exhibit intra-day variability due to the scintillation of their very compact components, caused by inhomogeneities of the intervening medium between the observer and the object. On time scales of one to several months, the variations of synchrotron emission often correlate with those of optical and/or x-ray radiation because of the nonuniform accretion rate and interaction between the jet and the ambient medium in the immediate vicinity of the nucleus. Variability on time scales of several years may be due to more substantial changes in the accretion rate, heating of the matter, and energy processing in the accretion disk.

Long-term variability of very bright AGNs with fluxes above 1 Jy is a subject of systematic studies; however, few such studies have been carried out for the population of fainter AGNs because of the lack of observational data. At the same time, the study of radio

variability of the sources with weak flux densities may prove to be a unique tool for investigating the evolution of AGNs and the nature of this phenomenon.

With the appearance of wide-field optical digital detectors, mass search for variable objects and transients became possible, and the attention to such research methods essentially increased. The same also refers to the radio range. At the end of the 20th century apart from the traditional monitoring of known objects, the archive data were used in searching for variability of radio sources. Thus, the papers [1]–[4] included the analysis of the archive data of the NVSS (NRAO VLA Sky Survey) [5] and FIRST (Faint Images of the Radio Sky at Twenty-Centimeters) [6] surveys. Let us also notice the 22-year survey of the southern sky MOST (Molonglo Observatory Synthesis Telescope) [7], the pilot survey ATCA (Australia Telescope Compact Array) at a frequency of 20 GHz (S_{20GHz} > 100 mJy) [8], the survey ATATS (Allen Telescope Array Twenty-Centimeter Survey), which comprises 12 epochs of observations ($S_{1.4GHz}$ > 20 nJy) [9]-[10], PiGSS (Pi GHz Sky Survey, Allen Telescope Array) [11]-[12], and many others.

The archive data of the surveys are also used for searching and estimating the frequency of radio transients [9]–[15]. Long-term radio transients are frequently thought to be associated with different types of events and objects. They can be supernovae [16–18] or afterglows of gamma-ray bursts [19]–[21]. The activity of stars and compact objects in the Galaxy can be also detected as a transient event in the radio range. For the new generation of radio surveys of the sky, tidal disruption event (TDE) or tidal disruption flares (TDF) are of special interest; they are associated with a sudden increase of the accretion rate due to tidal disruption of a star, appeared too close to an object with a mass of about 10^6–$10^8 M_\odot$, which can lead to an explosion in the soft x-ray band or, probably, to radio emission [22]–[24]. A considerable number of radio supernovae, isolated afterglows of gamma-ray bursts, outbursts due to tidal interaction are predicted in surveys with a sensitivity of about 0.1 mJy. All these events generate synchrotron radiation with self-absorption and, consequently, can be more likely observed at high radio frequencies.

There are a number of astrophysical phenomena that may plausibly produce gravitational waves in close coincidence with radio frequency emission [25]-[26]. Detection of transients coincident in these two channels would open up a new field for characterization of astrophysical transients involving massive compact objects. Transient gravitational-wave emission can occur when a temporary deformation of a rapidly rotating neutron star, a merger of a binary system of compact objects, specifically neutron stars or black holes. Recent evidence suggests that neutron star binary mergers may create at least some fraction of FRBs (Fast Radio Burst). Gamma-ray bursts (GRBs) may also result in radio emission. Core-collapse supernovae have also been proposed as plausible sources of short-duration radio pulses and GW emission.

2. Search for variable radio sources in the RATAN-600 blind surveys

We searched for variable radio sources from the archive data of surveys or observation cycles of the “Cold” experiment [27]. As a material for research, we used scans averaged throughout the multi-day runs. The work was carried out in several stages, which included (1) the compilation of a sample of calibration sources [28], (2) the search for candidates for variable radio sources [29]-[30], (3) searches for catalogs of the optical and infrared ranges of optical variability in the candidates we found for variables radio sources [31], (4) search for transient events [32]-[33]. Further, we describe in more detail the methods used by us.

2.1. RATAN-600 blind surveys of the experiment Cold

In 1980 the first 3.94 GHz deep blind survey was performed on the Northern sector of RATAN-600 within the framework of the "Cold" experiment [27] at the declination of the SS 433 source. A radio-source catalog (the RC catalog) with a detection threshold of 10 mJy [34] - [35] was produced based on the data of the survey. To refine the flux densities and coordinates of the RC catalog sources, several more observing runs were carried out at the same wavelength 7.6 cm and at the same declination SS433 ($Dec_{1980} = 4°57′\pm20′$) with RATAN-600 radio telescope. Soboleva et al. [36] reported the results obtained using data of surveys made in 1988-1999 and newly reduced data of the "Cold" survey (1980 - 1981) in the interval of right ascensions $7^h < RA < 17^h$. The list of objects found in this strip and identified with the objects of the NVSS catalog [5] can be found in the RCR (RATAN Cold Refined) catalog.

The reduction of the data of these surveys revealed that the flux densities of a number of objects vary from one observing run to another. The authors averaged the flux densities over all the observing runs, since identifying variable radio sources was not among their tasks. These averaged flux densities and their errors are reported in the RCR catalog [36].

We try to analyze whether it is possible to discover variable radio sources in the blind surveys. To solve this problem, we use the data of the 7.6-cm surveys carried out in 1980, 1988, 1993, and 1994 at the declination of $Dec_{1980} = 4°57′$ in the $7^h < RA < 17^h$ strip [29] and then in the $2^h < RA < 7^h$ strip [30].

The use of surveys to study the variability of radio sources has a certain advantage due to the fact that in the process of the survey the antenna is focused onto a certain elevation H (declination Dec^0 of the central survey section) and its configuration remains practically unchanged during the runs. This reduces the errors due to the repositioning of the antenna, which is especially important for the determination of flux densities of faint sources.

Another advantage of blind surveys is that due to the specificity of the power beam pattern (PBP) of RATAN-600 its field simultaneously covers many sources in a single run of the sky strip. The number of sources crossing the PBP that can be identified in records increases with the sensitivity of the telescope and integration time. Integration time is determined by the number of repeated transits of the given sky strip (i.e., the number of scans). The number of transits of the observed sky strip in the surveys considered varied from 20 to 35 depending on the survey and hour of observation. Thus repeated scanning of the same sky strip in the surveys not only increases the number of objects, but also makes it possible to study fainter sources.

Note that the data of the considered surveys can be used to study the long-term variability of radio sources on time scales of several years, which is known to be due to the nonstationary processes in AGNs.

2.2. Selection of sources for construction of calibrating curves and estimation of flux density errors

The principal aim of calibration source selection is to derive the calibration curves that can be used to compute the source flux densities and to estimate the flux density errors. We selected RCR radio sources with steep and well-studied spectra with available flux density data at several frequencies. We selected sufficiently bright objects with minimal scatter of data points in their spectra. Radio sources with steep spectra seldom exhibit variations at frequencies greater than 1 GHz. However, such variability is observed in objects where a

compact component is found, which is responsible for flux density variations. Our sample does not include known variable sources, which have mostly flat spectra. Most of the selected sources have spectral indices $\alpha_{3.94} < -0.75$ ($F_\nu \sim \nu^\alpha$) and r.m.s. errors of the scatter of data points on the spectrum $RMS^{sp} < 20\%$. According to the data of the used catalogs, the source flux density errors at different frequencies lie in the interval from 6% to 28%. The average flux density error for the entire sample of calibration sources is 15% ± 0.03%.

Let us recall some of the features of the observations on the RATAN-600 radio telescope whose PBP differs significantly from that of a parabolic dish [37]. In the mode of single-sector observations the PBP broadens with increasing angular distance from its central section. Correspondingly, the farther the source is from the central section, the broader is the response width and the weaker the signal. One-dimensional scans are superpositions of the sources that have crossed different horizontal sections of the power beam pattern.

To find variable sources in the data of the deep surveys carried out on the RATAN-600 radio telescope in 1980–1994, we performed a more thorough selection of calibration sources, constructed the experimental dependences F/T_a and computed calibration curves, performed a detailed analysis and estimated the relative standard errors for each survey.

To test the calibration sources for variability, we performed quantitative estimates of the parameters V_R [1], V_F [38], and the long-term variability index V [39] that characterize the variability of objects (our main parameter was the index V) and analyzed the statistical properties of suspected variable objects**.** Out of the entire sample of calibration sources (about 80 objects) 14 had positive long-term variability indices for at least one pair of surveys.

The estimates of relative standard deviations of flux densities from their mean values averaged over all the surveys, RMS^i (i is number of a survey), for the subsamples with $V > 0$ and $V < 0$ showed that they differ significantly. The RMS^i values for suspected variable sources and for "nonvariable" sources, averaged over the entire sample, are equal to $RMS^i = 0.23 \pm 0.07$ and $RMS^i = 0.08 \pm 0.04$, respectively. This leads us to conclude that the flux densities of the overwhelming majority of calibration sources varied only slightly from one survey to another, and that the flux density errors, on average, did not exceed 10%. Thus, we used for the calibration curve constructing only sources with $V < 0$ and with the χ^2 probability $p < 0.6$.

2.3. Candidates for long-term variable radio sources

As the initial data for the analysis of the variability of RCR-catalog sources, we use several-day average observational runs that have undergone primary reduction. After background subtraction we identified the sources on the averaged scans via Gaussian analysis. A detailed description of the technique used to reduce survey data has been published in [36].

We have searched for variable radio sources using the preserved averaged data from the "Cold" blind surveys carried out at RATAN-600 in 1980–1994. We studied those sources in the right ascension interval $2^h < RA_{2000} < 17^h$ which had flux density measurements at a frequency of 3.94 GHz in at least two surveys. We studied objects with 3.94-GHz flux densities $F \geq 15$ mJy, which are easily identifiable in the scans. We did not perform the study of variability of the objects, for which the flux density estimates in different surveys coincided within the measurement errors, or they were detected in a single survey only, as well as blended sources.

To reveal variable sources among the RCR objects of the considered sample, we estimated the long-term variability index V, the relative variability amplitude $V\chi$, the χ^2 probability p, and the parameters V_R and V_F.

In the interval of $2^h < RA_{2000} < 17^h$, 429 of 830 objects of the RCR catalog were studied for variability. We detected significant flux density variations for 73 of 429 objects studied for variability with a probability of $p > 0.6$ by the χ^2 criterion.

From our measurements, there are no significant flux density variations detected for five sources included in the OVRO monitoring program and/or marked as variable in NED database. Taking into account these 5 sources, we detected 78 variable sources in the region studied, which is equal to about 10% of the whole number of sources detected in the interval of $2^h < RA_{2000} < 17^h$, or 18% of the number of objects (429) that were studied for variability. This coincides with estimates for about 10 – 30% when searching for radio variability with the archive data [1, 40].

Radio luminosities of the studied sample of variable sources at 1.4 GHz fall within the range of $10^{24.5}$–$10^{29.5}$WHz^{-1}, i.e., all these objects are powerful radio sources. There are more galaxies (52%) than quasars (40%) among them. The number of objects with steep spectra ($\alpha_{3.94\ GHz} \leq -0.5$) is greater than with flat ones. Variable sources can have different kinds of morphological types, although, there are more point sources and sources with a core by 10 – 17% than among nonvariable objects.

The tenth part of variable objects are not compact and have significant angular and linear sizes (from 100 to 500 kpc), and also there are features in the morphological structure which are probably caused by a recurrent phase of the radio source activity. All the extended sources are associated with galaxies that have neighbors. One possible explanation of their variability is a change of internal jet orientation which does not coincide with the formed jets of a radio galaxy. In a number of cases, such changes could be caused by gravitational interaction with a close massive neighbor.

2.4. Search for optical variability for the candidates for long-term variable radio sources

To search for variability of host galaxies in the optical range [31], we used the USNO-B1 [41], GSC2.3 [42], SSS [43], and SDSS DR12 [44] catalogs, in the infrared range 2MASS [45], LAS and GPS UKIDSS [46]. The USNO-B1, SSS, and GSC-2.3 catalogs are based on the series of photographic sky surveys.

We estimated the V_R parameter which characterizes the amplitude of brightness variations. Fifteen objects from the list of variable radio sources are marked as variable in the optical range in the NED database. Thus, the variability in the optical and/or infrared ranges is observed for 35 (V_R>2.5) of 73 variable radio sources. Accounting for photometry errors, intrinsic for catalogs, the median amplitude of brightness variations of the objects under study is 1.0^m for USNO-B1, SSS, and GSC2.3, 0.15^m for SDSS and 0.36^m for 2MASS and the UKIDSS surveys.

All the host galaxies of the variable sources with brightness in the interval of R filter magnitudes in $13^m \div 18^m$ proved to be variable in the optical range. For the objects fainter than 18^m but brighter than 21^m, the percentage of optically variable objects decreases to 50% – 70%. Among even fainter objects ($R \approx 21^m$), the variability was not detected from the catalog data. The decrease of the percentage of optically variable objects with the brightness decrease is associated with observational selection due to insufficient survey depth and absence of systematic observations of faint objects. In most cases, variability in the radio

range is accompanied by variability in the optical range for the quite bright host objects ($R < 18^m$).

Assuming that emission of an active galaxy is determined by processes generated by the central engine and the core is surrounded by the dust torus, we can suppose that the amount of the observed optical emission depends on the degree of obscuring the central source by the torus, and the radio emission generated by the active core is detected to the full extent.

The ratio of optical luminosity to radio luminosity can be referred to a characteristic of the shading factor of the torus. To check this, we used the RCR sources with a known type of the host object and redshift (about a half of the catalog's objects) which allowed us to estimate their radio luminosity and absolute magnitude. We analyzed to which extent the ratio of absolute magnitude to logarithmic radio luminosity, $k = -M_r/\log(L_{3.94})$, taken with the opposite sign, differs for galaxies and quasars. We found that the quasars demonstrate quite constant value of this ratio, $k \approx 0.94$, independent of the power of a radio source; for the galaxies, it varies from 0.77 to 0.92. The k parameter for strongest galaxies is minimal, then with the radio luminosity decline after some value, it starts to grow up to the values observed for quasars. Different behavior of k for galaxies and quasars shows that there is a relation with obscuring characteristics of a torus. The dependence of this parameter on radio luminosity for radio galaxies indicates that the obscuring properties of the dust torus are different for the sources of different radio luminosity.

The comparison between the RCR sources for which there are no significant flux density variations detected and variable radio sources including those with brightness variations in the optical and/or infrared ranges according to the catalog data showed that the k median value and the proportion of the sources with flat spectra grow from the first group to the last one. If we view this as a manifestation of the dust torus orientation and its shading characteristics, then we can conclude that the core of variable sources is more open to an observer.

3. Search for long-term radio transients in the RATAN-600 blind surveys

Let us note that the sources detected at least in two surveys were included into the RCR catalog [36]. A number of sources detected in one survey only were not included in the RCR catalog. The reason is that due to precession they turned out at different distance in declination from the central cross-section of the survey in different years. With increasing source's distance from the central cross-section, the sensitivity of the survey turned out insufficient for detection. Moreover, the sensitivity of the surveys slightly changed from cycle to cycle. In an additional analysis of the survey scans, which was conducted in order to discover transient signals, we singled out twenty-two sources identified with the NVSS objects. They make about 4%of the number of the sources from the RCR catalog.

As a criterion of the transient nature of a source, apart from its absence in the NVSS and other catalogs, we adopted the condition of its detection in scans of only one single survey of 1980, 1988, 1993, and 1994 provided that the sensitivity of at least one another survey would be enough for its detection.

The characteristics of the surveys, taken from [30, 31], are given in Table 1, where column 1 shows the name of the survey, column 2 - the elevation of antenna positioning H, 3 - the begin and end dates of the survey, 4 - the duration time of the surveys Δt, in days, 5 - the number of scans N from which we obtained the averaged record, 6 - root-mean square error of noises in the averaged scans σ, in mJy, 7 - the detection threshold F_{min} in the averaged scan,

in mK. Notice that the search for transient events using the data from the Cold surveys is complicated by different sensitivity of the surveys and precession, due to which the region of the survey slightly shifts.

Table1. *Characteristics of the surveys conducted on RATAN-600 in 1980–1994*

Survey	H	Dates	Δt, days	N	σ, mK	F_{lim}, mJy
1980	51°07'.9	Mar 15, 1980–Jun 06, 1980	84	25-50	0.7	8.0
1988	51°08'.7	Dec 16, 1987–Jan 12, 1988	28	25	1.1	10.6
1993	51°09'.6	Sep 17, 1993–Nov 01, 1993	46	46	1.6	10.4
1994	51°22'.0	Apr 01, 1994–May 25, 1994	55	40	1.2	11.1

Upon the browsing the scans of the surveys in the right ascension range $2^h < RA < 17^h$, three transient events were discovered (see Table 2). All of them were found in the scans of the 1980 survey, which differs from the further ones by the best sensitivity, low noise, and also by longer duration (longer accumulation time). The antenna temperatures T_a of the detected events exceed 3–5σ. Transient radio sources completely meet the above requirements. Although the sensitivity of the 1988, 1993, and 1994 surveys suffices for their detection, they are not detected in the scans. The characteristics of transients are given in Table 1, where column 1 shows the name of the event, column 2 – right accession with error, 3 – declination with error, 4 – flux density on 3.94 GHz, in mJy, with error, column 5 shows the estimates of the ratio T_a/σ, which these sources should have had in the records of the 1988–1994 surveys with regard to the sensitivity of these surveys and the flux densities obtained from the 1980 survey.

Table2. *Transients in the interval $7^h < RA < 17^h$ in the 1980–1994 surveys*

Name	$R.A._{2000}$, hh mm ss.s	Dec, dd mm ss	F, mJy	T_a/σ, in 1988-1994
J111417+045530	11 14 16.7 ± 0.6	+04 55 30 ± 45	21.0 ± 2.0	5.2–7.5
J113344+045030	11 33 44.1 ± 0.6	+04 50 30 ± 45	24.3 ± 2.5	3.4–4.0
J165433+045457	16 54 33.1 ± 0.3	+04 54 57 ± 45	88.2 ± 8.5	11.1–16.6

Notice that the considered data are the average from 20 to 35 of the processed records of the sky stripe passing, depending on the survey and the observing hours, which excludes the presence of random noise, moreover, the level of man-made noise near the telescope was low in 1980–1994. The scans averaged over all observations of the surveys are time intervals from one to three months. Thus, the transient events detectable in the available data will refer to slow radio transients with the duration of the event from weeks to months. Unfortunately, neither the archive of the RATAN-600 observations nor the authors of the surveys preserved daily records or groups of the averaged records that could be of use for a more detailed analysis of the events and their interpretation.

As far as the goal of the paper is to study the possibilities of detection of transient events

using the observed data obtained in the RATAN-600 blind survey mode but not their investigation, we considered it possible to use the preserved scans averaged over the whole set of observations to search for long duration transients.

After the checking of the supernovae list, and the SIMBAD and NED databases including the catalogs of cataclysmic variables, Wolf-Rayet stars, Xray binaries, and M dwarfs, radio sources which are available in VizieR, SIMBAD, and NED databases, we have not found any coordinate coincidence (r = 2). A search for coincidences with detected transient events was also carried out. Using the data from radio, optical and infrared surveys, we made assumptions on the possible nature of these events. The first transient is probably associated with AGN activity, the second with a cataclysmic GRB event or with a supernova, the origin of the third is not determined.

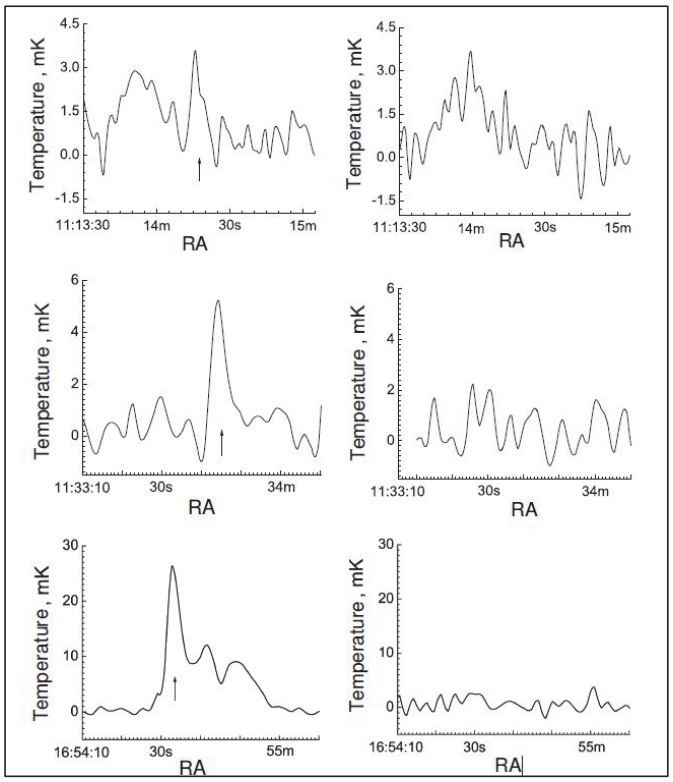

Fig1. *On the left: the regions of the averaged scan of the 1980 survey, which show the supposed transient sources J111417+045530, J113344+045030, and J165433+045457 (top to bottom). In the figures, they are marked with arrows. On the right: for comparison, with the scan of the 1994 survey where the same data regions are given.*

The survey area in the right-ascension interval $2^h < RA_{2000} < 17^h$ is 157.5 square degrees. Total accumulation time of the surveys is about 7 months. So the estimation of the radio transient surface density is $3 \times 10^{-2} deg^{-2}$ with the detection level 8–13.5 mJy on 3.94 GHz and 1 day duration of a transient. If it takes into account only accumulation time of the 1980 survey the density is more than twice higher.

4. Conclusion

Using the processed data from the Cold surveys conducted on RATAN-600 in 1980–1999, in a few our papers we tried to detect variable objects and transient events. The strategy of conducting the deep search Cold surveys was primarily aimed at obtaining data to search for microwave background fluctuations but not at the study of radio sources. Nevertheless, we discovered seventy-three sources suspected in variability, three transient events, and twenty-two radio sources which had not been included in the RCR catalog due to the

selection criterion applied: the presence of a source in two surveys at least.

In the attempt to interpret the origin of the detected transient signals, we found that they most likely refer to three different events. One of them can be referred to transient events associated with active galactic nuclei, the second one—to afterglows in the radio band of cataclysmic GRB events or supernova explosions, and the origin of the third one is undetermined.

Thus, taking into account the characteristics of the available radiometers and the observation strategy, the RATAN-600 radio telescope can be used not only for monitoring of the known variable radio sources but also as a tool to search for variable and transient events.

Acknowledgements

The study was carried out with the partial support of the RFBR grant 17-07-01367-a. The study was supported by the Ministry of Education and Science of the Russian Federation (government contract No.14.518.11.7054).In our research, we used the access to the Vizier catalogs, SIMBAD (CDS, Strasbourg, France) database, and also the NED (NASA/IPAC Extragalactic Database) database operated by the laboratory of the California Institute of Technology under contract with NASA.

References

[1] W. H. de Vries, R. H. Becker, R. L. White, and D. J. Helfand, Optical Properties of faint FIRST Variable Radio Sources. Astron. J., 2004; 127: 2565-2578.

[2] E. O. Ofek and D. A. Frail, The Structure Function of Variable 1.4 GHz Radio Sources Based on NVSS and FIRST Observations. Astrophys. J., 2011; 737: id 45 – 7 pp.

[3] N. Thyagarajan, D. J. Helfand, R. L. White, et al., Variable and Transient Radio Sources in the FIRST Survey. Astron. J., 2011; 742: 49-15 pp.

[4] E. O. Ofek, D. A. Frail, B. Breslauder, et al. A Very Large Array Search for 5 GHz Radio Transients and Variables at Low Galactic Latitudes. Astrophys. J., 2011; 740: 65 – 11 pp.

[5] J. J. Condon, W. D. Cotton, E. W. Greisen, et al. The NRAO VLA Sky Survey. Astron. J., 1998, 115: 1693-1716.

[6] D. J. Helfand, R. L. White ans R. H. Becker. The Last of FIRST: The Final Catalog and Source Identifications. Astrophys. J. , 2015, 801: id 25, 17 pp.

[7] K. W. Bannister, T. Murphy, B. M. Gaensler, et al. A 22-yr southern sky survey for transient and variable radio sources using the Molonglo Observatory Synthesis Telescope. MNRAS, 2011, 412, 634 – 664.

[8] E. M. Sadler, R. Ricci, R. D. Ekers, et al. The properties of extragalactic radio sources selected at 20GHz. MNRAS, 2006, 371, 898-914.

[9] S. Croft, G. C. Bower, R. Ackermann, et al., The Allen Telescope Array Twenty-centimeter Survey—A 690 deg^2, 12 Epoch Radio Data Set. I. Catalog and Long-duration Transient Statistics. Astrophys. J., 2010, 719, 45-58.

[10] S. Croft, G. C. Bower,G. Keating, et al. The Allen Telescope Array Twenty-centimeter Survey—A 700-square-degree, Multi-epoch Radio Data Set. II. Individual Epoch Transient Statistics. Astrophys. J., 2011, 731: id 34, 11 pp.

[11] S. Croft, G. C. Bower, and D.Whysong, The Allen Telescope Array Pi GHz Sky Survey. III. The ELAIS-N1, Coma, and Lockman Hole Fields, Astrophys. J., 2013, 762: 93, 25 pp.

[12] G. C. Bower, D. Saul, J. S. Bloom, et al., Submillijansky Transients in Archival Radio Observations, Astrophys. J., 2007, 666, 346-360.

[13] G. C. Bower, D. Whysong, S. Blair, et al., The Allen Telescope Array Pi GHz Sky Survey II. Daily and Monthly Monitoring for Transients and Variability in the Boötes Field, Astrophys. J., 2011, 739: id 76, 18 pp.

[14] T. Murphy, S. Chatterjee, D. L. Kaplan, et al., AST: An ASKAP Survey for Variables and Slow Transients, Publ. Astron. Soc. Australia, 2013, 30: e006, 27 pp.

[15] P. K. G. Williams,G. C. Bower, S. Croft, et al., ASGARD: A Large Survey for Slow Galactic Radio Transients. I. Overview and First Results, Astrophys. J., 2013, 762: id 85, 24 pp.

[16] S. R. Kulkarni, D. A. Frail, M. H. Wieringa, et al., Radio emission from the unusual supernova 1998bw and its association with the γ-ray burst of 25 April 1998, Nature, 1998, 395, 663-669.

[17] K.W.Weiler, R. A. Sramek, N. Panagia, et al., Radio supernovae, 1986, Astrophys. J. 301, 790-812.

[18] A. M. Soderberg, A. Brunthaler, E. Nakar, et al., Radio and X-ray Observations of the Type Ic SN 2007gr Reveal an Ordinary, Non-relativistic Explosion, Astrophys. J., 2019, 725: 922-930.

[19] D. A. Frail, S. R. Kulkarni, L. Nicastro, et al., The radio afterglow from the γ-ray burst of 8 May 1997, Nature, 1997, 389:261-263.

[20] T. Totani and A. Panaitescu, Orphan Afterglows of Collimated Gamma-Ray Bursts: Rate Predictions and Prospects for Detection, Astrophys. J., 2002, 576: 120-134.

[21] P. Chandra and D.A. Frail, A Radio-selected Sample of Gamma-Ray Burst Afterglows, Astrophys. J., 2012, 746: id 156, 28 pp.

[22] S. Gezari, D. C. Martin, B. Milliard, et al., Ultraviolet Detection of the Tidal Disruption of a Star by a Supermassive Black Hole, Astrophys. J., 2006, 653: L25-L28.

[23] B. A. Zauderer, E. Berger, A. M. Soderberg, et al., Birth of a relativistic outflow in the unusual γ-ray transient Swift J164449.3+573451, Nature, 2011, 476: 425-428.

[24] B. A. Zauderer, E. Berger, R. Margutti, et al., Illuminating the Darkest Gamma-Ray Bursts with Radio Observations, Astrophys. J., 2013, 767: id 152, 13 pp.

[25] Predoi, V.; Clark, J.; Creighton, T.; Daw, E.; et al. Prospects for joint radio telescope and gravitational-wave searches for astrophysical transients. Classical and Quantum Gravity. 2010, 27: id. 084018, 20 pp.

[26] Abbott, B. P.; Abbott, R.; Abbott, T. D.; et al. Search for transient gravitational waves in coincidence with short-duration radio transients during 2007-2013. Physical Review D, 2016; 93: id.122008, 13 pp.

[27] Pariiskii, Iu. N.; Korolkov, D. V. The Kholod experiment - The first deep sky survey using the RATAN-600 radio telescope. Itogi Nauki i Tekhniki, 1986, 31: 73-197.

[28] Majorova, E. K.; Zhelenkova, O. P., On possibility of detection of variable sources using the data of "Cold" surveys carried out on RATAN-600, Astrophysical Bulletin, 2012, 67: 318-339.

[29] Majorova, E. K.; Zhelenkova, O. P. Search for variable sources using data of "Cold" surveys,

Astrophysical Bulletin, 2013, 68: 418-441.

[30] Majorova, E. K.; Zhelenkova, O. P.; Temirova, A. V. Search for variable sources using the data of Cold surveys in the right-ascension interval $2^h \leq RA \leq 6^h$, Astrophysical Bulletin, 2015, 70: 33-44.

[31] Zhelenkova, O. P.; Majorova, E. K. Observational manifestations and intrinsic properties of the RCR sources in terms of a unified model, Astrophysical Bulletin, 2016, 71: 165-188.

[32] Zhelenkova, O. P.; Majorova, E. K. Search for radio transients and recent detection of radio sources in the RATAN-600 surveys of 1980-1994, Astrophysical Bulletin, 2016, 71: 14-23.

[33] Zhelenkova, Olga P.; Majorova, Elena K. The search of radio transients in the RATAN-600 radio telescope surveys. Astroinformatics, Proceedings of IAU Symposium, 2017, 325: 270-273.

[34] Yu. N. Parijskij, N. N. Bursov, N. M. Lipovka, et al., The RATAN-600 7.6 cm catalog of radio sources from Experiment Cold-80. A&AS, 1991, 87: 1-32.

[35] Yu. N. Parijskij, N. N. Bursov, N. M. Lipovka, et al., The RATAN-600 7.6 cm catalogue of radio sources within the interval 22h-4h at declination of SS433. A&AS, 1992, 96: 583-592.

[36] N. S. Soboleva, E. K. Majorova, O. P. Zhelenkova, et al., RATAN-600 7.6-cm deep sky strip surveys at the declination of the SS433 source during the 1980-1999 period. Data reduction and the catalog of radio sources in the right-ascension interval 7^h<R.A. < 17^hAstrophysical Bulletin, 2010, 65: 42-59.

[37] E. K. Majorova and S. A. Trushkin, Experimental studies of the beam pattern of RATAN-600. Bull. Spec. Astrophys. Obs., 2002, 54: 89-122.

[38] Ting-Gui Wang, Hong-Yan Zhou, Jung-Xian Wang, et al., Evidence for a Population of Beamed Radio-intermediate Quasars, Astrophys. J., 2006, 645: 856-860.

[39] A. G. Gorshkov, V. K. Konnikova, and M. G. Mingaliev, Variability of the flux densities of radio sources on timescales shorter than a month, Astron. Rep., 2010, 54: 908-924.

[40] A. G. Gorshkov, V. K. Konnikova, Variability at frequencies of 3.9 and 7.5 GHz of radio sources from the Zelenchuk survey with fluxes greater than 200 mJy, Astron. Rep., 1995, 39: 257-267.

[41] D. G. Monet, S. E. Levine, B. Casian, et al., The USNO-B Catalog, Astron. J., 2003, 125: 984-993.

[42] B. Lasker, M. G. Lattanzi, B. J. McLean, et al., The Second-Generation Guide Star Catalog: Description and Properties, Astron. J., 2008, 136: 735-766.

[43] N. C. Hambly, H. T. MacGillivray, M. A. Read, et al., The SuperCOSMOS Sky Survey - I. Introduction and description, MNRAS, 2001, 326: 1279-1294.

[44] C. P. Ahn, R. Alexandroff, C. Allende Prieto et al., The Tenth Data Release of the Sloan Digital Sky Survey: First Spectroscopic Data from the SDSS-III Apache Point Observatory Galactic Evolution Experiment, Astrophys. J. Suppl., 2014, 211: id 17, 16pp.

[45] M. F. Skrutskie, R. M. Cutri, R. Steining et al., The Two Micron All Sky Survey (2MASS), Astron. J., 2996, 131: 1163-1183.

[46] A. Lawrence, S. J. Warren, D. Almani et al., The UKIRT Infrared Deep Sky Survey (UKIDSS) MNRAS, 2007, 379: 1599-1617.

Detection of ultra-high-frequency variability with a deficit of quanta

B.E. Zhilyaev[1], A.V. Sergeev[2]

[1] Main Astronomical Observatory, National Academy of Sciences of Ukraine,
27 Zabolotnoho St., 03143 Kiev, Ukraine; zhilyaev@mao.kiev.ua

[2] Terskol branch of the Institute of Astronomy of the Russian Academy of Sciences
(TF INASAN)

Abstract A technique for detecting harmonics in sparse quantum flows is developed when it is impossible to describe a light curve. A problem that is insoluble in the time representation can be exactly solvable in the Fourier frequency representation. To demonstrate the capabilities of ultra-high-frequency photometry, we present a numerical experiment. We show that at a sampling time of one microsecond on the 2 m telescope, harmonics can be detected in the frequency range up to 500 kHz for an object with U = 14.5. We demonstrate the application of the described technique to the analysis of gamma-ray flare from the Compton Gamma Observatory CGRO. In the BATSE trigger No. 207 in an energy channel of 25-50 keV with flare duration of 0.030 ± 0.002 s, two significant harmonics at 190 and 310 kHz with half-widths of about 25 kHz are fixed, which correspond to velocities of 25,000 km / sec (~ 0.08 speed of light). The size of the object is estimated to be ~ 6000 km, and the size of the active region is ~ 484 km. A possible scenario for gamma ray flare is the merging of a black hole of stellar mass and a neutron star.

Keywords: techniques: photometric, methods: numerical, methods: miscellaneous, gamma-rays: general

1. Introduction

It would seem that the deficit of quanta puts insurmountable obstacles in the way of fast photometry. For the sparse flux of quanta, the concept of the light curve becomes vague. This creates a false impression of an almost insoluble problem when we are dealing with rapidly changing processes. Nevertheless, this unsolvable problem in the time representation can be exactly solvable in the Fourier frequency representation. We can obtain formal mathematical expressions for estimating the frequency, amplitude and phase of a harmonic, starting literally with three photons in a number of measurements. According to Fourier's theorem, there are no restrictions on the absolute values of the mean intensity, sampling frequency, etc. However, the minimum detectable signal amplitude depends on the total number of recorded photons ([1], [7]).

It can theoretically be shown that the minimum amplitude of the harmonic signal a_{min}, detected at the level of confidence probability 3 σ, has the form [7]:

$$a_{min} = < n >^{\frac{1}{2}} \left(\frac{72}{N}\right)^{\frac{1}{4}}$$

where <n> is the average intensity value, *N* is the number of measurements. Thus, for detecting a harmonic signal, about a hundred real quanta are needed, regardless of the intensity of the source.

To demonstrate the capabilities of ultra-high-frequency (UHF) photometry, we present the following numerical experiment. Let a series of measurements be a Poisson stream of quanta with an average intensity *a* equal to one ten-thousandth for the sampling time. This means that on average, we need ten thousand measurements to record one quantum, and the remaining data are zeros. The appearance of a quantum is a random process. The series consists of Poisson noise and a sinusoidal wave with an amplitude equal to one ten-thousandth and a period equal, say, half the Nyquist frequency. The length of the series of measurements is N.

$$B = a \cdot \left(1 + \cos\left(2 \cdot \frac{\pi}{4} \cdot (1{:}N)\right)\right) \tag{1}$$

Note that the signal frequency in this case is insignificant, if only it was less than the Nyquist frequency. A usable signal is a non-stationary Poisson process with the intensity described by a sinusoidal wave. The modeling conditions are such that for two hundred thousand measurements there are about two dozen photons. It is quite clear that under these conditions it is impossible to construct the light curve. An example of three such measurements with a time resolution of 1 microsecond is shown in Fig 1 Left.

We will perform formal calculations of the power spectrum of these "observations" to detect a harmonic signal and to estimate its frequency and amplitude. Compare the given signal parameters with the resulting parameters obtained as a result of the simulation.

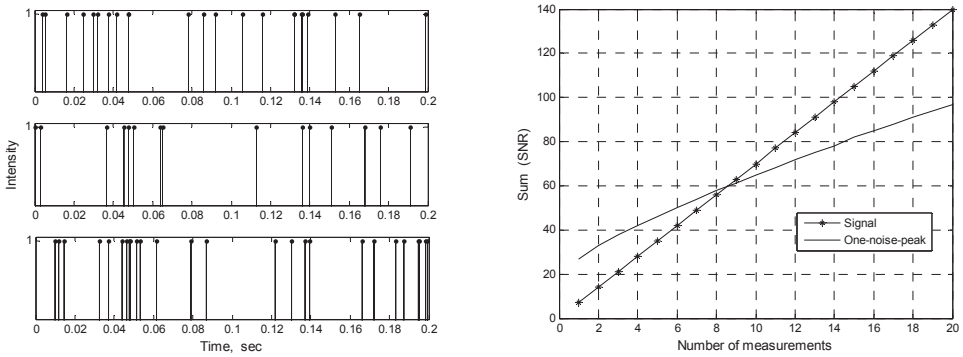

Fig1. *Left: Three arrays of random photocounts selected from the Poisson distribution with the intensity determined by the equation (1) by the amplitude a = 0.0001, the signal sampling time is one microsecond and the length of the series is N = 200000. Right: The cumulative sum of the SNR and snr elements depending on the number of measurements n.*

Define the signal-to-noise ratio (SNR) and detection criterion for the signal:

$$\mathrm{SNR} = \frac{\mathrm{a}^2}{2 \cdot \mathrm{cov}\left(\mathrm{poissrnd(B)}\right)} \cdot \mathrm{N} + \mathrm{M}$$

$$\mathrm{snr} = \mathrm{chi2inv}\left(1 - \frac{1}{\mathrm{N}}\right) \tag{2}$$

Here, SNR is the signal-to-noise ratio of a random variable chosen from the Poisson

distribution with the parameter *B* (equation 1), *poissrnd* is the random variable generator from the Poisson distribution, *cov* is the variance operator, *N* is the series length, *M* is the average value of the χ^2_2 chi-square distribution with 2 degrees of freedom. The value of *snr* is equal to *chi2inv* - the inverse distribution function, χ^2_2 is a chi-square with 2 degrees of freedom for the quantity (1-1 / N). Its value corresponds to the detection level "One noise peak" in the noise power spectrum.

From a computational point of view, the measurement data can conveniently be represented as an array of power spectra consisting of *n* measurements with sample length *N.* In Fig 1 Right shows the cumulative sum of the *SNR* and *snr* elements, depending on the number of measurements *n.* The *SNR> snr* condition defines the limit value of the number of measurements for the detection of a harmonic signal.

It can be seen from the figure that a sample of about ten such measurements makes it possible to detect a harmonic signal and to estimate its frequency and amplitude.

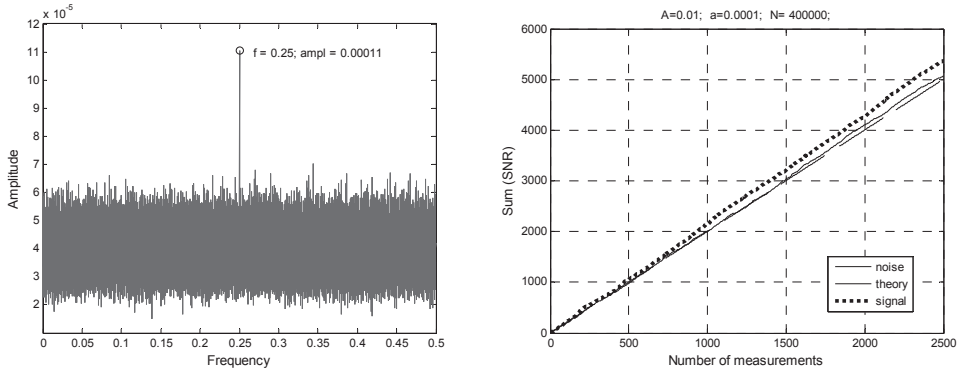

Fig2. *Left: Spectrum of signal amplitudes from equation (1) averaged over 10 samples. Right: The cumulative sum of SNR signals elements and noise peaks (a thin solid line) and its theoretical value is the cumulative sum of chi-square distribution elements with 2 degrees of freedom (discontinuous curve) depending on the number of measurements n.*

Fig 2 Left shows the amplitude spectrum averaged over 10 samples of the signal from equation (1). The specified signal amplitude $a = 10^{-4.}$ The calculated amplitude is $1.1 \cdot 10^{-4}$. The dimensionless frequency is equal to the specified frequency f = 0.25. The coincidence of the given and calculated signal parameters proves the effectiveness of the proposed algorithm.

100% variable sources with a Poisson intensity of 10^{-4} counts during signal accumulation can be detected after accumulating only about a hundred photocounts. Conditionally, with a sampling time of one second and the length of $N = 100000$ series, 10 photocounts is expected on average. For a sure detection of harmonics based on the criterion "One noise peak", it is enough to perform about 10 measurements. With a sampling time of one microsecond, the total measurement time is 0.7 seconds. For a 2 m telescope this corresponds to the source U = 14.5. The frequency range is 500 kHz.

Table 1 presents the computation data for sources with Poisson intensity *a* from 10^{-4} to 10^{-5} for a sampling time of one microsecond. The number of quanta during a single measurement is about 80 on the average. At the same time, 100% variable sources can be detected with a brightness of U from 14.5 to 17.0 magnitudes on a 2 m telescope. The length

of the series of measurements N ranges from one hundred thousand to one million, the total measurement time is from 0.7 to 9.0 seconds.

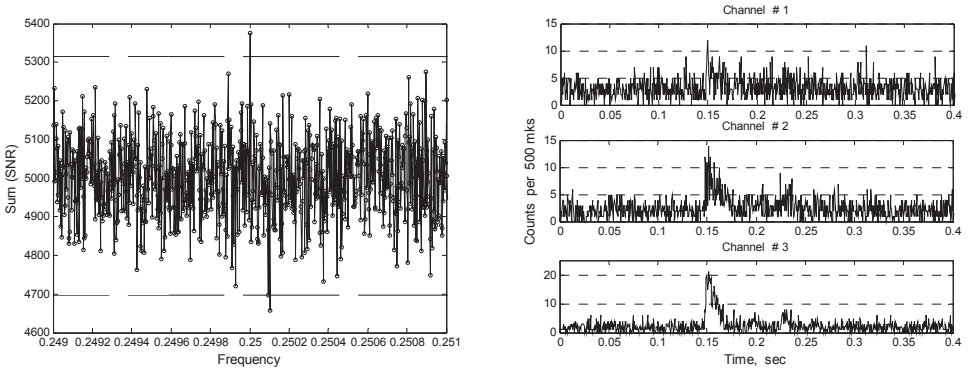

Fig 3. *Left: The cumulative sum of SNR elements for the critical number of measurements n is shown as solid line. The dashed lines correspond to the detection of a harmonic by the criterion "One noise peak". Right: Light curves with a resolution of 0.5 milliseconds in three energy channels 25-50 keV, 50-100 keV, and 100-300 keV.*

Table 1 Computation data for sources with different Poisson intensity. 100% variable sources.

a	N	n	Nq	U	T, sec
0.0001	100000	7	70	14.5	0.7
0.00009	111111	7	70	14.6	0.8
0.00008	125000	8	80	14.7	1.0
0.00007	142900	8	80	14.9	1.1
0.00006	166666	8	80	15.1	1.3
0.00005	200000	8	80	15.3	1.6
0.00004	250000	8	80	15.5	2.0
0.00003	333333	8	80	14.8	2.7
0.00002	500000	9	90	16.2	4.5
0.00001	1000000	9	90	17.0	9.0

NOTE:
a is Poisson amplitude (average number of quanta during the sampling time of the signal)
N is the length of the sample
n is the number of measurements for signal detection
N_q is the number of quanta in a single sample
U is the magnitude in the U filter
T - total measurement time

2. Stars

Above we considered 100% variable sources. Such sources, apparently, are of mainly methodological interest. Now consider real stars with a 1% variable source. Equation of source:

$$B = a \cdot \left(100 + \cos\left(2 \cdot \frac{\pi}{4} \cdot (1:N)\right)\right) \quad (3)$$

We simulate the detection of UHF variability in the range up to 500 kHz with amplitude of 0.01 mag in stars with U equal from 9.5 to 10.8 and for sources in white light W equal to 12.5 to 13.8 mag for the 2 m telescope.

Fig 2 Right shows the cumulative sum of *SNR* elements as a function of the number of measurements *n*. The figure also shows the calculated cumulative sum of elements for noise peaks (a thin solid line) and its theoretical value is the cumulative sum of elements with the chi-square distribution χ^2_2 with 2 degrees of freedom (discontinuous curve). The data correspond to the first line of the elements in Table 2: Poisson amplitude a = 0.0001, sample length N = 400000, number of measurements n = 2205, necessary to detect the harmonic signal, the number of quanta for the time of one measurement Nq = 88200, the limiting stellar magnitudes U = 9.5 and W = 12.5, the total measurement time is T = 882 seconds.

Fig 3 Left shows the cumulative sum of SNR elements for the critical number of measurements *n*. The dashed lines correspond to the detection of a harmonic by the criterion "One noise peak". Its theoretical value is the cumulative sum of the elements of the distribution χ^2_{2n}, the chi-square with $2 \cdot n$ degrees of freedom. It can be seen that a signal with a given amplitude a = 0.0001 is detected at a dimensionless frequency f = 0.25. The coincidence of the given and calculated signal parameters proves the effectiveness of the proposed detection algorithm.

Table 2 Computation data for 1% variable sources with different Poisson intensity.

a	N	n	Nq	U	W	T, sec
0.0001	400000	2205	88200	9.5	12.5	882
0.00009	444444	2231	89240	9.6	12.6	991
0.00008	499998	2256	90240	9.7	12.7	1128
0.00007	571428	2281	91240	9.9	12.9	1303
0.00006	666666	2316	92640	10.1	13.1	1544
0.00005	800000	2350	94000	10.3	13.3	1880
0.00004	999998	2396	95840	10.5	13.5	2396
0.00003	1333333	2456	98240	10.8	13.8	3274

NOTE: Notations as in Table 1

In the next section, we demonstrate the application of the described technique to the analysis of gamma-ray flare from the data of the Compton Gamma Observatory (CGRO).

3. BATSE Trigger No. 207

For our analysis, we used the TTE (time-tagged event) from the BATSE 3B catalog [5], obtained by the Compton Gamma Observatory. Because of the high temporal resolution, the TTE data is suitable for searching for high-frequency variability. Each TTE data set contains the arrival time of all registered photons within 2 μs of time, energy and detector number, in which each photon is registered. The energy boundaries of the channels are approximately 25-50 keV, 50-100 keV, 100-300 keV, and more than 300 keV. We chose one of four short flashes, namely trigger number 207.

The gamma-ray flare of the BATSE trigger No. 207 is fixed in three energy channels No. 1 25-50, No. 2 50-100, No. 3 100-300 keV. The sampling time is one microsecond. For trigger number 207, Cline et al. [2] give flare duration according to the TTE data of 0.030 ± 0.002 s.

Fig 3 Right shows the binned light curves with a resolution of 0.5 milliseconds. In Fig 4 Left initial (raw) light curves in the flare region. The length of the series of measurements is 1,545,916 the number of registered gamma quanta in the three channels is 9447, 7107, 6119. The degree of filling (Poisson's intensity) averages about 0.003. The number of recorded quanta during a flare period is about 300. The light curve "appears" when five hundred samples are combined (0.5 milliseconds, Fig 4 Right).

The duration of the flare in the first energy channel (25-50 keV) is about 20 milliseconds. The smoothed light curve clearly shows the fluctuations in the brightness of the flare with a frequency of about 180 Hz. Variations of brightness at high frequencies can not be traced because of the degradation of the light curve. However, they are clearly manifested in the power spectra (Fig 5 Left). Two significant harmonics are seen at frequencies of 190 and 310 kHz. Harmonics are detected at a spectral resolution of 13 kHz. The spectral resolution is regulated by the choice of the width of the Tukey spectral window when constructing the power spectrum. In the raw unsmoothed spectra, harmonics are not detected. This indicates modulation of the harmonics. Filtering the frequency spectra allows us to set the bandwidth of the modulation.

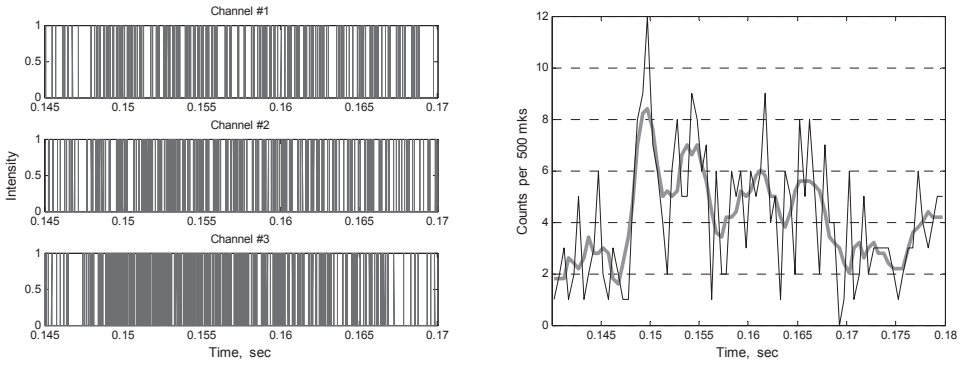

Fig 4. *Left: Initial (raw) light curves in the region of the flare. The degree of filling (Poisson's intensity) averages about 0.003. Right: Smoothed light curve in the first energy channel (25-50 keV). The fluctuations in the brightness of the flare with a frequency of about 180 Hz are clearly visible.*

We constructed the Fourier power spectrum of the first BATSE trigger channel counts of the 207 (25-50 keV) with a time resolution of 1 μs using the technique described above for signal simulation. The spectrum is presented in the form of the signal-to-noise-frequency

ratio in the frequency range up to 500 kHz. In the raw spectrum, there are no significant signal peaks visible in Fig 5 Left. We assumed that the signal is subject to strong frequency modulation and used a merger of frequencies to eliminate modulation. This procedure is equivalent to low-frequency filtering in the frequency representation. Since the signal-to-noise ratio (SNR) for noise peaks obeys the χ^2_2 statistic, summing the harmonics within a frequency window of width n leads to a χ^2_{2n} statistic for noise peaks.

Fig 5 Right shows the Fourier power spectrum after filtering with a frequency window of width n = 10. The detection threshold at the significance level of "One Noise Peak" for the statistics of χ^2_{20} is 49.6. Fig 5 Right shows two significant peaks at 190 and 310 kHz, which coincide with the signal peaks in Fig 5 Left.

Thus, the technique described above in modeling for the detection of harmonic signals in sparse quantum fluxes is confirmed by comparison with the full-scale experiment.
Approximation by the Gaussian allows one to estimate the half-width FWHM of the harmonics peaks at about 25 kHz. The half-widths of the peaks correspond to velocities of 25,000 km / sec (~ 0.08 speed of light). The size of the active region d of the oscillation source and the size of the object D can be estimated as:

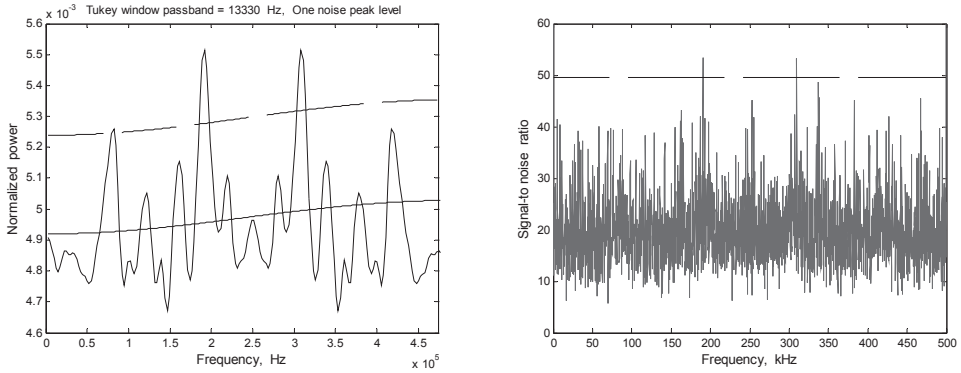

Fig 5. *Left: Power spectrum in the flare region is shown. The dashed curve corresponds to the detection of a harmonic by the criterion "One noise peak". Right: The Fourier power spectrum after filtering with a frequency window of width n = 10. The detection boundary at the significance level "One noise peak" is shown by a dashed line.*

$$d = \Delta f / f \cdot c \cdot \Delta t$$

$$D = c \cdot \Delta t$$

Here f and Δf are the frequencies of the harmonics and half-widths of the peaks, c is the speed of light, and Δt is the flare duration (0.02 sec). Thus, the size of the object can be estimated D = 6000 km, and the size of the active region d = 484 km. These estimates give grounds to consider the object to be relativistic.

A possible scenario for gamma-ray flare is the merger of black holes of stellar mass and neutron stars [8]. During the coalescence process, the substance circulating around the black hole demonstrates rapid fluctuations in the radiation intensity. Such a system will also emit gravitational waves, which lead to a decrease in the radius of the orbit. The time scale of the coalescence process is from several milliseconds to several tens of milliseconds and oscillation frequencies of hundreds of Hz ([4], [3], [6]).

4. Conclusion

We demonstrate a technique for estimating the frequency, amplitude, and phase of a harmonic in sparse fluxes of quanta.

We show that 100% variable sources can be detected after accumulating only about a hundred photocounts. For the 2 m telescope this corresponds to the source U = 14.5. The frequency range is 500 kHz.

For stars with a 1% variable source the detection is achievable for a stellar magnitude U = 9.5 and in white light W = 12.5 for a measurement time of T = 882 seconds.

We demonstrate the described technique to the analysis of gamma-ray flare, BATSE trigger No. 207. Two significant harmonics are seen at frequencies of 190 and 310 kHz.

The half-widths in harmonic spectra are of about 25 kHz, which correspond to velocities of 25,000 km / sec (~ 0.08 of the speed of light). The size of the object is estimated at 6000 km, and the size of the active region is 484 km. These estimates give grounds to consider the object to be relativistic. A possible scenario for gamma flare is the merger of a black hole of the stellar mass and the neutron star

4. References

[1] S. Bonazzola, M. Chevreton X - and gamma- ray Superfast Photometry, Astron. Astrophys.,1982, V. 105, P. 1-5.

[2] Cline, D.B., Matthey, C., Otwinowski, S., 1999, ApJ, 527, 827

[3] Faber, J.A., Baumgarte, T.W., Shapiro, S.L., Taniguchi, K., Rasio, F.A., 2006, PhRvD 73, 024012

[4] Lee, W.H., Kluzniak, W., 1999, ApJ, 526, 178

[5] Meegan, C.A., Pendleton, G.N., Briggs, M.S., et al., 1996, ApJS, 106, 65

[6] Shibata, M., Taniguchi, K.: 2008, PhRvD, 77, 084015

[7] Zhilyaev B.E. Statistical Photometry of Stars: Concept and Methods, Proceedings, Balkan Meeting of young Astronomers, 25-29 Sept. 2000, Belogradchik, Bulgaria, Eds. A. Antov, R. Konstantinova-Antova, R. Bogdanovski and M. Tsvetkov, Belogradchik, 2001, P. 185-198.

[8] B.E. Zhilyaev, D. Dubinovska , 2009, On the detection of high-frequency oscillations in short gamma-ray bursts, Astron. Nachr. ,AN 330, No. 4, 1-7

Научное издание

Труды Международной конференции
Сверхновая SN 1987A,
кварковый фазовый переход в компактных объектах
и многоволновая астрономия

Ответственные редакторы:
В.В. Соколов, Т.Н. Соколова, В.Б. Петков, В.В. Синев, Е.А. Горбачева
Корректоры *Т.Н. Соколова*, *Е.А. Горбачева*

Отпечатано с оригинала, предоставленного авторами
Подписано в печать 00.00.2018
Ф-т 60×84/8. Уч.-изд.л. 25,0. Зак. 22425. Тираж 100 экз. Бесплатно
Печать цифровая

Федеральное государственное бюджетное учреждение науки
Институт ядерных исследований Российской академии наук

Издательский отдел
117312, Москва, проспект 60-летия Октября, 7а